SETARIA AS A MODEL GENETIC SYSTEM TO ACCELERATE YIELD INCREASES IN CEREALS, FORAGE CROPS, AND BIOENERGY GRASSES

EDITED BY: Thomas P. Brutnell, Andrew Doust, Hari Deo Upadhyaya and Joyce Van Eck

PUBLISHED IN: Frontiers in Plant Science

frontiers Research Topics

frontiers

ISSN 1664-8714
ISBN 978-2-88963-282-4
DOI 10.3389/978-2-88963-282-4

About Frontiers

Frontiers is more than just an open-access publisher of scholarly articles: it is a pioneering approach to the world of academia, radically improving the way scholarly research is managed. The grand vision of Frontiers is a world where all people have an equal opportunity to seek, share and generate knowledge. Frontiers provides immediate and permanent online open access to all its publications, but this alone is not enough to realize our grand goals.

Frontiers Journal Series

The Frontiers Journal Series is a multi-tier and interdisciplinary set of open-access, online journals, promising a paradigm shift from the current review, selection and dissemination processes in academic publishing. All Frontiers journals are driven by researchers for researchers; therefore, they constitute a service to the scholarly community. At the same time, the Frontiers Journal Series operates on a revolutionary invention, the tiered publishing system, initially addressing specific communities of scholars, and gradually climbing up to broader public understanding, thus serving the interests of the lay society, too.

Dedication to Quality

Each Frontiers article is a landmark of the highest quality, thanks to genuinely collaborative interactions between authors and review editors, who include some of the world's best academicians. Research must be certified by peers before entering a stream of knowledge that may eventually reach the public - and shape society; therefore, Frontiers only applies the most rigorous and unbiased reviews.
Frontiers revolutionizes research publishing by freely delivering the most outstanding research, evaluated with no bias from both the academic and social point of view. By applying the most advanced information technologies, Frontiers is catapulting scholarly publishing into a new generation.

What are Frontiers Research Topics?

Frontiers Research Topics are very popular trademarks of the Frontiers Journals Series: they are collections of at least ten articles, all centered on a particular subject. With their unique mix of varied contributions from Original Research to Review Articles, Frontiers Research Topics unify the most influential researchers, the latest key findings and historical advances in a hot research area! Find out more on how to host your own Frontiers Research Topic or contribute to one as an author by contacting the Frontiers Editorial Office: researchtopics@frontiersin.org

SETARIA AS A MODEL GENETIC SYSTEM TO ACCELERATE YIELD INCREASES IN CEREALS, FORAGE CROPS, AND BIOENERGY GRASSES

Topic Editors:
Thomas P. Brutnell, Chinese Academy of Agricultural Sciences, China
Andrew Doust, Oklahoma State University, United States
Hari Deo Upadhyaya, International Crops Research Institute for the Semi-Arid Tropics (ICRISAT), India
Joyce Van Eck, Boyce Thompson Institute, United States

Citation: Brutnell, T. P., Doust, A., Upadhyaya, H. D., Van Eck, J., eds. (2019). Setaria as a Model Genetic System to Accelerate Yield Increases in Cereals, Forage Crops, and Bioenergy Grasses. Lausanne: Frontiers Media SA. doi: 10.3389/978-2-88963-282-4

Table of Contents

04 ***Editorial:* Setaria *as a Model Genetic System to Accelerate Yield Increases in Cereals, Forage Crops, and Bioenergy Grasses***
Andrew N. Doust, Thomas P. Brutnell, Hari Deo Upadhyaya and Joyce Van Eck

06 ***Optimization of Phenotyping Assays for the Model Monocot* Setaria viridis**
Biswa R. Acharya, Swarup Roy Choudhury, Aiden B. Estelle, Anitha Vijayakumar, Chuanmei Zhu, Laryssa Hovis and Sona Pandey

19 ***Arabidopsis Type III $G\gamma$ Protein AGG3 is a Positive Regulator of Yield and Stress Responses in the Model Monocot* Setaria viridis**
Jagdeep Kaur, Swarup Roy Choudhury, Anitha Vijayakumar, Laryssa Hovis, Zach Rhodes, Rob Polzin, Dylan Blumenthal and Sona Pandey

32 ***The Status of* Setaria viridis *Transformation:* Agrobacterium-*Mediated to Floral Dip***
Joyce Van Eck

37 ***Domestication and Improvement in the Model C4 Grass, Setaria***
Hao Hu, Margarita Mauro-Herrera and Andrew N. Doust

50 ***QTL Mapping Combined With Comparative Analyses Identified Candidate Genes for Reduced Shattering in* Setaria italica**
Sandra Odonkor, Soyeon Choi, Debkanta Chakraborty, Liliam Martinez-Bello, Xuewen Wang, Bochra A. Bahri, Maud I. Tenaillon, Olivier Panaud and Katrien M. Devos

59 ***SiSTL2 is Required for Cell Cycle, Leaf Organ Development, Chloroplast Biogenesis, and has Effects on C_4 Photosynthesis in* Setaria italica *(L.) P. Beauv.***
Shuo Zhang, Sha Tang, Chanjuan Tang, Mingzhao Luo, Guanqing Jia, Hui Zhi and Xianmin Diao

75 ***Species-Associated Differences in the Below-Ground Microbiomes of Wild and Domesticated* Setaria**
Srinivasa Chaluvadi and Jeffrey L. Bennetzen

87 ***SiYGL2 is Involved in the Regulation of Leaf Senescence and Photosystem II Efficiency in* Setaria italica *(L.) P. Beauv.***
Shuo Zhang, Hui Zhi, Wen Li, Jianguo Shan, Chanjuan Tang, Guanqing Jia, Sha Tang and Xianmin Diao

102 ***A Dynamic Co-expression Map of Early Inflorescence Development in* Setaria viridis *Provides a Resource for Gene Discovery and Comparative Genomics***
Chuanmei Zhu, Jiani Yang, Mathew S. Box, Elizabeth A. Kellogg and Andrea L. Eveland

119 ***Neural Net Classification Combined With Movement Analysis to Evaluate* Setaria viridis *as a Model System for Time of Day of Anther Appearance***
Jigar S. Desai, Erin Slabaugh, Donna J. Liebelt, Jacob D. Fredenberg, Benjamin N. Gray, S. V. Krishna Jagadish, Olivia Wilkins and Colleen J. Doherty

130 ***Screening of Mutants Related to the C_4 Photosynthetic Kranz Structure in Foxtail Millet***
Mingzhao Luo, Shuo Zhang, Chanjuan Tang, Guanqing Jia, Sha Tang, Hui Zhi and Xianmin Diao

frontiers in Plant Science

EDITORIAL
published: 10 October 2019
doi: 10.3389/fpls.2019.01211

Editorial: *Setaria* as a Model Genetic System to Accelerate Yield Increases in Cereals, Forage Crops, and Bioenergy Grasses

Andrew N. Doust[1], Thomas P. Brutnell[2], Hari Deo Upadhyaya[3] and Joyce Van Eck[4]*

[1] Oklahoma State University, Stillwater, OK, United States, [2] Chinese Academy of Agricultural Sciences, Beijing, China, [3] CGIAR Research Program on Climate Change, Agriculture and Food Security (CCAFS), South Asia, New Delhi, India, [4] Boyce Thompson Institute, Ithaca, IL, United States

Keywords: ***Setaria*, Green foxtail, foxtail millet, C4 photosynthesis, grass, Poaceae**

Editorial on the Research Topic

Setaria as a Model Genetic System to Accelerate Yield Increases in Cereals, Forage Crops, and Bioenergy Grasses

Setaria is a model C4 grass in the tribe Paniceae of the subfamily Panicoideae, closely related to switchgrass, napier grass, and, pearl millet, and, in the sister tribe, closely related to important crops such as maize, sorghum, and sugar cane. The model comprises two species, foxtail millet (*Setaria italica*), domesticated in the Yellow River valley in China approximately 9–11,000 years ago, and its wild progenitor, green foxtail (*Setaria viridis*), which is one of the world's most widespread weeds. *Setaria*, particularly green foxtail, differs from its more important biofuel and crop relatives in that it is small in stature and fast cycling and has a small genome. As such, it is ideally suited to greenhouse and growth experiments, as well as being capable of being grown in field plots. Over the last 10 years, numerous resources have been created for both species, including annotated genomes, mutant and field collections, transformation protocols, and gene atlases. Some of these advances were detailed in a volume in the Springer Crop Genetics and Genomics volume released in 2017 (Doust and Diao, 2017). The current collection of papers in this Research Topic, covering domestication, developmental genetics, mutant analysis, microbiomes, and technical advances, shows how far the field has progressed even in the short time since that volume.

Several papers deal with the genetics of domestication and improvement. Hu et al. present an overview of domestication and improvement in *Setaria*, focusing on key traits that differ between foxtail millet and its wild progenitor green foxtail. Concentrating on the domestication and improvement traits of shattering, plant architecture and flowering time, the paper summarizes known information and points out new opportunities for improvement in drought stress and nutrient efficiencies.

Odonkor et al. take the theme of domestication further and investigate the genetic basis of shattering in *Setaria* in more detail. Through mapping and gene expression analyses, the authors pinpoint the ortholog of sorghum SH1 as being likely to underlie the quantitative trait locus (QTL) of the largest effect, with a second small QTL in the vicinity of the ortholog of rice qSH1. These results are significant because they suggest that there might be a common genetic control of shattering across the grasses. Chaluvadi and Bennetzen also look at the effects of domestication but focus belowground, contrasting soil microbiome differences between wild and domesticated *Setaria*. They point out key differences in the microbiotic assemblages of domesticated versus wild accessions and

OPEN ACCESS

Edited and reviewed by:
Roberto Papa, Marche Polytechnic University, Italy

****Correspondence:***
Andrew N. Doust
andrew.doust@okstate.edu

Specialty section:
This article was submitted to Plant Breeding, a section of the journal Frontiers in Plant Science

Received: *03 April 2019*
Accepted: *03 September 2019*
Published: *10 October 2019*

Citation:
Doust AN, Brutnell TP, Upadhyaya HD and Van Eck J (2019) Editorial: Setaria as a Model Genetic System to Accelerate Yield Increases in Cereals, Forage Crops, and Bioenergy Grasses. Front. Plant Sci. 10:1211. doi: 10.3389/fpls.2019.01211

suggest that domestication has selected for specific associations in the root and rhizosphere.

Other papers deal with gene expression analyses. Zhu et al. present a co-expression study of early inflorescence development in green foxtail, which is canonical with that found in other panicoid grasses even though the resulting inflorescence is more complex. Six developmental stages were identified, containing stage-specific co-expression modules with homologs of known developmental genes from maize and rice, suites of transcription factors, and unknown genes. This study will be important for comparative analyses and gene discovery in *Setaria*.

Three papers detail screening and characterization of mutants related to C4 photosynthesis, Kranz structure, and chloroplast biogenesis in foxtail millet. Luo et al. detail their studies on identifying ethyl methanesulfonate (EMS) mutants of foxtail millet that show variation in anatomical structure, especially related to Kranz anatomy. The genetic basis of Kranz anatomy, an essential part of C4 photosynthesis in grasses, has been exceedingly difficult to elucidate, and the 14 mutants identified by Luo et al. represent an important new set of resources for genetic analysis. Another two papers describe the identification of genes responsible for chloroplast biogenesis and a range of other phenotypes. Zhang, Tang, et al. identify the *Setaria* ortholog of deoxycytidine monophosphate deaminase (DCD), a key enzyme in dTTP biosynthesis. Surprisingly, the expression of this gene in *Setaria* differs from that in rice (a C3 plant) and is affected by low CO_2 environments, showing similar patterns of expression to C4 photosynthesis genes. This may provide new avenues for understanding the differing roles of this essential gene in C3 and C4 grasses. Zhang, Zhi et al. describe the identification of an ATP-independent metalloprotease that is required for chloroplast development, photosystem II function, leaf senescence, and abscisic acid (ABA) signal response. This is the first report characterizing this gene's functions in C4 plants.

Setaria is also an excellent vehicle for stress studies, including drought, salt, and low nutrient levels. The paper by Kaur et al. details the role of an *Arabidopsis* type III Gγ protein AGG3 in monocots, using the over-expression of the *Arabidopsis* gene in *Setaria* to gain insight into its function in C4 grasses. In doing so, Kaur et al. reveal that several traits are correlated with gene expression level while others appear to exhibit allele-specific expression. Traits related to stress were positively affected, including responses to salt and low nitrogen.

The papers that seek to understand the genetic control of development and response to the environment all rest on a requirement for accurate and sensitive phenotyping. Two papers directly address this issue. Acharya et al. conduct multiple phenotypic assays of *Setaria* to optimize growth conditions under multiple hormonal and abiotic stresses. This is very important to provide a secure base of information for the *Setaria* community to conduct further phenotypic assays. A very different tack is taken by Desai et al., who use neural net classification combined with movement analysis of time-lapse imagery to track flower opening in *Setaria*. This trait is particularly tricky to track in *Setaria*, where the inflorescence architecture is complex, and flowers open briefly and in different parts of the inflorescence. Knowledge of timing of anther appearance is critical for the success of controlled crosses in *Setaria* as well as in breeding for favorable opening times in hot field environments.

Finally, Van Eck provides a review of *S. viridis* transformation approaches. In it, she discusses tissue culture-based and floral dip approaches and concludes that tissue culture-based methods are more reliable, though more technically demanding, than the floral dip method. Simplification of tissue-based approaches and further optimization of the floral dip method—the holy grail of monocot transformation—are necessary for *Setaria* to reach its full potential as a model system.

While by no means being a comprehensive review of all activity in *Setaria* to date, these articles provide a unique insight into the value and potential of the *Setaria* model system.

AUTHOR CONTRIBUTIONS

AD wrote manuscript; JE, HU, and TB provided comments and edits.

REFERENCE

Doust, A. N., and Diao, X. (eds.) (2017). The genetics and genomics of *Setaria*. *Plant genetics and genomics: crops and models*, vol. 19. Springer-Verlag, New York. doi: 10.1007/978-3-319-45105-3

Conflict of Interest: The authors declare that the research was conducted in the absence of any commercial or financial relationships that could be construed as a potential conflict of interest.

frontiers in Plant Science

ORIGINAL RESEARCH
published: 22 December 2017
doi: 10.3389/fpls.2017.02172

Optimization of Phenotyping Assays for the Model Monocot *Setaria viridis*

*Biswa R. Acharya†, Swarup Roy Choudhury†, Aiden B. Estelle, Anitha Vijayakumar, Chuanmei Zhu, Laryssa Hovis and Sona Pandey**

Donald Danforth Plant Science Center, St. Louis, MO, United States

Setaria viridis (green foxtail) is an important model plant for the study of C4 photosynthesis in panicoid grasses, and is fast emerging as a system of choice for the study of plant development, domestication, abiotic stress responses and evolution. Basic research findings in Setaria are expected to advance research not only in this species and its close relative *S. italica* (foxtail millet), but also in other panicoid grasses, many of which are important food or bioenergy crops. Here we report on the standardization of multiple growth and development assays for *S. viridis* under controlled conditions, and in response to several phytohormones and abiotic stresses. We optimized these assays at three different stages of the plant's life: seed germination and post-germination growth using agar plate-based assays, early seedling growth and development using germination pouch-based assays, and adult plant growth and development under environmentally controlled growth chambers and greenhouses. These assays will be useful for the community to perform large scale phenotyping analyses, mutant screens, comparative physiological analysis, and functional characterization of novel genes of *Setaria* or other related agricultural crops. Precise description of various growth conditions, effective treatment conditions and description of the resultant phenotypes will help expand the use of *S. viridis* as an effective model system.

Keywords: *Setaria viridis*, seedling growth and development, seed germination, phytohormones, abiotic stress, phenotyping

OPEN ACCESS

Edited by:
Andrew Doust, Oklahoma State University, United States

Reviewed by:
Jose Sebastian, Carnegie Institution for Science (CIS), United States
Kate Warpeha, University of Illinois at Chicago, United States

****Correspondence:***
Sona Pandey
spandey@danforthcenter.org

†These authors have contributed equally to this work.

Specialty section:
This article was submitted to Plant Breeding, a section of the journal Frontiers in Plant Science

Received: *06 October 2017*
Accepted: *11 December 2017*
Published: *22 December 2017*

Citation:
Acharya BR, Roy Choudhury S, Estelle AB, Vijayakumar A, Zhu C, Hovis L and Pandey S (2017) Optimization of Phenotyping Assays for the Model Monocot Setaria viridis. Front. Plant Sci. 8:2172. doi: 10.3389/fpls.2017.02172

INTRODUCTION

Setaria viridis (Setaria, hereafter), a C4 plant, belongs to the grass subfamily Panicoideae which also includes important crops like maize, sugarcane, sorghum and potential biofuel species such as Miscanthus and switchgrass. Setaria possesses all inherent characteristics of an ideal reference plant; the plants are easy to grow and maintain, have small stature (∼30 cm at maturity), rapid life cycle (6–8 weeks), produce large quantities of seed and are diploid with a small genome size of ∼500 Mb (Brutnell et al., 2010). The Setaria genome has been sequenced and *Agrobacterium*-mediated Setaria callus transformation and spike–dip transformation methods have been established (Bennetzen et al., 2012; Martins et al., 2015; Saha and Blumwald, 2016). There is large extant genetic diversity in this species and mapping populations and large-scale mutant populations are being developed (Huang et al., 2014, 2017; Layton and Kellogg, 2014; Schroder et al., 2017). Together with its close relative *S. italica,* with which it is interfertile, *S. viridis* also serves as a good model system to study crop domestication (Li and Brutnell, 2011). Furthermore, extensive genomics and transcriptomics resources are currently available and are being constantly

developed for this species (Xu J. et al., 2013; Huang et al., 2016; Singh et al., 2016; Pandey et al., 2017). A number of studies, many already harnessing these resources, have recently been published corroborating its considerable potential as a model system for gene discovery, physiological and developmental analyses, stress responses and nutrient use efficiency (Yue et al., 2014; Li et al., 2016; Mauro-Herrera and Doust, 2016; Pan et al., 2016; Bandyopadhyay et al., 2017; Huang et al., 2017). Given its similarity to and close phylogenetic relationship with a number of important food crops, it is expected that identification of novel gene functions in *S. viridis* that are associated with growth and development, grain size, yield and biomass, resistance to different pathogens and abiotic factors will have huge benefits for translational research geared toward improving food security.

Despite the progress made with resource development for Setaria, and its increasing usage across the world as a model system for the study of panicoid grasses, critical aspects of its growth and development and the factors affecting them are not as well-established as for other model plants such as Arabidopsis. The development of standardized and simple methods to perform efficient genetic and physiological analysis is critical at this stage to expand its use as an effective model species, as well as for comparing results across laboratories. Moreover, development of fast, efficient and standardized seed or seedling-based assays will also be useful for large-scale mutant screen or bulk segregant analysis, for the evaluation of abiotic or biotic stress responses of plants, and to study the effect of different plant hormones or other additives. Toward this goal, we have standardized a set of assays which describe optimum growth conditions for dormancy breakage and seed germination, early seedling growth and development and adult plant growth phenotypes for Setaria.

Seed germination is an important biological process in the plant life cycle which is tightly regulated by the antagonistic phytohormones abscisic acid (ABA) and gibberellic acid (GA_3). ABA serves as a negative regulator of seed germination whereas GA_3 is a positive regulator and their dynamic metabolic status determines whether a dormant seed will germinate or not (Finkelstein et al., 2008; Nonogaki, 2014; Gazzarrini and Tsai, 2015; Shu et al., 2015, 2016). In addition to hormonal signals, environmental cues such as light, temperature, and water also impact seed germination (Nonogaki, 2014; Gazzarrini and Tsai, 2015; Shu et al., 2015). Seed germination assays are a quick, easy and efficient way to evaluate seed dormancy, seed quality, effect of different phytohormones, response to various abiotic stresses and other environmental conditions. Many of the key Arabidopsis mutants, especially those related to ABA, GA, and ethylene signaling and metabolism were identified through seed germination screens (Bleecker et al., 1988; Guzman and Ecker, 1990; Saleki et al., 1993; Yang et al., 1995; Leon-Kloosterziel et al., 1996; Ogawa et al., 2003). These screens are usually performed with plate-based assays, which allow for easy, efficient screening of thousands of seeds in a short time. Similarly, post-germination growth and early-seedling growth assays are also key indicators of the plants' response to a multitude of environmental, abiotic and biotic stress signals and can be efficiently applied to large plant populations. Even though it is expected that different environmental signals, phytohormones or stresses will affect Setaria growth and development, a detailed analysis of those effects, the effective concentration ranges for different additives and the critical stages for observing specific plant phenotypes remain underexplored. Often such information is derived from more established model systems such as Arabidopsis, which may not be optimal in this case.

Several studies have reported on different aspects of seed germination in Setaria, including comparisons between different accessions or species, interspecies comparison of germination efficiencies and the effects of different environmental conditions on seed germination (Manthey and Nalewaja, 1987; Dekker and Hargrove, 2002; Liu et al., 2003, 2017; Mauro-Herrera et al., 2013; Sebastian et al., 2014; Amini et al., 2015a,b; Shu et al., 2015; Saha and Blumwald, 2016; Saha et al., 2016; Hodge and Doust, 2017). Assays have also been developed for germination on synthetic media plates under controlled conditions and genetic basis of seed germination efficiency has been explored (Mauro-Herrera et al., 2013; Qie et al., 2014; Sebastian et al., 2014; Muthamilarasan et al., 2015; Feng et al., 2016; Feldman et al., 2017; Huang et al., 2017; Liu et al., 2017); all with the aim of effectively breaking the seed dormancy, which remains a major problem in Setaria. Freshly harvested Setaria seeds are difficult to germinate on synthetic media and typically require various pretreatments such as long post-harvest storage (1–3 months), a cold shock treatment, liquid smoke or gibberellic acid treatment, etc. (Mauro-Herrera et al., 2013; Sebastian et al., 2014; Saha and Blumwald, 2016; Saha et al., 2016). Even under these conditions the consistent, homogenous germination is relatively difficult to achieve, which may be important for many physiological assays.

The goals of this research were to identify suitable conditions for breaking dormancy of Setaria seeds and to standardize media and growth conditions for efficient plate-based assays. In addition, the effect of each of the major phytohormones was analyzed on germination and/or on early seedling growth. Adult plants were also compared for growth in different conditions especially in the context of their photoperiod requirement, nutrient requirement and water stress response. The results presented in the following sections describe a set of optimum conditions which will be useful for the community at large for multiple phenotypic analyses and will help to improve the use of Setaria as a model system for important food, feed and fuel crops.

MATERIALS AND METHODS

Seed Selection, Liquid Smoke Treatment, and Seed Sterilization

Setaria viridis accession A10.1 is used for all assays described in this report, with accession ME034V also being tested in controlled growth chambers and greenhouse conditions for comparison. After seed collection, the papery glume and lower lemma were removed and black or dark brown seeds were separated from pale or greenish seeds, which are likely a mix of both mature and immature seeds. Darker seeds consistently showed better germination and have been used for the assays described in this report. Two different sterilization protocols were tested. In one, seed dormancy was broken by treating

seeds with Hickory liquid smoke obtained from a local grocery store at or 5% for 24 h (Sebastian et al., 2014) or 50% for 2 h (Brutnell Lab, Personal Communication) followed by five washes with autoclaved MQ water to remove liquid smoke. Seeds were then surface-sterilized with 20% bleach (Clorox) and 0.1% Tween-20 (Sigma-Aldrich) for 20 min with continuous shaking. Alternatively, seeds were treated with 20% bleach and 0.1% Tween-20 for 1 h with continuous shaking without liquid smoke treatment. The sterilized seeds were washed eight times with autoclaved MQ water and plated on 0.5X MS media (Caisson Labs, Smithfield, UT, United States) plates or inserted in seed germination pouches (PhytoAB, Redwood City, CA, United States; Catalogue No. CYG-38LB). Seeds sown on plates were stratified at 4°C in the dark for 2 days followed by transfer to controlled growth chamber with 12 h day/night (31°C/22°C) regime, with light intensity 450 μmol/m^2/sec and relative humidity 50–60%. Seeds sown on germination pouches or soil were transferred to growth chambers or greenhouse without any need of stratification. For growth in soil, seeds without sterilization were sown in 10 cm pots containing Metromix 360 (Hummert International, Earth City, MO, United States) and transferred to controlled growth chambers with 12 h day/night (31°C/22°C) regime, with light intensity 450 μmol/m^2/sec and relative humidity 50–60% or in greenhouses (28°C/22°C (day/night) temperature, 30–50% humidity, ∼300–450 μmol/m^2/sec light intensity depending on the weather and time of the day). In greenhouses, supplemental lighting was applied when the outside light level is <600 watts/sq. meter/sec. From May through September, supplemental lighting was available between 06:00 and 10:00 am. October through April it was available from 06:00 am to 8:00 pm. The lights are a mix of metal halide and high pressure sodium, and provide a minimum of 300 μmol/m^2/sec. When the outside light is >1000 W/sq. meter/sec., the shade cloth was pulled. Relative humidity was maintained at a minimum of 30%.

Seed Germination Assays

Seed germination assays were performed on 0.5X MS media plates. Germination was defined as radicle emergence which was recorded from day 1 to day 4 post-stratification (Hodge and Doust, 2017). For plate-based assays we evaluated the germination of 3 months old versus freshly harvested seeds, the effect of GA_3 (Caisson Labs) on the germination of freshly harvested seeds, the effect of agar (0.8%) or phytagel (0.4%) as gelling agents (Caisson Labs), the effect of liquid smoke treatment, and the effect of different sucrose concentrations (0, 0.5, 1.0, and 1.5% sucrose) in the media. To assess the effect of different stresses during germination, seeds were plated directly on media containing different concentrations of ABA (Caisson Labs), NaCl, or glucose.

Post-germination and Early Seedling Growth Assays

Effect of different phytohormones was assessed during post-germination, early seedling growth in both plate-based assays and in germination pouches. For plate-based assays, seeds were placed on media containing different concentrations of brassinosteroids (brassinolide, BL, Sigma-Aldrich, St. Louis, MO, United States), ethylene (ACC, ethylene precursor, Sigma), jasmonic acid (JA, Sigma) and auxin (IAA, indole-3- acetic acid, Caisson Labs) followed by stratification for two days at 4°C in the darkness. Plates were transferred to the growth chambers and incubated in light for 6 h to help germination. Plates were then covered with aluminum foil (except for auxin treatment) and seedlings were allowed to grow for 4–5 days. Seed germination percentage, root lengths, and coleoptile lengths were quantified. To evaluate the effect of ABA, NaCl, and glucose on post-germination growth and root length, seeds were first germinated on control media and then transferred to media plates supplemented with different concentrations of desired additives. Seedlings were grown in the 12 h dark/12 h light cycle and coleoptile lengths, root lengths, and secondary root numbers were measured from day 1 to day 7 post-transfer for each of the treatments.

For assays using germination pouches, seeds were germinated under control conditions by placing them on pouches pre-wet with autoclaved water. The water in germination pouches was replaced with desired media or additives 48 h post-imbibition. Seedlings were allowed to grow for 2 weeks. Root lengths were recorded every day.

Adult Plant Growth, Phenotyping, and Stress Treatment

To compare the growth of plants between greenhouses and growth chambers, seedlings were grown under similar conditions (except day length, which was maintained in the growth chambers at 12 h day/12 h night). To analyze the effect of nitrogen and water deficit, plants were grown under four different conditions; well-watered with sufficient nitrogen (W), well-watered, without nitrogen (W-N), low water, sufficient nitrogen (L), and low water without nitrogen (L-N). The amount of water need to be supplemented to the plant survival was determined prior to the experiment. Both W and L were provided with the nutrient medium supplemented with 15 mM nitrogen (added as KNO_3) whereas in the treatments without nitrogen (W-N and L-N) no exogenous nitrogen was added in the nutrient media. The L and L-N plants were provided with 50% the amount of water as compared to the W plants. All four treatments were conducted at the same time in the greenhouse with 50% humidity and 31°C/22°C (day/night) temperature. Four plants and three replicates were used for each treatment. Multiple growth parameters, including plant height, leaf number, day to heading, panicle number, and seed yield were recorded periodically starting from one-week post-germination till the plants matured and dried.

Statistical Analysis

All experiments were repeated at least three times independently and data were averaged. Means, standard deviation (seed germination assays) and standard errors (for root length and number, coleoptile length, leaf number, plant height, panicle number, and size and seed weight) for measurements were

calculated. Statistical significance of results was calculated using Student's *t*-test with a *P*-value threshold of less than 0.05.

RESULTS AND DISCUSSION

Standardization of Setaria Seed Germination Conditions

Optimization of conditions that result in uniform, 100% seed germination under a controlled environment is crucial for the success of many phenotypic assays. Achieving uniform germination in *S. viridis* has been a challenge as it displays huge discrepancies depending on the age of the seeds, dormancy breaking requirements and appropriate media and environmental conditions (Nonogaki, 2014; Sebastian et al., 2014; Saha et al., 2016; Hodge and Doust, 2017). To address this, we performed a set of assays to identify conditions that result in consistent, homogenous germination of seeds. All through this manuscript we have used the upper anthecium, i.e., entire upper floret that contains the caryopsis (fruit) with upper lemma and palea attached to it (**Figure 1A**) and referred to it as seed for the sake of simplicity. Our results show that seed quality and age have a huge effect on germination potential of Setaria seeds. First, seeds which were darker in color with glume and lower lemma removed from them show significantly improved, uniform germination compared to pale or green seeds harvested from the same panicle (**Figure 1B**). We have used dark seeds for all assays described in this report. Secondly, the age of the seeds also has a significant effect as has been previously reported (Sebastian et al., 2014; Hodge and Doust, 2017). In general, seeds stored in the dark at 4°C for at least 3 months after harvesting germinate at 100% efficiency, compared to freshly harvested seeds which show germination efficiency anywhere from 20 to 60%. Treatment of freshly harvested seeds (1-week-old) with exogenous GA_3 did significantly improve germination. By 4-day post-stratification up to 90% seeds germinated in the presence of 100 nM or 1 μM GA_3 compared to *ca.* 50% seeds in the absence of exogenous GA_3 (**Figure 2A**). This concentration of GA_3 is significantly lower that what has been reported previously (Sebastian et al., 2014). We did not observe any difference in germination efficiency between seeds aged 3 months to 1 year post-harvest. Moreover, liquid smoke treatment on freshly harvested Setaria seeds has been reported to promote germination efficiency (Sebastian et al., 2014). In our experiments, treatment with 5% liquid smoke for 24 h resulted in higher rates of contamination whereas a 50% liquid smoke for 2 h had a negative effect on the germination of 3- to 12-months post-harvest seeds (**Figure 2B**). At 2 days post-stratification, control seeds (without liquid smoke treatment) showed more than 80% seed germination compared to the liquid smoke treatment where less than 25% seeds germinated. By 3 days, all non-treated seeds had germinated, whereas seeds treated with liquid smoke showed 60 and 65% germination on by 3 and 4 days, respectively (**Figure 2B**). We consistently achieved 100% seed germination using 3-month-old, dark seeds with no smoke treatment, which were sterilized with 20% bleach and 0.1% Tween-20 for 1 h with continuous shaking, followed by extensive washing with autoclaved distilled water.

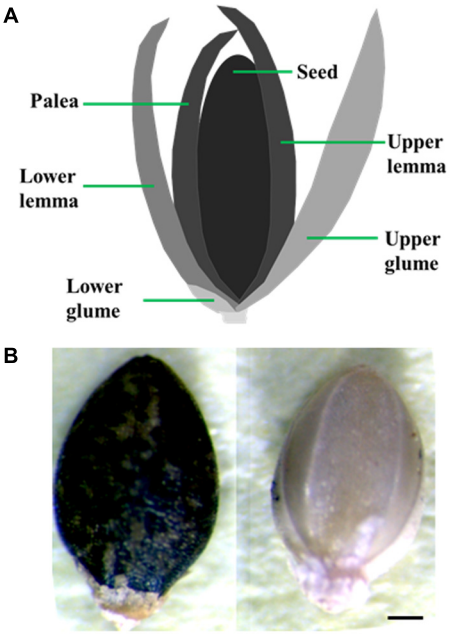

FIGURE 1 | Seeds used for germination and growth assays. **(A)** Diagrammatic representation of a Setaria floret. Upper anthecium which consists of hard upper lemma and palea attached to the caryopsis (fruit) was used in germination and growth assays. **(B)** Dark and pale seeds isolated form the same panicle. Dark seeds were used for all experiments. Scale bar is 250 μm.

Shorter sterilization times (15 or 30 min) resulted in occasional contamination on synthetic media plates or in germination pouches. These conditions were used for all assays described in this manuscript, although additional sterilization protocols have also been reported and may be useful according to the individual requirement (Saha and Blumwald, 2016; Saha et al., 2016).

For plate based assays we further tested seed germination and growth on different concentrations of phytagel- (0.3–1.5%) versus agar- (0.4–1.5%) based MS media, as both these gelling agents have been used previously (Boyes et al., 2001; Xu W. et al., 2013). We found 0.4% phytagel and 0.8% agar based media to be most effective in Setaria seed germination (data not shown). Parallel assays were then performed using both gelling agents to assess seed germination, root length, and secondary root number per seedling. No difference was observed in seed germination efficiency (**Figure 2C**) or root length (not shown) of the seedlings. However, seedlings that were grown on Phytagel-based media showed ∼60% more secondary roots than seedlings that were grown on Agar-based media (**Figure 2C**, inset), indicating that the Phytagel-based media may promote a more robust root system architecture (RSA) in Setaria. We used Phytagel-based media for subsequent assays, although the choice of gelling agent can be varied based on the specific experimental requirements.

We next assessed the amount of sucrose in the germination media as the presence, absence or variation of sucrose content is known to affect germination rate and seedling growth of plants such as Arabidopsis (Finkelstein and Lynch, 2000;

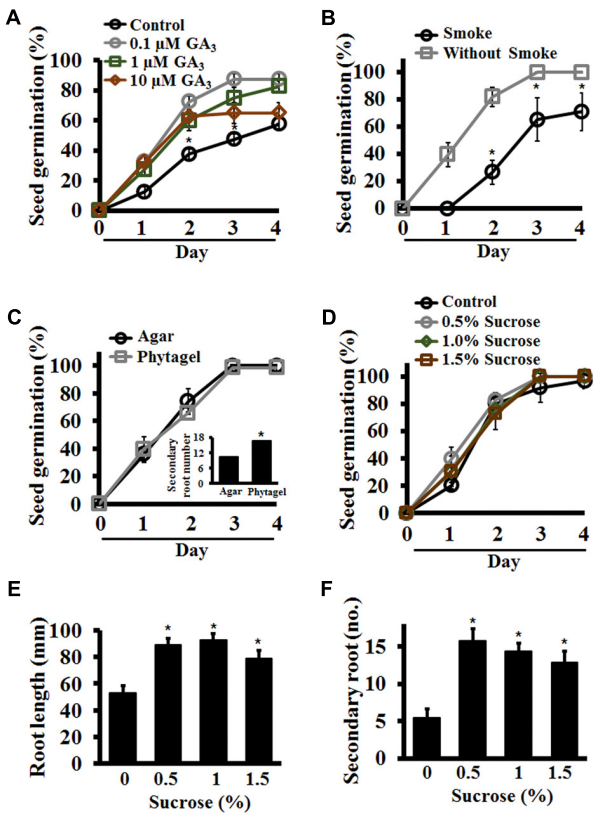

FIGURE 2 | Standardization of seed germination conditions for Setaria using synthetic media in plate-based assays. **(A)** Germination percentage of freshly harvested Setaria seeds was assessed in the presence of varying concentrations of exogenously added gibberellic acid (GA_3). **(B)** Seeds were treated with or without liquid smoke before sterilization and germination percentage was quantified from day 1 to day 4. **(C)** Percentage of seed germination of Setaria was counted from day 1 to day 4 on Phytagel- or Agar-based 0.5X MS media. The number of secondary roots at day 7 was also quantified (inset panel). **(D)** Effect of varying concentrations of sucrose on seed germination of Setaria was quantified for up to 4 days post-stratification. **(E)** The primary root length of Setaria seedlings were measured at 7 day post-stratification in the presence of varying concentrations of sucrose. **(F)** Secondary root number of Setaria seedlings was quantified at 7 day post-stratification. In all experiments, seeds sown on 0.5X MS media plates were stratified at 4 °C in the dark for 2 days followed by transfer to the growth chamber with light-12 h (31°C)/dark-12 h (22°C) cycle. Plates were placed vertically to measure the root length and secondary root number. Minimum 3 months old, dark-colored seeds were used in the experiments **(C–F)**. Data were averaged from three biological replicates and at least 60–70 seeds were used in each experiment. For **(A–D)**, error bars represent standard deviation (±SD). For **(E,F)** Error bars represent standard error (±SE). Asterisks represent *P*-values less than 0.05 as calculated using Student's *t*-test.

Dekkers et al., 2004, 2008). Media without sucrose or supplemented with 0.5, 1.0, and 1.5% sucrose were used to assess optimal sucrose content needed for seed germination and seedling growth. On day 1, different sucrose concentrations had some effect with less than 20% germination on media without sucrose versus ∼40% germination in media with sucrose. However, later on during germination, no significant differences were observed in germination frequency by the presence of sucrose in the media and by day 4 all seeds on all media had germinated (**Figure 2D**). This suggests that for seed germination *per se*, sucrose is not a requirement. However, post-germination growth was significantly affected by the presence of sucrose. Seedlings grown on MS media without sucrose showed smaller primary roots (∼55 mm) whereas the root lengths were ∼90 mm for media containing 0.5 and 1% sucrose and ∼80 mm for media with 1.5% sucrose (**Figure 2E**). The difference in secondary root numbers was also striking. Seedlings grown on media with no additional sucrose developed few secondary roots (5–6 secondary roots/primary root), whereas those growing on media with sucrose developed up to three times more roots (**Figure 2F**). These observations suggest that 0.5–1.0% sucrose containing MS-Phytagel media should be preferred for Setaria seedling growth in plate-based assays. We used 0.5% sucrose in the 0.5X MS, Phytagel media for all the assays described in this report. Identical sucrose concentration has been used in previously reported studies as well (Sebastian et al., 2014).

Effect of Different Abiotic Stresses on Setaria Seed Germination

Several exogenous factors affect seed germination, and germination in the presence of different hormones or stressors has been widely used for screening of mutant seeds, identification of abiotic stress sensitivity of plants, or to study the effect of plant hormones such as ABA, which is well-known to inhibit seed germination (Leon-Kloosterziel et al., 1996; Garciarrubio et al., 1997; Finkelstein et al., 2002, 2008; Brocard-Gifford et al., 2003). Similarly, the effect of different abiotic stresses have been studied on different aspects of Setaria growth and development (Dekker and Hargrove, 2002; Doust and Kellogg, 2006; Yue et al., 2014; Amini et al., 2015b; Muthamilarasan et al., 2015; Feng et al., 2016; Li et al., 2016; Pan et al., 2016; Saha et al., 2016; Singh et al., 2016; Feldman et al., 2017; Pandey et al., 2017). We evaluated the effect of different ABA concentrations ranging from 0.5 to 10 μM on Setaria seed germination. Media plates (0.5X MS media, 0.4% phytagel, 0.5% sucrose) were supplemented with different concentrations of ABA; an equimolar concentration of EtOH (an ABA solvent) was used as a control. Germination was recorded every 24 h post-stratification for 7 days and expressed as percentage of total seeds. Setaria seeds exhibited extreme sensitivity to ABA. More than 75% of seeds had germinated by 2 days on control media, whereas no germination was seen in the presence of ABA even at the lowest (0.5 μM) concentration. By day 3, 90% seed germination was observed on control media, and less than 10% seeds germinated on 0.5 μM ABA with almost no germination at higher ABA concentrations. By day 7, all seeds had germinated on the control media plates; seed germination was ∼40% and ∼10% on media containing 0.5 and 1.0 μM ABA, respectively (**Figure 3A**). One or two seeds occasionally germinated on 1.5 or 2 μM ABA, whereas no germination was ever seen at higher concentrations (5 μM ABA or above). These data show extremely high sensitivity of Setaria seeds for ABA during germination when compared with other model plants such as Arabidopsis, which shows

~40–50% germination at 1 μM ABA by 48 h (Pandey et al., 2006).

Salinity stress negatively affects seed germination. NaCl is commonly used as an agent to study the effect of salt stress on seed germination, growth and other physiological processes (Saleki et al., 1993; Yue et al., 2014; Duan et al., 2015; Muthamilarasan et al., 2015; Liu et al., 2017; Pandey et al., 2017). To assess the effect of salinity on Setaria seed germination, seeds were plated on media containing 50, 100, 150, and 200 mM NaCl and compared with control media with no added NaCl. As in the ABA experiment, by day 2 more than 75% of the seeds had germinated on control media plates, whereas no germination was seen in the presence of even the lowest NaCl concentrations (**Figure 3B**). Seeds plated on 50 and 100 mM NaCl showed considerably delayed germination (~20% by day 3, when almost all control seeds had germinated); however, all these seeds eventually germinated by day 7. Seed germination was even more delayed with higher NaCl concentrations, and by day 7 about 75 and 40% seeds germinated on media plates with 150 and 200 mM NaCl, respectively (**Figure 3B**). These data suggest that at lower salt concentrations, the seeds eventually overcome the effects of stress, and are able to germinate although slower than the germination on control plates. However, at more than 100 mM salt concentration, the stress is too severe for the seeds to overcome, and full germination potential was never achieved.

Sugars such as glucose play important regulatory roles during seed germination. High levels of glucose inhibit seed germination and seedling development in Arabidopsis (Dekkers et al., 2004). We tested the effect of different glucose concentrations on Setaria seed germination. Seeds were germinated on different concentrations of glucose (2, 4, and 6% glucose in MS media; no additional sucrose added). Control media had no glucose or sucrose added to it. A clear, concentration-dependent effect of glucose in delaying seed germination was obvious. By day 4, when all control seeds had germinated, only ~50% of the seeds had germinated on media containing 2% glucose, and significantly fewer on higher glucose concentrations (**Figure 3C**). By day 7 both control and 2% glucose-containing media showed 100% seed germination. Only 50 and 30% seeds germinated by 7 day on media containing 4 and 6% glucose, respectively. The seeds that did germinate on 4% or higher glucose concentrations exhibited high anthocyanin accumulation, showing the effects of stress.

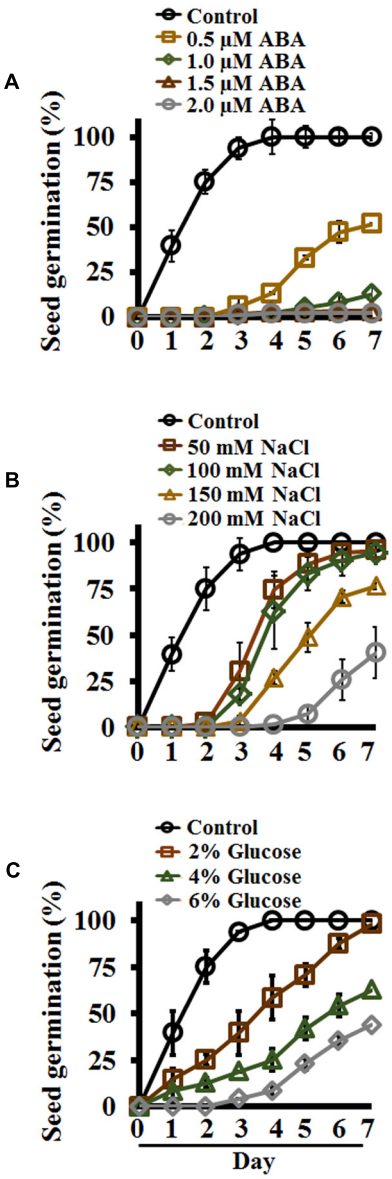

FIGURE 3 | Effect of exogenous abscisic acid (ABA), NaCl and glucose on Setaria seed germination in plate-based assays. Sterilized Setaria seeds were plated on varying concentrations of **(A)** ABA, **(B)** NaCl, and **(C)** glucose. Seed germination (n = 60 per treatment) was counted for up to 7 days and compared with germination on control media. Minimum 3 months old, dark-colored seeds were used. In all experiments, seeds were stratified at 4°C in the dark for 2 days followed by transfer to the growth chamber with light-12 h (31°C)/dark-12 h (22°C) cycle. Three biological replicates of each treatment were used for data analysis. Error bars represent standard deviation (±SD).

Effect of Different Hormones and Abiotic Stresses on Post-germination, Early Seedling Growth of Setaria Using Plate-Based Assays

Post-germination, early seedling growth of plants is extremely sensitive to multiple hormones, nutrients and additives. Seedling-stage assays are useful to evaluate the differences in root length, number of secondary roots, coleoptile or shoot length, and can be performed at a relatively large scale using simple plate-based assays. We assessed the effects of different plant hormones and abiotic stresses on early seedling growth of Setaria to determine their effective concentration ranges and the phenotypic differences that arise due to the treatments.

Auxins are well-known to affect root growth and development in a variety of plants. In general, auxins inhibit primary root length and promote secondary root formation (Overvoorde et al., 2010). To test the effect of auxins on Setaria roots,

seeds were germinated on media plates containing different IAA (Indole-3-acetic acid) concentrations. No effect of IAA was seen on Setaria seed germination. IAA at the concentration range 0.1–10 μM inhibited root growth. Four days post-imbibition, primary root length of seedlings on control, 0.1 and 1 μM IAA was *ca* 43, 16, and 7 mm, respectively (**Figure 4A**). At higher concentrations (10 μM), the roots stopped growing, and were deformed and frequently exhibited bulging (**Figure 4A**). At these concentrations, we did not observe any major differences in secondary root formation between control and IAA treated plants, but at 0.1 μM IAA, the roots were covered with root hairs. The emerging coleoptiles were not significantly different in length at the different IAA concentrations tested (**Figure 4A**).

Brassinosteroids also affect early seedling growth by promoting hypocotyl elongation and root inhibition in plants such as Arabidopsis (Clouse et al., 1996; Clouse, 2001). Although the effects of brassinosteroids are well-documented on later growth stages of monocots such as on lamina joint formation, branching and grain filling, their effects on early seedling growth are not as well-described (Cao and Chen, 1995; Wu et al., 2008; Zhang et al., 2014). Previous studies have reported that in the presence of BL, coleoptile and root growth were inhibited in maize whereas coleoptile growth was promoted (with twisted phenotype) and root growth was inhibited in rice (Yamamuro et al., 2000; Wang et al., 2006; Kir et al., 2015). To test the effect of brassinosteroid on Setaria seedling growth, we grew seeds on different Brassinolide (BL, active brassinosteroid) concentrations, in darkness, and measured primary root and coleoptile lengths. BL at 100 nM caused the most obvious phenotypic differences in the seedlings. After 4 days of post-imbibition growth, 100 nM BL resulted in more than 60% reduction in root length compared to control seedlings (**Figure 4B**). The coleoptiles were also shorter and exhibited the classic twisted, curved growth, as is reported for Arabidopsis seedlings. Not only were seedlings grown on BL stunted but occasionally they also showed tendril like structures on the coleoptiles, a phenotype not reported previously.

The gaseous plant hormone ethylene has a major effect on seedling growth, especially in darkness. Arabidopsis seedlings exhibit a classic triple response in the presence of ethylene or its precursor ACC (1-Aminocyclopropane-1-carboxylic acid), with shorter roots, shorter hypocotyl and apical hook formation (Bleecker et al., 1988; Guzman and Ecker, 1990; Yang et al., 2015). Reduced growth of coleoptiles and roots in the presence of ethylene is also reported for maize, wheat, sorghum and *Brachypodium*, although in rice ethylene is reported to promote coleoptile growth while inhibiting root growth (Satler and Kende, 1985; Ma et al., 2014; Yang et al., 2015). Setaria seedlings exhibited clear differences in root length and coleoptile length in the presence of different concentrations of ACC. ACC concentrations of 25–50 mM inhibited root lengths and coleoptile lengths by more than 50% (**Figure 4C**). However, an apical hook formation, which is typical of Arabidopsis (and other dicot) seedlings was not seen in Setaria. This is likely due to the evolutionary difference between monocots and dicots in how they protect their shoot apical meristem (SAM). As the seeds which are buried under soil germinate during skotomorphogenic developmental program, dicot seedlings protect the SAM by forming an apical hook while monocot seedlings develop a coleoptile for the protection of the SAM (Abbas et al., 2013).

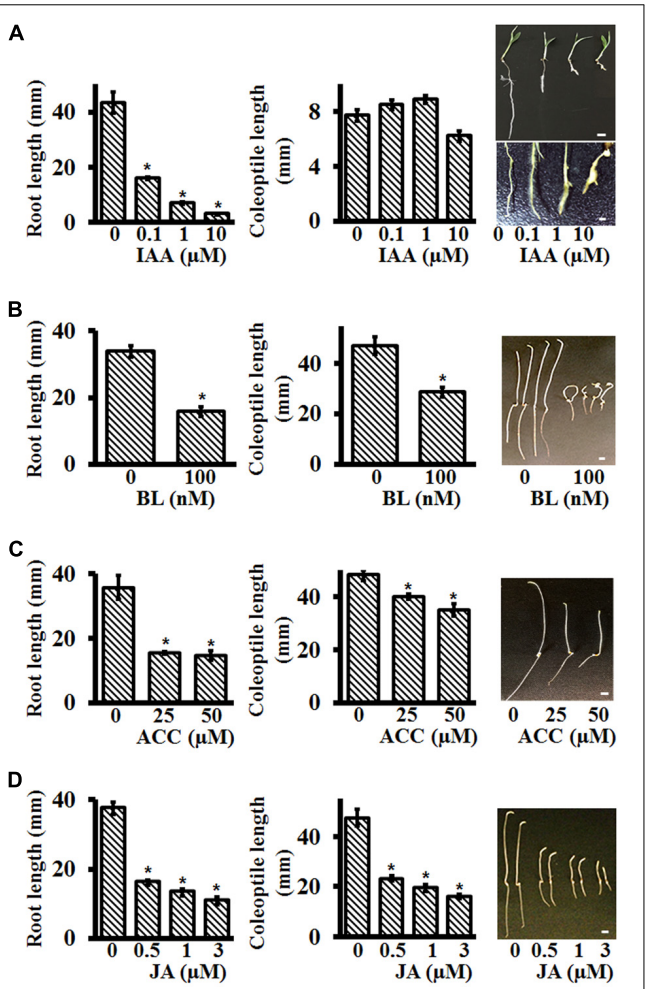

FIGURE 4 | Effect of different plant hormones on post-germination growth of Setaria seedlings using plate-based assays. Sterilized Setaria seeds were plated on varying concentrations of **(A)** indole-3 acetic acid (IAA), **(B)** brassinolide (BL), **(C)** 1-aminocyclopropane-1 carboxylic acid (ACC), and **(D)** methyl jasmonate (JA). The plates were placed vertically. Root and coleoptile lengths were measured after 5 days of growth. For IAA treatment, seedlings were grown in light-12 h (31°C)/dark-12 h (22°C) cycle. The upper and lower panels in the picture show the entire seedlings and terminal root phenotypes (20 X magnification), respectively. For BL, ACC, and JA treatments the seedlings were grown in the dark. The pictures on the right show the phenotypes of 5 day old seedlings in the presence of specific hormone treatments. At least 3 months old, dark-colored seeds were used in the experiment. Data were averaged from three biological replicates. At least 20–30 seeds were used in each experiment. Error bars represent standard error (±SE). For comparative analysis, appropriate controls were included for each treatment. Asterisks represent *P*-values less than 0.05 as calculated using Student's *t*-test. Scale bars are 5 mm for all figures except for the lower panel of IAA treated roots where it is 1 mm.

Although jasmonic acid (JA) is usually associated with the defense response of plants, it has a major effect on plant growth and development both directly or by interacting with other

plant hormones (Creelman and Mullet, 1995; Turner et al., 2002; Gray, 2004; Wasternack, 2007; Gazzarrini and Tsai, 2015; Shyu and Brutnell, 2015). We evaluated the effect of different concentrations of JA on skotomorphogenic growth of Setaria seedlings. Seeds were plated on control media or on media containing 0.5, 1.0, and 3.0 μM MeJA (methyl jasmonate). Coleoptile and root lengths were measured at 4 days post-imbibition. In comparison to seedlings grown on control media, root lengths were reduced by ∼60, 65, and 70%, and coleoptile lengths were reduced by ∼50, 60, and 65% in seedlings grown in media containing 0.5, 1.0, and 3.0 μM MeJA, respectively (**Figure 4D**). The negative regulatory role of JA during skotomorphogenic growth has been reported previously for the Arabidopsis and maize seedlings (Wasternack, 2007; Shyu and Brutnell, 2015).

Abscisic acid, NaCl and glucose, in addition to exerting a major effect on seed germination, also affect later stages of seedling development (Finkelstein et al., 2002; Dekkers et al., 2008). However, these effects are usually confounded by assay conditions where the seeds are allowed to germinate on media containing these stressors followed by extended growth on the same media. To clearly differentiate the effect of these additives on early seedling growth and development of Setaria, independent of their effects on germination, seeds were first plated on the control media plates and grown for 48 h. By this time all seeds had germinated, as examined by the radicle protrusion from the seeds. The germinated seeds were then transferred to new control media plates or media plates supplemented with different additives.

Abscisic acid is known to inhibit primary root length and secondary root formation (Harris, 2015). As was seen for seed germination assays, Setaria seedlings were extremely sensitive to ABA for post-germination growth as well. More than 60% reduction was seen in the primary root length at as low as 2 μM ABA, with almost complete growth arrest at 5 μM ABA (**Figure 5A**). This concentration is almost an order of magnitude lower than what is reported for Arabidopsis root growth inhibition assays (Pandey et al., 2006). Secondary root inhibition was also highly sensitive to exogenous ABA and no secondary roots were formed at 1 μM ABA. At concentrations as low as 0.2 μM ABA, more than 50% reduction in secondary root formation was observed (**Figure 5B**). **Figure 5C** shows representative seedlings growing in the presence of ABA.

We also determined the effect of NaCl and glucose on coleoptile and root length inhibition of Setaria seedlings. At 50 mM NaCl, more than 50% reduction in root length (**Figures 5C,E**) and ∼25% reduction in coleoptile length (**Figures 5D,E**) was observed, with higher concentrations (100 mM) leading to stronger effects. For growth in the presence of glucose, as low as 2% glucose had a significant effect on root (>50% reduction) and coleoptile (>25% reduction) lengths (**Figures 5G–I**). It should be noted that at this concentration of glucose, germination *per se*, though delayed, is not affected (**Figure 3C**). Stronger effects were seen at 4% glucose, and seedling growth was almost completely arrested at 6% glucose which could be due to the sugar-induced arrest of seedling development by meristem quiescence (Lastdrager et al., 2014).

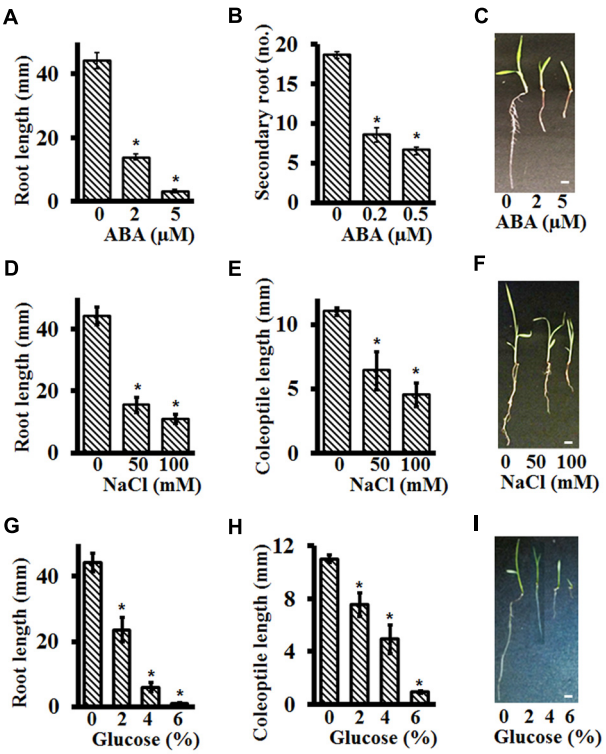

FIGURE 5 | Effect of different stresses on post-germination growth of Setaria using plate-based assays. Sterilized Setaria seeds sown on 0.5X MS media plates were stratified at 4°C in the darkness for 2 days followed by transfer to the growth chamber with light-12 h (31°C)/dark-12 h (22°C) cycle for another 2 days. The effect of ABA on post-germination growth was studied by measuring the primary root length at day 3 **(A)** and secondary root number at day 5 **(B)** after transfer to the media containing varying concentrations of ABA. The picture in **(C)** shows representative seedlings after growth in the presence of ABA. The effect of NaCl **(D,E)** and glucose **(G,H)** was analyzed by quantifying the primary root length and coleoptile length after transfer to the media containing varying concentrations of NaCl and glucose. Figures **(F,I)** show representative images of Setaria seedlings after growth in the presence of NaCl or glucose, respectively. For each experiment, 3 months old, dark-colored seeds were used. Three biological replicates of each treatment were performed and at least 20–30 seeds were used in each experiment. Appropriate controls were used for each treatment. Error bars represent standard errors (±SE). Asterisks represent *P*-values less than 0.05 as calculated using Student's *t*-test. Scale bars are 5 mm.

Effect of Different Hormones and Abiotic Stresses on Root Growth of Setaria Using Germination Pouch Assays

Analysis of early seedling growth and development of Setaria on media plates is restricted by time. Even when using 150 mm plates, seedlings could be grown at the most for 1 week. Furthermore, shoot development is not optimal when in the constant contact with media. To address these concerns, we standardized seedling growth assays using seed germination pouches (**Figure 6A**) which resulted in prolific RSA as well as effective growth of shoots exposed to air. We used the medium size pouches (18 cm × 12.5 cm) for Setaria seedling growth and planted 20–22 seeds per pouch. The ability to stack hundreds

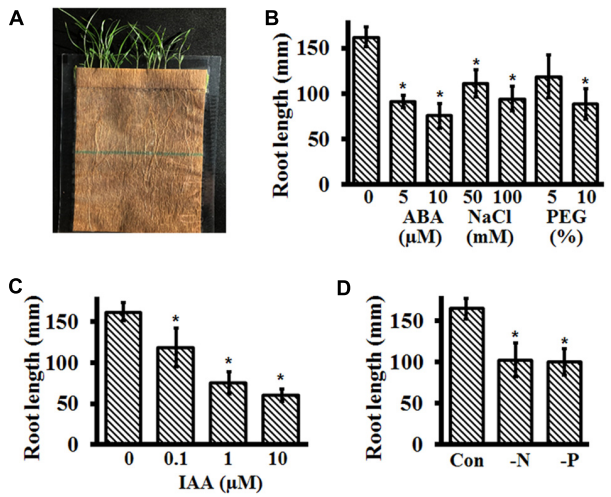

FIGURE 6 | Growth of Setaria in germination pouches and effect of different stresses on seedling growth. **(A)** Representative image of 2-week-old Setaria plants growing in germination pouch. At least 3 months old, dark-colored Setaria seeds were grown under control conditions by placing them on pre-wet pouches. **(B)** For different abiotic stress treatments, seeds were germinated on pre-wet germination pouches for 2 days. The media in the germination pouch was replaced with media supplemented with ABA (5 and 10 μM), NaCl (50 and 100 mM) and PEG (5% and 10%, equivalent to –0.05 and –0.15 MPa osmotic stress). **(C)** The media in germination pouches was replaced with different concentrations of IAA and **(D)** with either minus nitrogen or minus phosphate MS media. In all experiments, the primary root lengths were quantified after 2 weeks of growth. Appropriate controls were used in each experiment **(B–D)**. Three biological replicates of each treatment were performed and at least 20 seeds were used for each experiment. Error bars represent standard errors (±SE). Asterisks represent *P*-values less than 0.05 as calculated using Student's *t*-test.

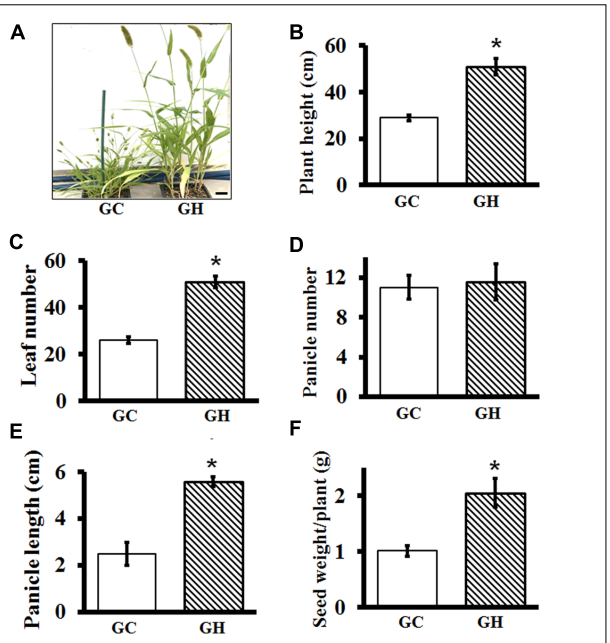

FIGURE 7 | Comparative analysis of vegetative and reproductive growth parameters of Setaria grown in controlled environment growth chambers and in greenhouses. **(A)** Representative images of 7-week-old Setaria plants grown in growth chamber (GC, left) and greenhouse (GH, right). **(B)** Plant height at 7 weeks, **(C)** Leaf number at 4 weeks **(D)** panicle number at 7 weeks and **(E)** length of mature panicle at 7 weeks were measured. **(F)** Total seed weight was quantified from the plants grown under in growth chambers versus greenhouse. Three biological replicates of each treatment and four plants in each experiment were used for data analysis. Error bars represent standard errors (±SE). Asterisks represent *P*-values less than 0.05 as calculated using Student's *t*-test. Scale bar is 5 cm.

of pouches in a small container also allowed growing large plant populations in limited space. Additional advantages of growing plants in germination pouches included the ability to change treatment condition without disturbing seedling growth, the ability to monitor and measure root growth at desired time points, and the ability to grow plants without requiring a specialized growth chamber. We successfully grew plants without any special requirements on lab benches (with additional lighting from fluorescent bulbs, ∼150 μmol/m^2/sec; 16 h/8 h day/night regime) for up to 2 weeks.

We tested the effect of different stresses and hormones on plants growing in germination pouches by first germinating the seeds in 0.5X MS media without sucrose (addition of sucrose results in contamination), followed by replacement with desired media 48 h post-imbibition. Root lengths were recorded every 24 h for 2 weeks. Additionally, because drought and salinity are some of the most critical factors affecting young seedling growth and plants typically respond to these stresses by changing their RSA, we also used the germination pouch assays to assess the effects of water stress on plant growth and development. We present the final root length data for the following experiments, but significant changes in overall RSA and young shoots were obvious by visual inspection and can be quantified as per the specific experimental need.

As expected, treatment with different concentrations of ABA and NaCl significantly inhibited root growth and development (**Figure 6B**). Overall root length of seedlings treated with 5 and 10 μM ABA were ∼55 and 45%, respectively, that of untreated seedlings. This suggests that 5 μM ABA is an optimum concentration to analyze the effect of ABA on Setaria root growth. In the presence of 50 and 100 mM NaCl, the root lengths were inhibited by 25 and 45%, respectively, compared with the untreated seedlings. The effect of glucose cannot be tested in germination pouches, as it results in a high level of contamination (due to growth in non-sterile conditions). However, we did test the effect of polyethylene glycol (PEG8000) as an osmotic stress in this system. Addition of PEG that resulted in an osmotic stress equivalent of −0.05 and −0.15 MPa led to 32 and 43% decrease in root length of Setaria seedlings (**Figure 6B**). Similarly, root growth was also significantly affected by different auxin concentrations (**Figure 6C**), with 1 μM IAA being the optimum.

Besides drought and salinity stresses, nutrient deficiency is a common problem in crop productivity and among the nutrients, nitrogen (N) and phosphorus (P) deficiency are major abiotic stresses that limit plant growth and productivity (Zhao et al., 2005; Balemi and Negisho, 2012; Ingram et al., 2012). Unavailability of nitrogen and phosphorus in the soil changes RSA by modulating root cell elongation or cell division

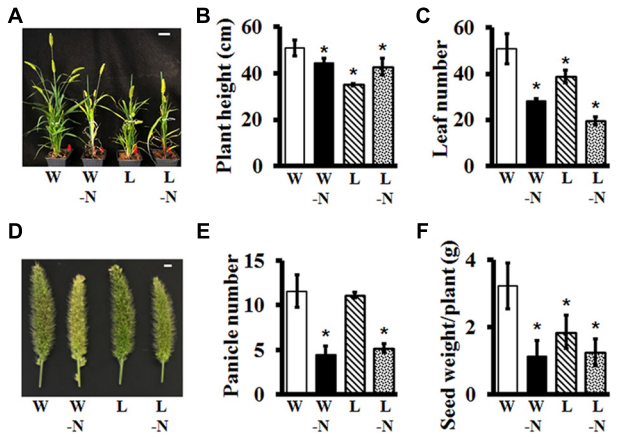

FIGURE 8 | Effect of water and nitrogen deficit on vegetative and reproductive growth parameters of Setaria. **(A)** Representative image of 7 weeks old Setaria plants grown in the greenhouse under four different conditions: W = well-watered +15 mM nitrogen supplemented in the media, W-N = well-watered, no nitrogen supplement, L = low watered (50% compared to the well-watered control) +15 mM nitrogen, and L-N = low-water and no nitrogen supplement in the media. Different growth parameters such as **(B)** plant height and **(C)** leaf number were measured from seven and 4 weeks old Setaria plants, respectively. **(D)** Representative image of main panicle from 7 weeks old Setaria plants. **(E)** Panicles number per plant was counted from 7 weeks old plants. **(F)** Seed weight/plant was calculated after harvesting. Three biological replicates of each treatment and four plants in each experiment were used for data analysis. Error bars represent standard errors (±SE). Asterisks represent *P*-values less than 0.05 as calculated using Student's *t*-test. Scale bars are 5 cm for **(A)** and 5 mm for **(D)**.

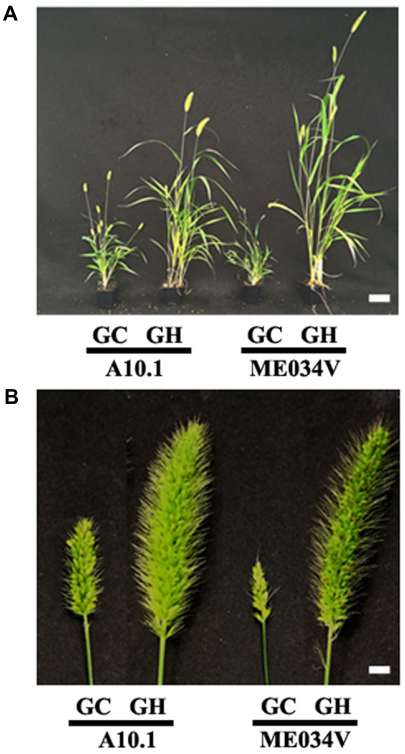

FIGURE 9 | Comparison of Setaria accessions A10.1 and ME034V grown in controlled environment growth chambers versus in greenhouses. **(A)** Representative images of 5 weeks old Setaria plants A10.1 (left) and ME034V (right) grown in growth chamber (GC) and greenhouse (GH). **(B)** Representative images of A10.1 (left) and ME034V (right) panicles grown in growth chamber (GC) and greenhouse (GH). The plants were growth conditions under similar conditions in growth chamber and greenhouse under conditions listed in Supplementary Table S1. Scale bars are 5 cm for **(A)** and 5 mm for **(B)**.

(Williamson et al., 2001; Smith and De Smet, 2012). Similar to the study of other abiotic stresses, we used germination pouch growth assays to investigate the effect of N and P deficiency on Setaria RSA. Seeds were germinated on pre-wet germination paper bags and supplemented with control MS media or MS media without N (MS-N, Caisson Labs) or without P (MS-P, Caisson Labs) 48 h post-imbibition. Seedlings were allowed to grow for 2 weeks and RSA as well as shoot phenotypes were examined. Both treatments resulted in a significant effect on the RSA of Setaria seedlings with ∼38 and 40% root growth inhibition in absence of N and P, respectively (**Figure 6D**). The young shoots of plants growing in the absence of N and P were pale green compared with the untreated seedlings.

Adult Plant Growth and Phenotypes in Controlled Growth Chambers versus Greenhouse

For plants such as Setaria, where yield is determined by the number and size of panicles, it is important to precisely define the conditions that result in optimal growth. Similarly, to study the effect of different stress conditions on adult plants, control plants should grow in conditions that result in optimal growth and development. It is known that Setaria growth and development is extremely sensitive to photoperiod and temperature (Swanton et al., 1999; Doust et al., 2017). As expected, huge differences in overall plant architecture were observed between plants grown in controlled environment growth chambers versus controlled environment greenhouses. Plants grown in greenhouses were in general healthier and grew almost twice as large compared to the ones grown in growth chambers under similar conditions (except for the day length) (**Figure 7A**). To precisely compare the effect of different growth conditions, we grew a set of plants in growth chambers and greenhouses for the entire life cycle and documented key phenotypes. The overall conditions were similar in the greenhouse versus growth chamber and are listed in Supplementary Table S1.

Plants grown in greenhouses were taller (**Figure 7B**) and produced more leaves compared to the plants grown in the growth chambers, which were significantly smaller and had fewer leaves (**Figure 7C**). Panicle number per plant was not significantly different between the two growth conditions (**Figure 7D**); however, panicles of greenhouse grown plants were ∼3 times bigger (**Figure 7E**) and possessed more seeds. Consequently, yield, expressed as the seed weight per plant, was more than double in greenhouse-grown plants, compared to those grown in the controlled environment growth chambers (**Figure 7F**). This suggests that for the physiological experiments to be performed

on adult Setaria plants, it may be important to grow them in conditions which result in their optimal growth.

Effect of Different Stresses on Adult Plant Growth and Development

We evaluated the effects of two different stresses, low water potential and low nitrogen, on Setaria growth and development, singly and in combination. The water level of the low-water (L) plants was maintained at the 50% level of the control, well-watered (W) plants; and the low N plants did not receive any exogenous nitrogen whereas the nitrogen-sufficient plants had 15 mM (KNO_3) added to the nutrient media. The stresses were applied from the time when the seedlings were 1-week-old and continued for the entire life cycle of the plant. The effects of single or combinatorial stresses were analyzed on overall plant architecture, plant height, leaf number, panicle number, and yield (expressed as total seed weight).

Setaria plants growing in soil in greenhouses grew fairly normally for the first 2 weeks of stress treatment, with no obvious differences when compared to control plants which were well-watered with nitrogen-containing nutrient media. However, the effects of different stresses became obvious as the plants grew and matured (**Figure 8A**). Low nitrogen led to pale coloration of the leaves, an effect that was more pronounced in the low nitrogen/low water combination stress. Overall plant height and biomass were significantly reduced in response to stresses (**Figure 8B**). Leaf number per plant was significantly lower in response to all stresses, but more pronounced in low nitrogen treatment with ∼50% reduction in response to low nitrogen and ∼60% reduction in response to low N in combination with low water (**Figure 8C**). Panicles exhibited unique characteristics in terms of color and size. Since Setaria is a relatively drought tolerant plant, it is not surprising that low water stress by itself did not have a huge effect on overall growth and development, panicle size or number of panicles per plant (**Figures 8D,E**); however, water-stressed plants did develop fewer seeds per panicle, which resulted in significantly reduced yield (**Figure 8F**). The effects of low nitrogen were more noticeable, both by itself and combined with water stress. These plants produced pale, thinner panicles, which were fewer in number and as a result had extremely poor yield (**Figures 8D–F**). These data suggest that even though Setaria is considered a wild, non-domesticated plant, it does exhibit consistent, obvious phenotypes in response to different stresses that can be used to characterize useful agronomic traits in various mutant populations, which will be valuable for their utilization in domesticated, food crops.

Applications to Other *Setaria* Accessions

Among more than 200 *S. viridis* accessions collected so far (Huang et al., 2014), A10.1 is of the greatest interest to the community because of the availability of different genetic tools, its sequenced genome (Bennetzen et al., 2012) and chemically induced mutant populations (Huang et al., 2017). Recently, increasing attention is also being paid to another accession ME034V, which is morphologically similar to A10.1 but shows significantly higher transformation efficiency (Zhu et al., 2017). Given the similarity of the two accessions, we believe that our findings with A10.1 can be applied to ME034V to a great extent. For example, we tested how ME034V grows in controlled growth chambers versus greenhouses. Similar to what we find in A10.1, ME034V grows much taller and healthier (**Figure 9A**) and produces much bigger panicles and more seeds (**Figure 9B**) in greenhouse conditions compared to in controlled growth chambers. This suggests that the methods presented in this paper can be used as a valuable reference for research using ME034V and other accessions in future.

CONCLUSION

Optimization of multiple growth and development assays for Setaria, at three different stages of its life cycle, will be helpful for the research community to utilize it for more functional studies in the future. The standardization of different growth conditions, media, hormone concentrations, stresses and the description of resultant phenotypes will aid further targeted studies, and in combination with additional genetic and genomic tools being developed in multiple labs will greatly increase its use as a favorite model system for the study of grasses. Finally, a description of a set of optimized conditions will also help eliminate differences observed between different labs due to slightly altered conditions. These assays will serve as the first important steps to promote Setaria as a key model for a number of monocot species, where such resources are relatively limited.

AUTHOR CONTRIBUTIONS

SP, BA, and SRC designed research; BA, SRC, AE, AV, CZ, and LH performed research; BA, SRC, AE, AV, and SP analyzed data; BA, SRC, AV, CZ, and SP wrote the paper.

FUNDING

Research in the Pandey lab is supported by NIFA/AFRI (2015-67013-22964) and NSF (IOS-1157942 and MCB-1714693) grants to SP. CZ is supported by National Science Foundation (NSF) grant IOS-1413824 to Elizabeth A. Kellogg.

ACKNOWLEDGMENTS

The authors thank our Danforth Center colleagues Dr. Elizabeth Kellogg, Dr. Malia Gehan, and Dr. Tom Brutnell for providing Setaria seeds and for useful discussion that helped tremendously with standardization of growth conditions.

SUPPLEMENTARY MATERIAL

The Supplementary Material for this article can be found online at: https://www.frontiersin.org/articles/10.3389/fpls.2017.02172/full#supplementary-material

REFERENCES

Abbas, M., Alabadi, D., and Blazquez, M. A. (2013). Differential growth at the apical hook: all roads lead to auxin. *Front. Plant Sci.* 4:441. doi: 10.3389/fpls.2013.00441

Amini, V., Zaefarian, F., and Rezvani, M. (2015a). Interspecific variations in seed germination and seedling emergence of three Setaria species. *Braz. J. Bot.* 38, 539–545. doi: 10.1007/s40415-015-0158-6

Amini, V., Zaefarian, F., and Rezvani, M. (2015b). Effect of pre-chilling and environmental factors on breaking seed dormancy and germination of three foxtail species. *Acta Agric. Slov.* 105, 269–278. doi: 10.14720/aas.2015.105.2.10

Balemi, T., and Negisho, K. (2012). Management of soil phosphorus and plant adaptation mechanisms to phosphorus stress for sustainable crop production: a review. *J. Soil Sci. Plant Nutr.* 12, 547–561. doi: 10.4067/S0718-95162012005000015

Bandyopadhyay, T., Muthamilarasan, M., and Prasad, M. (2017). Millets for next generation climate-smart agriculture. *Front. Plant Sci.* 8:1266. doi: 10.3389/fpls.2017.01266

Bennetzen, J. L., Schmutz, J., Wang, H., Percifield, R., Hawkins, J., Pontaroli, A. C., et al. (2012). Reference genome sequence of the model plant Setaria. *Nat. Biotechnol.* 30, 555–561. doi: 10.1038/nbt.2196

Bleecker, A. B., Estelle, M. A., Somerville, C., and Kende, H. (1988). Insensitivity to ethylene conferred by a dominant mutation in *Arabidopsis thaliana*. *Science* 241, 1086–1089. doi: 10.1126/science.241.4869.1086

Boyes, D. C., Zayed, A. M., Ascenzi, R., McCaskill, A. J., Hoffman, N. E., Davis, K. R., et al. (2001). Growth stage-based phenotypic analysis of Arabidopsis: a model for high throughput functional genomics in plants. *Plant Cell* 13, 1499–1510. doi: 10.1105/tpc.13.7.1499

Brocard-Gifford, I. M., Lynch, T. J., and Finkelstein, R. R. (2003). Regulatory networks in seeds integrating developmental, abscisic acid, sugar, and light signaling. *Plant Physiol.* 131, 78–92. doi: 10.1104/pp.011916

Brutnell, T. P., Wang, L., Swartwood, K., Goldschmidt, A., Jackson, D., Zhu, X. G., et al. (2010). *Setaria viridis*: a model for C4 photosynthesis. *Plant Cell* 22, 2537–2544. doi: 10.1105/tpc.110.075309

Cao, H. P., and Chen, S. K. (1995). Brassinosteroid-induced rice lamina joint inclination and its relation to indole-3-Acetic-Acid and Ethylene. *Plant Growth Regul.* 16, 189–196. doi: 10.1007/BF00029540

Clouse, S. D. (2001). Integration of light and brassinosteroid signals in etiolated seedling growth. *Trends Plant Sci.* 6, 443–445. doi: 10.1016/S1360-1385(01)02102-1

Clouse, S. D., Langford, M., and McMorris, T. C. (1996). A brassinosteroid-insensitive mutant in *Arabidopsis thaliana* exhibits multiple defects in growth and development. *Plant Physiol.* 111, 671–678. doi: 10.1104/pp.111.3.671

Creelman, R. A., and Mullet, J. E. (1995). Jasmonic acid distribution and action in plants: regulation during development and response to biotic and abiotic stress. *Proc. Natl. Acad. Sci. U.S.A.* 92, 4114–4119. doi: 10.1073/pnas.92.10.4114

Dekker, J., and Hargrove, M. (2002). Weedy adaptation in Setaria spp. V. Effects of gaseous environment on giant foxtail (*Setaria faberi*) (Poaceae) seed germination. *Am. J. Bot.* 89, 410–416. doi: 10.3732/ajb.89.3.410

Dekkers, B. J., Schuurmans, J. A., and Smeekens, S. C. (2008). Interaction between sugar and abscisic acid signalling during early seedling development in Arabidopsis. *Plant Mol. Biol.* 67, 151–167. doi: 10.1007/s11103-008-9308-6

Dekkers, B. J. W., Schuurmans, J. A. M. J., and Smeekens, S. C. M. (2004). Glucose delays seed germination in *Arabidopsis thaliana*. *Planta* 218, 579–588. doi: 10.1007/s00425-003-1154-9

Doust, A. N., and Kellogg, E. A. (2006). Effect of genotype and environment on branching in weedy green millet (*Setaria viridis*) and domesticated foxtail millet (*Setaria italica*) (Poaceae). *Mol. Ecol.* 15, 1335–1349. doi: 10.1111/j.1365-294X.2005.02791.x

Doust, A. N., Mauro-Herrera, M., Hodge, J. G., and Stromski, J. (2017). The C-4 model grass Setaria is a short day plant with secondary long day genetic regulation. *Front. Plant Sci.* 8:1062. doi: 10.3389/fpls.2017.01062

Duan, L., Sebastian, J., and Dinneny, J. R. (2015). Salt-stress regulation of root system growth and architecture in Arabidopsis seedlings. *Plant Cell Expans.* 1242, 105–122. doi: 10.1007/978-1-4939-1902-4_10

Feldman, M. J., Paul, R. E., Banan, D., Barrett, J. F., Sebastian, J., Yee, M. C., et al. (2017). Time dependent genetic analysis links field and controlled environment phenotypes in the model C4 grass Setaria. *PLOS Genet.* 13:e1006841. doi: 10.1371/journal.pgen.1006841

Feng, Z. J., Xu, Z. S., Sun, J., Li, L. C., Chen, M., Yang, G. X., et al. (2016). Investigation of the ASR family in foxtail millet and the role of ASR1 in drought/oxidative stress tolerance. *Plant Cell Rep.* 35, 115–128. doi: 10.1007/s00299-015-1873-y

Finkelstein, R., Reeves, W., Ariizumi, T., and Steber, C. (2008). Molecular aspects of seed dormancy. *Annu. Rev. Plant Biol.* 59, 387–415. doi: 10.1146/annurev.arplant.59.032607.092740

Finkelstein, R. R., Gampala, S. S., and Rock, C. D. (2002). Abscisic acid signaling in seeds and seedlings. *Plant Cell* 14(Suppl.), S15–S45. doi: 10.1105/tpc.010441

Finkelstein, R. R., and Lynch, T. J. (2000). Abscisic acid inhibition of radicle emergence but not seedling growth is suppressed by sugars. *Plant Physiol.* 122, 1179–1186. doi: 10.1104/pp.122.4.1179

Garciarrubio, A., Legaria, J. P., and Covarrubias, A. A. (1997). Abscisic acid inhibits germination of mature Arabidopsis seeds by limiting the availability of energy and nutrients. *Planta* 203, 182–187. doi: 10.1007/s004250050180

Gazzarrini, S., and Tsai, A. Y. (2015). Hormone cross-talk during seed germination. *Essays Biochem.* 58, 151–164. doi: 10.1042/bse0580151

Gray, W. M. (2004). Hormonal regulation of plant growth and development. *PLOS Biol.* 2:e311. doi: 10.1371/journal.pbio.0020311

Guzman, P., and Ecker, J. R. (1990). Exploiting the triple response of Arabidopsis to identify ethylene-related mutants. *Plant Cell* 2, 513–523. doi: 10.1105/tpc.2.6.513

Harris, J. M. (2015). Abscisic acid: hidden architect of root system structure. *Plants (Basel)* 4, 548–572. doi: 10.3390/plants4030548

Hodge, J. G., and Doust, A. N. (2017). Morphological development of *Setaria viridis* from germination to flowering. *Plant Genet. Genomics.* 19, 161–175. doi: 10.1007/978-3-319-45105-3_10

Huang, P., Feldman, M., Schroder, S., Bahri, B. A., Diao, X., Zhi, H., et al. (2014). Population genetics of *Setaria viridis*, a new model system. *Mol. Ecol.* 23, 4912–4925. doi: 10.1111/mec.12907

Huang, P., Jiang, H., Zhu, C., Barry, K., Jenkins, J., Sandor, L., et al. (2017). Sparse panicle1 is required for inflorescence development in *Setaria viridis* and maize. *Nat. Plants* 3:17054. doi: 10.1038/nplants.2017.54

Huang, P., Shyu, C., Coelho, C. P., Cao, Y., and Brutnell, T. P. (2016). *Setaria viridis* as a model system to advance millet genetics and genomics. *Front. Plant Sci.* 7:1781. doi: 10.3389/fpls.2016.01781

Ingram, P. A., Zhu, J. M., Shariff, A., Davis, I. W., Benfey, P. N., and Elich, T. (2012). High-throughput imaging and analysis of root system architecture in *Brachypodium distachyon* under differential nutrient availability. *Philos. Trans. R. Soc. B Biol. Sci.* 367, 1559–1569. doi: 10.1098/rstb.2011.0241

Kir, G., Ye, H., Nelissen, H., Neelakandan, A. K., Kusnandar, A. S., Luo, A., et al. (2015). RNA interference knockdown of BRASSINOSTEROID INSENSITIVE1 in maize reveals novel functions for brassinosteroid signaling in controlling plant architecture. *Plant Physiol.* 169, 826–839. doi: 10.1104/pp.15.00367

Lastdrager, J., Hanson, J., and Smeekens, S. (2014). Sugar signals and the control of plant growth and development. *J. Exp. Bot.* 65, 799–807. doi: 10.1093/jxb/ert474

Layton, D. J., and Kellogg, E. A. (2014). Morphological, phylogenetic, and ecological diversity of the new model species *Setaria viridis* (Poaceae: Paniceae) and its close relatives. *Am. J. Bot.* 101, 539–557. doi: 10.3732/ajb.1300428

Leon-Kloosterziel, K. M., van de Bunt, G. A., Zeevaart, J. A., and Koornneef, M. (1996). Arabidopsis mutants with a reduced seed dormancy. *Plant Physiol.* 110, 233–240. doi: 10.1104/pp.110.1.233

Li, P., and Brutnell, T. P. (2011). *Setaria viridis* and *Setaria italica*, model genetic systems for the Panicoid grasses. *J. Exp. Bot.* 62, 3031–3037. doi: 10.1093/jxb/err096

Li, W., Chen, M., Wang, E., Hu, L., Hawkesford, M. J., Zhong, L., et al. (2016). Genome-wide analysis of autophagy-associated genes in foxtail millet (*Setaria italica* L.) and characterization of the function of SiATG8a in conferring tolerance to nitrogen starvation in rice. *BMC Genomics* 17:797. doi: 10.1186/s12864-016-3113-4

Liu, K., Qi, S., Li, D., Jin, C., Gao, C., Duan, S., et al. (2017). TRANSPARENT TESTA GLABRA 1 ubiquitously regulates plant growth and development from Arabidopsis to foxtail millet (*Setaria italica*). *Plant Sci.* 254, 60–69. doi: 10.1016/j.plantsci.2016.10.010

Liu, Z., Li, X., Li, R., Jiang, D., and Cao, C. (2003). A comparative study on seed germination of 15 grass species in Keeqin Sandyland. *Ying Yong Sheng Tai Xue Bao* 14, 1416–1420.

Ma, B., Yin, C. C., He, S. J., Lu, X., Zhang, W. K., Lu, T. G., et al. (2014). Ethylene-induced inhibition of root growth requires abscisic acid function in

rice (*Oryza sativa* L.) Seedlings. *PLOS Genet.* 10:e1004701. doi: 10.1371/journal.pgen.1004701

Manthey, D. R., and Nalewaja, J. D. (1987). Germination of two foxtail (Setaria) Species. *Weed Technol.* 1, 302–304.

Martins, P. K., Ribeiro, A. P., Cunha, B., Kobayashi, A. K., and Molinari, H. B. C. (2015). A simple and highly efficient Agrobacterium-mediated transformation protocol for *Setaria viridis*. *Biotechnol. Rep. (Amst)* 6, 41–44. doi: 10.1016/j.btre.2015.02.002

Mauro-Herrera, M., and Doust, A. N. (2016). Development and genetic control of plant architecture and biomass in the panicoid grass, Setaria. *PLOS ONE* 11:e0151346. doi: 10.1371/journal.pone.0151346

Mauro-Herrera, M., Wang, X., Barbier, H., Brutnell, T. P., Devos, K. M., and Doust, A. N. (2013). Genetic control and comparative genomic analysis of flowering time in Setaria (Poaceae). *G3* 3, 283–295. doi: 10.1534/g3.112.005207

Muthamilarasan, M., Bonthala, V. S., Khandelwal, R., Jaishankar, J., Shweta, S., Nawaz, K., et al. (2015). Global analysis of WRKY transcription factor superfamily in Setaria identifies potential candidates involved in abiotic stress signaling. *Front. Plant Sci.* 6:910. doi: 10.3389/fpls.2015.00910

Nonogaki, H. (2014). Seed dormancy and germination-emerging mechanisms and new hypotheses. *Front. Plant Sci.* 5:233. doi: 10.3389/fpls.2014.00233

Ogawa, M., Hanada, A., Yamauchi, Y., Kuwalhara, A., Kamiya, Y., and Yamaguchi, S. (2003). Gibberellin biosynthesis and response during Arabidopsis seed germination. *Plant Cell* 15, 1591–1604. doi: 10.1105/tpc.011650

Overvoorde, P., Fukaki, H., and Beeckman, T. (2010). Auxin control of root development. *Cold Spring Harb. Perspect. Biol.* 2:a001537. doi: 10.1101/cshperspect.a001537

Pan, Y., Li, J., Jiao, L., Li, C., Zhu, D., and Yu, J. (2016). A Non-specific *Setaria italica* lipid transfer protein gene plays a critical role under abiotic stress. *Front. Plant Sci.* 7:1752. doi: 10.3389/fpls.2016.01752

Pandey, G., Yadav, C. B., Sahu, P. P., Muthamilarasan, M., and Prasad, M. (2017). Salinity induced differential methylation patterns in contrasting cultivars of foxtail millet (*Setaria italica* L.). *Plant Cell Rep.* 36, 759–772. doi: 10.1007/s00299-016-2093-9

Pandey, S., Chen, J. G., Jones, A. M., and Assmann, S. M. (2006). G-protein complex mutants are hypersensitive to abscisic acid regulation of germination and postgermination development. *Plant Physiol.* 141, 243–256. doi: 10.1104/pp.106.079038

Qie, L., Jia, G., Zhang, W., Schnable, J., Shang, Z., Li, W., et al. (2014). Mapping of quantitative trait locus (QTLs) that contribute to germination and early seedling drought tolerance in the interspecific cross *Setaria italica* x *Setaria viridis*. *PLOS ONE* 9:e101868. doi: 10.1371/journal.pone.0101868

Saha, P., and Blumwald, E. (2016). Spike-dip transformation of *Setaria viridis*. *Plant J.* 86, 89–101. doi: 10.1111/tpj.13148

Saha, P., Sade, N., Arzani, A., Rubio Wilhelmi, M. D. M., Coe, K. M., Li, B., et al. (2016). Effects of abiotic stress on physiological plasticity and water use of *Setaria viridis* (L.). *Plant Sci.* 251, 128–138. doi: 10.1016/j.plantsci.2016.06.011

Saleki, R., Young, P. G., and Lefebvre, D. D. (1993). Mutants of *Arabidopsis thaliana* capable of germination under saline conditions. *Plant Physiol.* 101, 839–845. doi: 10.1104/pp.101.3.839

Satler, S. O., and Kende, H. (1985). Ethylene and the growth of rice seedlings. *Plant Physiol.* 79, 194–198. doi: 10.1104/pp.79.1.194

Schroder, S., Bahri, B. A., Eudy, D. M., Layton, D. J., Kellogg, E. A., and Devos, K. M. (2017). Genetic diversity and origin of North American green foxtail [*Setaria viridis* (L.) Beauv.] accessions. *Genet. Resour. Crop Evol.* 64, 367–378. doi: 10.1007/s10722-016-0363-6

Sebastian, J., Wong, M. K., Tang, E., and Dinneny, J. R. (2014). Methods to promote germination of dormant *Setaria viridis* seeds. *PLOS ONE* 9:e95109. doi: 10.1371/journal.pone.0095109

Shu, K., Liu, X. D., Xie, Q., and He, Z. H. (2016). Two faces of one seed: hormonal regulation of dormancy and germination. *Mol. Plant* 9, 34–45. doi: 10.1016/j.molp.2015.08.010

Shu, K., Meng, Y. J., Shuai, H. W., Liu, W. G., Du, J. B., Liu, J., et al. (2015). Dormancy and germination: how does the crop seed decide? *Plant Biol. (Stuttg)* 17, 1104–1112. doi: 10.1111/plb.12356

Shyu, C., and Brutnell, T. P. (2015). Growth-defence balance in grass biomass production: the role of jasmonates. *J. Exp. Bot.* 66, 4165–4176. doi: 10.1093/jxb/erv011

Singh, R. K., Jaishankar, J., Muthamilarasan, M., Shweta, S., Dangi, A., and Prasad, M. (2016). Genome-wide analysis of heat shock proteins in C4 model, foxtail millet identifies potential candidates for crop improvement under abiotic stress. *Sci. Rep.* 6:32641. doi: 10.1038/srep32641

Smith, S., and De Smet, I. (2012). Root system architecture: insights from Arabidopsis and cereal crops Introduction. *Philos. Trans. R. Soc. B Biol. Sci.* 367, 1441–1452. doi: 10.1098/rstb.2011.0234

Swanton, C. J., Huang, J. Z., Deen, W., Tollenaar, M., Shrestha, A., and Rahimian, H. (1999). Effects of temperature and photoperiod on *Setaria viridis*. *Weed Sci.* 47, 446–453.

Turner, J. G., Ellis, C., and Devoto, A. (2002). The jasmonate signal pathway. *Plant Cell* 14(Suppl.), S153–S164. doi: 10.1105/tpc.000679

Wang, L., Xu, Y. Y., Ma, Q. B., Li, D., Xu, Z. H., and Chong, K. (2006). Heterotrimeric G protein alpha subunit is involved in rice brassinosteroid response. *Cell Res.* 16, 916–922. doi: 10.1038/sj.cr.7310111

Wasternack, C. (2007). Jasmonates: an update on biosynthesis, signal transduction and action in plant stress response, growth and development. *Ann. Bot.* 100, 681–697. doi: 10.1093/aob/mcm079

Williamson, L. C., Ribrioux, S. P. C. P., Fitter, A. H., and Leyser, H. M. O. (2001). Phosphate availability regulates root system architecture in Arabidopsis. *Plant Physiol.* 126, 875–882. doi: 10.1104/pp.126.2.875

Wu, C. Y., Trieu, A., Radhakrishnan, P., Kwok, S. F., Harris, S., Zhang, K., et al. (2008). Brassinosteroids regulate grain filling in rice. *Plant Cell* 20, 2130–2145. doi: 10.1105/tpc.107.055087

Xu, J., Li, Y., Ma, X., Ding, J., Wang, K., Wang, S., et al. (2013). Whole transcriptome analysis using next-generation sequencing of model species *Setaria viridis* to support C4 photosynthesis research. *Plant Mol. Biol.* 83, 77–87. doi: 10.1007/s11103-013-0025-4

Xu, W., Ding, G., Yokawa, K., Baluska, F., Li, Q. F., Liu, Y., et al. (2013). An improved agar-plate method for studying root growth and response of *Arabidopsis thaliana*. *Sci. Rep.* 3:1273. doi: 10.1038/srep01273

Yamamuro, C., Ihara, Y., Wu, X., Noguchi, T., Fujioka, S., Takatsuto, S., et al. (2000). Loss of function of a rice brassinosteroid insensitive1 homolog prevents internode elongation and bending of the lamina joint. *Plant Cell* 12, 1591–1606. doi: 10.1105/tpc.12.9.1591

Yang, C., Lu, X., Ma, B., Chen, S. Y., and Zhang, J. S. (2015). Ethylene signaling in rice and Arabidopsis: conserved and diverged aspects. *Mol. Plant* 8, 495–505. doi: 10.1016/j.molp.2015.01.003

Yang, Y. Y., Nagatani, A., Zhao, Y. J., Kang, B. J., Kendrick, R. E., and Kamiya, Y. (1995). Effects of gibberellins on seed germination of phytochrome-deficient mutants of *Arabidopsis thaliana*. *Plant Cell Physiol.* 36, 1205–1211.

Yue, J., Li, C., Liu, Y. W., and Yu, J. J. (2014). A remorin gene SiREM6, the target gene of SiARDP, from foxtail millet (*Setaria italica*) promotes high salt tolerance in transgenic Arabidopsis. *PLOS ONE* 9:e100772. doi: 10.1371/journal.pone.0100772

Zhang, C., Bai, M. Y., and Chong, K. (2014). Brassinosteroid-mediated regulation of agronomic traits in rice. *Plant Cell Rep.* 33, 683–696. doi: 10.1007/s00299-014-1578-7

Zhao, D. L., Reddy, K. R., Kakani, V. G., and Reddy, V. R. (2005). Nitrogen deficiency effects on plant growth, leaf photosynthesis, and hyperspectral reflectance properties of sorghum. *Eur. J. Agron.* 22, 391–403. doi: 10.1016/j.eja.2004.06.005

Zhu, C., Yang, J., and Shyu, C. (2017). Setaria comes of age: meeting report on the second international Setaria genetics conference. *Front. Plant Sci.* 8:1562. doi: 10.3389/fpls.2017.01562

Conflict of Interest Statement: The authors declare that the research was conducted in the absence of any commercial or financial relationships that could be construed as a potential conflict of interest.

frontiers in Plant Science

ORIGINAL RESEARCH
published: 09 February 2018
doi: 10.3389/fpls.2018.00109

Arabidopsis Type III Gγ Protein AGG3 Is a Positive Regulator of Yield and Stress Responses in the Model Monocot *Setaria viridis*

*Jagdeep Kaur†, Swarup Roy Choudhury, Anitha Vijayakumar, Laryssa Hovis, Zach Rhodes, Rob Polzin, Dylan Blumenthal and Sona Pandey**

Donald Danforth Plant Science Center, St. Louis, MO, United States

OPEN ACCESS

Edited by:
Andrew Doust, Oklahoma State University, United States

Reviewed by:
Lucía Jordá, Universidad Politécnica de Madrid (UPM), Spain
Yi Shang, Yunnan Normal University, China

***Correspondence:**
Sona Pandey
spandey@danforthcenter.org

†Present address:
Jagdeep Kaur, Monsanto Company, St. Louis, MI, United States

Specialty section:
This article was submitted to Plant Breeding, a section of the journal Frontiers in Plant Science

Received: *15 November 2017*
Accepted: *19 January 2018*
Published: *09 February 2018*

Citation:
Kaur J, Roy Choudhury S, Vijayakumar A, Hovis L, Rhodes Z, Polzin R, Blumenthal D and Pandey S (2018) Arabidopsis Type III Gγ Protein AGG3 Is a Positive Regulator of Yield and Stress Responses in the Model Monocot Setaria viridis. Front. Plant Sci. 9:109. doi: 10.3389/fpls.2018.00109

Heterotrimeric G-proteins are key regulators of a multitude of growth and development pathways in eukaryotes. Along with the conserved G-protein components found in all organisms, plants have certain novel variants with unique architecture, which may be involved in the regulation of plant-specific traits. The higher plant-specific type III (or Class C) Gγ protein, which possesses a large C terminal extension, represented by AGG3 in Arabidopsis, is one such variant of canonical Gγ proteins. The type III Gγ proteins are involved in regulation of many agronomically important traits in plants, including seed yield, organ size regulation, abscisic acid (ABA)-dependent signaling and stress responses, and nitrogen use efficiency. However, the extant data, especially in the monocots, present a relatively complex and sometimes contradictory picture of the regulatory role of these proteins. It remains unclear if the positive traits observed in certain naturally occurring populations are due to the presence of specific allelic variants of the proteins or due to the altered expression of the gene itself. To address these possibilities, we have overexpressed the Arabidopsis *AGG3* gene in the model monocot *Setaria viridis* and systematically evaluated its role in conferring agriculturally relevant phenotypes. Our data show that *AtAGG3* is indeed functional in Setaria and suggest that a subset of the traits affected by the type III Gγ proteins are indeed positively correlated with the gene expression level, while others might have more complex, allele specific regulation.

Keywords: *Setaria viridis*, heterotrimeric G-proteins, AGG3, type III Gγ, yield, stress response

INTRODUCTION

Food security has become an imminent challenge especially with the ever increasing human population on the planet and is now thought to be worse than it was 20 years ago (Alexandratos, 1999). The population of the planet is projected to increase by almost 50% within the next 35 years. With the drastic increase in population, food production also must increase. Without appropriate solutions the need for increased land for crops could irreversibly change terrestrial and aquatic environments (Tilman et al., 2002). Identification of specific genes/targets that confer increased yield potential in non-optimal environment and elucidation of their mode of action is, therefore,

central to our future needs. The type III Gγ proteins of the heterotrimeric G-protein complex are fast emerging as one such agronomically important target (Botella, 2012).

Heterotrimeric GTP-binding proteins (G-proteins hereafter) composed of Gα, Gβ, and Gγ subunits mediate signaling in response to a variety of stimuli in all eukaryotes and control critical growth and developmental processes (Urano and Jones, 2014; Stateczny et al., 2016). The G-protein core components and their basic biochemical properties are largely conserved across phyla; however, key differences emerge when comparing plants with metazoan systems. The genomes of most plants encode fewer canonical G-protein subunits, e.g., 1 Gα and 1 Gβ proteins exist in Arabidopsis compared to 23 Gα and 5 Gβ proteins in humans (Hackenberg et al., 2017). Intriguingly, plant genomes also encode certain divergent G-protein components, which may be involved in the control of plant-specific functions. One such plant-specific component is exemplified by the novel type III Gγ proteins, which are emerging as a major target for plant breeding (Chakravorty et al., 2011; Roy Choudhury et al., 2011).

The plant Gγ proteins are classified into three different groups based on their C-terminal region. The type I are the canonical Gγ proteins found in all organisms. These are 100–120 aa proteins, represented in Arabidopsis by AGG1 and AGG2. The type II Gγ proteins are very similar to the type I Gγ proteins but they lack the signature C-terminal prenylation motif present in canonical Gγ (Roy Choudhury et al., 2011; Thung et al., 2012). Both type I and type II Gγ proteins have been shown to be involved in plant-microbe interaction and various hormone signaling pathways (Trusov et al., 2006, 2007, 2008, 2009; Delgado-Cerezo et al., 2012; Yadav et al., 2012; Roy Choudhury and Pandey, 2013).

The type III Gγ proteins, represented by Arabidopsis AGG3, rice DEP1, GS3 and GGC2, wheat TaDEP1, barley HvDEP1 and soybean GmGγ8, GmGγ9, and GmGγ10 are at least twice as large as the type I or type II proteins and have a modular architecture (Roy Choudhury et al., 2011; Botella, 2012; Trusov et al., 2012). The N-terminal region of these proteins is similar in size and sequence to the type I and II Gγ proteins and is connected with the C-terminal region with a putative transmembrane domain. The C-terminal region is extremely rich in amino acid Cysteine (Cys), which can account for up to 38% of total amino acids in this region (Roy Choudhury et al., 2011). Interestingly, there is an expansion of the C-terminal region in plants that have more than one homolog of type III Gγ protein. For example, the three rice proteins possess 100, 200, and 300 amino acids in their C-terminal region, while the N-terminal region is fairly conserved. Similar expansion of the C-terminal region is seen in the soybean type III Gγ proteins. This unique Cys-rich region has predicted segments showing some similarity to tumor necrosis/nerve growth factor receptor (TNFR/NGFR) and multiple repeats of the von Willebrand factor type C modules and a Sprouty domain, which are thought to be involved in large protein complex formation (Roy Choudhury et al., 2011; Botella, 2012; Trusov et al., 2012; Wolfenstetter et al., 2014).

Type III Gγ proteins regulate two of the most critical plant processes; seed yield and stress responses. The *AGG3* gene of Arabidopsis was discovered as the missing Gγ protein that could explain a subset of Gβ mutant phenotypes, especially those related to ABA-responses, unaccounted for by the previously identified *AGG1* and *AGG2* genes (Chakravorty et al., 2011; Wolfenstetter et al., 2014). Additionally, an independent study in Arabidopsis identified *AGG3* by map-based cloning as an organ size regulator, as loss-of-function of *AGG3* resulted in smaller leaves and flowers (Li et al., 2012b). Surprisingly, a survey of rice literature revealed that the homologs of this gene were already characterized, although not as Gγ protein. The rice proteins, named GS3 (grain size 3) and DEP1 (dense and erect panicle 1), were identified as major quantitative trait loci (QTL) for panicle density, seed size and seed number (Fan et al., 2006; Huang et al., 2009; Mao et al., 2010; Li et al., 2012a; Kunihiro et al., 2013).

Several studies in the past years have revealed a relatively complex picture of the type III Gγ regulated processes in plants. Overall, the situation seems to be clearer in dicots such as Arabidopsis and Camelina, where AGG3 protein has been shown to be a positive regulator of stress response and organ size. Overexpression of *AGG3* in both Arabidopsis and Camelina results in larger plants, bigger seeds and better stress tolerance, while the knockout mutants of *AGG3* in Arabidopsis have an opposite phenotype suggesting a direct, positive correlation between the protein level and the observed phenotypes (Chakravorty et al., 2011; Li et al., 2012b; Roy Choudhury et al., 2014; Alvarez et al., 2015). However in monocots, especially in rice where the gene has been studied extensively at the genetic level, extant data present a complex scenario.

The *GS3* gene, as the name suggests, regulates grain size in rice and plants with different allelic variants of this gene produce differently sized grains (Mao et al., 2010). Varieties containing naturally occurring mutations resulting in the potential loss-of-function alleles produce extremely long grains, whereas a variant causing deletion of the C-terminal region but leaving the most of the Gγ-like domain intact, results in plants producing extremely short grains. Additional variants which produce normal, short or long grains, depending on the location of the mutation are also reported (Fan et al., 2006, 2009; Mao et al., 2010; Botella, 2012). Overall, it has been concluded that the GS3 locus is a negative regulator of grain size, which incidentally is opposite of the role of *AGG3* gene in Arabidopsis and Camelina.

Different allelic variants of the *DEP1* locus, which was initially identified as a major QTL for dense and erect panicles, also confer distinct phenotypes (Huang et al., 2009). For examples plants possessing *dep1* or *qPE9-1* alleles, which code for almost identical proteins with only one amino acid difference in their lengths have different phenotypes. *dep1,* which is a gain of function mutation, leads to increased panicle branching and improved grain yield whereas *qPE9-1,* which is a loss-of-function mutation, exhibits no change in branching and causes reduced yield (Huang et al., 2009; Zhou et al., 2009; Yi et al., 2011). RNAi-mediated suppression of *DEP1* locus in *dep1* allelic background resulted in curved panicles and fewer grains, whereas expression of a *DEP1* promoter-driven expression of *dep1* allele resulted in erect panicles and increased yield. Furthermore, a constitutive promoter-driven expression of the *dep1* resulted in dwarf plants with erect panicles, whereas similar expression of *DEP1* allele had no phenotypic effect. Finally, a recent CRISPR/CaS9 based editing of *DEP1* gene

resulted in erect panicles, similar to what was reported with the *dep1* allele, but the plants were also dwarfed and the grain size was not affected, which is not what was seen with the naturally occurring *dep1* mutation (Li et al., 2016; Xu et al., 2016; Zhao et al., 2016). In wheat, an RNAi-mediated downregulation of *TaDEP1* led to longer and less compact spikes, whereas a similar loss-of-function mutation in barley *HvDEP1* resulted in dwarf plants, with compact, shorter spikes and improved seed yield (Wendt et al., 2016). Recently *DEP1* has also been identified as a major QTL for nitrogen use efficiency (NEU) in rice (Sun et al., 2014; Wendt et al., 2016; Xu et al., 2016). Finally, a 12 year field study in barley concluded that the effect of *DEP1* locus is highly dependent on the environmental conditions and may result in significantly higher or lower yields, compared to the wild type control plants (Wendt et al., 2016).

Based on these studies, the overall consensus is that the type III *G*γ genes are critical regulators of important agronomic traits, and have been subjected to artificial selection all through domestication. However, there seem to be a huge effect of the genetic background as well as specific environmental conditions that determine the eventual yield and stress responses of the plants possessing specific alleles. To gain a better understanding of the role of type III Gγ proteins, we have overexpressed a monocot codon optimized *AGG3* gene in *Setaria viridis* (green foxtail), a member of the Panicoideae subfamily of grasses which also include food crops like maize and sorghum. The availability of a sequenced genome, efficient transformation system and rapid life cycle with ample seed production makes it an ideal model system for the study of physiological, developmental and yield traits of important grain crops (Acharya et al., 2017). The data presented in this manuscript confirm that the *AGG3* gene is functional in Setaria and while some of the traits are indeed positively regulated by constitutive overexpression of *AGG3* gene, others might have a more complex regulation, dependent on the presence of specific alleles, genetic background or environmental conditions.

MATERIALS AND METHODS

Construction of Plant Expression Vectors and *S. viridis* Plant Transformation

A 759 bp *AGG3* (*At5g20635*) gene (Supplementary Figure S1) was chemically synthesized (GeneScript Incorporated, Piscataway, NJ, United States) using the monocot-preferred codons. Employing Gateway® (GW) strategy, the full-length *AGG3* gene was cloned into *pCR8/GW/TOPO* vector (Invitrogen, Waltham, MA, United States) using manufacturer's instructions. The resulting *pCR8/GW/AGG3* entry clone after sequence confirmation was recombined into *pANIC10A* expression vector (Mann et al., 2012) using LR clonase enzyme (Invitrogen, Waltham, MA, United States) which allowed constitutive expression of *AGG3* driven by *ZmUbi1* (*Zea mays* ubiquitin 1) promoter. The sequence confirmed *pANIC10A::AGG3* and *pANIC10A* (empty vector, EV, hereafter) constructs were transformed into *Agrobacterium tumefaciens* strain AGL1 using standard protocol. Transgenic *S. viridis* (A10.1) plants expressing these two constructs were generated by the plant transformation facility at Boyce Thompson Institute, Ithaca, NY (Van Eck and Swartwood, 2015). The transformed *S. viridis* T_0 events were genotyped for the presence of selectable marker gene *hph* using primers listed in Supplementary Table S1. T_0 events positive for *hph* gene were grown to maturity and T_1 seeds were shipped to the Danforth Center for further characterization.

Characterization of Transgenic *S. viridis* Plants

Seeds were propagated by growing in metro mix 360 potting mix (Hummert International, Earth City, MO, United States), in a growth chamber which was maintained at 31°C day/ 22°C night temperature, with a relative humidity 50–60% at a 12 h day/12 h night photoperiod. Plants were watered once a day and fertilized twice a week.

One hundred mg of leaf tissue from the T_1 families of transgenic plants (*AGG3-OE* and *EV*) was used for DNA isolation following a CTAB method. DNA was quantified on a Nanodrop 2000c (Thermo Fisher Scientific, Austin, TX, United States) and used for genotyping, Southern blot analysis and TaqMan assays. Plants carrying the *AGG3* transgene were identified by genomic PCR. To determine the insert integration pattern a DIG (Digoxigenin)-labeled Southern hybridization protocol was used as described in https://docs.wixstatic.com/ugd/45ed6d_bbc4921f988e4aa7afd873237555a42a.pdf. Briefly, 10 μg of DNA was digested with *Mfe*I, run on a 1.0% agarose gel and transferred to a positively charged nitrocellulose membrane. The membrane was UV-crosslinked and prepared for hybridization (pre-hybridization) using the DIG Easy Hyb (Roche, Indianapolis, IN, United States) solution. The hybridization probe complimentary to the *hph* gene was prepared using DIG-labeled dNTPs and *pANIC10A* plasmid DNA as template. The membrane was hybridized overnight followed by washing with low (2X SSC, 0.1% SDS) and high (0.5 X SSC, 0.1% SDS) stringency washes and blocked with 1X blocking buffer (1X maleic acid buffer, Blocking Reagent- Roche). Afterward the membrane was treated with anti-DIG AP Fab Fragments (Roche) prepared in blocking buffer. The membrane was washed three times with 1X washing buffer (1X maleic acid buffer, Tween 20). Detection was done using the CDP-Star reagent (Thermo Fisher Scientific, St. Peters, MO, United States) for 5 min.

To identify the homozygous families from single insert transgenic *S. viridis AGG3-OE* and *EV* lines, a TaqMan assay was performed using https://docs.wixstatic.com/ugd/45ed6d_4ce1ccdacf3243c794ad1f9f9f19b8b3.pdf. Briefly, the multiplex reaction (10 μL total) contained 5 μL of genotype master mix (Thermo Fisher Scientific, St. Peters, MO, United States), 0.3 μL of nuclease-free water, 0.9 μL of each of *hph* (marker gene) and *SvPCKR* (*S. viridis* phosphoenolpyruvate carboxykinase gene, internal control) forward and reverse primers, 0.025 *hph* (5′ FAM 3′ QSY) and *SvPCKR* (5′ VIC 3′ TAMRA) dually labeled probes (see sequence information of primer and probes in Supplementary Table S1) and 1 μL of genomic DNA (1 μg equivalent). Each sample including wild type A10.1 and non-template controls (NTC) was run in triplicate. The data were imported into CopyCaller Software (Thermo Fisher Scientific,

Carlsbad, CA, United States) and analyzed for CNV, without the use of a calibrator. The software generated a graphical output of the copies of the gene of interest that were present in the genome of each individual.

RNA Isolation, DNase Treatment, cDNA Synthesis, and qRT-PCR Analysis

Total RNA from *EV* and *AGG3-OE* transgenic plants was extracted from 2 weeks old seedlings using TRIzol reagent and was digested with RNase-free DNaseI (Ambion®, Thermo Fisher Scientific). The quantity and the quality of the RNA were assessed with nanodrop spectrophotometer. Total RNA (500 ng) was reverse transcribed into cDNA using first-strand cDNA synthesis kit (Invitrogen, Carlsbad, CA, United States) and used for quantitative real-time PCR (qPCR) using SYBR mix (Invitrogen). qRT-PCR was conducted in 10 μL reaction mix in three biological replicates. Similar setup was used to check the expression levels of a subset of nitrate transporter and signaling genes. Differences in transcript level were calculated using the $^{\Delta\Delta}$CT method (Bustin et al., 2009). Data represent the means and standard errors (SE) of three biological replicates. The gene specific primers and the reference gene used in the qPCR reactions are listed in Supplementary Table S1.

Germination and Early Seedling Growth Assays

Sterilized Setaria seeds were plated on 0.5 X MS media (Caisson labs, Smithfield, UT, United States) with 0.4% phytagel. Seeds were stratified at 4°C in the darkness for 2 days followed by transfer to the growth chamber maintained at a 12 h (31°C)/ 12 h (22°C) light/dark cycle (Acharya et al., 2017). Germination was defined as protrusion of the radicle from seeds and quantified as the percentage of total seeds at 5 days after plating. To quantify the seed germination in the presence of ABA or glucose, sterilized seeds were plated directly on 0.5 X MS media containing 0.5 μM ABA or 3% glucose. Three biological replicates of each experiment were performed with 24 seeds per genotype per treatment per replicate and data were averaged. Significant differences were analyzed using the Student's *t*-test.

To examine early seedling growth, Setaria seeds sown on 0.5 X MS media plates were stratified at 4°C in the dark for 2 days followed by transfer to the growth chamber with 12 h (31°C)/ 12 h (22°C) light/dark cycle for another 2 days. To evaluate the effect of ABA, glucose or salt (NaCl) on post-germination growth, germinated seeds were transferred on plates containing 2 μM ABA, 3% glucose or 100 mM NaCl (Acharya et al., 2017). Seedlings (20–24 seedlings per genotype per treatment) were grown vertically in the 12 h dark/12 h light cycle and coleoptile and root lengths were measured after 3 days of growth. Germinated seeds transferred to control plates and grown under identical conditions were used as control. To determine the effect of nitrogen or phosphorus limiting conditions, seeds were plated on nitrogen or phosphate deficient 0.5 X MS media (Caisson Labs), and coleoptile and root lengths were measured after 7 days of growth. All experiments were repeated three times and data were averaged.

Adult Plant Growth and Development Assays and Stress Treatment

Plants were grown by sowing the seeds directly into 10 cm pots containing metro mix 360 potting mix in the environmentally controlled greenhouse maintained at 50–60% relative humidity, 31°C/22°C day/night temperature and 12 h of day length (250 μmol m^{-2} s^{-1}) to maturity (Acharya et al., 2017). The phenotypic parameters such as plant height, leaf number, days to heading, size and the number of the panicles were measured weekly. Plants were also grown under low water (50% of the water compared to the well-watered control), nitrogen limiting (no exogenous N_2 added during fertilization versus 15 mM added in control set), and a combination of low water, N_2 limiting conditions. After 8 weeks of growth, plants were allowed to dry and bagged to avoid seed loss. Seeds were collected from completely dried plants. Each experiment contained 12 plants per genotype and the experiment was repeated three times, independently. Data were averaged and are presented as the mean of three biological replicates. Significant differences between EV and transgenic plants' phenotypes was evaluated using Student's *t*-test.

Statistical Analysis

All experiments were repeated at least three times independently and data were averaged. Means, standard deviation (seed germination assays) and standard errors (for root length and number, coleoptile length, leaf number, plant height, panicle number and size, seed weight and qRT-PCR) for measurements were calculated. Statistical significance of results was calculated using Student's *t*-test with a *P*-value threshold of ≤0.05 (*), ≤0.01 (**) or ≤0.001(***).

RESULTS

Generation of Monocot Codon Optimized *AGG3* Overexpressing (*AGG3-OE*) *S. viridis* Plants

The homologs of type III *G*γ genes are present in all higher plants. Using Arabidopsis *AGG3* and rice *DEP1* and *GS3* as query sequences we identified three type III *G*γ genes *Sevir.6G177400.1, Sevir.2G229300.1* and *Sevir.9G375000.1* referred as *SvGG3a, SvGG3b* and *SvGG3c,* respectively, in the *Setaria viridis* genome (Supplementary Table S1). These genes share ∼25%, 31% and 29% identity, respectively, with Arabidopsis *AGG3*; ∼24%, 57% and 22% identity, respectively, with the rice *DEP1* and ∼21%, 20% and 46% identity, respectively, with the rice *GS3* at the amino acid level. The homology mostly exists within the Gγ-like domain of the protein sequences (Supplementary Table S2) and is typical of sequence homologies found within the Gγ proteins. Each one of these Setaria Gγ proteins might be involved in the regulation of one or more developmental, yield-related or stress-response pathways. Because our goal was to evaluate the extent to which the response regulation is dependent on the prototypical type III Gγ protein's expression level, and not on the presence of a specific variant or allele in the

genome, we decided to overexpress a monocot codon-optimized version of the Arabidopsis *AGG3* gene and assess its effect on plant growth, development, yield, and stress response in Setaria.

For strong constitutive expression, the monocot codon-optimized *AGG3* (Supplementary Figure S1) was driven by maize *ZmUbi1* promoter and intron, flanked by octapine synthase polyadenylation signal in *pANIC10A::AGG3* (**Figure 1A**). We obtained eight and two independent T_0 events belonging to *pANIC10A::AGG3* and *EV* constructs, respectively. Between 13 and 16 T_1 families/event were tested for the presence/absence of the plant selectable marker *hph* gene and the data were subjected to goodness of fit for single locus Mendelian segregation of 3:1 using chi-squared analysis. As reported in **Table 1**, 6/8 events (AGG3-1A, AGG3-2A, AGG3-3A, AGG3-4A, AGG3-5A, and AGG3-6B) for *pANIC10A::AGG3* and 2/2 events (EV-2A and EV-3A) for *EV* construct showed single locus inheritance. T_1 events AGG3-1B and AGG3-6A did not conform to 3:1 segregation (**Table 1**).

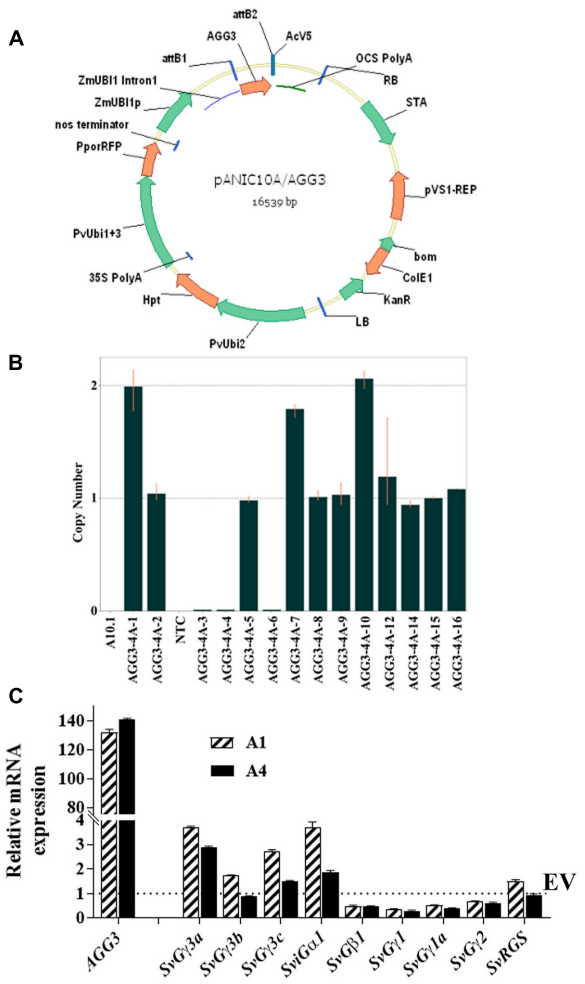

FIGURE 1 | Generation of Setaria *AGG3* overexpression lines. **(A)** Map of the expression vector used for cloning a monocot codon optimized Arabidopsis *AGG3* gene. **(B)** Identification of the homozygous families from single insert AGG3-4A transgenic plants in T1 generation using Taqman assay **(C)** Expression analysis of *AGG3* transgene and endogenous Setaria G-protein genes by qRT-PCR analysis. Transcript levels of indicated genes were determined in *EV* and *AGG3-OE* (A1 and A4) lines using cDNA isolated from 10-day-old *S. viridis* seedlings. The expression values of EV, A1 and A4 were normalized with Setaria ubiquitin gene. Dotted line represents the expression level of *SvGγ3a, SvGγ3b, SvGγ3c, SviGα1, SvGβ1, SvGγ1, SvGγ1a, SvGγ2, SvRGS* in the EV (assigned as 1). The values are presented as the mean ± SE of three biological replicates and represented as fold changes. EV, Setaria plants overexpressing the empty vector; A1, A4 are the two independent transgenic lines for *AGG3* overexpression (*AGG3-OE*).

All T_1 events showing 3:1 segregation were tested for stable integration of the expression cassette using Southern hybridization using a DIG-labeled *hph* probe. Events AGG3-1A and AGG3-2A showed the presence of two copies, AGG3-3A and AGG3-4A carried a single copy while AGG3-5A and AGG3-6A showed three copies of the insert. Both the *EV* events EV-2A and EV-3A showed the presence of single insert. From the distinct banding pattern, all of these lines seemed to be independent events (Supplementary Figure S2). We also used a TaqMan assay to identify homozygous families from single copy events. Thus, 4, 3, 3 and 6 homozygous lines each from AGG3-3A, AGG3-4A, EV-2A and EV-3A, respectively, were identified (**Table 1**). As expected, these single copy events conformed to 1:2:1 segregation pattern (**Table 1**). **Figure 1B** shows representative data for AGG3-4A event, where families numbered AGG3-4A-1, -7, and -10 were homozygous with 2 copies, while families -2, -5, -8, -9, -12, -14, -15 and -16 were heterozygous. PCR null families -3, -4 and -6 were nulls. No amplification was observed in wild type A10.1 and NTC control as expected (**Figure 1B**).

The T_1 seeds from *pANIC10A::AGG3* and *EV* events were self-fertilized to obtain T_2 seeds. Seeds from each of the T_2 family were collected individually. Sixteen T_2 families from each event were progeny tested for *hph* gene (**Table 2**). Based on these data, AGG3-1A-10, AGG3-1B-15, AGG3-1B-16, AGG3-2A-2, AGG3-2A-7, AGG3-3A-9, AGG3-4A-7, AGG3-5A-2, AGG3-6A-4, AGG3-6A-6, AGG3-6B-12, EV-2A-5 and EV-3C-2 families were all PCR positives and considered homozygous, while AGG3-5A-1 and AGG3-6B-13 were segregating (**Table 2**). All the events were advanced to T_3 generation by self-fertilization. Under normal growth and development conditions no phenotypic differences were observed between different T3 lines (Supplementary Figure S3). Two independent, homozygous lines, designated as A1 (AGG3-1B-15-1) and A4 (AGG3-4A-7-4), and the EV containing line EV-2A-5-1 (EV) were selected for further molecular and phenotypic characterization (**Table 2**).

Expression Analysis of *AGG3* and Native G-Protein Genes in Transgenic *S. viridis* Plants

To confirm the higher expression level of the introduced transgene, the transcript level of *AGG3* in Setaria was quantified using qPCR. The analysis showed more than 100 fold increase in the level of *AGG3* transcript in A1 and A4 lines compared to the ubiquitin gene, which was used as control. No *AGG3* transcript was detected in the EV containing plants. Because G-proteins typically work as a protein complex, we also determined the

TABLE 1 | Genetic and molecular characterization of transgenic T_1 *S. viridis* lines.

Line	PCR segregation		Chi-square (χ^2)	Insert number[b]	Zygosity[c]			Chi-square (χ^2)
	hph+	*hph−*	Value (3:I)[a]		Homo	Hetero	Null	Value (I:2:I)[a]
pANIC10A::AGG3								
AGG3-1A	14	1	2.69	2		Not Tested		
AGG3-1B	16	0	5.33*	2		Not Tested		
AGG3-2A	14	2	1.33	2		Not Tested		
AGG3-3A	9	5	0.86	1	4	5	3	0.50
AGG3-4A	11	3	0.94	1	3	8	3	0.28
AGG3-5A	14	2	1.33	3		Not Tested		
AGG3-6A	16	0	5.33*	3		Not Tested		
AGG3-6B	15	1	3.00	3		Not Tested		
pANICIOA (empty vector, EV)								
EV-2A	12	2	0.86	1	3	9	3	0.60
EV-3C	12	4	0.00	1	6	5	3	2.42

[a]*At 1 and 2 degree of freedom and P = 0.05, χ^2 critical values are 3.84 and 5.99, respectively.* [b]*Based on Southern hybridization data on pooled Ti families.* [c]*Based on TaqMan assay, Homo (homozygous), Hetero (Heterozygous) and Null transgenic lines were identified.* *Significant at P = 0.05.

TABLE 2 | Genetic and molecular characterization of transgenic T_2 and T_3 *S. viridis* lines.

Line	T_2 generation			T_3 generation
	PCR segregation[a]		Zygosity status	Family selected for further characterization and their designation[b]
	hph+	*hph −*		
pANIC10A::AGG3				
AGG3-1A-10	16	0	Homo	/
AGG3-1B-15	16	0	Homo	AGG3-1B-15-1 (Al)
AGG3-1B-16	16	0	Homo	/
AGG3-2A-2	16	0	Homo	AGG3-2A-2-3 (A2)
AGG3-2A-7	16	0	Homo	/
AGG3-3A-9	16	0	Homo	AGG3-3A-9-2 (A3)
AGG3-4A-7	16	0	Homo	AGG3-4A-7-4 (A4)
AGG3-5A-1	5	11	Segregating	/
AGG3-5A-2	16	0	Homo	AGG3-5A-2-2 (A5)
AGG3-6A-4	16	0	Homo	/
AGG3-6A-6	16	0	Homo	AGG3-6A-6-1 (A6)
AGG3-6B-12	16	0	Homo	AGG3-6B-12-4(A7)
AGG3-6B-13	13	3	Segregating	
pANICIOA (empty vector, EV)				
EV-2A-5	16	0	Homo	EV-2A-5-1 (EV)
EV-3C-2	16	0	Homo	EV-3C-2-1 (EV-2)

[a]*Absence of hph negative plants indicate homozygosity (Homo) status of parent line.* [b]*Families were phenotyped.*

expression levels of other native G-protein genes of Setaria (gene names and accession numbers listed in Supplementary Table S1) upon *AGG3* overexpression (**Figure 1C**). The transcript levels of the Setaria G-protein complex genes were not significantly and consistently different between EV control versus A1 and A4 plants. These data confirm that a higher expression of *AGG3* does not significantly affect the expression level of other members of the G-protein complex. This also ascertains that any differences observed in the overall traits of the transgenic plants is indeed due to the overexpression of *AGG3* and not due to alteration in the level of other proteins of the complex.

Effect of *AGG3* Overexpression on Early Plant Development

Constitutive overexpression of the *AGG3* has an overall positive effect on the growth and stress responses in Arabidopsis and Camelina, the two species where it has been evaluated. The effects of *AGG3* overexpression in Camelina are obvious from the early seedling stage as the transgenic plants are bigger and more robust (Roy Choudhury et al., 2014). However, in Setaria, the germination and early seedling growth of EV containing plants was indistinguishable from the A1 and A4 plants when grown on synthetic media plates, under control conditions. We then evaluated the effect of different stresses on early development as it has been shown that higher expression of *AGG3* results in hyposensitivity to exogenous ABA during seed germination and early seedling growth in Arabidopsis, and the knockout mutants of *AGG3* gene are hypersensitive to ABA (Chakravorty et al., 2011). Similarly, transgenic Camelina plants overexpressing *AGG3* exhibit reduced sensitivity to ABA as well as other abiotic stresses such as exogenous sucrose and NaCl during germination and early seedling growth (Roy Choudhury et al., 2014; Alvarez et al., 2015). Incidentally, in monocot plants, the functional role of type III Gγ genes related to stress response has been not investigated in sufficient detail. There is one study in rice where *qPE9-1* (a mutation in *DEP1* locus) has been shown to negatively regulate ABA responses during seed germination and post-germination root growth (Zhang et al., 2015) suggesting that the stress-related regulatory role of AGG3 and its homologs might be conserved among dicots and monocots.

Seeds of both A1 and A4 transgenic plants germinated similar to the EV seeds in the ABA-free medium, indicating that there is no change in their sensitivity to endogenous ABA (**Figure 2A**). However, in the presence of 0.5 μM exogenous ABA, the

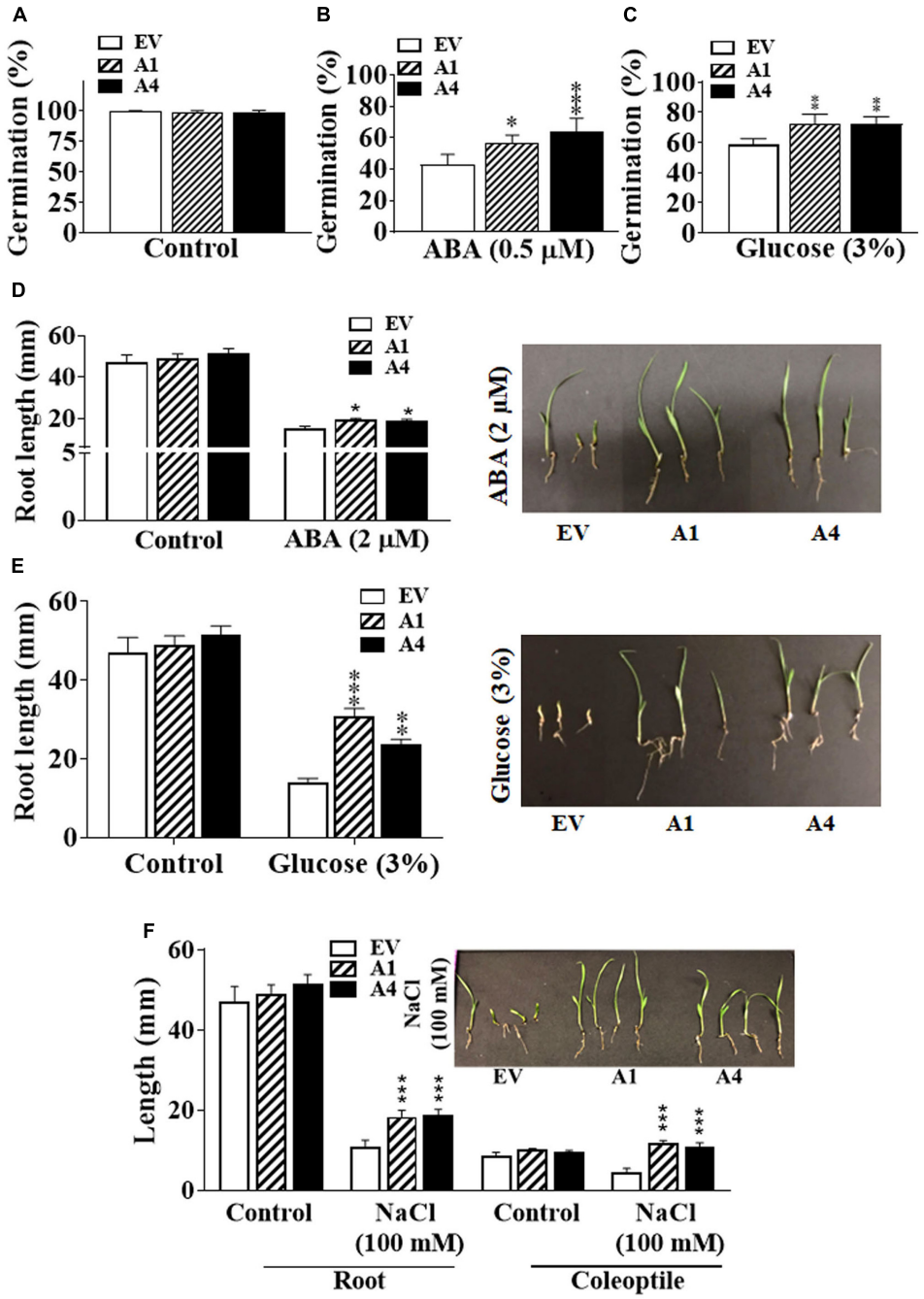

FIGURE 2 | Effect of different abiotic stresses on early development of Setaria *AGG3OE* plants. **(A)** Percentage of seed germination in EV, A1, and A4 transgenic seeds under control conditions. **(B)** Percentage of seed germination in EV, A1 and A4 transgenic seeds in the presence of 0.5 X MS media containing 0.5 µM ABA or **(C)** 3% glucose. For these experiments, 24 seeds per genotype, per treatment were used. Seeds were sterilized and stratified at 4°C for 2 days. Seed germination was calculated as the percentage of total seeds that germinated after 5 days post-stratification. The data represent mean values (±SE) of three biological replicates. **(D)** Post-germination seedling growth of EV and A1 and A4 transgenic plants in the presence of 2 µM ABA, **(E)** 3% glucose or **(F)** 100 mM NaCl. Seeds were germinated on 0.5 X MS agar for 2 days followed by their transfer to the media containing different additives and grown for another 3 days. Root and coleoptile lengths were measured. The graphs represent the mean values (±SE) from sixty seedlings. The corresponding representative pictures are also shown. Asterisks represent *P*-values ≤ 0.05 (*), ≤0.01 (**), or ≤0.001 (***) as calculated using Students *t*-test.

germination of A1 and A4 seeds was considerably improved compared to the EV seeds, and a clear ABA hyposensitivity was observed. Five days after plating, approximately 55–65% of A1 and A4 seeds had germinated, respectively, compared with 40% germination observed in EV seeds on ABA (0.5 µM) containing media (**Figure 2B**).

Because *AGG3* gene is also known to regulate sugar sensitivity and both ABA and glucose signaling pathways are intricately linked (Rook et al., 2006; Seki et al., 2007; Hey et al., 2010; Vishwakarma et al., 2017), we investigated whether the overexpression of *AGG3* resulted in altered responsiveness to glucose. Similar to what was observed for ABA, the A1 and A4 seeds showed better germination compared with the EV seeds in the presence of exogenous glucose. After 5 days of growth on 3% glucose containing media, ∼70% germination was seen in the A1 and A4 seeds, compared with ∼55% germination in EV seeds (**Figure 2C**).

Inhibition of primary root length in the early seedling stage is one of the important phenotypic effects of ABA or glucose-mediated responses (Fedoroff, 2002; Rook et al., 2006; Hey et al., 2010). We compared the effect of exogenous ABA and glucose on primary root length of the EV, A1 and A4 seedlings. Under control conditions, the primary root lengths of all plants were comparable. However, similar to the ABA-mediated inhibition of seed germination, the A1 and A4 seedlings showed less sensitivity to ABA for primary root length inhibition. In the presence of 2 μM exogenous ABA, the primary root length of EV containing seeds was inhibited by ∼57%, compared to ∼43% and ∼36% inhibition observed in A1 and A4 seedlings, respectively (**Figure 2D**). Similar results were obtained in the presence of 3% glucose where the primary roots of the A1 and A4 seedlings was significantly bigger compared to the EV seedlings. Almost 60% reduction in root length was seen for the EV seeds compared to ∼35% and 40% reduction seen in A1 and A4 seedlings, respectively (**Figure 2E**) in the presence of glucose.

We have previously shown that overexpression of *AGG3* gene also enhances salt tolerance in transgenic Camelina (Roy Choudhury et al., 2014). To evaluate the salt tolerance of *AGG3*-overexpressing Setaria plants, seeds were first germinated on 0.5 X MS media and after 2 days of growth, transferred to 0.5 X MS media supplemented with 100 mM NaCl. In the presence of NaCl, A1 and A4 seedlings grew larger than those of the EV seedlings, exhibiting significantly increased primary root length (1.7 times bigger that EV roots) and coleoptile length (2.5 times bigger than EV coleoptiles), exhibiting a hyposensitive response to salt stress (**Figure 2F**). Taken together, these data suggest a general improvement of stress tolerance in the *AGG3*-overexpressing transgenic Setaria plants during germination and at the early seedling stage.

Besides stress tolerance, improved nitrogen and phosphate use efficiency of crops is one of the important needs for sustainable agricultural production. Functional study on one of the type III *Gγ* in rice (*DEP1* allele) has shown the regulation of NUE by this protein (Sun et al., 2014). To assess whether *AGG3*-overexpressing transgenic Setaria exhibited improved growth in nitrogen limiting conditions, we compared the primary root and coleoptile length of transgenic lines with EV lines by growing them under nitrogen limiting condition. We observed ∼26% and 44% longer roots in A1 and A4 seedlings, respectively, compared with the EV line; whereas coleoptile lengths were unaffected by the reduction in nitrogen availability (**Figure 3A**). It suggests that the overexpression of *AGG3* in Setaria can improve the root growth at the early seedling stage for maintaining better plant survival in the nitrogen limiting condition. To verify whether the effect of *AGG3*-overexpression was specific to nitrogen we also investigated their early seedling growth under phosphate limiting condition. No differences were seen in root and coleoptile growth between A1, A4 and EV lines (**Figure 3A**) under these conditions, suggesting the role of type III Gγ genes is specific to nitrogen. The transgenic plants continued to exhibit better growth in the nitrogen limiting conditions (**Figure 3B**). When grown in controlled environment growth chambers for 5 weeks under these conditions, the flag leaves of EV containing plants showed clear nitrogen-responsive chlorosis, accumulated anthocyanin and senesced; whereas the flag leaves of A1 and A4 transgenic plants remained green and exhibited no stress-related phenotype (**Figure 3C**). We compared the transcript levels of key transporters and signaling proteins related to nitrogen uptake, sensing and metabolism in EV control versus A1 and A4 transgenic plants (**Figure 3D**). Several of these genes showed modest (2–5 fold) increase in A1 and A4 compared to the EV plants, suggesting that a general improvement in the NUE of these plants is likely correlated with better uptake and/or sensing.

Overall these data suggest that for seed germination and early plant development, the type III Gγ proteins are a direct, positive regulator of stress responses and their role seems to be conserved between dicot and monocot plants, possibly independent of specific variant of the gene present in the genome.

Effect of *AGG3* Overexpression on Overall Plant Growth, Development and Yield

The type III Gγ proteins are also a major determinant of organ size, especially reproductive organs and seeds. In Arabidopsis, overexpression of *AGG3* results in significantly larger floral organs and bigger seeds whereas opposite was seen with the loss-of-function *agg3* mutant plants (Chakravorty et al., 2011; Li et al., 2012b). Likewise, overexpression of *AGG3* in Camelina increased the seed size and number, in addition to improved biomass production (Roy Choudhury et al., 2014). To determine the effect of *AGG3* overexpression on yield traits reported to be regulated by *DEP1* or *GS3* in rice (Fan et al., 2006; Huang et al., 2009; Mao et al., 2010; Li et al., 2012a), we grew the EV containing and *AGG3* overexpressing plants in greenhouses for their entire life cycle and recorded multiple growth and development traits starting 1 week post-germination for 8 weeks, till the plants were left for drying. Final seed yield was quantified from completely dried plants.

After the first 2 weeks when all plants were indistinguishable from each other, the A1 and A4 plants displayed more robust growth. By 4 weeks, the transgenic plants produced a higher number of leaves per plant compared to the EV containing plants (**Figure 4A**). No difference in the flowering time was observed and the first panicle emerged at a similar time for both EV containing and *AGG3* overexpressing plants. At 7 weeks, when the plants had fully matured, the A1 and A4 plants maintained

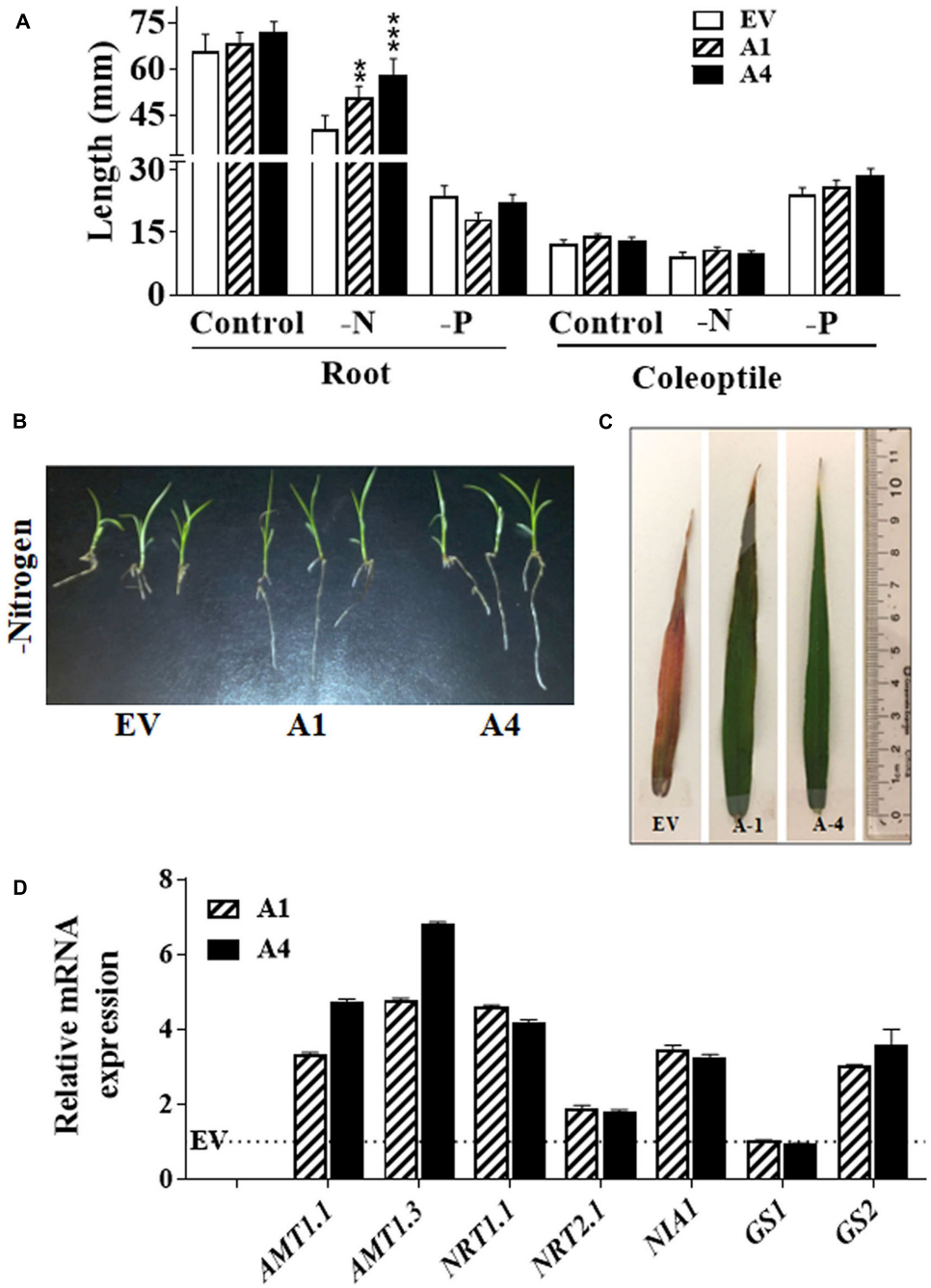

FIGURE 3 | Effect of nitrogen limiting conditions on growth of *AGG3OE* Setaria plants. **(A)** Root and coleoptile lengths of 1 week old seedling grown on 0.5 X MS media lacking nitrogen or phosphate sources. The data represent the mean values (±SE) from sixty seedlings. Asterisks represent *P*-values ≤ 0.01 (**) or ≤0.001 (***) as calculated using Students *t*-test. **(B)** Representative picture of 2 weeks old seedlings of *EV* control and *AGG3OE* lines grown on nitrogen free media. **(C)** Representative picture of the flag leaf of 5 weeks old EV, A1 and A4 plants under nitrogen-limiting condition. **(D)** Expression levels of nitrate transporter and metabolism genes in 2-week old *S. viridis* A1 and A4 plants. Dotted line represents the expression values of the genes (assigned as 1) in EV control plants. The data represent mean values (±SE) of three biological replicates.

the higher leaf numbers (**Figure 4B** and Supplementary Table S3) and were taller than the EV containing plants (**Figure 4C** and Supplementary Table S3), resulting in an overall increased biomass of the transgenic plants.

The overexpression of *AGG3* resulted in more panicles per plant as recorded at 7 weeks (**Figure 4D** and Supplementary Table S3); however, no difference in the panicle length, density or erectness was observed. The panicles from EV plants were

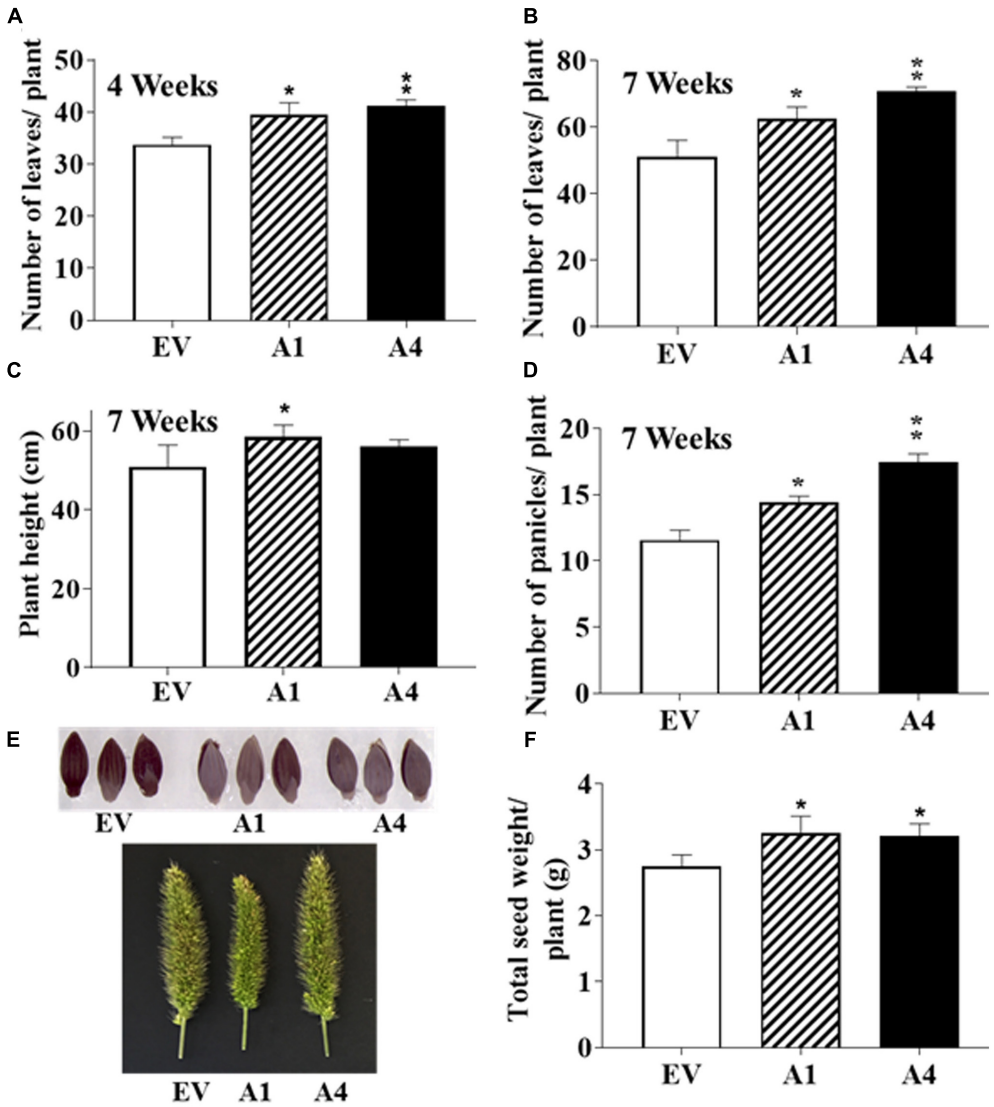

FIGURE 4 | Effect of *AGG3OE* on adult *S. viridis* plants. Adult plant phenotypes of EV, A1 and A4 plants grown under control conditions. Twelve plants per genotype for each of the transgenics were evaluated. The parameters measured were **(A)** number of leaves at 4-weeks, **(B)** leaf number at 7-weeks, **(C)** plant height at 7-weeks, **(D)** number of panicles per plant at 7-weeks. **(E)** Representative pictures of the panicles and seeds of EV versus A1 and A4 transgenic plants. **(F)** The total seed yield per plant. The data represent mean values (±SE) of three biological replicates. Asterisks represent *P*-values ≤ 0.05 (*) or ≤0.01 (**) as calculated using Students *t*-test.

phenotypically indistinguishable from the A1 and A4 plants (**Figure 4E**). Finally, we measured the seed size and seed weight from the A1 and A4 plants and compared it to EV plants. No differences in seed size (**Figure 4E**) or seed weight (100 seed weight per genotype) were observed. However, due to the presence of more panicles per plant, the overall seed produced from A1 and A4 plants was significantly higher than the EV plants (**Figure 4F** and Supplementary Table S3), translating into improved yield per plant.

We also tested the effect of low water stress and nitrogen limiting growth conditions, individually and in combination, on various growth parameters and yield of EV, A1 and A4 plants. Although the transgenic plants exhibited improved stress tolerance at the seed germination and seedling stage and in the growth chambers, in the greenhouse conditions various growth parameters and the yield of A1 and A4 plants were affected by the stress treatment to the similar extent as the EV plants and no noticeable improvement was seen under any of the above listed stress conditions tested (Supplementary Table S3). The *AGG3* transgene was expressed at a significantly higher level in plants grown in the greenhouse, although its expression level was lower under stress conditions compared to the control conditions (Supplementary Figure S4).

These data indicate that while some of the phenotypes ascribed to the regulation by type III Gγ proteins might have a simple causal relationship with the gene expression level; others are more

complex and may depend on the presence of specific protein variant or specific environmental conditions.

DISCUSSION

Naturally occurring or engineered changes in the expression of type III Gγ-proteins result in profound changes in plant architecture, abiotic stress responses and yield potential (Huang et al., 2009; Mao et al., 2010; Botella, 2012; Li et al., 2012a,b; Roy Choudhury et al., 2014; Wendt et al., 2016; Zhao et al., 2016). The distinctive architecture of these proteins, the presence of an extremely Cys-rich region (likely one of the highest Cys containing proteins in nature), and the presence of certain unusual domains (e.g., TNFR or Sprouty) makes them a novel component of the conventional G-protein complex and suggests their possibly unique mechanism of action, which remains largely unknown. The type III Gγ-proteins proteins are clearly a part of the G-protein heterotrimer, as has been confirmed by multiple protein–protein interaction studies as well as genetic analysis (Sun et al., 2014; Wolfenstetter et al., 2014). Homology searches show relatively high sequence conservation in the Gγ domain within the type III family (Supplementary Table S2) as well as when compared with type I or type II family proteins. The C terminal region of the proteins is highly variable, both in its length which could range from 100 to 400 amino acids, as well as in its sequence. However, this region is critical for the proteins' function, as shown by analysis of rice *GS3* and *DEP1* alleles and by complementation studies in Arabidopsis and rice (Li et al., 2012b; Sun et al., 2014; Wolfenstetter et al., 2014). Most of the naturally occurring mutations that define panicle branching or grain size in rice map to the C-terminal region of DEP1 and GS3, respectively (Mao et al., 2010; Botella, 2012; Wendt et al., 2016). Moreover, the phenotypes of the Arabidopsis *agg3* mutants cannot be complemented with the N-terminal Gγ-like domain and the C-terminal region is required to restore the wild-type phenotypes. Surprisingly, no effect of the deletion of specific domains within the C-terminal region was observed. Mutant *agg3* plants transformed with variants of *AGG3,* which were missing the TNFR, TM or VWFC regions, exhibited WT phenotypes.

In order to determine the role of higher expression levels of a prototypical type III Gγ protein, we chose to overexpress a monocot codon optimized *AGG3* gene in Setaria. Because the overexpression of this gene results in multiple growth and development phenotypes in Arabidopsis and in Camelina (Chakravorty et al., 2011; Li et al., 2012b; Roy Choudhury et al., 2014), it allowed for a direct comparison between phenotypes which are directly correlated with the expression level versus those which are dependent of the presence of specific allelic variants of the gene in the genome.

Our data show both similarities and dissimilarities with the effect of overexpression of *AGG3* in Camelina versus Setaria. Camelina seedlings overexpressing *AGG3* are robust and show a clearly improved growth early on, which is distinguishable from the wild type or EV plants. This was not seen in *Setaria AGG3* overexpressors. One possibility is that the Camelina seeds overexpressing *AGG3* are significantly bigger than the EV seeds resulting in better nutrient availability to the germinating seeds, which is not the case with Setaria *AGG3* overexpressing seeds (**Figure 4E**). However, after 2 weeks an improvement in growth of Setaria *AGG3OE* lines was observed, as seen by more leaves per plant and relatively taller plants compared to the EV plants. An improved growth of plants and more branching was also seen in Camelina *AGG3OE* plants.

The seedling stress responses of Setaria *AGG3-OE* lines were similar to what has been reported for Arabidopsis and Camelina *AGG3-OE* lines. The plants showed less sensitivity to ABA, glucose and NaCl and exhibited improved seedling growth compared to the EV containing seedlings on media containing these additives (**Figure 2**). These responses are predicted to be mediated by the classic G-protein signaling pathways, and therefore, are potentially conserved between different plant species. However, unexpectedly we did not see an effect of improved stress tolerance in mature plants grown under greenhouse conditions. Both *EV* containing and *AGG3-OE* lines of Setaria responded similarly to low water stress. Similar trend was seen in response to nitrogen limiting conditions, where the plants exhibited clearly improved growth at the seedling stage and at the young plant stage (**Figure 3**), but the overall growth, development and yield of mature plants was affected similarly in EV versus *AGG3-OE* lines. Incidentally, rice plants possessing specific *DEP1* alleles have been shown to exhibit significantly improved NUE. The lack of improved stress response of adult plants could be due to the specific growth conditions used in our experiments or due to the fact that *Setaria viridis* is an undomesticated plant and therefore has mechanisms to overcome stresses during the growth over its life cycle. Additionally, a developmental stage dependent effect of AGG3 on plants' stress tolerance cannot be ruled out.

One of the most crucial phenotypes ascribed to the type III Gγ proteins is the regulation of grain size and panicle density and erectness. These were the traits that led to the discovery and cloning of the rice homologs of these proteins, GS3 and DEP1 (Fan et al., 2006; Huang et al., 2009; Mao et al., 2010; Xu et al., 2016). Even though we observed a clear difference in panicle number per plants in the transgenic lines, which resulted in improved yield (**Figure 4**), the panicle morphology, seed morphology and the seed size of the *AGG3-OE* plants were indistinguishable from the EV control plants. This is surprising as the overexpression of the same gene in Arabidopsis and in Camelina resulted in significantly larger floral organs and seeds. It may be that AGG3 type proteins interact differently with the developmental programs that control seed size in dicots versus monocots. While in dicots, there seems to be a direct positive correlation between the organ size and protein expression level, the regulation seems to be much more complex in monocots and might involve specific regions of the protein or interaction with specific protein complexes.

Overall, our data confirm that at least a subset of the type III Gγ protein regulated processes are directly linked to the gene's expression level. These include major agronomical traits such as an improved biomass and seed yield. However, our data also emphasize that the roles of these proteins are complex and there are possible allele specific regulatory

circuits. The proteins are clearly an important target for breeding or engineering of important traits in plants, and a thorough investigation of different domains, specific regions or specific variants, under different environmental conditions is required, especially in the context of their role as a part of the G-protein heterotrimer, to fully harness their agronomic potential (Botella, 2012). Finally, identification of specific effector proteins, which act downstream of the heterotrimeric G-protein complex, and evaluation of their role in affecting yield and stress-related traits regulated by G-proteins will also be of critical importance. Only few of such effectors are known in plants to date, and some of these may provide for the specificity of response regulation during G-protein signaling.

AUTHOR CONTRIBUTIONS

The present study was conceived and directed by SP. JK, SRC, and AV conducted the majority of the experimental work with technical help and contribution from LH, ZR, RP, and DB. SP, JK, SRC, and AV contributed toward designing of experiments, interpretation of results, and writing of the manuscript.

FUNDING

Research in the Pandey Lab is supported by NIFA/AFRI (2015-67013-22964) and NSF (IOS-1557942 and MCB-1714693) grants to SP. JK was supported by a grant from the James S. McDonnell Foundation to the Institute for International Crop Improvement at DDPSC.

ACKNOWLEDGMENTS

We are thankful to Drs. Paul Anderson, Nigel Taylor, and Tom Brutnell at the DDPSC for their help and support. Our special thanks to Hui Jiang and Kimberly Maxson-Stein at DDPSC for sharing their Setaria expertise with us.

SUPPLEMENTARY MATERIAL

The Supplementary Material for this article can be found online at: https://www.frontiersin.org/articles/10.3389/fpls.2018.00109/full#supplementary-material

REFERENCES

Acharya, B. R., Roy Choudhury, S., Estelle, A. B., Vijayakumar, A., Zhu, C., Hovis, L., et al. (2017). Optimization of phenotyping assays for the model monocot *Setaria viridis*. *Front. Plant Sci.* 8:2172. doi: 10.3389/fpls.2017.02172

Alexandratos, N. (1999). World food and agriculture: outlook for the medium and longer term. *Proc. Natl. Acad. Sci. U.S.A.* 96, 5908–5914. doi: 10.1073/pnas.96.11.5908

Alvarez, S., Roy Choudhury, S., Sivagnanam, K., Hicks, L. M., and Pandey, S. (2015). Quantitative proteomics analysis of *Camelina sativa* seeds overexpressing the AGG3 gene to identify the proteomic basis of increased yield and stress tolerance. *J. Proteome Res.* 14, 2606–2616. doi: 10.1021/acs.jproteome.5b00150

Botella, J. R. (2012). Can heterotrimeric G proteins help to feed the world? *Trends Plant Sci.* 17, 563–568. doi: 10.1016/j.tplants.2012.06.002

Bustin, S. A., Benes, V., Garson, J. A., Hellemans, J., Huggett, J., Kubista, M., et al. (2009). The MIQE guidelines: minimum information for publication of quantitative real-time PCR experiments. *Clin. Chem.* 55, 611–622. doi: 10.1373/clinchem.2008.112797

Chakravorty, D., Trusov, Y., Zhang, W., Acharya, B. R., Sheahan, M. B., McCurdy, D. W., et al. (2011). An atypical heterotrimeric G-protein γ-subunit is involved in guard cell K^+-channel regulation and morphological development in *Arabidopsis thaliana*. *Plant J.* 67, 840–851. doi: 10.1111/j.1365-313X.2011.04638.x

Delgado-Cerezo, M., Sanchez-Rodriguez, C., Escudero, V., Miedes, E., Fernandez, P. V., Jorda, L., et al. (2012). *Arabidopsis* heterotrimeric G-protein regulates cell wall defense and resistance to necrotrophic fungi. *Mol. Plant* 5, 98–114. doi: 10.1093/mp/ssr082

Fan, C., Xing, Y., Mao, H., Lu, T., Han, B., Xu, C., et al. (2006). GS3, a major QTL for grain length and weight and minor QTL for grain width and thickness in rice, encodes a putative transmembrane protein. *Theor. Appl. Genet.* 112, 1164–1171. doi: 10.1007/s00122-006-0218-1

Fan, C., Yu, S., Wang, C., and Xing, Y. (2009). A causal C-A mutation in the second exon of GS3 highly associated with rice grain length and validated as a functional marker. *Theor. Appl. Genet.* 118, 465–472. doi: 10.1007/s00122-008-0913-1

Fedoroff, N. V. (2002). Cross-talk in abscisic acid signaling. *Sci. STKE* 2002:re10. doi: 10.1126/stke.2002.140.re10

Hackenberg, D., McKain, M. R., Lee, S. G., Roy Choudhury, S., McCann, T., Schreier, S., et al. (2017). Galpha and regulator of G-protein signaling (RGS) protein pairs maintain functional compatibility and conserved interaction interfaces throughout evolution despite frequent loss of RGS proteins in plants. *New Phytol.* 216, 562–575. doi: 10.1111/nph.14180

Hey, S. J., Byrne, E., and Halford, N. G. (2010). The interface between metabolic and stress signalling. *Ann. Bot.* 105, 197–203. doi: 10.1093/aob/mcp285

Huang, X., Qian, Q., Liu, Z., Sun, H., He, S., Luo, D., et al. (2009). Natural variation at the DEP1 locus enhances grain yield in rice. *Nat. Genet.* 41, 494–497. doi: 10.1038/ng.352

Kunihiro, S., Saito, T., Matsuda, T., Inoue, M., Kuramata, M., Taguchi-Shiobara, F., et al. (2013). Rice DEP1, encoding a highly cysteine-rich G protein gamma subunit, confers cadmium tolerance on yeast cells and plants. *J. Exp. Bot.* 64, 4517–4527. doi: 10.1093/jxb/ert267

Li, M., Li, X., Zhou, Z., Wu, P., Fang, M., Pan, X., et al. (2016). Reassessment of the four yield-related Genes Gn1a, DEP1, GS3, and IPA1 in rice using a CRISPR/Cas9 system. *Front. Plant Sci.* 7:377. doi: 10.3389/fpls.2016.00377

Li, S., Liu, W., Zhang, X., Liu, Y., Li, N., and Li, Y. (2012a). Roles of the Arabidopsis G protein γ subunit AGG3 and its rice homologs GS3 and DEP1 in seed and organ size control. *Plant Signal. Behav.* 7, 1357–1359. doi: 10.4161/psb.21620

Li, S., Liu, Y., Zheng, L., Chen, L., Li, N., Corke, F., et al. (2012b). The plant-specific G protein γ subunit AGG3 influences organ size and shape in *Arabidopsis thaliana*. *New Phytol.* 194, 690–703. doi: 10.1111/j.1469-8137.2012.04083.x

Mann, D. G., Lafayette, P. R., Abercrombie, L. L., King, Z. R., Mazarei, M., Halter, M. C., et al. (2012). Gateway-compatible vectors for high-throughput gene functional analysis in switchgrass (*Panicum virgatum* L.) and other monocot species. *Plant Biotechnol. J.* 10, 226–236. doi: 10.1111/j.1467-7652.2011.00658.x

Mao, H., Sun, S., Yao, J., Wang, C., Yu, S., Xu, C., et al. (2010). Linking differential domain functions of the GS3 protein to natural variation of grain size in rice. *Proc. Natl. Acad. Sci. U.S.A.* 107, 19579–19584. doi: 10.1073/pnas.1014419107

Rook, F., Hadingham, S. A., Li, Y., and Bevan, M. W. (2006). Sugar and ABA response pathways and the control of gene expression. *Plant Cell Environ.* 29, 426–434. doi: 10.1111/j.1365-3040.2005.01477.x

Roy Choudhury, S., Bisht, N. C., Thompson, R., Todorov, O., and Pandey, S. (2011). Conventional and novel Gγ protein families constitute the heterotrimeric G-protein signaling network in soybean. *PLOS ONE* 6:e23361. doi: 10.1371/journal.pone.0023361

Roy Choudhury, S., and Pandey, S. (2013). Specific subunits of heterotrimeric G proteins play important roles during nodulation in soybean. *Plant Physiol.* 162, 522–533. doi: 10.1104/pp.113.215400

Roy Choudhury, S., Riesselman, A. J., and Pandey, S. (2014). Constitutive or seed-specific overexpression of Arabidopsis *G-protein γ subunit 3 (AGG3)* results in

increased seed and oil production and improved stress tolerance in *Camelina sativa*. *Plant Biotechnol. J.* 12, 49–59. doi: 10.1111/pbi.12115

Seki, M., Umezawa, T., Urano, K., and Shinozaki, K. (2007). Regulatory metabolic networks in drought stress responses. *Curr. Opin. Plant Biol.* 10, 296–302. doi: 10.1016/j.pbi.2007.04.014

Stateczny, D., Oppenheimer, J., and Bommert, P. (2016). G protein signaling in plants: minus times minus equals plus. *Curr. Opin. Plant Biol.* 34, 127–135. doi: 10.1016/j.pbi.2016.11.001

Sun, H., Qian, Q., Wu, K., Luo, J., Wang, S., Zhang, C., et al. (2014). Heterotrimeric G proteins regulate nitrogen-use efficiency in rice. *Nat. Genet.* 46, 652–656. doi: 10.1038/ng.2958

Thung, L., Trusov, Y., Chakravorty, D., and Botella, J. R. (2012). Ggamma1+Ggamma2+Ggamma3 = Gbeta: the search for heterotrimeric G-protein gamma subunits in Arabidopsis is over. *J. Plant Physiol.* 169, 542–545. doi: 10.1016/j.jplph.2011.11.010

Tilman, D., Cassman, K. G., Matson, P. A., Naylor, R., and Polasky, S. (2002). Agricultural sustainability and intensive production practices. *Nature* 418, 671–677. doi: 10.1038/nature01014

Trusov, Y., Chakravorty, D., and Botella, J. R. (2012). Diversity of heterotrimeric G-protein gamma subunits in plants. *BMC Res. Notes* 5:608. doi: 10.1186/1756-0500-5-608

Trusov, Y., Rookes, J. E., Chakravorty, D., Armour, D., Schenk, P. M., and Botella, J. R. (2006). Heterotrimeric G proteins facilitate Arabidopsis resistance to necrotrophic pathogens and are involved in jasmonate signaling. *Plant Physiol.* 140, 210–220. doi: 10.1104/pp.105.069625

Trusov, Y., Rookes, J. E., Tilbrook, K., Chakravorty, D., Mason, M. G., Anderson, D., et al. (2007). Heterotrimeric G protein γ subunits provide functional selectivity in G$\beta\gamma$ dimer signaling in Arabidopsis. *Plant Cell* 19, 1235–1250. doi: 10.1105/tpc.107.050096

Trusov, Y., Sewelam, N., Rookes, J. E., Kunkel, M., Nowak, E., Schenk, P. M., et al. (2009). Heterotrimeric G proteins-mediated resistance to necrotrophic pathogens includes mechanisms independent of salicylic acid-, jasmonic acid/ethylene- and abscisic acid-mediated defense signaling. *Plant J.* 58, 69–81. doi: 10.1111/j.1365-313X.2008.03755.x

Trusov, Y., Zhang, W., Assmann, S. M., and Botella, J. R. (2008). Ggamma1 + Ggamma2 not equal to Gbeta: heterotrimeric G protein Ggamma-deficient mutants do not recapitulate all phenotypes of Gbeta-deficient mutants. *Plant Physiol.* 147, 636–649. doi: 10.1104/pp.108.117655

Urano, D., and Jones, A. M. (2014). Heterotrimeric G protein-coupled signaling in plants. *Annu. Rev. Plant Biol.* 65, 365–384. doi: 10.1146/annurev-arplant-050213-040133

Van Eck, J., and Swartwood, K. (2015). *Setaria viridis*. *Methods Mol. Biol.* 1223, 57–67. doi: 10.1007/978-1-4939-1695-5_5

Vishwakarma, K., Upadhyay, N., Kumar, N., Yadav, G., Singh, J., Mishra, R. K., et al. (2017). Abscisic acid signaling and abiotic stress tolerance in plants: a review on current knowledge and future prospects. *Front. Plant Sci.* 8:161. doi: 10.3389/fpls.2017.00161

Wendt, T., Holme, I., Dockter, C., Preuss, A., Thomas, W., Druka, A., et al. (2016). *HvDep1* is a positive regulator of culm elongation and grain size in barley and impacts yield in an environment-dependent manner. *PLOS ONE* 11:e0168924. doi: 10.1371/journal.pone.0168924

Wolfenstetter, S., Chakravorty, D., Kula, R., Urano, D., Trusov, Y., Sheahan, M. B., et al. (2014). Evidence for an unusual transmembrane configuration of AGG3, a class C Ggamma subunit of Arabidopsis. *Plant J.* 81, 388–398. doi: 10.1111/tpj.12732

Xu, H., Zhao, M., Zhang, Q., Xu, Z., and Xu, Q. (2016). The *DENSE AND ERECT PANICLE 1 (DEP1)* gene offering the potential in the breeding of high-yielding rice. *Breed. Sci.* 66, 659–667. doi: 10.1270/jsbbs.16120

Yadav, D. K., Islam, S. M., and Tuteja, N. (2012). Rice heterotrimeric G-protein gamma subunits (RGG1 and RGG2) are differentially regulated under abiotic stress. *Plant Signal. Behav.* 7, 733–740. doi: 10.4161/psb.20356

Yi, X., Zhang, Z., Zeng, S., Tian, C., Peng, J., Li, M., et al. (2011). Introgression of *qPE9-1* allele, conferring the panicle erectness, leads to the decrease of grain yield per plant in japonica rice (*Oryza sativa* L.). *J Genet Genomics* 38, 217–223. doi: 10.1016/j.jgg.2011.03.011

Zhang, D. P., Zhou, Y., Yin, J. F., Yan, X. J., Lin, S., Xu, W. F., et al. (2015). Rice G-protein subunits *qPE9-1* and *RGB1* play distinct roles in abscisic acid responses and drought adaptation. *J. Exp. Bot.* 66, 6371–6384. doi: 10.1093/jxb/erv350

Zhao, M., Sun, J., Xiao, Z., Cheng, F., Xu, H., Tang, L., et al. (2016). Variations in *DENSE AND ERECT PANICLE 1 (DEP1)* contribute to the diversity of the panicle trait in high-yielding japonica rice varieties in northern China. *Breed. Sci.* 66, 599–605. doi: 10.1270/jsbbs.16058

Zhou, Y., Zhu, J., Li, Z., Yi, C., Liu, J., Zhang, H., et al. (2009). Deletion in a quantitative trait gene qPE9-1 associated with panicle erectness improves plant architecture during rice domestication. *Genetics* 183, 315–324. doi: 10.1534/genetics.109.102681

Conflict of Interest Statement: The authors declare that the research was conducted in the absence of any commercial or financial relationships that could be construed as a potential conflict of interest.

frontiers in Plant Science

MINI REVIEW
published: 25 May 2018
doi: 10.3389/fpls.2018.00652

The Status of *Setaria viridis* Transformation: *Agrobacterium*-Mediated to Floral Dip

Joyce Van Eck[1,2]*

[1] Boyce Thompson Institute, Ithaca, NY, United States, [2] Plant Breeding and Genetics Section, School of Integrative Plant Science, Cornell University, Ithaca, NY, United States

Setaria viridis has many attributes, including small stature and simple growth requirements, that make it attractive as a model species for monocots. Genetic engineering (transformation) methodology is a key prerequisite for adoption of plant species as models. Various transformation approaches have been reported for *S. viridis* including tissue culture-based and *in planta* by *Agrobacterium tumefaciens* infection of floral organs referred to as the floral dip method. The tissue culture-based method utilizes *A. tumefaciens* infection of mature seed-derived callus with subsequent recovery of stable transgenic lines. Vectors found to be most effective contain the hygromycin phosphotransferase selectable marker gene driven by either *Panicum virgatum* or *Zea mays* ubiquitin promoters. As for the floral dip method, there are two reports based on *Agrobacterium* infection of young *S. viridis* inflorescences. Plants were allowed to mature, seeds were collected, and analysis of the progeny verified the presence of transgenes. Each transformation approach, tissue culture-based and floral dip, has advantages and disadvantages depending on the expertise of personnel and resources available. While the tissue culture-based method results in a higher transformation efficiency than floral dip, implementation requires a specific technical skillset that limits availability of experienced personnel to successfully perform transformations. Less technical experience is required for floral dip; however, a lack of high-quality growth chambers or greenhouses that provide the necessary optimum growing conditions would reduce an already low transformation efficiency or would not result in recovery of transgenic lines. An overview of transformation methods reported for *S. viridis* is presented in this review.

Keywords: AGL1, *Agrobacterium tumefaciens*, green bristlegrass, *in planta* transformation, mature-seed derived callus, monocot transformation, *Setaria italica*

Edited by:
Susana Araújo,
Instituto de Tecnologia Química e Biológica (ITQB-NOVA), Portugal

Reviewed by:
Mireille Chabaud,
Institut National de la Recherche Agronomique de Toulouse, France
Kumrop Ratanasut,
Naresuan University, Thailand

***Correspondence:**
Joyce Van Eck
jv27@cornell.edu

Specialty section:
This article was submitted to Plant Breeding, a section of the journal Frontiers in Plant Science

Received: *22 January 2018*
Accepted: *27 April 2018*
Published: *25 May 2018*

Citation:
Van Eck J (2018) The Status of Setaria viridis Transformation: Agrobacterium- Mediated to Floral Dip. Front. Plant Sci. 9:652. doi: 10.3389/fpls.2018.00652

INTRODUCTION

Setaria viridis is the weedy, wild ancestor of the domesticated *Setaria italica* (foxtail millet), which is an important food crop in some eastern Asian countries (Dekker, 2003). *S. viridis*, also known as green bristlegrass, green millet, and green foxtail, is a self-pollinating, small, diploid annual grass (Defelice, 2002). The short stature (10–15 cm) of *S. viridis* compared to the larger size of *S. italica* and other closely related Poaceae family members such as maize, *Miscanthus*, and sugarcane

is an attribute that sparked interest in its development as a model species for important food and bioenergy crops (Brutnell et al., 2010). Being that *S. viridis* is a C4 photosynthesis grass, further interest in *S. viridis* as a model monocot species was driven by the potential of its usefulness in advancing knowledge of the cellular and biochemical mechanisms of C4 photosynthesis (Brutnell et al., 2015).

Setaria viridis has a small genome size (510 Mb) for which genome sequence is available, it has a short generation time of 6–9 weeks, and with its simple growth requirements, large populations can be grown under greenhouse and growth chamber conditions (Li and Brutnell, 2011; Bennetzen et al., 2012). Li and Brutnell (2011) showed that under a short-day photoperiod, *S. viridis* grows to less than 10 cm in height at flowering. *S. viridis* also has a high level of seed production with the potential to produce approximately 34,000 seeds per plant under suitable growing conditions (Stevens, 1932).

Development of genetic engineering methodology, often referred to as transformation, is a key factor when building a model species platform and this was certainly true for establishing *S. viridis* as a model. The ability to introduce or modify genes plays a critical role in gene identification and elucidation of function, which leads to an enhanced understanding of gene networks and mechanisms. Over the past three decades, various techniques have been developed to introduce genes of interest into plant cells. These gene transfer techniques include: direct DNA uptake into protoplasts (Paszkowski et al., 1984), delivery of DNA by particle bombardment (biolistics; Sanford et al., 1987), and by *Agrobacterium tumefaciens*-mediated methods (Gelvin, 2003). There are advantages and disadvantages of each of these approaches that need to be taken into consideration when choosing gene transfer methods for particular plant species. Direct DNA uptake into protoplasts requires methods for plant regeneration, which can be difficult depending on the plant species. For the biolistics method, a gene gun and related supplies are required, which can make this method cost prohibitive for many research groups. In addition, copy number of the introduced transgene needs to be taken into consideration from the standpoint of potential complications with transgene expression, namely, gene silencing (Tang et al., 2007). *Agrobacterium*-mediated transformation results in a lower transgene copy number than delivery by biolistics and the newly reported pollen magnetofection transformation (Zhao et al., 2017). As for *Agrobacterium*-mediated transformation, it is important that the plant material that works best for plant regeneration under tissue culture conditions is amenable to infection yet not adversely affected by the bacterial infection.

Agrobacterium tumefaciens is a soil-borne plant pathogenic bacterium that engineers infected cells to produce metabolites needed to support its growth. More than 30 years ago, researchers modified a strain of *A. tumefaciens* to investigate its utility for transformation of petunia, tobacco, and tomato (Horsch et al., 1985). In the intervening years, there has been a significant number of reports of genetic engineering of both dicots and monocots using *A. tumefaciens*; however, initially, monocots proved to be more problematic (Sood et al., 2011). This was partially due to low efficiency of plant regeneration at that time and, in addition, monocots are not natural hosts of *A. tumefaciens*. Over time, strategies were designed to overcome the barriers of plant regeneration and infection which led to more routine methods for *Agrobacterium*-mediated transformation of several monocot species. Various tissues including immature embryos (Ishida et al., 2007) and regenerable callus derived from immature embryos, immature inflorescences, and mature seeds (Lee et al., 2004; Burris et al., 2009; Song et al., 2011) have been used for *A. tumefaciens*-mediated transformation of monocots. Efforts by researchers worldwide led to advancement of *Agrobacterium* and biolistics approaches for monocot transformation that allowed genetic engineering of the major cereal crops (maize, rice, wheat, barley, sorghum, oats, and millets), which represents roughly two-thirds of the world food supply (Ji et al., 2013). For *S. viridis* transformation methods, there are reports of *Agrobacterium*-mediated transformation of mature seed-derived callus (Brutnell et al., 2010; Van Eck and Swartwood, 2015; Van Eck et al., 2017) and non-tissue culture methods (*in planta*) through infection of immature inflorescences followed by recovery of transgenic seed (Martins et al., 2015a; Saha and Blumwald, 2016).

The purpose of this review is to provide an overview of information presented at the Second International *Setaria* Genetics Conference on the status of genetic engineering approaches developed for *S. viridis* (Zhu et al., 2017). The first report of transformation was based on *Agrobacterium* infection of mature-seed derived callus of *S. viridis* A10.1 (Brutnell et al., 2010). Modifications of this method and strategies to improve the efficiency including decreasing the time for recovery of transgenic lines have been made. In addition to details regarding the tissue-culture-based approach for transformation, a summary of two reports on infection of floral organs in immature inflorescences, commonly referred to as the floral dip method, will also be described here. As evidenced from the collection of reports in this research topic, *S. viridis* has proven to be an effective model and the availability of engineering strategies has contributed to its utility to advance investigations.

AGROBACTERIUM TUMEFACIENS-MEDIATED TRANSFORMATION OF MATURE SEED-DERIVED CALLUS

As indicated earlier, methods for *Agrobacterium*-mediated transformation of *S. viridis* were first reported in 2010 (Brutnell et al., 2010). In brief, the method was based on infection of mature seed-derived callus of *S. viridis* A10.1 with the *A. tumefaciens* strain AGL1 that contained a vector optimized for monocot transformation. The time from infection of callus to recovery of mature T1 seed was approximately 4 months. Depending on the composition of the selectable marker gene cassette in the vectors used for transformation, the transformation efficiency, based on infection of the total number of mature seed-derived calli per experiment, ranged from 5 to 15% (Van Eck et al., 2017). Transformation efficiency is defined as the percentage of infected material that gives rise to at least one independent transgenic line.

The most effective vectors for *S. viridis* transformation were those that contained the hygromycin phosphotransferase selectable marker gene (*hpt*), which confers resistance to the antibiotic hygromycin. The promoter driving *hpt* was also found to be key for efficient transformation. Vectors that contained *hpt* driven by a monocot promoter resulted in recovery of a greater number of transgenic lines compared to vectors where *hpt* expression was under the control of promoters best suited for dicots (Van Eck et al., 2017). In addition, those vectors that had an intron in the *hpt* gene resulted in a greater number of transgenic lines than when an intron was not present in the gene. Similar findings were also reported when a vector with an intron-containing *hpt* was used for rice transformation (Wang et al., 1998). Gene constructs designed with the following vectors were found to be best for *S. viridis* transformation: pWBVec8 (Wang et al., 1998), pOL001 (Vogel and Hill, 2008), pMDC (Curtis and Grossniklaus, 2003), and pANIC (Mann et al., 2012).

In addition to the *hpt* selectable marker gene, vectors used for the development of the *S. viridis* transformation methodology also contained the beta-glucuronidase (GUS) and green fluorescent protein (GFP) reporter genes (Martins et al., 2015b; Van Eck and Swartwood, 2015).

Additional modifications of the *Agrobacterium*-mediated transformation methodology of *S. viridis* A10.1 were also reported by a second group (Martins et al., 2015b). Martins et al. (2015b) followed similar methodology as reported by Van Eck et al. (2017). A comparison of the primary components that make up the various reported transformation methods (Martins et al., 2015b; Van Eck and Swartwood, 2015; Van Eck et al., 2017) is outlined in **Table 1**. The vectors used for transformation, more specifically the type of selectable marker gene and its promoter contained in the vector, were the key parameters that influenced transformation efficiency in the methods described by Martins et al. (2015b). The vector designated p7U resulted in the lowest transformation efficiency at 6%. p7U contained the bialaphos resistance selectable marker gene (*bar*) under control of the ubiquitin promoter from maize. The vectors used for their transformation efforts that resulted in higher transformation efficiencies than p7U contained *hpt* under control of either the CaMV 35S promoter or an enhanced version. In addition, *hpt* in the vectors that resulted in higher levels of transgenic line recovery was either codon optimized for expression in monocots or contained an intron. Wang et al. (1998) demonstrated that an intron-containing version of *hpt* resulted in higher transformation efficiencies for rice than a non-intron-containing version. This result combined with those reported by Van Eck et al. (2017) points to the importance of vector selection, namely, the composition of the selectable marker gene cassette, for *S. viridis* transformation. Researchers should be aware that perhaps a vector that works efficiently for transformation of one monocot species might not work efficiently in a different monocot.

In the years since the first report by Brutnell et al. (2010) on *S. viridis*' potential as a model that also included preliminary information on *Agrobacterium*-mediated transformation of mature seed-derived callus, some key factors related to callus generation and plant regeneration were identified that improved the efficiency of transgenic line recovery (Van Eck and Swartwood, 2015; Van Eck et al., 2017). One of these factors included the gelling agent used in the callus induction medium (CIM). When agar was used as the gelling agent in the CIM, the callus quality was poor and resulted in a low level of plant regeneration. However, the substitution of a gellan gum-type gelling agent (Phytagel or Gelzan) in the CIM greatly improved the callus quality and subsequent plant regeneration. Additional changes such as the substitution of maltose for sucrose, addition of $ZnSO_4$ in the CIM and inclusion of an agar (Phytoblend) as the gelling agent in the plant regeneration medium instead of Phytagel or Gelzan enhanced the recovery of transgenic lines (Van Eck et al., 2017).

TABLE 1 | Comparison of parameters reported for *Agrobacterium tumefaciens*-mediated transformation of mature seed-derived callus of *Setaria viridis*.

Parameters	Van Eck et al.[1]	Martins et al.[1]
Setaria viridis accession	A10.1	A10.1
Agrobacterium tumefaciens strains	AGL1	EHA105
Medium components[1]	MS[2] salts-based CIM[3], zinc sulfate, maltose, and Gelzan	MS salts-based CIM, biotin, sucrose, and Phytagel
Age of callus infected	6–8-weeks-old	4–6-weeks-old
Selectable marker genes[4]	*hpt*	*hpt* and *bar*
Transformation efficiency[5]	A10.1: 5–15%	A10.1: 8–29%

[1]For additional details on media components, see the following: Martins et al., 2015b; Van Eck and Swartwood, 2015; Van Eck et al., 2017. [2]Murashige and Skoog salts' formulation (Murashige and Skoog, 1962). [3]CIM – callus induction medium. [4]hpt – hygromycin phosphotransferase gene which confers resistance to hygromycin; bar – bialaphos resistance gene. [5]Transformation efficiency: percentage of infected callus that gives rise to at least one independent transgenic line. The range in Setaria viridis transformation efficiency resulted from the composition of plant selectable marker gene cassette (gene and its promoter) present in the binary vectors used for transformation experiments.

TABLE 2 | Comparison of parameters reported for floral dip transformation of *Setaria viridis*.

Parameters	Martins et al., 2015b	Saha and Blumwald, 2016
Setaria viridis accession	A10.1	A10.1, 132, 98HT-80
Inflorescence stage	Boot stage	5-days-old spikes
Agrobacterium tumefaciens strain	AGL1	AGL1, EHA105, GV3101, and LBA4404
Vectors	pANIC 6A	Multiple
Selectable marker gene	*hpt*[1]	*hpt*
Transformation efficiency	0.6%[2]	0.5–0.8%[3]

[1]hpt – hygromycin phosphotransferase gene which confers resistance to hygromycin. [2]Transformation efficiency based on the number of PCR-verified transformants/1000 mature seeds collected from infiltrated immature inflorescences. [3]Transformation efficiency based on the number of hygromycin-resistant seedlings recovered after germination on hygromycin-containing medium/total number of seeds tested. The range of transformation efficiency is a result of the effects of different parameters tested.

FLORAL DIP TRANSFORMATION

The ability to deliver genes of interest into plant cells through bypassing tissue culture-based methods, often referred to as *in planta* transformation, has advantages such as specialized equipment (e.g., laminar flow hood) is not required and the introduction of somaclonal variation, that can result in off-type plants, is avoided (Bairu et al., 2011). A non-tissue culture-based method that involves application of *A. tumefaciens* containing gene constructs of interest to floral organs is referred to as floral dip transformation. This method is routinely used for Arabidopsis transformation. Development and modifications of this approach greatly advanced the utilization of Arabidopsis as a model (Clough and Bent, 1998; Somerville and Koornneef, 2002; Zhang et al., 2006). Floral dip methods have also been reported for other plant species including wheat (Agarwal et al., 2009), maize (Mu et al., 2012), and rice (Ratanasut et al., 2017). However, the floral dip transformation approach for these species has not been widely adopted and they are generally transformed by *Agrobacterium*-mediated tissue-culture-based methods or biolistics.

There are two reports for floral dip transformation of *S. viridis* (Martins et al., 2015a; Saha and Blumwald, 2016). In brief, both methods involved exposure of immature inflorescences of *S. viridis* to *A. tumefaciens* containing a gene construct followed by recovery of mature seed that gave rise to plants that were confirmed to be transgenic. Martins et al. (2015a) indicated that 1.5–2 months following floral dipping were required to identify T1 seeds by assessment for red fluorescence. Saha and Blumwald (2016) reported recovery of fertile, transgenic plants within 8–10 weeks of floral dip. Various parameters were evaluated to develop the best approach for this *in planta* transformation method in *S. viridis* and a comparison of parameters reported by both groups is presented in **Table 2**. Martins et al. (2015a) focused their efforts on *S. viridis* A10.1, whereas Saha and Blumwald (2016) utilized three different genotypes: A10.1, 132, and 98HT-80. The 98HT-80 genotype resulted in the highest transformation efficiency at 0.8% and the efficiency of A10.1 reported by both groups was approximately 0.6%. Approaches for determining transformation efficiency differed in the reports. Martins et al. (2015a) based their transformation efficiency on the number of PCR-verified transgenic plants recovered from germination of 1000 seeds harvested from *Agrobacterium*-infected immature inflorescences. However, Saha and Blumwald (2016) based the transformation efficiency on the number of hygromycin-resistant plants recovered following germination of a pre-determined number of seeds on hygromycin-containing medium. These *in planta* methods provide alternative approaches to the tissue culture-based *Agrobacterium* method of infection of callus derived from mature seeds of *S. viridis*.

CONCLUSION

Robust methods for genetic engineering whether it be tissue culture-based or *in planta* are critical for dissecting the intricacies of gene function and networks. Knowledge gained from gene function studies helps guide development of strategies for crop improvement. This is true whether these gene function studies are performed directly in crop species or models that result in translatable information to crops. The genetic engineering resources described here for *S. viridis* combined with attributes that make it an ideal model system have advanced many studies that might not otherwise have been realized (Huang et al., 2016). The availability of tissue culture-based and *in planta* transformation methods provides options for performing gene function studies in *S. viridis* and allows application of new technologies such as gene editing. While there are advantages and disadvantages as described in this review for each transformation method, researchers need to investigate the different methods to determine the approach that is most feasible and reproducible in their labs. Advances in genetic engineering methods, such as the recently reported pollen magnetofection in cotton (Zhao et al., 2017), along with continued development of genetic and genomic resources will greatly benefit the *Setaria* research community.

AUTHOR CONTRIBUTIONS

The author confirms being the sole contributor of this work and approved it for publication.

FUNDING

The author acknowledges the National Science Foundation Plant Genome Research Program (IOS-1546882) for support related to her research on genetic engineering of *Setaria viridis*.

REFERENCES

Agarwal, S., Loar, S., Steber, C., and Zale, J. (2009). "Floral transformation of wheat," in *Transgenic Wheat, Barley and Oats: Production and Characterization Protocols*, eds D. H. Jones and R. P. Shewry (Totowa, NJ: Humana Press), 105–113. doi: 10.1007/978-1-59745-379-0_6

Bairu, M. W., Aremu, A. O., and Van Staden, J. (2011). Somaclonal variation in plants: causes and detection methods. *Plant Growth Regul.* 63, 147–173. doi: 10.1007/s10725-010-9554-x

Bennetzen, J. L., Schmutz, J., Wang, H., Percifield, R., Hawkins, J., Pontaroli, A. C., et al. (2012). Reference genome sequence of the model plant Setaria. *Nat. Biotechnol.* 30, 555–561. doi: 10.1038/nbt.2196

Brutnell, T. P., Bennetzen, J. L., and Vogel, J. P. (2015). *Brachypodium distachyon* and *Setaria viridis*: model genetic systems for the grasses. *Annu. Rev. Plant Biol.* 66, 465–485. doi: 10.1146/annurev-arplant-042811-105528

Brutnell, T. P., Wang, L., Swartwood, K., Goldschmidt, A., Jackson, D., Zhu, X. G., et al. (2010). *Setaria viridis*: a model for C4 photosynthesis. *Plant Cell* 22, 2537–2544. doi: 10.1105/tpc.110.075309

Burris, J. N., Mann, D. G., Joyce, B. L., and Stewart, C. N. (2009). An improved tissue culture system for embryogenic callus production and plant regeneration in switchgrass (*Panicum virgatum* L.). *Bioenergy Res.* 2, 267–274. doi: 10.1007/s12155-009-9048-8

Clough, S. J., and Bent, A. F. (1998). Floral dip: a simplified method for *Agrobacterium*-mediated transformation of *Arabidopsis thaliana*. *Plant J.* 16, 735–743. doi: 10.1046/j.1365-313x.1998.00343.x

Curtis, M. D., and Grossniklaus, U. (2003). A gateway cloning vector set for high-throughput functional analysis of genes in planta. *Plant Physiol.* 133, 462–469. doi: 10.1104/pp.103.027979

Defelice, M. S. (2002). Green foxtail, *Setaria viridis* (L.) P. Beauv. *Weed Technol.* 16, 253–257. doi: 10.1614/0890-037X(2002)016[0253:GFSVLP]2.0.CO;2

Dekker, J. (2003). The foxtail (*Setaria*) species-group. *Weed Sci.* 51, 641–656. doi: 10.1614/P2002-Ir

Gelvin, S. B. (2003). *Agrobacterium*-mediated plant transformation: the biology behind the "gene-jockeying" tool. *Microbiol. Mol. Biol. Rev.* 67, 16–37. doi: 10.1128/MMBR.67.1.16-37.2003

Horsch, R. B., Fry, J. E., Hoffmann, N. L., Eichholtz, D., Rogers, S. G., and Fraley, R. T. (1985). A simple and general-method for transferring genes into plants. *Science* 227, 1229–1231. doi: 10.1126/science.227.4691.1229

Huang, P., Shyu, C., Coelho, C. P., Cao, Y., and Brutnell, T. P. (2016). *Setaria viridis* as a model system to advance millet genetics and genomics. *Front. Plant Sci.* 7:1781. doi: 10.3389/fpls.2016.01781

Ishida, Y., Hiei, Y., and Komari, T. (2007). *Agrobacterium*-mediated transformation of maize. *Nat. Protoc.* 2, 1614–1621. doi: 10.1038/nprot.2007.241

Ji, Q., Xu, X., and Wang, K. (2013). Genetic transformation of major cereal crops. *Int. J. Dev. Biol.* 57, 495–508. doi: 10.1387/ijdb.130244kw

Lee, S. H., Lee, D. G., Woo, H. S., and Lee, B. H. (2004). Development of transgenic tall fescue plants from mature seed-derived callus via *Agrobacterium*-mediated transformation. *Asian Australas. J. Anim.* 17, 1390–1394. doi: 10.5713/ajas.2004.1390

Li, P., and Brutnell, T. P. (2011). *Setaria viridis* and *Setaria italica*, model genetic systems for the Panicoid grasses. *J. Exp. Bot.* 62, 3031–3037. doi: 10.1093/jxb/err096

Mann, D. G., Lafayette, P. R., Abercrombie, L. L., King, Z. R., Mazarei, M., Halter, M. C., et al. (2012). Gateway-compatible vectors for high-throughput gene functional analysis in switchgrass (*Panicum virgatum* L.) and other monocot species. *Plant Biotechnol. J.* 10, 226–236. doi: 10.1111/j.1467-7652.2011.00658.x

Martins, P. K., Nakayama, T. J., Ribeiro, A. P., Cunha, B., Nepomuceno, A. L., Harmon, F. G., et al. (2015a). *Setaria viridis* floral-dip: a simple and rapid *Agrobacterium*-mediated transformation method. *Biotechnol. Rep.* 6, 61–63. doi: 10.1016/j.btre.2015.02.006

Martins, P. K., Ribeiro, A. P., Cunha, B., Kobayashi, A. K., and Molinari, H. B. C. (2015b). A simple and highly efficient *Agrobacterium*-mediated transformation protocol for *Setaria viridis*. *Biotechnol. Rep.* 6, 41–44. doi: 10.1016/j.btre.2015.02.002

Mu, G., Chang, N., Xiang, K., Sheng, Y., Zhang, Z., and Pan, G. (2012). Genetic transformation of maize female inflorescence following floral dip method mediated by *Agrobacterium*. *Biotechnology* 11, 178–183. doi: 10.3923/biotech.2012.178.183

Murashige, T., and Skoog, F. (1962). A revised medium for rapid growth and bio assays with tobacco tissue cultures. *Physiol. Plant.* 15, 473–497. doi: 10.1111/j.1399-3054.1962.tb08052.x

Paszkowski, J., Shillito, R. D., Saul, M., Mandak, V., Hohn, T., Hohn, B., et al. (1984). Direct gene transfer to plants. *EMBO J.* 3, 2717–2722. PMCID: PMC557758

Ratanasut, K., Rod-In, W., and Sujipuli, K. (2017). *In planta Agrobacterium*-mediated transformation of rice. *Rice Sci.* 24, 181–186. doi: 10.1016/j.rsci.2016.11.001

Saha, P., and Blumwald, E. (2016). Spike-dip transformation of *Setaria viridis*. *Plant J.* 86, 89–101. doi: 10.1111/tpj.13148

Sanford, J. C., Klein, T. M., Wolf, E. D., and Allen, N. (1987). Delivery of substances into cells and tissues using a particle bombardment process. *Particul. Sci. Technol.* 5, 27–37. doi: 10.1080/02726358708904533

Somerville, C., and Koornneef, M. (2002). A fortunate choice: the history of *Arabidopsis* as a model plant. *Nat. Rev. Genet.* 3, 883–889. doi: 10.1038/nrg927

Song, G. Q., Walworth, A., and Hancock, J. F. (2011). Factors influencing *Agrobacterium*-mediated transformation of switchgrass cultivars. *Plant Cell Tissue Organ Cult.* 108, 445–453. doi: 10.1007/s11240-011-0056-y

Sood, P., Bhattacharya, A., and Sood, A. (2011). Problems and possibilities of monocot transformation. *Biol. Plant.* 55, 1–15. doi: 10.1007/s10535-011-0001-2

Stevens, O. A. (1932). The number and weight of seeds produced by weeds. *Am. J. Bot.* 19, 784–794. doi: 10.2307/2436042

Tang, W., Newton, R. J., and Weidner, D. A. (2007). Genetic transformation and gene silencing mediated by multiple copies of a transgene in eastern white pine. *J. Exp. Bot.* 58, 545–554. doi: 10.1093/jxb/erl228

Van Eck, J., and Swartwood, K. (2015). "*Setaria viridis*," in *Agrobacterium Protocols*, Vol. 1, ed. K. Wang (New York, NY: Springer), 57–67. doi: 10.1007/978-1-4939-1695-5_5

Van Eck, J., Swartwood, K., Pidgeon, K., and Maxson-Stein, K. (2017). "*Agrobacterium tumefaciens*-mediated transformation of *Setaria viridis*," in *Genetics and Genomics of Setaria*, eds A. Doust and X. Diao (Cham: Springer International Publishing), 343–356. doi: 10.1007/978-3-319-45105-3_20

Vogel, J., and Hill, T. (2008). High-efficiency *Agrobacterium*-mediated transformation of *Brachypodium distachyon* inbred line Bd21-3. *Plant Cell Rep.* 27, 471–478. doi: 10.1007/s00299-007-0472-y

Wang, M. B., Li, Z. Y., Matthews, P. R., and Upadhyaya, N. M. (1998). Improved vectors for *Agrobacterium tumefaciens*-mediated transformation of monocot plants. *Acta Hortic.* 461, 401–407. doi: 10.17660/ActaHortic.1998.461.46

Zhang, X., Henriques, R., Lin, S. S., Niu, Q. W., and Chua, N. H. (2006). *Agrobacterium*-mediated transformation of *Arabidopsis thaliana* using the floral dip method. *Nat. Protoc.* 1, 641–646. doi: 10.1038/nprot.2006.97

Zhao, X., Meng, Z., Wang, Y., Chen, W., Sun, C., Cui, B., et al. (2017). Pollen magnetofection for genetic modification with magnetic nanoparticles as gene carriers. *Nat. Plants* 3, 956–964. doi: 10.1038/s41477-017-0063-z

Zhu, C., Yang, J., and Shyu, C. (2017). Setaria comes of age: meeting report on the Second International Setaria Genetics Conference. *Front. Plant Sci.* 8:1562. doi: 10.3389/fpls.2017.01562

Conflict of Interest Statement: The author declares that the research was conducted in the absence of any commercial or financial relationships that could be construed as a potential conflict of interest.

frontiers in Plant Science

REVIEW
published: 29 May 2018
doi: 10.3389/fpls.2018.00719

Domestication and Improvement in the Model C4 Grass, Setaria

*Hao Hu, Margarita Mauro-Herrera and Andrew N. Doust**

Department of Plant Biology, Ecology, and Evolution, Oklahoma State University, Stillwater, OK, United States

Setaria viridis (green foxtail) and its domesticated relative *S. italica* (foxtail millet) are diploid C4 panicoid grasses that are being developed as model systems for studying grass genomics, genetics, development, and evolution. According to archeological evidence, foxtail millet was domesticated from green foxtail approximately 9,000 to 6,000 YBP in China. Under long-term human selection, domesticated foxtail millet developed many traits adapted to human cultivation and agricultural production. In comparison with its wild ancestor, foxtail millet has fewer vegetative branches, reduced grain shattering, delayed flowering time and less photoperiod sensitivity. Foxtail millet is the only present-day crop in the genus *Setaria*, although archeological records suggest that other species were domesticated and later abandoned in the last 10,000 years. We present an overview of domestication in foxtail millet, by reviewing recent studies on the genetic regulation of several domesticated traits in foxtail millet and discuss how the foxtail millet and green foxtail system could be further developed to both better understand its domestication history, and to provide more tools for future breeding efforts.

Keywords: Setaria, foxtail millet, genetic control, domestication, shattering, plant architecture, flowering time, photoperiod

OPEN ACCESS

Edited by:
Roberto Papa,
Università Politecnica delle Marche, Italy

Reviewed by:
Karolina Susek,
Institute of Plant Genetics (PAN), Poland
Matthew Nicholas Nelson,
Royal Botanic Gardens, Kew, United Kingdom

***Correspondence:**
Andrew N. Doust
andrew.doust@okstate.edu

Specialty section:
This article was submitted to Plant Breeding, a section of the journal Frontiers in Plant Science

Received: *13 January 2018*
Accepted: *14 May 2018*
Published: *29 May 2018*

Citation:
Hu H, Mauro-Herrera M and Doust AN (2018) Domestication and Improvement in the Model C4 Grass, Setaria. Front. Plant Sci. 9:719. doi: 10.3389/fpls.2018.00719

INTRODUCTION

The evolution of human civilization is in many ways written on the back of grass domestication. Cereal grains directly or indirectly provide approximately half of the calories that support human populations (Emily et al., 2013). Furthermore, forage provided by both wild and improved grasses feed domesticated animal herds in much of the world. Grasses have also figured prominently in unraveling the domestication process and its relationship to evolution via natural selection (Doust, 2007a; Glemin and Bataillon, 2009). Despite this importance, differences in the details of domestication amongst the various lineages of grasses raise the question of whether there is a single model of domestication in the grasses or unique paths to similar phenotypes. Some phenotypes appear conserved (at least for cereal crops like rice, wheat, and maize), such as the change from a freely dispersed propagule to one that is hard to dislodge, and therefore reliably harvested from the plant ("non-shattering") (Purugganan and Fuller, 2009). However, even this change, which has the practical result of retaining seeds on the plant, appears to involve different combinations of floral and inflorescence parts, and be controlled by different genes in different domestication events (Doust et al., 2014b). In this context, it is worth considering whether increasing the number of cereal domestication events that we study can help us better understand underlying processes of domestication. Here, we use the term 'event' to signify an independent domestication, while recognizing that the process of domestication is not an instantaneous change from wild to domesticated forms (Allaby et al., 2017). In recent years,

insights into the domestication process have increased rapidly, in part driven by the increased ease of genome sequencing. Rice (*Oryza sativa*)was the first sequenced grass genome (Goff et al., 2002; Yu et al., 2002; Matsumoto et al., 2005), followed by sorghum (*Sorghum bicolor*) (Paterson et al., 2009), *Brachypodium* (Vogel et al., 2010), maize (*Zea mays*) (Schnable et al., 2009), and various others, including foxtail millet (*Setaria italica*) (Bennetzen et al., 2012; Zhang et al., 2012), pearl millet (*Pennisetum glaucum*) (Varshney et al., 2017), *Oropetium* (VanBuren et al., 2015), and *Dichanthelium* (Studer et al., 2016). A new wave of investigation has recently started to target the wild progenitors of crop species, including the ancestor of maize, teosinte, and several ancestors of wheat (Jia et al., 2013a; Ling et al., 2013; Yang et al., 2017). These resources are providing new insights into domestication, and new opportunities for selection and improvement of under-utilized grain crops.

Foxtail millet (*S. italica*) is an ancient cereal grain crop of Northern China, that was grown in rotation with winter wheat in the regions around the Yellow River (Diao and Jia, 2017b). It is now grown in China, India, and Africa, excelling as a drought and low nutrient tolerant grain (Goron and Raizada, 2015; Nadeem et al., 2018). Its wild ancestor, green foxtail (*S. viridis*), is a widespread weed of temperate regions worldwide (Dekker, 2003). Foxtail millet principally differs from green foxtail in reduced vegetative branching, greater height, increased inflorescence branching, and larger seeds (**Figure 1**). Draft genomes are now available for both foxtail millet (*S. italica*) and its wild ancestor, green foxtail (*S. viridis*) (*Setaria viridis* v1.1, DOE-JGI[1]).

The genus *Setaria* belongs to the subtribe Cenchrinae and tribe Paniceae within the subfamily Panicoideae (Kellogg, 2017). All species possess the C4 photosynthetic pathway, and close relatives include pearl millet (formerly *Pennisetum glaucum*, now *Cenchrus glaucum*), (Chemisquy et al., 2010), napier grass (*C. purpureum*), and switchgrass (*Panicum virgatum*). The sister tribe is the Andropogoneae, which includes the important crop species maize (*Z. mays*), sorghum (*Sorghum bicolor*), and sugar cane (*Saccharum officinarum*) (Doust et al., 2009). *Setaria* is the largest genus in the Cenchrinae, and consists of approximately 100 species that are widely distributed in warm and temperate regions worldwide (Kellogg, 2017). The known domesticated crops in this genus include foxtail millet, yellow foxtail (*S. pumila*), and plains bristle grass (*S. macrostachya*), but foxtail millet is the only one that remains a major crop (Austin, 2006; Diao and Jia, 2017b). Other members of the genus, including green foxtail, are invasive weeds in corn and soybean field in many parts of the world (Dekker, 2003; Darmency et al., 2017). Besides *Setaria* and *Cenchrus*, the Cenchrinae clade also includes several smaller genera whose evolutionary relationships are not well understood (Doust et al., 2007; Kellogg, 2015, 2017). The relationships of foxtail millet and its wild progenitor, green foxtail, with respect to other species in the genus are unclear, as all studies to date have shown *Setaria* to be either para- or polyphyletic, depending on its circumscription (Doust et al., 2007; Kellogg et al., 2009; Kellogg, 2015). However, foxtail millet and green foxtail belong to a small well-supported clade, along with the tetraploid species, *S. verticillata* and *S. faberi* (Wang et al., 2009). *S. faberi* is an allotetraploid, with both genomes closely related to green foxtail, whereas *S. verticillata* appears to have one genome related to green foxtail, and the other to more distantly related species (Kellogg et al., 2009; Layton and Kellogg, 2014; Kellogg, 2017). The clade appears to be Asian in origin, even though the three wild species are all now widely distributed weeds.

Genetic analyses on foxtail millet, which date from at least the 1930's, concentrated on the genetics of distinct phenotypes, such as spikelet-tipped bristles and purple bristles (Ayyangar et al., 1933). Experiments on crossing in foxtail millet were also performed, and the difficulties in crossing the small flowers of these inbreeding plants was first discussed (Li et al., 1935). Much breeding work continued in China over the years since that time (Diao and Jia, 2017a), but only a few population genetic and herbicide resistance papers were published in English until the end of the last century. These included investigations into the origin of domestication of foxtail millet, which used a variety of markers to test hypotheses of origins in Northern China, South Asia, and the hypothesis of twin origins, in both China and Europe (Kawase and Sakamoto, 1984; Jusuf and Pernes, 1985; Darmency et al., 1987; Wang et al., 1995b; Fukunaga et al., 1997; Li et al., 1998; Nakayama et al., 1998; Le Thierry d'Ennequin et al., 2000). More recently, comparative genomic studies used common SSR markers to infer syntenic relationships between multiple grass genomes, including foxtail millet (Wang et al., 1998), and showed how the nine chromosomes of *Setaria* are simple rearrangements of the twelve chromosomes of rice (Brutnell et al., 2015). In addition, the same mapping population used to create the genetic maps that were the basis of comparative genome analyses was later used to identify quantitative trait loci (QTL) underlying phenotypic traits of both the vegetative body and inflorescence of *Setaria* (Doust et al., 2004, 2005; Doust and Kellogg, 2006). After the creation of advanced generation RILs, this population was also used to analyze the genetic determinants of traits such as branching (Mauro-Herrera and Doust, 2016; Doust, 2017), shattering (Doust et al., 2014a; Odonkor, 2015), height (Mauro-Herrera and Doust, 2016; Doust, 2017; Feldman et al., 2017), flowering time (Mauro-Herrera et al., 2013; Doust, 2017), and biomass (Mauro-Herrera et al., 2013; Mauro-Herrera and Doust, 2016; Doust, 2017; Feldman et al., 2017; Banan et al., 2018).

In 2012, the Setaria reference genome was independently released by two groups from the United States (Bennetzen et al., 2012) and China (Zhang et al., 2012). The United States group sequenced the foxtail millet inbred line *Yugu1* using the Sanger platform, and generated a 396.7 Mb assembly with 80% genome coverage and 35,158 annotated loci (Bennetzen et al., 2012). The Chinese group reported a genome from cultivated foxtail millet cv. *Zhanggu* sequenced with the Illumina platform, producing a ∼423 Mb draft that covered ∼86% of the total genome, with 38,801 genes annotated (Zhang et al., 2012). The genome assemblies allowed many more markers to be identified and denser linkage maps to be created, resulting in increased precision of QTL analysis (Kumari et al., 2013; Mauro-Herrera et al., 2013; Pandey et al., 2013; Zhang et al., 2014; Fang

[1]http://phytozome.jgi.doe.gov/

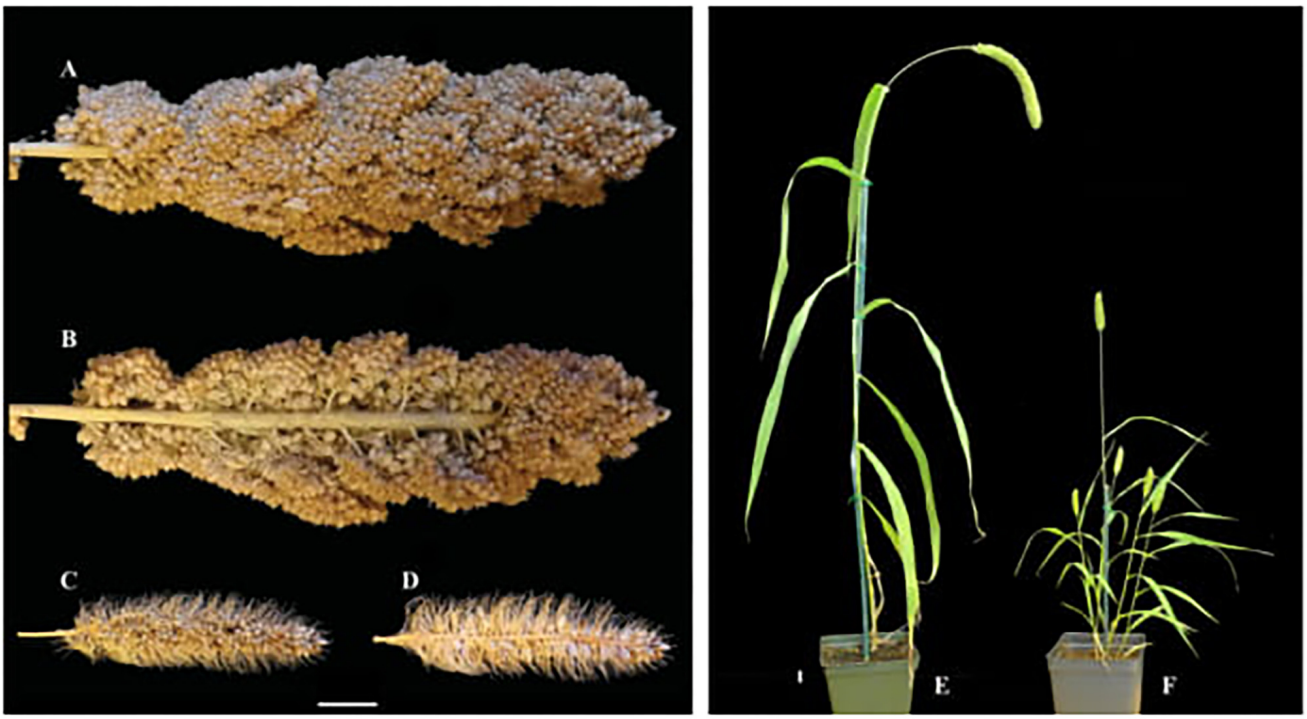

FIGURE 1 | Morphological comparison of domesticated foxtail millet and its wild ancestor green foxtail. Whole and longitudinal section of foxtail millet **(A,B)** and green foxtail **(C,D)** panicles. Whole plant of foxtail millet **(E)** and green foxtail **(F)**.

et al., 2016; Mauro-Herrera and Doust, 2016). Further reduced representation sequencing has also allowed dense marker maps to be generated for mapping populations (Fahlgren et al., 2015; Feldman et al., 2017). The genome sequence of the wild parent, green foxtail, of the Wang et al. (1998) mapping population is available (acc. *A10.1*), although there is as yet no publicly available genome for the foxtail millet accession, *B100*, the female parent of this population. Several other mapping populations have been created, both between foxtail millet and green foxtail (Qie et al., 2014), and within foxtail millet (Zhang K. et al., 2017), although none of them have been used to directly address the genetic changes that occurred during domestication.

In the last 10 years, the Setaria system (comprising foxtail millet and its wild progenitor green foxtail) has been promoted as an experimental model system for studying grass genetics and biofuel production (Doust et al., 2009; Brutnell et al., 2010, 2015; Li and Brutnell, 2011) (**Figure 1**). Both species possess several significant advantages over related C4 panicoid grasses such as maize and sorghum, including short life cycle, small size, simple growth requirements and ease of transformation (Brutnell et al., 2010). Difficulties with making controlled crosses between accessions, owing to small size of the individual flowers, has been addressed successfully by both temperature and chemical interventions to kill pollen in the female parent (Jiang et al., 2013; Zhang H.Y. et al., 2017), and much work has also been done on overcoming seed dormancy issues (Sebastian et al., 2014; Brenner et al., 2015; Acharya et al., 2017). Following recommendations made at the First international Setaria Genetics Conference in Beijing in 2014, we have adopted the name Setaria (capitalized, no italics) for this model system (foxtail millet and green foxtail) while *Setaria* (capitalized, italics) remains the correct form for the genus name (Diao et al., 2014; Doust and Diao, 2017).

THE DOMESTICATION OF FOXTAIL MILLET

The most recent evidence to date suggests that domestication of foxtail millet occurred between 9,000 and 6,000 YBP in China, before being brought west into Europe (Diao and Jia, 2017b). Other hypotheses have included origins in Europe and in west Asia (Jones, 2004; Nasu et al., 2007). A separate origin in Europe is based on the relatively early appearance of foxtail millet grains in the European archeological record (4,000–3,000 YBP) (Nasu et al., 2007), and genetic evidence that European foxtail millet genotypes are more closely related to co-occurring green foxtail genotypes than to foxtail millet from China (Le Thierry d'Ennequin et al., 2000). However, recent studies of the movement of starchy grains across Eurasia have concluded that movement can be much faster by trade than formerly assumed (Lightfoot et al., 2013), and that the close relationship of foxtail millet and green foxtail in Europe is likely the result of hybridization between foxtail millet and green foxtail in Europe (Le Thierry d'Ennequin et al., 2000; Austin, 2006). Beyond archeological evidence, a recent genomic study that sequenced

916 foxtail millet accessions suggested a single domestication event of foxtail millet in China (Jia et al., 2013b). Green foxtail accessions in China show a strong relationship to Chinese foxtail millet accessions, indicative of continued gene flow after domestication. The Chinese green foxtail accessions are distinct from populations in North America, some of which apparently arrived there prior to European settlement (Huang et al., 2014; Huang and Feldman, 2017; Schroder et al., 2017).

A recent review of archeological finds from China suggests that the domestication and widespread adoption of foxtail millet in China involved three phases (Diao and Jia, 2017b). The first was the pre-domestication phase (23,000 to 9,000 YBP), where several archeological finds of plant starches and stone tools for processing green foxtail and/or foxtail millet seeds have been found (Yang et al., 2012; Jia et al., 2013b). However, intact grains have not been recovered for this phase. The second phase was that of domestication (9,000 to 6,000 YBP), where foxtail millet grains have been found in multiple archeological sites in northern China, especially in the Yellow River region (Lü et al., 2009). These finds indicate that foxtail millet was being cultivated as a food crop. The third phase was the expansion phase (after 6,000 YBP), a phase during which large quantities of foxtail millet grains have been found in hundreds of archeological sites, especially in southern and western China (Lü et al., 2005, 2014). The evidence from archeological sites in the expansion phase suggests that foxtail millet had spread to several major regions of ancient China, and that cultivation had become widespread. In addition, after 6,000 YBP, foxtail millet had quickly spread to other regions, and foxtail millet grains have been recovered from archeological sites from Eastern Siberia (5,550–4,050 YBP) (Sergusheva and Vostretsov, 2009), Korea (5,500 YBP) (Lee, 2011), and Japan (4,000 YBP) (Crawford, 1992).

THE GENETICS OF DOMESTICATION

Although green foxtail and foxtail millet are usually described as separate species (Austin, 2006), recent studies have increasingly led to the conclusion that foxtail millet is just a domesticated version of green foxtail (Doust et al., 2009). The genetic evidence includes both isozyme (Wang et al., 1995a) and DNA marker analyses (Wang et al., 1998; Hirano et al., 2011; Li et al., 2012). Wang et al. (2010), using 50 accessions of cultivated foxtail and 34 of green foxtail, determined that foxtail millet only contained 55% of the diversity of green foxtail, and that domestication occurred in China approximately 8700 years ago. They did not find fixed differences between the cultivars and their wild relatives, but did find a high proportion of shared polymorphisms, particularly for the cultivars. On average, domesticated foxtail millet shared almost 75% of its polymorphisms with green foxtail, whereas the proportion for green foxtail was 36%. Unique polymorphisms were present in both species, but were much less prevalent in cultivars than in the wild species. They suggested that the domestication bottleneck in foxtail millet was more severe than in maize, but slightly less than in rice. More recent studies, on Chinese and on two sets of North American collections, have provided new insights into the relationships and diversity of foxtail and green foxtail. The large degree of overlap found by Wang et al. (2010) in Chinese foxtail millet and green foxtail accessions may be due to their long shared history, as recent analyses of green foxtail accessions from North America, China, and other regions, found two main groups in North America, and a third group that was more foxtail millet-like, and to which all of the Chinese accessions belonged (Huang et al., 2014; Schroder et al., 2017). A recent sequence study of multiple varieties of foxtail millet identified selective sweeps between landrace and improved varieties indicative of selection after domestication, as well as regions of low diversity in all varieties, indicative of a domestication bottleneck (Jia et al., 2013c). Jia et al. (2013c) focused on a low-diversity region on chromosome 9 that contains the SH1 locus, whose orthologous locus in sorghum has been shown to control abscission of the grain (shattering) (Lin et al., 2012). Further analysis of the genetic signature of domestication is necessary to understand the extent to which domestication in foxtail millet is similar to processes in other cereal grains.

GENES CONTRIBUTING TO DOMESTICATION-RELATED TRAITS

The identification of genes responsible for domestication traits in Setaria is still in its early stages, although multiple studies have highlighted genomic regions which appear to harbor causal loci (Doust et al., 2004, 2005, 2017; Mauro-Herrera et al., 2013; Odonkor, 2015; Mauro-Herrera and Doust, 2016; Coelho et al., 2017; Feldman et al., 2017; Wang et al., 2017). Some of these also appear to colocate with regions controlling domestication or improvement traits in other species (Mauro-Herrera et al., 2013; Doust et al., 2014b). Conservation of genes responsible for domestication was first noted by Paterson et al. (1995), and may indicate a shared genetic mechanism for changes in traits between wild and domesticated species. However, Bennetzen et al. (2012) compared sequences of several candidate domestication genes, such as *Q*, *qSH1*, *tb1*, etc., between foxtail millet and green foxtail, and found no coding differences, suggesting that the domestication of foxtail millet involved either a different set of loci, or regulation mechanisms that were not obvious by simple sequence comparison. Further work has refined and extended these observations, and we discuss below the evidence for genetic control of several domestication and improvement phenotypes.

Shattering

Seed shattering, or seed dispersal, is the mechanism by which plants disperse seeds at maturity. However, it is an unfavorable trait for cereal crops in agricultural production, because it leads to reduction in harvesting and grain yield (Li and Olsen, 2016). The loss of the seed-shattering habit is thought to be one of the most important events in seed crop domestication, and it is a critical feature that distinguishes modern crops from their wild progenitors (Li and Olsen, 2016). In grasses, the position and method of seed shattering is regulated by where abscission zones are formed. An abscission zone (AZ) can be formed in a variety of positions on the pedicel of the spikelet or on subtending branches, but in Setaria is underneath the glumes, so that the whole spikelet,

containing one seed, falls off as a unit (Doust et al., 2014b). Hodge and Kellogg (2016) studied the anatomy and histology of AZs in both green foxtail and foxtail millet, but, unlike sorghum, rice or barley, no notable lignification was observed in the AZ of Setaria. However, cellular staining identified subtle differences of cell size, orientation and arrangement between green foxtail and foxtail millet, particularly in the non-shattering foxtail millet line *Yugu1*. The tensile strength that is required to remove a spikelet from the pedicel is much lower in wild green foxtail than domesticated foxtail millet, and a discrete cup-shaped structure remains after dispersal of the grain. In foxtail millet, however, a force able to remove the grain from the inflorescence usually results in a break in the pedicel rather than in the abscission zone beneath the glumes (Doust et al., 2014a).

Doust et al. (2014a) evaluated seed shattering in an F7 RIL mapping population of Setaria, and identified two significant QTLs – one locus (QTL1) on chromosome 9 that contributes more than 35% of the phenotypic variation, and the other locus (QTL2) on chromosome 5 that is responsible for about 8% (**Table 1**). They also found that there was no significant genetic interaction between QTL1 and any other loci, including QTL2, whereas QTL2 shows epistatic interactions with several other genomic locations. QTL1 is syntenic to the region on sorghum chromosome 1 that contains the SH1 locus, identified as the major locus controlling shattering in that species (Lin et al., 2012). The same locus was also detected in an analysis of genome variability in 916 diverse foxtail millet varieties (Jia et al., 2013b), where an 855-bp indel in coding sequence was found when compared with green foxtail (**Figure 2**). In addition, all foxtail millet varieties show very low sequence diversity in this region when compared with the wild progenitor green foxtail. Odonkor (2015) identified the sorghum SH1 homologous in chromosome 9 as a candidate gene for seed shattering in foxtail millet, and suggested that a miniature inverted-repeat transposable element (MITE) insertion leads to the non-shattering phenotype in foxtail millet. These lines of evidence strongly suggest that the *Setaria* ortholog of the SH1 locus controls much of the shattering phenotype in and Setaria. The second QTL, QTL2, identified by Doust et al. (2014a), is overlapped by a region showing a strong selective sweep in the GWAS study by Jia et al. (2013b) (**Figure 2**). However, the selective sweep differentiates landrace and modern varieties, with greater diversity in landrace varieties, suggesting that QTL2 was selected upon after domestication and during the improvement of the crop. This region harbors the ortholog of *qSH1*, a major seed shattering gene in rice. If the *qSH1* homolog is confirmed as the causal gene in QTL2 it may suggest that it was selected upon during crop improvement rather than in the initial stages of domestication. Thus for shattering it is possible that there is a shared conserved genetic mechanism that spans multiple species.

Plant Height

Height is a trait that may be targeted by human selection during crop domestication and improvement, and there is significant variation in height in landrace varieties of foxtail millet, and within green foxtail accessions (Li and Yang, 2008; Chander et al., 2017a,b; Ghimire et al., 2018). Differences in height amongst landrace varieties may reflect both an ancestral increase in height took place as selection for losing unproductive tillers, followed by differentiation as farmers in different localities targeted height for a variety of reasons, including grain production and foraging. The GWAS analysis of 916 foxtail millet varieties by Jia et al. (2013b) documented genomic regions showing strong association with plant height on chromosomes 2, 4, and 6, while Fang et al. (2016) used an F2 population from a cross between two foxtail millet varieties, and found four height related QTLs on chromosomes 1, 3, 6, and 7. Recent studies on height in the F7 recombinant inbred line mapping population derived from that of Wang et al. (1998) identified major height-related QTLs on chromosomes 5, 7, and 9, with the effect of the different QTL being expressed at different developmental stages. Thus, for example, the QTL on chromosome 5 controls at least half of the variation in height at the seedling stage, but less variation at flowering and during seed maturation (Mauro-Herrera and Doust, 2016; Feldman et al., 2017). Only a few QTL overlap between the different studies (**Figure 2**), suggesting that both environmental and genotypic variation between trials contribute to differences in genetic regulation. The genes underlying these QTL have yet to be definitively isolated, but mapping efforts of several mutants are ongoing (Xue et al., 2016; Fan et al., 2017). The QTL regions also contain known candidate genes for height change, including, on chromosome V, the ortholog of *SEMIDWARF 1* (*SD1*), a gene that was important in breeding semi-dwarf rice varieties for the Green Revolution (Ashikari et al., 2002; Asano et al., 2011). Further work needs to be done to show that these genes actually control height, or to explain how different genes control height at different developmental stages.

Plant Branching

Vegetative branching significantly contributes to the determination of plant architecture (Doust, 2007a,b; McSteen, 2009; Hodge and Doust, 2017), and involves complicated genetic and environmental regulation (Finlayson et al., 2010). Human-directed selection and domestication has led to a dramatic reduction in vegetative branching in Setaria, presumably as a response to increased planting density and increases in seed weight and number of seeds per inflorescence (Doust, 2007a). Doust et al. (2004) reported the first QTL analysis of basal (tillering) and aerial branching in Setaria, and identified four QTLs for tillering on chromosomes 1, 3, and 4, and four QTLs for aerial branching on chromosomes 4, 5, and 9. Interestingly, the ortholog of *tb1*, a major gene controlling branching in maize, was found to associate with only a minor QTL for branching in Setaria (Doust et al., 2004), as was also reported in the closely related species, pearl millet (Poncet et al., 2002). A further study of trials in different greenhouse conditions and between greenhouse and field trials revealed substantial genotype by environment (G × E) relationships (Doust and Kellogg, 2006; Mauro-Herrera and Doust, 2016). Comparison with the GWAS analysis of 916 foxtail millet varieties by Jia et al. (2013b) showed several regions of overlap but also many unique QTL, emphasizing that branching has a high G × E component (**Figure 2**).

TABLE 1 | Summary of published quantitative trait loci (QTLs) of key domestication traits in Setaria.

Trait	Method	Population	Chromosome and candidate genes	Reference
Shattering	QTL	*S. viridis* × *S. italica*	5: Seita.5G381300 (*qSH1*) 9: Seita.9G154300 (*SbSH1*)	Doust et al., 2014a
	QTL	*S. viridis* × *S. italica*	9: Seita.9G154300 (*SbSH1*)	Odonkor, 2015
	Comparative mapping	*S. italica*	9: Seita.9G154300 (*SbSH1*)	Lin et al., 2012
	GWAS	*S. italica*	9: Seita.9G154300 (*SbSH1*)	Jia et al., 2013b
Branching	QTL	*S. viridis* × *S. italica*	1: Seita.1G136300 (*AtSUR1*) 3: Unknown 4: Seita.4G219200 (*OsMOC1*) 5: Unknown 6: Unknown 9: Seita.9G034300 (*AtAXR1*), Seita.9G123400 (*ZmTB1*)	Doust et al., 2004; Mauro-Herrera and Doust, 2016
	QTL	*S. viridis* × *S. italica*	5: Seita.5G368600 (*ZmBA1*) 9: Seita.9G123400 (*ZmTB1*)	Doust and Kellogg, 2006
	GWAS	*S. italica*	1: Unknown 2: Unknown 5: Unknown 8: Unknown 9: Unknown	Jia et al., 2013b
	QTL	*S. italica*	1: Unknown 7: Unknown	Fang et al., 2016
Height	QTL	*S. viridis* × *S. italica*	5: Seita.5G404900 (*OsSD1*) 9: Unknown	Mauro-Herrera and Doust, 2016
	QTL	*S. viridis* × *S. italica*	2: Seita.2G291300 (*ZmDFL1*) 5: Seita.5G404900 (*OsSD1*) 9: Unknown	Feldman et al., 2017
	GWAS	*S. italica*	2: Unknown 4: Unknown 6: Unknown	Jia et al., 2013b
	QTL	*S. italica*	1: Unknown 3: Unknown 6: Unknown 7: Unknown	Fang et al., 2016
	QTL	*S. italica*	1: Unknown	Wang et al., 2017
Inflorescence branching	QTL	*S. viridis* × *S. italica*	3: Unknown 7: Seita.7G222300 (*ZmFL1*) 9: Unknown	Doust et al., 2005
	GWAS	*S. italica*	2: Unknown 5: Unknown	Jia et al., 2013b
Flowering time	QTL	*S. viridis* × *S. italica*	4: Seita.4G067600 (*OsHD3a*) 8: Seita.8G034000 (*ZmTFL1*)	Mauro-Herrera et al., 2013
Flowering time	QTL	*S. viridis* × *S. italica*	2: Seita.2G436800 (*AtCDF1*), Seita.2G444300 (*SbPRR37*) 3: Seita.3G307200 (*OsREF6*) 4: Seita.4G116600 (*OsHD1/CONSTANS*) 5: Seita.5G317600 (*ZCN12*) 8: Seita.8G040100 (*OsPRR59*)	Doust, 2017; Doust et al., 2017
	GWAS	*S. italica*	1: Seita.1G236100 (*OsTOC1*), Seita.1G304900 (*OsHd1*), Seita.1G334800 (*OsCOP1*) 2: Seita.2G436800 (*OsCDF3*), Seita.2G444300 (*OsPPR37*)	Jia et al., 2013b

(Continued)

TABLE 1 | Continued

Trait	Method	Population	Chromosome and candidate genes	Reference
			3: Seita.3G044600 (*OsTOE1*)	
			4: Seita.4G282900 (*OsFD1*)	
			6: Seita.6G240100 (*OsABF3*), Seita.6G248900 (*OsSPY*)	
			7: Seita.7G007800 (*OsP*), Seita.7G119400 (*OsCRY1b*)	
			8: Seita.8G146800 (*OsGF14d*), Seita.8G146900 (*OsFKF1*)	
			9: Seita.9G342700 (*OsMADS56*)	

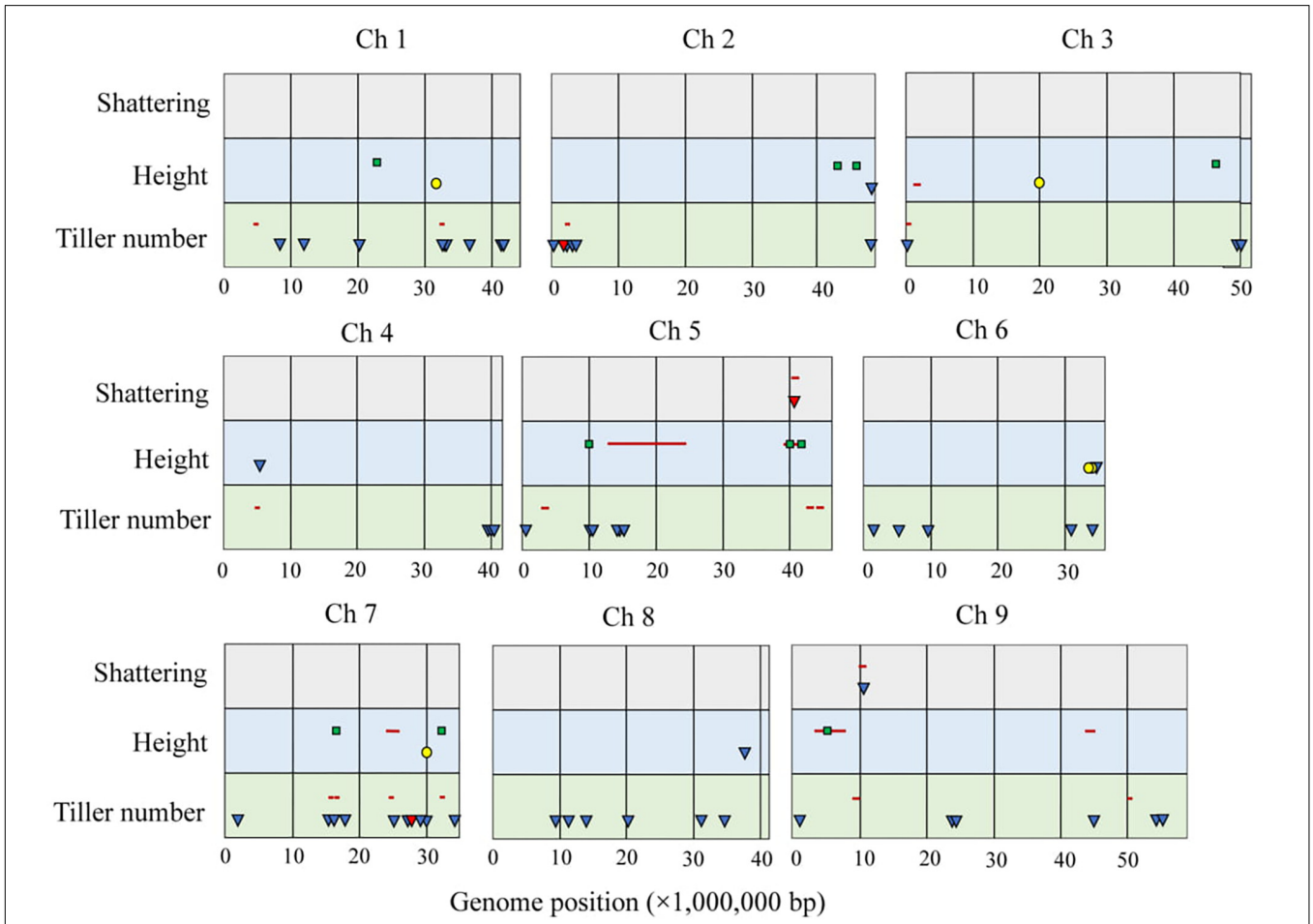

FIGURE 2 | Summary of domesticated and modern improvement loci across the Setaria genome. Each box represents an individual chromosome, where the values along the *x*-axis are physical position in the foxtail millet genome, *y*-axis indicates different traits. In each trait, the first row represents the foxtail millet × green foxtail F7 RIL population used in studies of Doust et al. (2014a) and Mauro-Herrera and Doust (2016) (QTLs displayed by red bars), and Feldman et al. (2017) (QTLs indicated by green squares). The second row represents the foxtail millet population studies of Jia et al. (2013b) (blue triangles correspond to GWAS signals of modern improvement, and red triangles show selective sweeps), and Fang et al. (2016) (QTLs represented by yellow circles).

The size and branching architecture of the inflorescence (panicle) also directly affects yield, as it determines the number of grains per panicle and hence final grain yield. Foxtail millet and green foxtail differ in the number of orders of branching within the inflorescence (**Figures 1A–D**), and Doust et al. (2005) identified three QTL for primary branch number/density on chromosomes 3, 7, and 9, whilst Jia et al. (2013b) identified three GWAS associations of chromosomes 2 and 5 (**Table 1**). Several of the QTL identified for primary inflorescence branch number in Doust et al. (2005) overlapped with QTL identified for vegetative branching (Doust et al., 2004). Other studies have focused on traits

indicative of total yield, including panicle length, diameter, and weight (Jia et al., 2013b; Wang et al., 2017; Zhang K. et al., 2017). However, few of these QTL overlap, suggesting multiple genes underlying these traits and/or environmental regulation. However, the latter seems surprising given the tight control over inflorescence form exhibited by plants, and it may be that present methods of analysis have not been able to satisfactorily decompose the inflorescence branch system in a way that can reveal underlying developmental drivers. An attempt to do this was done within the clade that *Setaria* belongs to (Doust and Kellogg, 2002), but a detailed analysis of inflorescence development in Setaria using emerging technologies such as x-ray tomography and other non-invasive techniques, along with new ways of analyzing data such as persistent homology analysis, remains to be accomplished (Bucksch et al., 2017).

Flowering Time and Photoperiod Sensitivity

Flowering is a critical indicator of the transition from vegetative growth to reproduction in the development of plants. The wild progenitors of crop species typically are photoperiod sensitive, because they are required to maximize their adaptability to their growing location. Crop species, on the other hand, may be selected for reduced photoperiod sensitivity in order to increase the range of localities in which they can be grown, and may have longer growing time, later flowering, and thus increased yield (Cockram et al., 2007). Thus selection on flowering time is unlikely to be a direct response to domestication but is best considered as a target for crop improvement. However, flowering time and photoperiod sensitivity also interact with other important traits, such as branching, height and biomass (Doust, 2017;Doust et al., 2017), making it relevant to discuss here.

Setaria has a wide latitudinal and longitudinal distribution around the world, and genetic evidence suggests that foxtail millet was domesticated from green foxtail in northern China, at temperate latitudes. Both foxtail millet and green foxtail show variation in photoperiod sensitivity (Swanton et al., 1999; Li and Yang, 2008; Jia et al., 2013b). In China, the four different growing regions are distinguished on the basis of spring or summer growing season and on variation in sensitivity to photoperiod and altitude (Diao and Jia, 2017a). Jia et al. (2013b) grew 916 accessions in four different latitudinal localities, and recorded differences in both morphology and heading date, along with differing significant SNP associations. A recent multiplexed shotgun genotyping (MSG) resequencing analysis of 439 RILs (derived from a cross between foxtail millet accessions Zhanggu and A2) under short (<12 h light) and long photoperiods (>14 h light), uncovered a total of 59 QTLs for 14 agronomic traits which were influenced by different photoperiods (Zhang K. et al., 2017). Doust et al. (2017) examined flowering responses in short (8 or 12 h light) and long (16 h light) photoperiods in a QTL mapping population, and demonstrated differences between short and long day regulation, with the 8 and 12 h photoperiods sharing QTL on chromosomes 4 and 5, and the 12 and 16 h having a shared QTL on chromosome 8. In addition there were QTLs on chromosomes 2 and 3 that were unique to the 16 h photoperiod. Mauro-Herrera et al. (2013) identified 16 flowering time QTLs across eight independent trials with varying climatic and photoperiod conditions, with domesticated foxtail millet alleles contributing to increased days to flowering. These QTL regions contained many candidate flowering genes identified from rice, maize, sorghum, and Arabidopsis, suggesting that the major genetic components in Setaria flowering and photoperiod response pathways are the same as in other plant species, even if the regulatory mechanisms are different between long and short day environments.

PERSPECTIVES FOR FUTURE BREEDING

Foxtail millet is well adapted to harsh environments, particularly under drought (Tang et al., 2017). It serves as an important staple grain in arid and semi-arid regions of Asia, particularly in northern China and India (Diao, 2017). The modern breeding programs of foxtail millet were initiated in the 1930s in India and 1950s in China, and were mostly focused on yield-related traits, because compared with other major crops, such as rice, wheat, and maize, the yield of foxtail millet is still relatively low (Diao and Jia, 2017a). However, global climate change, coupled with increasing population and reduction in arable lands, is adversely affecting cereal grain production in multiple regions (Wheeler and von Braun, 2013; Asseng et al., 2014). Stress tolerant foxtail millet is a potential crop that would be suitable for growing in drier and warmer conditions with few available inputs, particularly in developing countries in Asia and Africa (Huang et al., 2016).

There have been several studies exploring drought stress resistance traits in Setaria. Qie et al. (2014) investigated drought tolerance-related QTLs controlling germination and early seedling growth, using an F7 population of a cross between foxtail millet *Yugu1* and green foxtail W53, and identified a total of 18 QTLs. Tang et al. (2017) compared the transcriptomes of drought-tolerant foxtail millet *Yugu1* and drought-sensitive *An04*, and suggested that there was intense transcriptomic remodeling caused by genotype × drought stress interactions. Qi et al. (2013) studied differential gene expression patterns under PEG-induced drought treatment and found a total of 2,824 drought-responsive genes, including a large number of small RNAs and long non-coding RNAs that were actively involved in regulating drought-responsive genes. A dehydration-responsive element binding protein gene, *SiDREB2* (Lata et al., 2011; Lata and Prasad, 2014) and an ABA-responsive DREB, *SiARDP* (Li et al., 2014), were found to contribute to drought tolerance in foxtail millet. Peng et al. (2010) reported that the overexpression of phospholipase D (PLD) from foxtail millet could enhance the drought tolerance in Arabidopsis by elevating the sensitivity to ABA. These studies suggest that there is much scope for future breeding of foxtail millet with enhanced drought tolerance that

may provide new opportunities for increased food production in marginal crop production areas. Besides stress tolerance, other traits like resistance to leaf rust or blast diseases, and pests such as nematodes and other insects, are also important future breeding goals.

The traditional "phenotype-to-gene" forward genetics approach has been applied in the breeding and basic research of Setaria for many decades. Although several QTLs have been successfully identified from agronomically important traits, as reviewed above, the fine mapping of candidate genes is still challenging, mostly due to the lack of high density marker maps and high-quality reference genomes (Huang et al., 2016). However, the application of next generation sequencing in diverse collections of foxtail millet cultivars (Jia et al., 2013b) and wild green foxtail accessions (Huang and Feldman, 2017) are enabling the discovery of genomic variations on a large-scale. Meanwhile, the use of bulked segregant analysis (BSA) to quickly analyze mutant collections generated by chemical mutagenesis (Jiang et al., 2017) is accelerating Setaria gene discovery (Xue et al., 2016; Fan et al., 2017; Huang et al., 2017). New genes contributing to leaf color (Li et al., 2016), height, and inflorescence architecture (Masumoto et al., 2016; Huang et al., 2017; Xiang et al., 2017; Yang et al., 2018) have been successfully identified with this approach, substantially advancing our understanding of important traits.

In addition to forward genetics, transgenic-based reverse genetics tools are also being developed. Green foxtail can be easily transformed, unlike other panicoid model systems such as maize, sorghum, and Brachypodium, which are recalcitrant to transformation. Agrobacterium-mediated transformation methods starting with mature seeds have been successfully established (Van Eck et al., 2011, 2017; Van Eck and Swartwood, 2015), and faster floral-dip transformation methods have also been proposed (Martins et al., 2015; Saha and Blumwald, 2016, 2017). The rise of genome editing via CRISPR/Cas9 system will also enhance the future of Setaria genetics (Kikuchi et al., 2017; Zhu et al., 2017). The development of the Setaria genetic toolkit and resources will accelerate gene discovery and functional genomics analysis, benefiting not only millet breeding programs, but also enabling translational research from Setaria to other panicoid crops.

CONCLUSION

The Setaria system provides a window into domestication processes in the panicoid grasses that expands the discoveries that have already been made in the major crops of sorghum and maize. Differences between foxtail millet and those crops include an experimentally amenable wild ancestor that is widespread in temperate latitudes of the world and a domestication process that occurred at temperate latitudes, meaning that selection during improvement for adaptation to temperate latitudes was likely less intense than for maize and sorghum. The evidence from the traits presented here is that some conservation of genetic programs for domestication is shared between Setaria and other grasses, although definitive studies are still lacking. However, the Setaria system is not yet fully developed, and there are several areas that could be improved for future studies. These include a great need for additional and larger mapping populations, especially multi-parental mapping populations that will increase the power to identify causal genes. This approach has been very powerful for the sorghum, maize, rice, and Arabidopsis communities (Buckler et al., 2009; Kover et al., 2009; McMullen et al., 2009; Bandillo et al., 2013; Holland, 2015; Ongom and Ejeta, 2017), and would be of undoubted value for Setaria. Availability of genetic resources is also an issue, as the great diversity within China is essentially unavailable to outside researchers. Therefore, studies on the full diversity of the crop, foxtail millet, are limited to Chinese researchers at this time. Fortunately, studies on North American green foxtail wild diversity reveal that much of the species diversity is found there (Huang et al., 2014; Huang and Feldman, 2017; Schroder et al., 2017), a finding that will be important for future researchers. Another important aspect of the Setaria system is the promise of easy transformability, although there is as yet no published reports of transformation being used to confirm gene function. Routine transformation methods, including the possibility of a successful floral dip protocol, will help propel Setaria into a powerful system for gene discovery, as well as illuminating its domestication history and enhancing its future potential as a crop for a changing world.

AUTHOR CONTRIBUTIONS

AD conceived the idea. HH and MM-H compiled genetic studies. HH, MM-H, and AD interpreted the data, wrote, and revised the manuscript.

FUNDING

This research was supported by the Natural Science Foundation (NSF-IOS 1339332 and NSF-IOS 1557640 to AD).

REFERENCES

Acharya, B. R., Choudhury, S. R., Estelle, A. B., Vijayakumar, A., Zhu, C. M., Hovis, L., et al. (2017). Optimization of phenotyping assays for the model monocot *Setaria viridis*. *Front. Plant Sci.* 8:2172. doi: 10.3389/fpls.2017.02172

Allaby, R. G., Stevens, C., Lucas, L., Maeda, O., and Fuller, D. Q. (2017). Geographic mosaics and changing rates of cereal domestication. *Philos. Trans. R. Soc. B* 372:20160429. doi: 10.1098/rstb.2016.0429

Asano, K., Yamasaki, M., Takuno, S., Miura, K., Katagiri, S., Ito, T., et al. (2011). Artificial selection for a green revolution gene during japonica rice domestication. *Proc. Natl. Acad. Sci. U.S.A.* 108, 11034–11039. doi: 10.1073/pnas.1019490108

Ashikari, M., Sasaki, A., Ueguchi-Tanaka, M., Itoh, H., Nishimura, A., Datta, S., et al. (2002). Loss-of-function of a rice gibberellin biosynthetic gene, GA20 oxidase (GA20ox-2), led to the rice 'green revolution'. *Breed. Sci.* 52, 143–150. doi: 10.1270/jsbbs.52.143

Asseng, S., Ewert, F., Martre, P., Rötter, R. P., Lobell, D. B., Cammarano, D., et al. (2014). Rising temperatures reduce global wheat production. *Nat. Clim. Change* 5, 143–147. doi: 10.1038/nclimate2470

Austin, D. F. (2006). Fox-tail millets (*Setaria*: Poaceae) - abandoned food in two hemispheres. *Econom. Bot.* 60, 143–158. doi: 10.1663/0013-0001(2006)60[143:FMSPFI]2.0.CO;2

Ayyangar, G. N. R., Narayanan, T. R., and Rao, T. N. (1933). The inheritance of characters in *Setaria italica* (Beauv.), the Italian millet. Part IV. *Spikelet-tipped bristles. Ind. J. Agric. Sci.* 3, 552–558.

Banan, D., Paul, R. E., Feldman, M. J., Holmes, M. W., Schlake, H., Baxter, I., et al. (2018). High-fidelity detection of crop biomass quantitative trait loci from low-cost imaging in the field. *Plant Direct* 2:e00041. doi: 10.1002/pld3.41

Bandillo, N., Raghavan, C., Muyco, P. A., Sevilla, M. A., Lobina, I. T., Dilla-Ermita, C. J., et al. (2013). Multi-parent advanced generation inter-cross (MAGIC) populations in rice: progress and potential for genetics research and breeding. *Rice* 6:11. doi: 10.1186/1939-8433-6-11

Bennetzen, J. L., Schmutz, J., Wang, H., Percifield, R., Hawkins, J., Pontaroli, A. C., et al. (2012). Reference genome sequence of the model plant Setaria. *Nat. Biotechnol.* 30, 555–561. doi: 10.1038/nbt.2196

Brenner, D. M., Dekker, J., Niemi, J., and Pfiffner, L. (2015). Medical oxygen concentrators for releasing seed dormancy. *Crop Sci.* 55, 2291–2293. doi: 10.2135/cropsci2014.11.0783

Brutnell, T. P., Bennetzen, J. L., and Vogel, J. P. (2015). Brachypodium distachyon and *Setaria viridis*: model genetic systems for the grasses. *Annu. Rev. Plant Biol.* 66, 465–485. doi: 10.1146/annurev-arplant-042811-105528

Brutnell, T. P., Wang, L., Swartwood, K., Goldschmidt, A., Jackson, D., Zhu, X.-G., et al. (2010). *Setaria viridis*: a model for C4 photosynthesis. *Plant Cell* 22, 2537–2544. doi: 10.1105/tpc.110.075309

Buckler, E. S., Holland, J. B., Bradbury, P. J., Acharya, C. B., Brown, P. J., Browne, C., et al. (2009). The genetic architecture of maize flowering time. *Science* 325, 714–718. doi: 10.1126/science.1174276

Bucksch, A., Atta-Boateng, A., Azihou, A. F., Battogtokh, D., Baumgartner, A., Binder, B. M., et al. (2017). Morphological plant modeling: unleashing geometric and topological potential within the plant sciences. *Front. Plant Sci.* 8:900. doi: 10.3389/fpls.2017.00900

Chander, S., Bhat, K. V., Gowda, M. V. C., and Dikshit, N. (2017a). Identification, characterization and validation of core collection of foxtail millet (*Setaria italica*). *Ind. J. Agric. Sci.* 87, 899–910.

Chander, S., Bhat, K. V., Kumari, R., Sen, S., Gaikwad, A. B., Gowda, M. V. C., et al. (2017b). Analysis of spatial distribution of genetic diversity and validation of Indian foxtail millet core collection. *Physiol. Mol. Biol. Plants* 23, 663–673. doi: 10.1007/s12298-017-0448-5

Chemisquy, M. A., Giussani, L. M., Scataglini, M. A., Kellogg, E. A., and Morrone, O. (2010).). Phylogenetic studies favour the unification of *Pennisetum, Cenchrus* and *Odontelytrum* (Poaceae): a combined nuclear, plastid and morphological analysis, and nomenclatural combinations in *Cenchrus*. *Ann. Bot.* 106, 107–130. doi: 10.1093/aob/mcq090

Cockram, J., Jones, H., Leigh, F. J., O'sullivan, D., Powell, W., Laurie, D. A., et al. (2007). Control of flowering time in temperate cereals: genes, domestication, and sustainable productivity. *J. Exp. Bot.* 58, 1231–1244. doi: 10.1093/jxb/erm042

Coelho, C., Huang, P., and Brutnell, T. P. (2017). *Setaria viridis* as a Model for C-4 Photosynthesis. *Plant Cell* 22, 2537–2544. doi: 10.1007/978-3-319-45105-3_17

Crawford, G. W. (1992). "The transitions to agriculture in Japan," in *Transitions to Agriculture in Prehistory*, eds A. B. Gebauer and T. D. Price (Madison, WI: Prehistory Press), 117–132.

Darmency, H., Wang, T., and Délye, C. (2017). "Herbicide resistance in *Setaria*," in *Genetics and Genomics of Setaria*, eds A. Doust and X. Diao (Cham: Springer International Publishing), 251–266. doi: 10.1007/978-3-319-45105-3_15

Darmency, H., Zangre, G. R., and Pernes, J. (1987). The wild-weed-crop complex in setaria - a hybridization study. *Genetica* 75, 103–107. doi: 10.1016/j.bbrc.2010.02.068

Dekker, J. (2003). The foxtail (*Setaria*) species-group. *Weed Sci.* 51, 641–656. doi: 10.1614/P2002-IR

Diao, X., and Jia, G. (2017a). "Foxtail millet breeding in China," in *Genetics and Genomics of Setaria*, eds A. Doust and X. Diao (Cham: Springer International Publishing), 93–113. doi: 10.1007/978-3-319-45105-3_6

Diao, X., and Jia, G. (2017b). "Origin and domestication of foxtail millet," in *Genetics and Genomics of Setaria*, eds A. Doust and X. Diao (Cham: Springer International Publishing), 61–72. doi: 10.1007/978-3-319-45105-3_4

Diao, X., Schnable, J., Bennetzen, J. L., and Li, J. (2014). Initiation of *Setaria* as a model plant. *Front. Agric. Sci. Eng.* 1, 16–20. doi: 10.15302/J-FASE-2014011

Diao, X. M. (2017). Production and genetic improvement of minor cereals in China. *Crop J.* 5, 103–114. doi: 10.1093/mp/ssn039

Doust, A. (2007a). Architectural evolution and its implications for domestication in grasses. *Ann. Bot.* 100, 941–950.

Doust, A. N. (2007b). Grass architecture: genetic and environmental control of branching. *Curr. Opin. Plant Biol.* 10, 21–25.

Doust, A. N. (2017). "The effect of photoperiod on flowering time, plant architecture, and biomass in *Setaria*," in *Genetics and Genomics of Setaria*, eds A. Doust and X. Diao (Cham: Springer International Publishing), 197–210.

Doust, A. N., Devos, K. M., Gadberry, M. D., Gale, M. D., and Kellogg, E. A. (2004). Genetic control of branching in foxtail millet. *Proc. Natl. Acad. Sci. U.S.A.* 101, 9045–9050. doi: 10.1073/pnas.0402892101

Doust, A. N., Devos, K. M., Gadberry, M. D., Gale, M. D., and Kellogg, E. A. (2005). The genetic basis for inflorescence variation between foxtail and green millet (Poaceae). *Genetics* 169, 1659–1672. doi: 10.1534/genetics.104.035543

Doust, A. N., and Diao, X. (2017). *Genetics and Genomics of Setaria*. Switzerland: Springer International Publishing. doi: 10.1007/978-3-319-45105-3

Doust, A. N., and Kellogg, E. A. (2002). Inflorescence diversification in the panicoid "bristle grass" clade (Paniceae, Poaceae): evidence from molecular phylogenies and developmental morphology. *Am. J. Bot.* 89, 1203–1222. doi: 10.3732/ajb.89.8.1203

Doust, A. N., and Kellogg, E. A. (2006). Effect of genotype and environment on branching in weedy green millet (*Setaria viridis*) and domesticated foxtail millet (*Setaria italica*) (Poaceae). *Mol. Ecol.* 15, 1335–1349. doi: 10.1111/j.1365-294X.2005.02791.x

Doust, A. N., Kellogg, E. A., Devos, K. M., and Bennetzen, J. L. (2009). Foxtail millet: a sequence-driven grass model system. *Plant Physiol.* 149, 137–141. doi: 10.1104/pp.108.129627

Doust, A. N., Lukens, L., Olsen, K. M., Mauro-Herrera, M., Meyer, A., and Rogers, K. (2014a). Beyond the single gene: how epistasis and gene-by-environment effects influence crop domestication. *Proc. Natl. Acad. Sci. U.S.A.* 111, 6178–6183. doi: 10.1073/pnas.1308940110

Doust, A. N., Mauro-Herrera, M., Francis, A. D., and Shand, L. C. (2014b). Morphological diversity and genetic regulation of inflorescence abscission zones in grasses. *Am. J. Bot.* 101, 1759–1769. doi: 10.3732/ajb.1400186

Doust, A. N., Mauro-Herrera, M., Hodge, J. G., and Stromski, J. (2017). The C4 model grass Setaria is a short day plant with secondary long day genetic regulation. *Front. Plant Sci.* 8:1062. doi: 10.3389/fpls.2017.01062

Doust, A. N., Penly, A. M., Jacobs, S. W., and Kellogg, E. A. (2007). Congruence, conflict, and polyploidization shown by nuclear and chloroplast markers in the monophyletic "bristle clade" (Paniceae, Panicoideae, Poaceae). *Syst. Bot.* 32, 531–544. doi: 10.1600/036364407782250670

Emily, S. C., Paul, C. W., James, S. G., and Jonathan, A. F. (2013). Redefining agricultural yields: from tonnes to people nourished per hectare. *Environ. Res. Lett.* 8:3.

Fahlgren, N., Feldman, M., Gehan, M. A., Wilson, M. S., Shyu, C., Bryant, D. W., et al. (2015). A versatile phenotyping system and analytics platform reveals diverse temporal responses to water availability in Setaria. *Mol. Plant* 8, 1520–1535. doi: 10.1016/j.molp.2015.06.005

Fan, X. K., Tang, S., Zhi, H., He, M. M., Ma, W. S., Jia, Y. C., et al. (2017). Identification and Fine mapping of SiDWARF3 (D3), a Pleiotropic Locus controlling environment-independent dwarfism in foxtail millet. *Crop Sci.* 57, 2431–2442. doi: 10.2135/cropsci2016.11.0952

Fang, X., Dong, K., Wang, X., Liu, T., He, J., Ren, R., et al. (2016). A high density genetic map and QTL for agronomic and yield traits in Foxtail millet [*Setaria italica* (L.) P. Beauv.]. *BMC Genomics* 17:336. doi: 10.1186/s12864-016-2628-z

Feldman, M. J., Paul, R. E., Banan, D., Barrett, J. F., Sebastian, J., Yee, M. C., et al. (2017). Time dependent genetic analysis links field and controlled environment phenotypes in the model C-4 grass Setaria. *PLoS Genet.* 13:e1006841. doi: 10.1371/journal.pgen.1006841

Finlayson, S. A., Krishnareddy, S. R., Kebrom, T. H., and Casal, J. J. (2010). Phytochrome regulation of branching in Arabidopsis. *Plant Physiol.* 152, 1914–1927. doi: 10.1104/pp.109.148833

Fukunaga, K., Domon, E., and Kawase, M. (1997). Ribosomal DNA variation in foxtail millet, *Setaria italica* (L.) P. Beauv., and a survey of variation from Europe and Asia. *Theor. Appl. Genet.* 95, 751–756. doi: 10.1007/s001220050621

Ghimire, K. H., Joshi, B. K., Gurung, R., and Sthapit, B. R. (2018). Nepalese foxtail millet *Setaria italica* (L.) P. Beauv. genetic diversity revealed by morphological markers. *Genet. Resour. Crop Evol.* 65, 1147–1157. doi: 10.1007/s10722-017-0602-5

Glemin, S., and Bataillon, T. (2009). A comparative view of the evolution of grasses under domestication. *New Phytol.* 183, 273–290. doi: 10.1111/j.1469-8137.2009.02884.x

Goff, S. A., Ricke, D., Lan, T. H., Presting, G., Wang, R. L., Dunn, M., et al. (2002). A draft sequence of the rice genome (*Oryza sativa* L. ssp japonica). *Science* 296, 92–100. doi: 10.1126/science.1068275

Goron, T. L., and Raizada, M. N. (2015). Genetic diversity and genomic resources available for the small millet crops to accelerate a New Green Revolution. *Front. Plant Sci.* 6:157. doi: 10.3389/fpls.2015.00157

Hirano, R., Naito, K., Fukunaga, K., Watanabe, K. N., Ohsawa, R., and Kawase, M. (2011). Genetic structure of landraces in foxtail millet (*Setaria italica* (L.) P. Beauv.) revealed with transposon display and interpretation to crop evolution of foxtail millet. *Genome* 54, 498–506. doi: 10.1139/g11-015

Hodge, J. G., and Doust, A. N. (2017). "Morphological development of *Setaria viridis* from germination to flowering," in *Genetics and Genomics of Setaria*, eds A. Doust and X. Diao (Cham: Springer International Publishing), 161–175.

Hodge, J. G., and Kellogg, E. A. (2016). Abscission zone development in *Setaria viridis* and its domesticated relative, *Setaria italica*. *Am. J. Bot.* 103, 998–1005. doi: 10.3732/ajb.1500499

Holland, J. B. (2015). MAGIC maize: a new resource for plant genetics. *Genome Biol.* 16:163. doi: 10.1186/s13059-015-0713-2

Huang, P., and Feldman, M. (2017). "Genetic diversity and geographic distribution of north American *Setaria viridis* populations," in *Genetics and Genomics of Setaria*, eds A. Doust and X. Diao (Cham: Springer International Publishing), 45–59.

Huang, P., Feldman, M., Schroder, S., Bahri, B. A., Diao, X., Zhi, H., et al. (2014). Population genetics of *Setaria viridis*, a new model system. *Mol. Ecol.* 23, 4912–4925. doi: 10.1111/mec.12907

Huang, P., Jiang, H., Zhu, C. M., Barry, K., Jenkins, J., Sandor, L., et al. (2017). Sparse panicle1 is required for inflorescence development in *Setaria viridis* and maize. *Nat. Plants* 3:17054. doi: 10.1038/nplants.2017.54

Huang, P., Shyu, C., Coelho, C. P., Cao, Y., and Brutnell, T. P. (2016). *Setaria viridis* as a model system to advance millet genetics and genomics. *Front. Plant Sci.* 7:1781. doi: 10.3389/fpls.2016.01781

Jia, J., Zhao, S., Kong, X., Li, Y., Zhao, G., He, W., et al. (2013a). *Aegilops tauschii* draft genome sequence reveals a gene repertoire for wheat adaptation. *Nature* 496, 91–95. doi: 10.1038/nature12028

Jia, G., Huang, X., Zhi, H., Zhao, Y., Zhao, Q., Li, W., et al. (2013b). A haplotype map of genomic variations and genome-wide association studies of agronomic traits in foxtail millet (*Setaria italica). Nat. Genet.* 45, 957–961. doi: 10.1038/ng.2673

Jia, G., Shi, S., Wang, C., Niu, Z., Chai, Y., Zhi, H., et al. (2013c). Molecular diversity and population structure of Chinese green foxtail *Setaria viridis* (L.) Beauv. revealed by microsatellite analysis. *J. Exp. Bot.* 64, 3645–3655. doi: 10.1093/jxb/ert198

Jiang, H., Barbier, H., and Brutnell, T. (2013). Methods for performing crosses in *Setaria viridis,* a new model system for the grasses. *J. Vis. Exp.* 1:80. doi: 10.3791/50527

Jiang, H., Huang, P., and Brutnell, T. P. (2017). "Forward genetics in *Setaria viridis*," in *Genetics and Genomics of Setaria*, eds A. Doust and X. Diao (Cham: Springer International Publishing)), 303–322. doi: 10.1007/978-3-319-45105-3_18

Jones, M. (2004). "Between fertile crescents: minor grain crops and agricultural origins," in *Traces of Ancestry: Studies in Honour of Colin Renfrew*, ed. M. Jones (Cambridge: McDonald Institute for Archaeological Research), 127–135.

Jusuf, M., and Pernes, J. (1985). Genetic-variability of foxtail millet (*Setaria-italica* P Beauv) - electrophoretic study of 5 isoenzyme systems. *Theor. Appl. Genet.* 71, 385–391. doi: 10.1007/BF00251177

Kawase, M., and Sakamoto, S. (1984). Variation, geographical-distribution and genetic-analysis of esterase isozymes in foxtail millet, *Setaria-italica* (L) P-BEAUV. *Theor. Appl. Genet.* 67, 529–533. doi: 10.1007/BF00264899

Kellogg, E. A. (2015). *Flowering Plants. Monocots: Poaceae*. New York, NY: Springer International Publishing. doi: 10.1007/978-3-319-15332-2

Kellogg, E. A. (2017). "Evolution of Setaria," in *Genetics and Genomics of Setaria*, eds A. Doust and X. Diao (Cham: Springer International Publishing), 3–27. doi: 10.1007/978-3-319-45105-3_1

Kellogg, E. A., Aliscioni, S. S., Morrone, O., Pensiero, J., and Zuloaga, F. (2009). A phylogeny of *Setaria* (Poaceae, Panicoideae, Paniceae) and related genera based on the chloroplast gene *ndhF*. *Int. J. Plant Sci.* 170, 117–131. doi: 10.1086/593043

Kikuchi, K., Shyu, C., and Brutnell, T. P. (2017). "Transposon Tagging in *Setaria viridis*," in *Genetics and Genomics of Setaria*, eds A. Doust and X. Diao (Cham: Springer International Publishing), 323–342. doi: 10.1007/978-3-319-45105-3_19

Kover, P. X., Valdar, W., Trakalo, J., Scarcelli, N., Ehrenreich, I. M., Purugganan, M. D., et al. (2009). A Multiparent advanced generation inter-cross to fine-map quantitative traits in *Arabidopsis thaliana*. *PLoS Genet.* 5:e1000551. doi: 10.1371/journal.pgen.1000551

Kumari, K., Muthamilarasan, M., Misra, G., Gupta, S., Subramanian, A., Parida, S. K., et al. (2013). Development of eSSR-Markers in *Setaria italica* and their applicability in studying genetic diversity, cross-transferability and comparative mapping in millet and non-millet species. *PLoS One* 8:e67742. doi: 10.1371/journal.pone.0067742

Lata, C., Bhutty, S., Bahadur, R. P., Majee, M., and Prasad, M. (2011). Association of an SNP in a novel DREB2-like gene SiDREB2 with stress tolerance in foxtail millet [*Setaria italica* (L.)]. *J. Exp. Bot.* 62, 3387–3401. doi: 10.1093/jxb/err016

Lata, C., and Prasad, M. (2014). Association of an allele-specific marker with dehydration stress tolerance in foxtail millet suggests SiDREB2 to be an important QTL. *J. Plant Biochem. Biotechnol.* 23, 119–122. doi: 10.1007/s13562-013-0193-y

Layton, D. J., and Kellogg, E. A. (2014). Morphological, phylogenetic, and ecological diversity of the new model species *Setaria viridis* (Poaceae: Paniceae) and its close relatives. *Am. J. Bot.* 101, 539–557. doi: 10.3732/ajb.1300428

Le Thierry d'Ennequin, M., Panaud, O., Toupance, B., and Sarr, A. (2000). Assessment of genetic relationships between Setaria italica and its wild relative *S. viridis* using AFLP markers. *Theor. Appl. Genet.* 100, 1061–1066. doi: 10.1007/s001220051387

Lee, G.-A. (2011). The transition from foraging to farming in prehistoric Korea. *Curr. Anthropol.* 52, S307–S329. doi: 10.1086/658488

Li, C., Yue, J., Wu, X., Xu, C., and Yu, J. (2014). An ABA-responsive DRE-binding protein gene from *Setaria italica*, SiARDP, the target gene of SiAREB, plays a critical role under drought stress. *J. Exp. Bot.* 65, 5415–5427. doi: 10.1093/jxb/eru302

Li, H. W., Meng, C. J., and Liu, T. N. (1935). Problems in the breeding of millet [*Setaria italica* (L.) Beauv.]. *J. Am. Soc. Agron.* 27, 670–693. doi: 10.2134/agronj1935.00021962002700120002x

Li, H. Y., and Yang, Y. F. (2008). Phenotypic plasticity of life history characteristics: quantitative analysis of delayed reproduction of green foxtail *(Setaria viridis*) in the Songnen Plain of China. *J. Integr. Plant Biol.* 50, 641–647. doi: 10.1111/j.1744-7909.2008.00646.x

Li, L. F., and Olsen, K. M. (2016). "To have and to hold: selection for seed and fruit retention during crop domestication," in *Current Topics in Developmental Biology*, ed. V. Orgogozo (Cambridge, MA: Academic Press), 63–109. doi: 10.1016/bs.ctdb.2016.02.002

Li, P., and Brutnell, T. P. (2011). *Setaria viridis* and *Setaria italica*, model genetic systems for the Panicoid grasses. *J. Exp. Bot.* 62, 3031–3037. doi: 10.1093/jxb/err096

Li, W., Tang, S., Zhang, S., Shan, J., Tang, C., Chen, Q., et al. (2016). Gene mapping and functional analysis of the novel leaf color gene SiYGL1 in foxtail millet [*Setaria italica* (L.) P. Beauv]. *Physiol. Plant.* 157, 24–37. doi: 10.1111/ppl.12405

Li, W., Zhi, H., Wang, Y.-F., Li, H.-Q., and Diao, X.-M. (2012). Assessment of genetic relationship of foxtail millet with its wild ancestor and close relatives by ISSR markers. *J. Integr. Agric.* 11, 556–566. doi: 10.1016/S2095-3119(12)60042-2

Li, Y., Jia, J. Z., Wang, Y., and Wu, S. Z. (1998). Intraspecific and interspecific variation in Setaria revealed by RAPD analysis. *Genet. Resour. Crop Evol.* 45, 279–285. doi: 10.1023/A:1008600123509

Lightfoot, E., Liu, X., and Jones, M. K. (2013). Why move starchy cereals? A review of the isotopic evidence for prehistoric millet consumption across Eurasia. *World Archaeol.* 45, 574–623. doi: 10.1080/00438243.2013.852070

Lin, Z., Li, X., Shannon, L. M., Yeh, C.-T., Wang, M. L., Bai, G., et al. (2012). Parallel domestication of the Shattering1 genes in cereals. *Nat. Genet.* 44, 720–724. doi: 10.1038/ng.2281

Ling, H. Q., Zhao, S., Liu, D., Wang, J., Sun, H., Zhang, C., et al. (2013). Draft genome of the wheat A-genome progenitor *Triticum urartu*. *Nature* 496, 87–90. doi: 10.1038/nature11997

Lü, H., Li, Y., Zhang, J., Yang, X., Ye, M., Li, Q., et al. (2014). Component and simulation of the 4,000-year-old noodles excavated from the archaeological site of Lajia in Qinghai. China. *Chin. Sci. Bull.* 59, 5136–5152. doi: 10.1007/s11434-014-0663-1

Lü, H., Yang, X., Ye, M., Liu, K.-B., Xia, Z., Ren, X., et al. (2005). Millet noodles in Late Neolithic China. *Nature* 437, 967–968. doi: 10.1038/437967a

Lü, H., Zhang, J., Liu, K.-B., Wu, N., Li, Y., Zhou, K., et al. (2009). Earliest domestication of common millet (*Panicum miliaceum*) in East Asia extended to 10,000 years ago. *Proc. Natl. Acad. Sci. U.S.A.* 106, 7367–7372. doi: 10.1073/pnas.0900158106

Martins, P. K., Ribeiro, A. P., Cunha, B. A. D. B. D., Kobayashi, A. K., and Molinari, H. B. C. (2015). A simple and highly efficient Agrobacterium-mediated transformation protocol for *Setaria viridis*. *Biotechnol. Rep.* 6, 41–44. doi: 10.1016/j.btre.2015.02.002

Masumoto, H., Takagi, H., Mukainari, Y., Terauchi, R., and Fukunaga, K. (2016). Genetic analysis of NEKODE1 gene involved in panicle branching of foxtail millet, *Setaria italica* (L.) P. Beauv., and mapping by using QTL-seq. *Mol. Breed.* 36:59. doi: 10.1007/s11032-016-0481-z

Matsumoto, T., Wu, J. Z., Kanamori, H., Katayose, Y., Fujisawa, M., Namiki, N., et al. (2005). The map-based sequence of the rice genome. *Nature* 436, 793–800. doi: 10.1038/nature03895

Mauro-Herrera, M., and Doust, A. N. (2016). Development and genetic control of plant architecture and biomass in the panicoid grass. Setaria. *PLoS One* 11:e0151346. doi: 10.1371/journal.pone.0151346

Mauro-Herrera, M., Wang, X., Barbier, H., Brutnell, T. P., Devos, K. M., and Doust, A. N. (2013). Genetic control and comparative genomic analysis of flowering time in Setaria (Poaceae). *G3*, 283–295. doi: 10.1534/g3.112.005207

McMullen, M. D., Kresovich, S., Villeda, H. S., Bradbury, P., Li, H., Sun, Q., et al. (2009). Genetic properties of the maize nested association mapping population. *Science* 325, 737–740. doi: 10.1126/science.1174320

McSteen, P. (2009). Hormonal regulation of branching in grasses. *Plant Physiol.* 149, 46–55. doi: 10.1104/pp.108.129056

Nadeem, F., Ahmad, Z., Wang, R., Han, J., Shen, Q., Chang, F., et al. (2018). Foxtail Millet [*Setaria italica* (L.) Beauv.] Grown under low nitrogen shows a smaller root system, enhanced biomass accumulation, and nitrate transporter expression. *Front. Plant Sci.* 9:205. doi: 10.3389/fpls.2018.00205

Nakayama, H., Afzal, M., and Okuno, K. (1998).). Intraspecific differentiation and geographical distribution of Wx alleles for low amylose content in endosperm of foxtail millet, *Setaria italica* (L.) Beauv. *Euphytica* 102, 289–293. doi: 10.1023/A:1018344819531

Nasu, H., Momohara, A., Yasuda, Y., and He, J. (2007). The occurrence and identification of *Setaria italica* (L.) P. Beauv. (foxtail millet) grains from the Chengtoushan site (ca. 5800 cal B.P.) in central China, with reference to the domestication centre in Asia. *Veg. Hist. Archaeobot.* 16, 481–494. doi: 10.1007/s00334-006-0068-4

Odonkor, S. E. (2015). *Quantitative trait locus (QTL) Mapping Of Seed Weight, Pericarp Color, Bristling and Seed Shattering in Setaria*. Master of Science, University of Georgia, Athens, GA.

Ongom, P. O., and Ejeta, G. (2017). Mating Design and genetic structure of a multi-parent advanced generation inter-cross (MAGIC) population of Sorghum (*Sorghum bicolor* (L.) Moench). *G3* 8, 331–341. doi: 10.1534/g3.117.300248

Pandey, G., Misra, G., Kumari, K., Gupta, S., Parida, S. K., Chattopadhyay, D., et al. (2013). Genome-wide development and use of microsatellite markers for large-scale genotyping applications in foxtail millet [*Setaria italica* (L.)]. *DNA Res.* 20, 197–207. doi: 10.1093/dnares/dst002

Paterson, A. H., Bowers, J. E., Bruggmann, R., Dubchak, I., Grimwood, J., Gundlach, H., et al. (2009). The Sorghum bicolor genome and the diversification of grasses. *Nature* 457, 551–556. doi: 10.1038/nature07723

Paterson, A. H., Lin, Y.-R., Li, Z., Schertz, K. F., Doebley, J. F., Pinson, S. R., et al. (1995). Convergent domestication of cereal crops by independent mutations at corresponding genetic loci. *Science* 269, 1714–1718. doi: 10.1126/science.7695305231.1714

Peng, Y., Zhang, J., Cao, G., Xie, Y., Liu, X., Lu, M., et al. (2010). Overexpression of a PLDα1 gene from *Setaria italica* enhances the sensitivity of *Arabidopsis* to abscisic acid and improves its drought tolerance. *Plant Cell Rep.* 29, 793–802. doi: 10.1007/s00299-010-0865-1

Poncet, V., Martel, E., Allouis, S., Devos, K., Lamy, F., Sarr, A., et al. (2002). Comparative analysis of QTLs affecting domestication traits between two domesticated × wild pearl millet (*Pennisetum glaucum* L., Poaceae) crosses. *Theor. Appl. Genet.* 104, 965–975. doi: 10.1007/s00122-002-0889-1

Purugganan, M. D., and Fuller, D. Q. (2009). The nature of selection during plant domestication. *Nature* 457, 843–848. doi: 10.1038/nature07895

Qi, X., Xie, S., Liu, Y., Yi, F., and Yu, J. (2013). Genome-wide annotation of genes and noncoding RNAs of foxtail millet in response to simulated drought stress by deep sequencing. *Plant Mol. Biol.* 83, 459–473. doi: 10.1007/s11103-013-0104-6

Qie, L., Jia, G., Zhang, W., Schnable, J., Shang, Z., Li, W., et al. (2014). Mapping of quantitative trait locus (QTLs) that contribute to germination and early seedling drought tolerance in the interspecific cross *Setaria italica* × *Setaria viridis*. *PLoS One* 9:e101868. doi: 10.1371/journal.pone.0101868

Saha, P., and Blumwald, E. (2016). Spike-dip transformation of *Setaria viridis*. *Plant J.* 86, 89–101. doi: 10.1111/tpj.13148

Saha, P., and Blumwald, E. (2017). "Spike-Dip transformation method of *Setaria viridis*," in *Genetics and Genomics of Setaria*, eds A. Doust and X. Diao (Cham: Springer International Publishing), 357–369. doi: 10.1007/978-3-319-45105-3_21

Schnable, P. S., Ware, D., Fulton, R. S., Stein, J. C., Wei, F. S., Pasternak, S., et al. (2009). The B73 maize genome: complexity, diversity, and dynamics. *Science* 326, 1112–1115. doi: 10.1126/science.1178534

Schroder, S., Bahri, B. A., Eudy, D. M., Layton, D. J., Kellogg, E. A., and Devos, K. M. (2017). Genetic diversity and origin of North American green foxtail *Setaria viridis* (L.) Beauv. accessions. *Genet. Resour. Crop Evol.* 64, 367–378. doi: 10.1007/s10722-016-0363-6

Sebastian, J., Wong, M. K., Tang, E., and Dinneny, J. R. (2014). Methods to promote germination of dormant *Setaria viridis* seeds. *PLoS One* 9:e95109. doi: 10.1371/journal.pone.0095109

Sergusheva, E. A., and Vostretsov, Y. E. (2009). "The advance of agriculture in the coastal zone of East Asia," in *From Foragers to Farmers: Papers in Honour of Gordon C. Hillman*, ed. A. S. Fairbairn (Oxford: Oxbow Books), 205–219.

Studer, A. J., Schnable, J. C., Weissmann, S., Kolbe, A. R., Mckain, M. R., Shao, Y., et al. (2016). The draft genome of the C-3 panicoid grass species *Dichanthelium oligosanthes*. *Genome Biol.* 17:223. doi: 10.1186/s13059-016-1080-3

Swanton, C. J., Huang, J. Z., Deen, W., Tollenaar, M., Shrestha, A., and Rahimian, H. (1999). Effects of temperature and photoperiod on *Setaria viridis*. *Weed Sci.* 47, 446–453.

Tang, S., Li, L., Wang, Y., Chen, Q., Zhang, W., Jia, G., et al. (2017). Genotype-specific physiological and transcriptomic responses to drought stress in *Setaria italica* (an emerging model for Panicoideae grasses). *Sci. Rep.* 7:10009. doi: 10.1038/s41598-017-08854-6

Van Eck, J., and Swartwood, K. (2015). "*Setaria viridis*," in *Agrobacterium Protocols*, Vol. 1, ed. K. Wang (New York, NY: Springer), 57–67.

Van Eck, J., Swartwood, K., and Brutnell, T. (2011). Development of an *Agrobacterium tumefaciens*-mediated transformation method for *Setaria viridis* (Green Millet). *In Vitro Cell. Dev. Biol. Anim.* 47, S79–S79.

Van Eck, J., Swartwood, K., Pidgeon, K., and Maxson-Stein, K. (2017). "*Agrobacterium tumefaciens*-Mediated Transformation of *Setaria viridis*," in *Genetics and Genomics of Setaria*, eds A. Doust and X. Diao (Cham: Springer International Publishing), 343–356.

VanBuren, R., Bryant, D., Edger, P. P., Tang, H. B., Burgess, D., Challabathula, D., et al. (2015). Single-molecule sequencing of the desiccation-tolerant grass *Oropetium thomaeum*. *Nature* 527, 508–U209. doi: 10.1038/nature15714

Varshney, R. K., Shi, C. C., Thudi, M., Mariac, C., Wallace, J., Qi, P., et al. (2017). Pearl millet genome sequence provides a resource to improve agronomic traits in arid environments. *Nat. Biotechnol.* 35, 969–976. doi: 10.1038/nbt.3943

Vogel, J. P., Garvin, D. F., Mockler, T. C., Schmutz, J., Rokhsar, D., Bevan, M. W., et al. (2010). Genome sequencing and analysis of the model grass *Brachypodium distachyon*. *Nature* 463, 763–768. doi: 10.1038/nature08747

Wang, C., Chen, J., Zhi, H., Yang, L., Li, W., Wang, Y., et al. (2010). Population genetics of foxtail millet and its wild ancestor. *BMC Genet.* 11:90. doi: 10.1186/1471-2156-11-90

Wang, J., Wang, Z., Du, X., Yang, H., Han, F., Han, Y., et al. (2017). A high-density genetic map and QTL analysis of agronomic traits in foxtail millet [*Setaria italica* (L.) P. Beauv.] using RAD-seq. *PLoS One* 12:e0179717. doi: 10.1371/journal.pone.0179717

Wang, R.-L., Wendel, J. F., and Dekker, J. H. (1995a). Weedy adaptation in *Setaria* spp. II. Genetic diversity and population genetic structure in *S. glauca, S. geniculata,* and *S. faberii* (Poaceae). *Am. J. Bot.* 82, 1031–1039. doi: 10.3732/ajb.89.3.410

Wang, R. L., Wendel, J. F., and Dekker, J. H. (1995b). Weedy adaptation in *Setaria* Spp.1. isozyme analysis of genetic diversity and population genetic-structure in *Setaria-viridis*. *Am. J. Bot.* 82, 308–317. doi: 10.3732/ajb.89.3.410

Wang, Y., Zhi, H., Li, W., Li, H., Wang, Y., Huang, Z., et al. (2009). A novel genome of C and the first autotetraploid species in the *Setaria* genus identified by genomic in situ hybridization. *Genet. Resour. Crop Evol.* 56, 843–850. doi: 10.1186/1471-2164-14-244

Wang, Z. M., Devos, K. M., Liu, C. J., Wang, R. Q., and Gale, M. D. (1998). Construction of RFLP-based maps of foxtail millet, *Setaria italica* (L.) P. Beauv. *Theor. Appl. Genet.* 96, 31–36. doi: 10.1007/s001220050705

Wheeler, T., and von Braun, J. (2013). Climate change impacts on global food security. *Science* 341, 508–513. doi: 10.1126/science.1239402

Xiang, J. S., Tang, S., Zhi, H., Jia, G. Q., Wang, H. J., and Diao, X. M. (2017). Loose Panicle1 encoding a novel WRKY transcription factor, regulates panicle development, stem elongation, and seed size in foxtail millet *Setaria italica* (L.) P. Beauv. *PLoS One* 12:e0178730. doi: 10.1371/journal.pone.0178730

Xue, C. X., Zhi, H., Fang, X. J., Liu, X. T., Tang, S., Chai, Y., et al. (2016). Characterization and Fine mapping of SiDWARF2 (D2) in foxtail millet. *Crop Sci*. 56, 95–103. doi: 10.2135/cropsci2015.05.0331

Yang, J., Thames, S., Best, N. B., Jiang, H., Huang, P., Dilkes, B. P., et al. (2018). Brassinosteroids modulate meristem fate and differentiation of unique inflorescence morphology in *Setaria viridis*. *Plant Cell* 30, 48–66. doi: 10.1105/tpc.17.00816

Yang, N., Xu, X. W., Wang, R. R., Peng, W. L., Cai, L., Song, J. M., et al. (2017). Contributions of *Zea mays* subspecies mexicana haplotypes to modern maize. *Nat. Commun.* 8:1874. doi: 10.1038/s41467-017-02063-5

Yang, X., Wan, Z., Perry, L., Lu, H., Wang, Q., Zhao, C., et al. (2012). Early millet use in northern China. *Proc. Natl. Acad. Sci. U.S.A.* 109, 3726–3730. doi: 10.1073/pnas.1115430109

Yu, J., Hu, S., Wang, J., Wong, G. K., Li, S. G., Liu, B., et al. (2002). A draft sequence of the rice genome (*Oryza sativa* L. ssp indica). *Science* 296, 79–92.

Zhang, G., Liu, X., Quan, Z., Cheng, S., Xu, X., Pan, S., et al. (2012). Genome sequence of foxtail millet (*Setaria italica*) provides insights into grass evolution and biofuel potential. *Nat. Biotechnol.* 30, 549–554. doi: 10.1038/nbt.2195

Zhang, H. Y., Guo, P. Y., Wang, Y. G., Yuan, X. Y., Dong, S. Q., Song, X. E., et al. (2017). Assessment of male sterility and antioxidant enzyme activities induced by the chemical hybridization agent SQ-1 in foxtail millet (*Setaria italica*). *Emirates J. Food Agric.* 29, 212–221. doi: 10.9755/ejfa.2016-10-1530

Zhang, K., Fan, G., Zhang, X., Zhao, F., Wei, W., Du, G., et al. (2017). Identification of QTLs for 14 agronomically important traits in Setaria italica based on SNPs generated from high-throughput sequencing. *G3* 7, 1587–1594. doi: 10.1534/g3.117.041517

Zhang, S., Tang, C., Zhao, Q., Li, J., Yang, L., Qie, L., et al. (2014). Development of highly polymorphic simple sequence repeat markers using genome-wide microsatellite variant analysis in Foxtail millet [*Setaria italica* (L.) P. Beauv.]. *BMC Genomics* 15:78. doi: 10.1186/1471-2164-15-78

Zhu, C., Yang, J., and Shyu, C. (2017). Setaria comes of age: meeting report on the second international Setaria genetics conference. *Front. Plant Sci.* 8:1562. doi: 10.3389/fpls.2017.01562

Conflict of Interest Statement: The authors declare that the research was conducted in the absence of any commercial or financial relationships that could be construed as a potential conflict of interest.

frontiers in Plant Science

ORIGINAL RESEARCH
published: 19 July 2018
doi: 10.3389/fpls.2018.00918

QTL Mapping Combined With Comparative Analyses Identified Candidate Genes for Reduced Shattering in *Setaria italica*

*Sandra Odonkor[1†], Soyeon Choi[2], Debkanta Chakraborty[3], Liliam Martinez-Bello[1,4†], Xuewen Wang[1,2,4], Bochra A. Bahri[1,4,5], Maud I. Tenaillon[6], Olivier Panaud[7] and Katrien M. Devos[1,4]**

[1] Institute of Plant Breeding, Genetics and Genomics, University of Georgia, Athens, GA, United States, [2] Department of Genetics, University of Georgia, Athens, GA, United States, [3] Institute of Bioinformatics, University of Georgia, Athens, GA, United States, [4] Department of Plant Biology, University of Georgia, Athens, GA, United States, [5] Laboratory of Bioagressors and Integrated Protection in Agriculture (LR14AGR02), The National Agronomic Institute of Tunisia, University of Carthage, Tunis, Tunisia, [6] UMR8120 Génétique Quantitative et Evolution Le Moulon, Institut National de la Recherche Agronomique, Université Paris-Sud, Centre National de la Recherche Scientifique, AgroParisTech, Université Paris-Saclay, Paris, France, [7] Laboratoire Génome et Développement des Plantes, UMR UPVD/CNRS, Université de Perpignan Via Domitia, Perpignan, France

Setaria (L.) P. Beauv is a genus of grasses that belongs to the *Poaceae* (grass) family, subfamily Panicoideae. Two members of the *Setaria* genus, *Setaria italica* (foxtail millet) and *S. viridis* (green foxtail), have been studied extensively over the past few years as model species for C4-photosynthesis and to facilitate genome studies in complex Panicoid bioenergy grasses. We exploited the available genetic and genomic resources for *S. italica* and its wild progenitor, *S. viridis*, to study the genetic basis of seed shattering. Reduced shattering is a key trait that underwent positive selection during domestication. Phenotyping of $F_{2:3}$ and recombinant inbred line (RIL) populations generated from a cross between *S. italica* accession B100 and *S. viridis* accession A10 identified the presence of additive main effect quantitative trait loci (QTL) on chromosomes V and IX. As expected, enhanced seed shattering was contributed by the wild *S. viridis*. Comparative analyses pinpointed *Sh1* and *qSH1*, two shattering genes previously identified in sorghum and rice, as potentially underlying the QTL on *Setaria* chromosomes IX and V, respectively. The *Sh1* allele in *S. italica* was shown to carry a *PIF/Harbinger* MITE in exon 2, which gave rise to an alternatively spliced transcript that lacked exon 2. This MITE was universally present in *S. italica* accessions around the world and absent from the *S. viridis* germplasm tested, strongly suggesting a single origin of foxtail millet domestication. The *qSH1* gene carried two MITEs in the 5′UTR. Presence of one or both MITEs was strongly associated with cultivated germplasm. If the MITE insertion(s) in *qSH1* played a role in reducing shattering in *S. italica* accessions, selection for the variants likely occurred after the domestication of foxtail millet.

Keywords: domestication, miniature inverted-repeat transposable element (MITE), QTL analysis, seed shattering, *Setaria italica*, *Setaria viridis*, transcription factors

OPEN ACCESS

Edited by:
Andrew Doust, Oklahoma State University, United States

Reviewed by:
Mingsheng Chen, Institute of Genetics and Developmental Biology (CAS), China
Xinguang Zhu, University of Chinese Academy of Sciences (UCAS), China
Manoj Prasad, National Institute of Plant Genome Research (NIPGR), India

***Correspondence:**
Katrien M. Devos
kdevos@uga.edu

†Present address:
Sandra Odonkor, West African Centre for Crop Improvement, University of Ghana, Legon, Ghana
Liliam Martinez-Bello, Horticultural Sciences Department, University of Florida, Gainesville, FL, United States

Specialty section:
This article was submitted to Plant Breeding, a section of the journal Frontiers in Plant Science

Received: *23 February 2018*
Accepted: *11 June 2018*
Published: *19 July 2018*

Citation:
Odonkor S, Choi S, Chakraborty D, Martinez-Bello L, Wang X, Bahri BA, Tenaillon MI, Panaud O and Devos KM (2018) QTL Mapping Combined With Comparative Analyses Identified Candidate Genes for Reduced Shattering in Setaria italica. Front. Plant Sci. 9:918. doi: 10.3389/fpls.2018.00918

INTRODUCTION

Setaria italica, foxtail millet, and its wild ancestor *Setaria viridis*, green foxtail, are two of the ∼100 species that comprise the genus *Setaria*, tribe Paniceae, subtribe Cenchrinae, subfamily Panicoideae (Kellogg, 2017). The cultivated foxtail millet is grown both as a grain crop and for forage. The wild *S. viridis* is a weed found around the world in disturbed habitats. Cultivation of *S. italica* began approximately 5,900 years ago in the northern region of China, making it one of the oldest known domesticated crops (Barton et al., 2009). Domestication is the result of convergent selection for a limited number of traits aimed at making the crop better adapted to agricultural environments, higher yielding, and easier to harvest. The main traits favored in domesticated cereals are non-shattering seeds, larger grain size, increased grain number, larger panicle size, higher grain quality, and reduced sensitivity to photoperiod (Gepts, 2010).

Over the past decade, genes involved in a number of traits targeted by domestication have been characterized in cereal crops. One of the first genes isolated underlying a domestication quantitative trait locus was *Teosinte-branched* (*Tb1*) in maize, a transcription factor that controls axillary branch formation, sex expression, and inflorescence architecture (Doebley et al., 1997). Transition from the highly branched maize ancestor, teosinte, to the single-stalk phenotype of cultivated maize was caused by increased expression of *Tb1*, effected by the insertion of a transposable element 63 kb upstream of *Tb1*. Transcription factors have also been shown to be involved in the control of seed shattering in cereals (Doebley, 2006). *SH4* and *qSH1* are the two major disarticulation genes that underwent selection during rice domestication. *SH4*, located on rice chromosome 4, is a member of the trihelix family of transcription factors and carries a Myb3 DNA binding domain (Li et al., 2006). A single nucleotide polymorphism (SNP) in the Myb3 domain greatly reduced shattering. More recently, a frameshift mutation in *SH4* was identified that completely eliminated shattering (Zhou et al., 2012). *qSH1* on rice chromosome 1 encodes a BEL1-type transcription factor (Konishi et al., 2006). A SNP in the 5′ regulatory region eliminated *qSH1* expression at the abscission layer leading to loss of shattering ability. In sorghum, selection for non-shattering phenotypes during domestication largely occurred at the *Sh1* locus on chromosome 1 (Lin et al., 2012). At least three independent mutations have been identified that either inactivate the gene or reduce its expression significantly. Syntenic regions on rice chromosome 3, maize chromosomes 1 and 5, and *Setaria* chromosome IX have been shown to harbor disarticulation QTL, suggesting parallel selection at the *Sh1* locus during the domestication of cereals (Lin et al., 2012). Free-threshing ability in wheat is conferred by mutations in the *Q* gene on wheat chromosome 5A, which encodes a transcription factor belonging to the APETALA2 family. Wild and cultivated alleles differ in their expression as well as by the presence of a non-synonymous SNP which causes reduced homodimer formation (Simons et al., 2006). Triticeae also display disarticulation of the rachis, which is controlled by two tightly linked genes on chromosome 3 (Komatsuda et al., 2007). Inactivation of one of the two genes is sufficient to yield a non-brittle rachis phenotype. One of the genes (*BTR1*) is predicted to encode a membrane-bound protein. The other gene (*BTR2*) likely encodes a soluble protein. BTR2 has some similarity to, but is not considered an ortholog of, the *Arabidopsis thaliana INFLORESCENCE DEFICIENT IN ABSCISSION* (Butenko et al., 2003).

Setaria has recently been brought to the spotlight as a model plant system to study agronomically relevant traits in C_4-photosynthetic biofuel grasses and cereals (Doust et al., 2009; Li and Brutnell, 2011). *S. italica* and *S. viridis* have small diploid genomes (∼450 Mb), a short stature, rapid life cycle, and prolific seed production. Genetic and genomic resources include whole-genome sequence assemblies for both *S. italica* (Bennetzen et al., 2012; Zhang et al., 2012) and *S. viridis* (*Setaria viridis* v1.1, DOE-JGI[1]), a recombinant inbred line (RIL) population derived from a cross between B100 (*S. italica*) and A10 (*S. viridis*) (Bennetzen et al., 2012), high-density genetic maps (Bennetzen et al., 2012; Fang et al., 2016; Wang et al., 2017), a high-density haplotype map of genome variation (Jia et al., 2013) and transformation capability (Van Eck et al., 2017). QTL for seed shattering have previously been reported on *Setaria* chromosomes V and IX (Devos and Gale, 2000; Doust et al., 2014a). Here, we exploit the available genetic and genomic resources to further determine the genetic basis of shattering loss in foxtail millet.

MATERIALS AND METHODS

Plant Material

Seed shattering was measured on $F_{2:3}$ progeny (Devos et al., 1998; Wang et al., 1998) as well as on F_{10} recombinant inbred lines (RIL) (Bennetzen et al., 2012) from a cross between *S. italica* accession B100 and *S. viridis* accession A10. A total of 112 $F_{2:3}$ families of 6–13 plants together with the parents were grown in a randomized block design with two replications during the period from May to September 1998 in the field at Orsay, France. Replicate 2 consisted of only 66 $F_{2:3}$ families because of insufficient seed for some of the lines. For the RIL population, four plants per line for a total of 188 lines were grown in hill plots in a randomized block design with three replications at the University of Georgia (UGA) Plant Sciences Farm, Watkinsville, GA, during the period June to August, 2011. The *S. italica* accessions Yugu1 and B100 and the *S. viridis* accession A10 were part of the UGA *Setaria* collection. Their sources have been described previously (Wang et al., 1998; Bennetzen et al., 2012). *S. italica* accessions Ise-3 and Ise-5 were obtained from ICRISAT, Patancheru.

Genetic Maps and Markers

A linkage map for the F_2 population had been developed by Wang and colleagues using restriction fragment length polymorphism (RFLP) markers (Devos et al., 1998; Wang et al., 1998). This map consisted of 257 loci spanning 1050 cM across the nine foxtail millet chromosomes. The genetic map generated in

[1]http://phytozome.jgi.doe.gov

the RIL population and reported by Bennetzen et al. (2012) consisted of 990 single nucleotide polymorphism (SNP) markers and comprised a total map length of 1416 cM. The genotypic data used for the generation of both maps are attached as **Supplementary Table S1**.

Phenotypic Evaluation of Traits

Shattering ability, that is the ease with which spikelets are released from the pedicel, was scored subjectively from 0 (florets remaining intact as in the cultivated *S. italica*) to 3 (freely shattering as in the wild *S. viridis*) by clasping the panicle in a clenched fist. The phenotypic data used in the QTL mapping are provided in **Supplementary Table S1**.

QTL Mapping and Candidate Gene Identification

QTL mapping in both the $F_{2:3}$ and RIL populations was done using composite interval mapping (CIM) in Windows QTL Cartographer 2.5 (Basten et al., 1995; Wang et al., 2012). We used model 6 with forward and backward regression, a 10 cM window size, and a mapping step size of 1 cM. The logarithm of odds (LOD) threshold that defined a significant QTL was determined based on 500 permutations and a significance level of $P = 0.05$. Analyses were done for each replicate separately, as well as across replicates. To find candidate genes underlying the QTL, QTL regions, delineated by the most distal flanking markers with LOD scores above the significance threshold, were located on the *S. italica* Yugu1 genome sequence assembly v2.2[2]. Using comparative knowledge between *Setaria* and other grass species (Bennetzen et al., 2012; Devos et al., 2017), the orthologous regions in rice, sorghum, and maize were scanned for the presence of known shattering genes.

Comparative Analysis at the DNA Sequence Level of the *S. italica* and *S. viridis* Alleles at the *Sh1* and *qSH1* Loci

The sorghum *Sh1* (Sobic.001G152901; Lin et al., 2012) and rice *qSH1* (LOC_Os01g62920) coding sequences were used in BLASTN searches against the *S. italica* Yugu1 and *S. viridis* A10 whole genome sequence assemblies[2] to identify the corresponding orthologs. For each gene, the genomic sequences of the *S. italica* and *S. viridis* alleles were aligned and compared. To determine whether the same structural variations were present in B100 as in Yugu1, we exploited the ∼43 Gb of sequence data that were available from a bulk of 48 B100 × A10 RIL lines (Bennetzen et al., 2012; SRX030717 and SRX030718). The RIL bulk sequencing data had been generated to identify the SNPs used in the construction of the RIL genetic map (Bennetzen et al., 2012). The Illumina reads (2 × 75 bp) were aligned against the Yugu1 genome assembly using Bowtie (Langmead and Salzberg, 2012) with default parameters. Alignments in the *Sh1* and *qSH1* regions were inspected visually using the Integrated genome viewer (IGV) v2.3 (Robinson et al., 2011).

The structural variants identified in *Setaria* in *Sh1* and *qSH1* were further validated by PCR-amplification using primer set SiSh1-91F (5′-GGATCATGCCTTGCACTCCT-3′) / SiSh1-91R (5′-CATGCATGCACATTTCGGCT-3′) for *Sh1* and qSHIns1_F (5′-GCTTCCTGGAGTGGTCAAAC-3′) / qSHIns1_R (5′-GG ACGTGGTAGAGCTGCTG-3′) for *qSH1*, and genomic DNA of *S. italica* accessions Yugu1 and B100, and *S. viridis* accession A10. PCR reactions consisted of 1.5 mM $MgCl_2$, 200 nM dNTPs, 0.5 μM of forward and reverse primer and 4 U of GoTaq DNA polymerase (Promega) in 50 μl 1X GoTaq buffer (Promega) either with or without 5% DMSO. PCR conditions for *Sh1* were initial denaturation at 95°C for 3 min, 40 cycles of denaturation at 95°C, annealing at 58°C for 40 s, ramping to 72°C at a rate of 1°C/s and extension at 72°C for 3 min, followed by a final extension of 5 min at 72°C after which reactions were held at 10°C. The same conditions were used for *qSH1* except that reaction volumes were decreased to 10 or 20 μl, annealing was done at 60.9°C, and the number of cycles was reduced to 35. Amplicons were gel extracted using the Zymoclean™ Gel DNA Recovery Kit (The Epigenetics Company) and Sanger sequenced. Because of low amplification efficiency, *Sh1* fragments amplified from B100 were reamplified following gel extraction using the same reaction conditions, gel extracted again, and then sequenced.

Assessing the Presence of the MITEs in *Sh1* and *qSH1* in *S. italica* and *S. viridis* Germplasm

We downloaded Illumina reads obtained from whole-genome resequencing of 200 *S. italica* accessions (Jia et al., 2013) and 100 *S. viridis* accessions[3] and used sequences that spanned the boundary between genic and MITE sequence, as well as genic sequence that flanked the MITE insertion sites (*S. viridis* control) as queries in BLASTN analyses to test for the presence of the MITEs in the sequence data. The absence of hits when the *S. viridis* control was used as query combined with the presence of hits when the boundary region between genic sequence and MITE was used as query was taken as evidence for the presence of the MITE.

Transcript Analysis of *Sh1* and *qSH1* in *S. italica* and *S. viridis*

Total RNA was isolated from seedling leaves and from panicles 15 and 40 days after panicle emergence (15 DAPE) from A10 (*S. viridis*) and B100 (*S. italica*) using Trizol. Genomic DNA contamination was removed using the Turbo DNA-*free* kit (Invitrogen). cDNA was prepared using 500 ng of total RNA using the RevertAid First Strand cDNA Synthesis Kit (Thermo Scientific) according to the manufacturer's instructions. To assess the effect of the MITE on *Sh1* transcript processing in *S. italica*, 2 μg of cDNA was used as template in a PCR reaction (total volume 25 μl) consisting of 2 mM $MgCl_2$, 200 nM dNTPs, 1 μM forward primer Sh1-09f-MITE (5′-GTGCTACGTACACTGCAACTT-3′;

[2] phytozome.jgi.doe.gov

[3] genome.jgi.doe.gov

located in exon 1), 1 μM reverse primer Sh1-09r-MITE (5′-ATGATCCTGATCGCCTTTTG-3′; located in exon 3), and 0.025 U of GoTaq (Promega) in 25 μl of GoTaq Reaction Buffer (Promega). Amplicons were checked on a 1% agarose gel, purified from the gel using the GeneJET Gel Extraction Kit (Thermo Scientific), cloned into the pGEM-T Easy Vector (Promega) and Sanger sequenced. Semi-quantitative (semi-q) RT-PCR was conducted to determine transcript levels of *qSH1* in A10 and B100 using primer sets qSH_expr1_F (Seq: 5′- TC CAACTGATGGTGACAAGC-3′) and qSH_expr1_R (Seq: 5′- CT TGTGGACCTGCCTCATCT-3′). Actin was used as control. Reaction conditions were the same as used for amplification of genomic DNA. The semi-qRT-PCR conditions for analyzing *qSH1* expression levels were initial denaturation at 95°C for 5 min, 30 cycles of denaturation at 95°C for 45 s, annealing at 60°C for 45 s, and extension at 72°C for 1 min, followed by a final extension of 5 min at 72°C after which reactions were held at 10°C. A total of 5 μl reaction product was run on a 2.0% agarose gel and the intensity of the bands was measured using the software ImageJ (Abràmoff et al., 2004). Band intensity for *qSH1* was normalized using the intensity of the actin amplicon. *qSH1/Actin* ratios of technical replicates were averaged for statistical analysis.

RESULTS

Phenotypic Variation

Shattering in *S. viridis* acc. A10 was scored as 3 (highly shattering) and in *S. italica* acc. B100 as 0 (non-shattering). Some 39% of $F_{2:3}$ families displayed little shattering (mean score ≤ 1.3) and 2% displayed high shattering (mean score ≥ 2.7). Similarly, in the RIL population, an average of 35% of RILs were low shattering and 5% were highly shattering.

QTL Detection

QTL for seed shattering were identified on chromosomes V, VI, and IX in the $F_{2:3}$ population and on chromosomes V, VII, and IX in the RIL population (**Table 1**). For all QTL, the A10 allele led to increased shattering. The chromosome IX QTL in the $F_{2:3}$ population was located between the rice cDNA sequences C0595 (Genbank accession number AU091626) and C1361 (C98269), which identify loci on the *S. italica* acc. Yugu1 genome sequence (Bennetzen et al., 2012) at positions 6.2 and 14.6 Mb, respectively. This QTL explained 30.6% of the variation in the across-replicate analysis. The main chromosome IX QTL in the RIL population was located in the region 6.2 Mb–11.9 Mb (**Figure 1A**) and explained 35.2% of the variation in the across-replicate analysis (**Table 1**). QTL on chromosome V were also identified in all replicates in both populations although the location of the QTL varied by replicate and population. The chromosome V QTL in the $F_{2:3}$ population mapped to non-overlapping regions on the *S. italica* genome sequence (0.6–8.8 Mb and 29.5–to 43.7 Mb for replicate 1 and replicate 2, respectively). No QTL was identified on chromosome V when mean values across replicates 1 and 2 were used as trait data. In the RIL population, the chromosome V QTL was delineated to the region 35.8–36.9 Mb in replicate 1, 28.5–35.4 Mb in replicate 2, 32.3–35.4 Mb in replicate 3, and 28.1–36.9 Mb in the across-replicate analysis (**Figure 1B**). This QTL explained 12.5% of the variation in the across-replicate analysis (**Table 1**). The QTL on chromome VI was significant only in replicate 2 in the $F_{2:3}$ population. Similarly, the QTL on chromosome VII was significant only in replicate 2 in the RIL population.

Identification of Candidate Genes Underlying the Chromosome V and IX QTL

Several genes controlling seed shattering have been identified in cereals. Considering the known grass syntenic relationships (Gale and Devos, 1998; Devos, 2005), *qSH1* (Konishi et al., 2006) and *Sh1* (Lin et al., 2012) were of specific interest as candidate genes for the shattering QTL in our study. These genes had also been identified by Doust et al. (2014a,b) as candidates for shattering QTL they had mapped to *Setaria* chromosomes V and IX. *qSH1* is a BEL1-type homeobox gene on rice chromosome 1 which is syntenic with *Setaria* chromosome V. *Sh1* is a YABBY transcription factor on sorghum chromosome 1, which is syntenic with *Setaria* chromosome IX. The ortholog for *Sh1* in *S. italica* accession Yugu1 (Seita.9G154300) was located at position 10.1 Mb (corresponding to ∼44.5 cM on the genetic map) and thus within the interval carrying the shattering QTL on chromosome IX (6.2–11.9 Mb; **Figure 1A**). Furthermore, the marker most highly associated with the shattering trait on chromosome IX in the RIL population, UGSF31, was also the marker most closely linked to the *Sh1* gene. A comparison of the genomic and coding sequences of Seita.9G154300 and its ortholog in *S. viridis* acc. A10 (Sevir.9G153200) showed the presence of an 854 bp miniature inverted-repeat transposable element (MITE) in exon 2 in Seita.9G154300. The MITE belonged to the *P-Instability Factor (PIF)/Harbinger* family of DNA transposons. Scrutiny of this region in the alignment of Illumina reads generated from a pool of 48 B100 × A10 RILs showed the presence of reads that spanned the boundaries between *Sh1* and MITE sequence, suggesting that the MITE was also present in *S. italica* accession B100. PCR amplification of the MITE-containing region in *S. italica* accessions Yugu1 and B100 using primers located in intron 1 and intron 2 yielded no product using standard PCR conditions, and a faint ∼1500 bp product when amplification was done in the presence of 5% DMSO. In contrast, both sets of reaction conditions yielded a strong ∼700 bp product in *S. viridis* accession A10. Sequencing of the B100 amplicon showed that this accession carried the same MITE that was present in *S. italica* accession Yugu1 (**Supplementary Figure S1**).

The *Setaria* orthologs for *qSH1* were Seita.5G381300 in *S. italica* acc. Yugu1 and Sevir.5G386500 in *S. viridis* acc. A10. Seita.5G381300 maps to position 41.4 Mb (corresponding to ∼86 cM on the genetic map) in the *S. italica* Yugu1 genome assembly. Although none of the chromosome V QTL identified in our study spanned the *qSH1* locus (**Figure 1B**), we nevertheless considered *qSH1* as putatively underlying the shattering QTL on *Setaria* chromosome V because of its close proximity to

TABLE 1 | QTL for seed shattering detected in the $F_{2:3}$ and RIL populations.

	Replicate	Chromosome	Flanking Markers (Position in cM)	Marker at Peak (Position in cM)	LOD at Peak	Additive Effect	Dominant Effect	R^2 (%)
F_2 population[1]	Rep1	V	psf63.1 (37.9) – rgc643.1 (42)	psf63.1 (37.9)	5.7	−0.411	0.020	15.5
	Rep2	V	rgc409 (66.3) – psf386 (80.9)	rgc409 (66.3)	9.7	−0.499	0.015	35.4
	Rep2	VI	rgc83.4 (61.6) – psf420 (69.6)	psf420 (69.6)	5.0	−0.290	−0.050	9.7
	Rep1	IX	rgc1361 (100.2) – rgc595 (128.5)	rgc136 (124.5)	9.4	−0.306	0.393	29.0
	Rep2	IX	rgc136 (124.5) – rgc595 (128.5)	psm176 (127.6)	7.8	−0.444	−0.086	16.8
	All	IX	rgc1361 (100.2) – rgc595 (128.5)	rgc136 (124.5)	10.7	−0.374	0.259	30.6
RIL population[2]	Rep1	V	UGSF364 (76.2) – UGSF365 (78.2)	UGSF365 (78.2)	4.1	0.218	0	7.6
	Rep2	V	UGSF345 (63.4) – UGSF364 (76.2)	UGSF350 (66.9)	6.2	0.302	0	12.7
	Rep3	V	UGSF352 (70.0) – UGSF361 (74.7)	UGSF356 (71.3)	4.4	0.247	0	7.7
	All	V	UGSF343 (61.7) – UGSF365 (78.2)	UGSF356 (71.3)	9.3	0.253	0	12.5
	Rep2	VII	UGSF621 (12.9)	UGSF621 (12.9)	3.5	0.223	0	6.7
	Rep1	IX	UGSF21 (33.2) – UGSF39 (54.3)	UGSF31 (44.4)	12.7	0.395	0	24.5
	Rep2	IX	UGSF22 (34.7) – UGSF34 (48.9)	UGSF31 (44.4)	7.6	0.388	0	16.0
	Rep3	IX	UGSF21 (33.2) – UGSF38 (52.1)	UGSF30 (44.2)	11.5	0.489	0	22.3
	All	IX	UGSF21 (33.2) – UGSF39 (54.3)	UGSF31 (44.4)	21.8	0.481	0	35.2
	All	IX	UGSF48 (58.4) – UGSF83 (68.3)	UGSF54 (64.6)	6.7	−0.273	0	8.7
	Rep3	IX	UGSF96 (75.6) – UGSF109 (83.9)	UGSF96 (75.6)	4.5	0.317	0	7.9
	All	IX	UGSF96 (75.6) – UGSF108 (82.8)	UGSF103 (81.8)	5.1	0.242	0	6.5

[1]B100 = Parent A; A10 = Parent B; LOD thresholds for QTL significance were 3.8 in Rep1, 3.7 in Rep2 and 3.8 across-replicates. [2]A10 = Parent A; B100 = Parent B; LOD thresholds for QTL significance were 3.1 for Reps 1, 2 and across-replicates, and 3.0 for Rep 3.

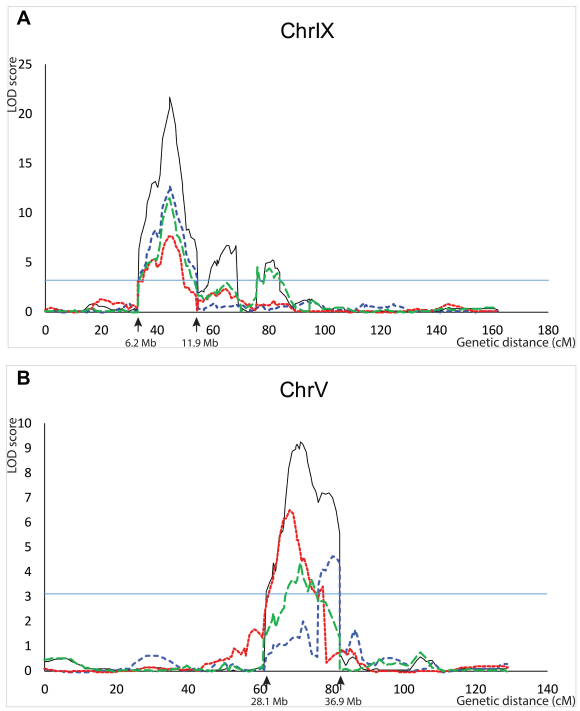

FIGURE 1 | QTL identified in the B100 × A10 RIL population on chromosomes IX **(A)** and V **(B)**. QTL in replicate 1 are in blue, in replicate 2 in red, in replicate 3 in green, and across-replicates in black. The horizontal line indicates the LOD threshold for significance at the 5% level.

the QTL. A comparison of Sevir.5G386500 and Seita.5G381300 showed that the two genes differed by a non-synonymous SNP in the coding region leading to a $Q_{77} \rightarrow H_{77}$ amino acid substitution, and by the presence of two MITEs belonging to the *PIF/Harbinger* family in the 5′UTR region. The insertion of both MITEs had been accompanied or followed by a rearrangement (**Supplementary Figure S2**). In case of the most 5′ located MITE (MITE 1), the deletion which spanned the 5′ boundary region of the *qSH1* 5′UTR and MITE was flanked by a short direct CGG repeat. This suggests that the deletion occurred by non-homologous end-joining during DNA break repair, possibly as part of the MITE insertion event. The insertion of the most 3′ located MITE (MITE 2) was accompanied/followed by both a deletion and an insertion (**Supplementary Figure S2**). Scrutiny of the alignment of the bulked B100 × A10 RIL reads against the Yugu1 genome assembly showed that the SNP and both MITEs were also present in *S. italica* accession B100. The presence of the two MITEs in the 5′UTR of B100 was confirmed by PCR and Sanger sequencing of the amplicons (**Supplementary Figure S3**). Semi-quantitative RT-PCR of *qSH1* in leaves of B100 and A10 showed that transcript levels were significantly lower in B100 compared to A10 (P = 0.015) (**Supplementary Table S2**). *qSH1* transcript levels in panicles were higher than in leaves (**Supplementary Table S2**), but not significantly different between A10 and B100 (P = 0.212).

Effect of the MITE on Transcript Processing of *Sh1* in *S. italica*

Because the MITE in Yugu1 and B100 *Sh1* was inserted close to the 3′ end of exon 2, we investigated whether its presence affected splicing. Sequencing of four clones from a single PCR reaction using *S. viridis* accession A10 cDNA as template with primer set sh1-09f-MITE/sh-09r-MITE, which was located in exon 1/exon 3 and hence amplified across the MITE insertion

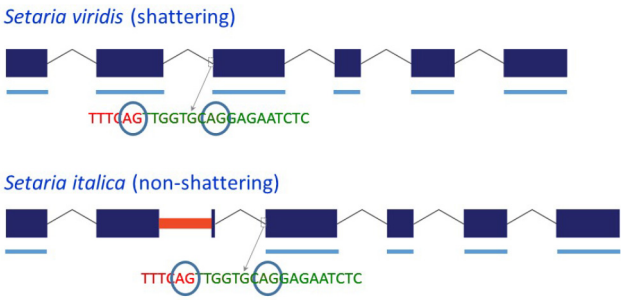

FIGURE 2 | Schematic representation of the structure of the *Sh1* gene and its transcript in *S. viridis* and *S. italica*. Blue boxes represent exons and thin lines represent introns. The red bar in exon 2 represents the MITE insertion. Thick blue lines underneath the exons represent exonic sequence present in the transcript. The circled "AG" indicates alternative splice sites.

site in exon 2, indicated the presence of two potential 3′ splice sites for intron 2 that were separated by 9 bp (**Figure 2** and **Supplementary Figure S1**). Reads corresponding to both splice products were also identified by BLASTN analysis against *S. viridis* A10 transcriptome data (NCBI SRA Experiment SRX875196), supporting the occurrence of alternative splicing. Sequencing of the same region (two clones from the same PCR reaction) in a *S. italica* B100 transcript also showed two alternative splice products that differed by nine basepairs. Furthermore, B100 transcripts lacked exon 2 (**Figure 2** and **Supplementary Figure S1**). The presence of the MITE resulted in the simultaneous splicing of intron 1, exon 2 plus the MITE and intron 2. The transcript data obtained by RT-PCR were confirmed by alignment of available RNA-Seq data from *S. italica* Yugu1 (NCBI SRA Experiment SRX2832831) against Seita.9G154300. The alignments further suggested that the MITE presence led to an additional alternatively spliced product in which introns 1 and 2 were retained (**Supplementary Figure S4**). We were unable to confirm the formation of this putatively alternatively spliced product by RT-PCR with primers located in exon 2 and exon 3. This could be due to the difficulty in amplifying across the GC-rich MITE. The overall GC content of the MITE was 66%, but was as high as 90% in several 50 bp windows. Alternatively, the presence of introns 1 and 2 in the RNA-Seq data may have been caused by genomic DNA contamination. This, however, is unlikely, because no evidence was obtained of retention of introns 3, 4, and 5 (**Supplementary Figure S4**). Of the two alternative splice sites 9 bp apart between intron 2 and exon 3, use of only the most 5′ splice site was observed in the RNA-Seq reads.

Presence of the MITEs in *S. italica* and *S. viridis* Germplasm

To determine the prevalence of the MITEs in *Sh1* and *qSH1* in *Setaria* germplasm, regions of, on average 87 bp, that covered either the boundary between genic sequence and MITE sequence or were comprised of genic sequence flanking the MITEs, were used in BLASTN searches against resequencing data from 200 *S. italica* and 100 *S. viridis* accessions. One or more reads in 59 *S. italica* accessions had hits against the boundary region that covered the 3′ end of exon 2 and the 5′ end of the MITE in *Sh1*. A total of 95 *S. italica* accessions had hits using the last 40 bp of the MITE, the last 5 bp of exon 2 and the first 39 bp of intron 2 of Yugu1 *Sh1* as query sequence. Thirty-five accessions had hits for both the 5′ and 3′ boundary regions, bringing the total number of *S. italica* accessions that carried a MITE to 119. None of the *S. italica* accessions had BLAST hits against the *S. viridis* control query sequence which covered the last 28 bp of exon 2 and the first 44 bp of intron 2 of A10 *Sh1*. In contrast, all 100 *S. viridis* accessions had BLAST hits using the MITE flanking sequence (*S. viridis* control) as query; none has BLAST hits using genic-MITE boundary regions as queries.

We found significant variation for the presence of the two MITEs in *qSH1* in *S. italica* germplasm. Of the 122 *S. italica* accessions with one or more identified blast hits, 54% carried at least one of the two MITEs, 43% lacked one of the MITEs but the presence of the other MITE was unknown and 2.5% (3 accessions) lacked both MITEs (**Supplementary Table S3**). Both MITEs were absent from the 5′UTR in *qSH1* in all *S. viridis* germplasm tested.

DISCUSSION

Although shattering ability was evaluated in a simple manner by scoring seed loss on a 0–3 scale, QTL were consistently (i.e., across replicates and populations) identified on chromosomes V and IX. However, only the QTL on chromosome IX colocalized across populations and replicates. This suggests that the clenched-fist method was sufficiently accurate to identify shattering loci of large effect. Precise mapping of smaller-effect QTL, however, may require the use of a force gauge to more precisely measure the strength needed to disarticulate a spikelet. The presence of wild-type alleles at both the chromosomes V and IX loci was required for a high level of shattering, indicating that the chromosomes V and IX effects are additive. Although the two QTL combined explained less than 50% of the variation in shattering, this is likely an underestimation due to the imprecise phenotyping. Nevertheless, it is possible that smaller-effect QTL for shattering are present in the population which were not, or not consistently, detected. The QTL on chromosomes VI and VII which were identified in only one replicate in the $F_{2:3}$ population and RIL population, respectively, could be such examples. Furthermore, additional QTL peaks were identified in some replicates on chromosome IX, and it is possible that they represent additional shattering genes that are present in the B100 × A10 population.

Although no visual abscission layer is present in *Setaria* (Hodge and Kellogg, 2016), our data show that the function of *Sh1* in seed disarticulation is conserved with *Sh1* function in other grass species despite differences in structure and/or location of the abscission zone (Doust et al., 2014b). The YABBY transcription factor (*Sh1* gene) underlying the shattering QTL on chromosome IX has previously been identified as the main gene controlling disarticulation in domesticated sorghum (Lin et al., 2012). *Sh1* also underlies shattering QTL on rice and

maize, suggesting parallel selection in different grass crops on this gene during domestication (Lin et al., 2012). In *S. italica,* the insertion of a *PIF/Harbinger* MITE close to the 3′ end of exon 2 led to the formation of a transcript that lacked exon 2. Exon 2 comprises 123 basepairs. Deletion of 41 amino acids in the SH1 protein in *S. italica* will almost certainly reduce or eliminate its activity. The same is true for proteins translated from transcripts in which introns 1, 2 and the MITE are retained. Analysis of resequencing data of *S. italica* (Jia et al., 2013) showed that 119 of the 200 accessions analyzed carried the MITE in *Sh1*. Of the 119 accessions, 75 were from China, and the remainder originated from other countries in Asia, Europe, and Africa. For the remaining 81 accessions, we could not establish presence/absence of the MITE because of the overall low depth of the resequencing data (average and median sequencing depth: 0.94 and 1.04, respectively). Importantly, none of the *S. italica* accessions tested were positive for the *S. viridis* control query sequence, supporting further that all *S. italica* germplasm carried the MITE in *Sh1*. Two additional *S. italica* lines, Ise-3 and Ise-5, that originated from India were also shown to carry the MITE in *Sh1* by PCR (**Supplementary Figure S1**).

Several hypotheses exist regarding the center of domestication of foxtail millet (reviewed by Diao and Jia, 2017). Some consider China the primary and possibly the only center of domestication for *Setaria*. Other studies advocate the existence of further independent centers of domestication in Europe and the region comprising central Asia, Pakistan, Afghanistan, and Northwest India. The presence of identical MITE insertions sites in *Sh1* in all 119 *S. italica* accessions for which sequence reads were available in the target region, irrespective of their country of origin, and the absence of this MITE in all *S. viridis* lines analyzed, strongly suggest a single center of domestication for foxtail millet. This is supported by the fact that alleles at SNP positions extending to at least 100 kb on either side of *Sh1* were close to fixation (99%) in our set of *S. italica* accessions (D. Chakraborty and K.M. Devos, unpublished data). The average frequency in this region of the *S. italica* SNP alleles in our set of *S. viridis* germplasm was 67%. The absence of the MITE in *Sh1* in the *S. viridis* germplasm analyzed may be due to (1) a low frequency of the low-shattering *Sh1* allele in wild populations, (2) insertion of the MITE early in the domestication process, or (3) a lack in our *S. viridis* collection of accessions from the center of domestication. Most of the resequencing data was for *S. viridis* accessions collected in the United States that belong to two major genetic subpopulations. Asian *S. viridis* germplasm largely forms a third subpopulation (Huang et al., 2014; Schröder et al., 2016)

It is unclear whether *qSH1* is the gene that underlies the shattering QTL on *Setaria* chromosome V. The presence of MITEs near genes can affect transcript levels, and both positive and negative effects have been reported (Naito et al., 2009; Lu et al., 2012; Han et al., 2013; Mao et al., 2015). It is therefore conceivable that the presence of either of the two MITEs in the 5′UTR of *qSH1* reduces expression of this transcription factor, leading to a strengthening of the abscission zone. In our analyses, transcript levels were lower in leaves of B100 than in A10, but no differences were observed in panicles. However, expression specifically in the abscission zone will need to be examined. In rice, *qSH1* expression was observed in both non-shattering and shattering lines in the shoot apical meristem during floral transition and in the anther regions, but only in shattering lines at the position of the abscission layer (Konishi et al., 2006). Although the coding sequence of the *qSH1* allele in *S. italica* acc. Yugu1 and B100 also differs from that in *S. viridis* accession A10 by the presence of a non-synonymous SNP, the lack of conservation of this region in different grass species (**Supplementary Figure S5**) suggests that this SNP is unlikely to affect *qSH1* gene function. An analysis of the presence of the two MITEs in *qSH1* across a worldwide collection of *S. italica* germplasm showed that 39% of Chinese germplasm (26 accessions) but only 7% (2) of accessions originating from countries other than China carried MITE 1. MITE 2 was predominantly present in *S. italica* worldwide. All *S. viridis* accessions tested lacked both MITEs. Genome-wide linkage disequilibrium in cultivated foxtail millet has been estimated at ∼100 kb (Jia et al., 2013), so our study could not differentiate between causal mutations and tightly linked variants. Of the three *S. italica* accessions that lacked both MITE 1 and MITE 2, two were from Hungary and one was from Turkey. The Turkish accession (Ci879) was listed as a "weedy foxtail" by Jia et al. (2013). Our study showed Ci879 to carry the MITE in *Sh1* so this accession was presumably low shattering. More precise phenotyping is necessary to determine the degree of shattering in *S. italica* lines that differ in the presence of the MITEs in *qSH1*.

CONCLUSION

We identified *Sh1* on *Setaria* chromosome IX as the main target for reduced shattering during the domestication of foxtail millet. The variant allele, which carries a *PIF/Harbinger* MITE, was present in *S. italica* lines from around the world and absent from all *S. viridis* accessions tested, supporting the hypothesis of a single center of domestication for foxtail millet. The *S. italica* accession B100 carries at least one other gene for reduced shattering located on chromosome V. Structural variation is present at the *qSH1* locus between *S. italica* and *S. viridis*, and the presence of two MITEs in the 5′UTR of *qSH1* is strongly associated with cultivated genotypes. Complementation tests or knock-out experiments are needed to unambiguously demonstrate that the MITE insertions represent the causal mutations to shattering rather than linked variants.

AUTHOR CONTRIBUTIONS

SO participated in the experimental design and QTL analysis, conducted the comparative analysis, and drafted the manuscript. SC did the *qSH1* transcript analysis, conducted the PCR to confirm the presence of the MITEs in *Sh1* and *qSH1*, and analyzed the RNA-Seq reads in the *Sh1* region. DC conducted the bioinformatic analysis of the presence of the MITEs in the *S. viridis* and *S. italica* germplasm. LM-B did the experimental *Sh1* transcript analysis. MT and OP conducted the phenotyping of the F_2 population. XW conducted the phenotyping of the

RIL population. BB conducted the QTL analyses. KD designed the study, participated in all aspects of data analysis and data interpretation, and wrote the manuscript. All authors critically read and approved the manuscript.

FUNDING

SO was partially funded through a graduate fellowship from the Institute of Plant Breeding, Genetics and Genomics. KD acknowledges funding from the National Institute of Food and Agriculture Plant Feedstock Genomics for Bioenergy Program (grant #2008-35504-04851).

SUPPLEMENTARY MATERIAL

The Supplementary Material for this article can be found online at: https://www.frontiersin.org/articles/10.3389/fpls.2018.00918/full#supplementary-material

FIGURE S1 | Multi-sequence alignment of the *Sh1* alleles and transcripts in *S. viridis* accession A10 and *S. italica* accessions Yugu1, B100, Ise-3 and Ise-5. Genomic and cDNA sequences are indicated with "genomic" and "cDNA," respectively, in the sequence name. Intron sequences have a white background, exon sequences have brown (A), yellow (C), green (T), and purple (G) backgrounds, and MITE sequences have green (A), orange (C), blue (T), and red (G) backgrounds.

FIGURE S2 | Insertion of **(A)** MITE 1 and **(B)** MITE 2 in the 5′UTR of *qSH1* was accompanied or followed by rearrangements. The MITE sequence is delineated by "|". Deletions are in red, insertions in green. [ ] indicates SSR units. Microhomology flanking the deletion is highlighted in yellow.

FIGURE S3 | Multi-sequence alignment of the *qSH1* alleles in *S. viridis* accession A10, and *S. italica* accessions B100 and Yugu1. MITE sequences have green (A), orange (C), blue (T), and red (G) backgrounds. The "ATG" start codon has a white background.

FIGURE S4 | Alignment of RNA-Seq reads against *Sh1* genomic sequence. **(A)** A10 reads (SRX875196) against Sevir.9G153200 (only the read coverage is shown) and **(B)** Yugu1 reads (SRX2832831) against Seita.9G154300 (both read coverage and individual read alignments are shown). Exon locations are indicated with red boxes. The MITE location in Seita9G.154300 is shown in blue.

FIGURE S5 | Multi-sequence alignment at the protein level across different grass species of the *qSH1* region carrying the non-synonymous SNP that differentiates *S. italica* from *S. viridis* (position 31 in this alignment).

TABLE S1 | Genotypic and phenotypic data for the B100 × A10 $F_{2:3}$ and RIL populations.

TABLE S2 | Semi-quantitative RT-PCR of *qSH1* in leaves and panicles of A10 and B100.

TABLE S3 | Presence/absence of MITEs 1 and 2 in *qSH1* in *S. italica* germplasm.

REFERENCES

Abràmoff, M. D., Magalhães, P. J., and Ram, S. J. (2004). Image processing with ImageJ. *Biophotonics Int.* 11, 36–42.

Barton, L., Newsome, S. D., Chen, F. H., Wang, H., Guilderson, T. P., and Bettinger, R. L. (2009). Agricultural origins and the isotopic identity of domestication in northern China. *Proc. Natl. Acad. Sci. U.S.A.* 106, 5523–5528. doi: 10.1073/pnas.0809960106

Basten, C. J., Weir, B. S., and Zeng, Z. B. (1995). *QTL Cartographer: A Reference Manual and Tutorial for QTL Mapping*. Raleigh, NC: North Carolina State University.

Bennetzen, J. L., Schmutz, J., Wang, H., Percifield, R., Hawkins, J., Pontaroli, A. C., et al. (2012). Reference genome sequence of the model plant Setaria. *Nat. Biotechnol.* 30, 555–561. doi: 10.1038/nbt.2196

Butenko, M. A., Patterson, S. E., Grini, P. E., Stenvik, G.-E., Amundsen, S. S., Mandal, A., et al. (2003). *INFLORESCENCE DEFICIENT IN ABSCISSION* controls floral organ abscission in Arabidopsis and identifies a novel family of putative ligands in plants. *Plant Cell* 15, 2296–2307. doi: 10.1105/tpc.014365

Devos, K. M. (2005). Updating the 'Crop Circle'. *Curr. Opin. Plant Biol.* 8, 155–162. doi: 10.1016/j.pbi.2005.01.005

Devos, K. M., and Gale, M. D. (2000). Genome relationships: the grass model in current research. *Plant Cell* 12, 637–646. doi: 10.1105/tpc.12.5.637

Devos, K. M., Wang, Z. M., Beales, J., Sasaki, T., and Gale, M. D. (1998). Comparative genetic maps of foxtail millet (*Setaria italica*) and rice (*Oryza sativa*). *Theor. Appl. Genet.* 96, 63–68. doi: 10.1111/tpj.12842

Devos, K. M., Wu, X., and Qi, P. (2017). "Genome structure and comparative genomics," in *Genetics and Genomics of Setaria – Plant Genetics and Genomics: Crops and Models*, eds A. Doust and X. Diao (Cham: Springer), 135–147.

Diao, X., and Jia, G. (eds) (2017). "Origins and domestication of foxtail millet," in *Genetics and Genomics of Setaria – Plant Genetics and Genomics: Crops and Models*, eds A. Doust and X. Diao (Cham: Springer), 61–72.

Doebley, J. (2006). Unfallen grains: How ancient farmers turned weeds into crops. *Science* 312, 1318–1319. doi: 10.1126/science.1128836

Doebley, J., Stec, A., and Hubbard, L. (1997). The evolution of apical dominance in maize. *Nature* 386, 485–488. doi: 10.1038/386485a0

Doust, A. N., Kellogg, E. A., Devos, K. M., and Bennetzen, J. L. (2009). Foxtail millet: a sequence-driven grass model system. *Plant Physiol.* 149, 137–141. doi: 10.1104/pp.108.129627

Doust, A. N., Lukens, L., Olsen, K. M., Mauro-Herrera, M., Meyer, A., and Rogers, K. (2014a). Beyond the single gene: How epistasis and gene-by-environment effects influence crop domestication. *Proc. Natl. Acad. Sci. U.S.A.* 111, 6178–6183. doi: 10.1073/pnas.1308940110

Doust, A. N., Mauro-Herrera, M., Francis, A. D., and Shand, L. C. (2014b). Morphological diversity and genetic regulation of inflorescence abscission zones in grasses. *Am. J. Bot.* 101, 1759–1769. doi: 10.3732/ajb.1400186

Fang, X., Dong, K., Wang, X., Liu, T., He, J., Ren, R., et al. (2016). A high density genetic map and QTL for agronomic and yield traits in Foxtail millet [*Setaria italica* (L.) P. Beauv.]. *BMC Genomics* 17:336. doi: 10.1186/s12864-016-2628-z

Gale, M. D., and Devos, K. M. (1998). Comparative genetics in the grasses. *Proc. Natl. Acad. Sci. U.S.A.* 95, 1971–1974. doi: 10.1073/pnas.95.5.1971

Gepts, P. (2010). Crop domestication as a long-term selection experiment. *Plant Breed. Rev.* 24, 1–44.

Han, Y., Qin, S., and Wessler, S. R. (2013). Comparison of class 2 transposable elements at superfamily resolution reveals conserved and distinct features in cereal grass genomes. *BMC Genomics* 14:71. doi: 10.1186/1471-2164-14-71

Hodge, J. G., and Kellogg, E. A. (2016). Abscission zone development in *Setaria viridis* and its domesticated relative, *Setaria italica*. *Am. J. Bot.* 103, 998–1005. doi: 10.3732/ajb.1500499

Huang, P., Feldman, M., Schroder, S., Bahri, B. A., Diao, X., Zhi, H., et al. (2014). Population genetics of *Setaria viridis*, a new model system. *Mol. Ecol.* 20, 4912–4925. doi: 10.1111/mec.12907

Jia, G., Huang, X., Zhi, H., Zhao, Y., Zhao, Q., Li, W., et al. (2013). A haplotype map of genomic variations and genome-wide association studies of agronomic traits in foxtail millet (*Setaria italica*). *Nat. Genet.* 45, 957–961. doi: 10.1038/ng.2673

Kellogg, E. A. (2017). "Evolution of Setaria," in *Genetics and Genomics of Setaria – Plant Genetics and Genomics: Crops and Models*, eds A. Doust and X. Diao (Cham: Springer), 3–27. doi: 10.1007/978-3-319-45105-3_1

Komatsuda, T., Pourkheirandish, M., He, C. F., Azhaguvel, P., Kanamori, H., Perovic, D., et al. (2007). Six-rowed barley originated from a mutation in a homeodomain-leucine zipper I-class homeobox gene. *Proc.*

Natl. Acad. Sci. U.S.A. 104, 1424–1429. doi: 10.1073/pnas.0608580104

Konishi, S., Izawa, T., Lin, S. Y., Ebana, K., Fukuta, Y., Sasaki, T., et al. (2006). An SNP caused loss of seed shattering during rice domestication. *Science* 312, 1392–1396. doi: 10.1126/science.1126410

Langmead, B., and Salzberg, S. L. (2012). Fast gapped-read alignment with Bowtie 2. *Nat. Methods* 9, 357–359. doi: 10.1038/nmeth.1923

Li, C., Zhou, A., and Sang, T. (2006). Rice domestication by reducing shattering. *Science* 311, 1936–1939. doi: 10.1126/science.1123604

Li, P., and Brutnell, T. (2011). *Setaria viridis* and *Setaria italica*, model genetic systems for the Panicoid grasses. *J. Exp. Bot.* 62, 3031–3037. doi: 10.1093/jxb/err096

Lin, Z., Li, X., Shannon, L. M., Yeh, C.-T., Wang, M. L., Bai, G., et al. (2012). Parallel domestication of the *Shattering1* genes in cereals. *Nat. Genet.* 44, 720–724. doi: 10.1038/ng.2281

Lu, C., Chen, J., Zhang, Y., Hu, Q., Su, W., and Kuang, H. (2012). Miniature Inverted–Repeat Transposable Elements (MITEs) have been accumulated through amplification bursts and play important roles in gene expression and species diversity in *Oryza sativa*. *Mol. Biol. Evol.* 29, 1005–1017. doi: 10.1093/molbev/msr282

Mao, H., Wang, H., Liu, S., Li, Z., Yang, X., Yan, J., et al. (2015). A transposable element in a NAC gene is associated with drought tolerance in maize seedlings. *Nat. Commun.* 6:8326. doi: 10.1038/ncomms9326

Naito, K., Zhang, F., Tsukiyama, T., Saito, H., Hancock, C. N., Richardson, A. O., et al. (2009). Unexpected consequences of a sudden and massive transposon amplification on rice gene expression. *Nature* 461, 1130–1134. doi: 10.1038/nature08479

Robinson, J. T., Thorvaldsdóttir, H., Winckler, W., Guttman, M., Lander, E. S., Getz, G., et al. (2011). Integrative genomics viewer. *Nat. Biotechnol.* 29, 24–26. doi: 10.1038/nbt.1754

Schröder, S., Bahri, B. A., Eudy, D. M., Layton, D. J., Kellogg, E. A., and Devos, K. M. (2016). Genetic diversity and origin of North American green foxtail [*Setaria* viridis (L.) Beauv.] accessions. *Genet. Resour. Crop Evol.* 64, 367–378. doi: 10.1007/s10722-016-0363-6

Simons, K. J., Fellers, J. P., Trick, H. N., Zhang, Z. C., Tai, Y. S., Gill, B. S., et al. (2006). Molecular characterization of the major wheat domestication gene Q. *Genetics* 172, 547–555. doi: 10.1534/genetics.105.044727

Van Eck, J., Swartwood, K., Pidgeon, K., and Maxson-Stein, K. (2017). "*Agrobacterium tumefaciens*-mediated transformation of *Setaria viridis*," in *Genetics and Genomics of Setaria – Plant Genetics and Genomics: Crops and Models*, eds A. Doust and X. Diao (Cham: Springer), 343–356.

Wang, J., Wang, Z., Du, X., Yang, H., Han, F., Han, Y., et al. (2017). A high-density genetic map and QTL analysis of agronomic traits in foxtail millet [*Setaria italica* (L.) P. Beauv.] using RAD-seq. *PLoS One* 12:e0179717. doi: 10.1371/journal.pone.0179717

Wang, S., Basten, C. J., and Zeng, Z.-B. (2012). *Windows QTL Cartographer 2.5*. Raleigh, NC: North Carolina State University.

Wang, Z. M., Devos, K. M., Liu, C. J., Wang, R. Q., and Gale, M. D. (1998). Construction of RFLP-based maps of foxtail millet, *Setaria italica* (L.) P.Beauv. *Theor. Appl. Genet.* 96, 31–36. doi: 10.1007/s001220050705

Zhang, G., Liu, X., Quan, Z., Cheng, S., Xu, X., Pan, S., et al. (2012). Genome sequence of foxtail millet (*Setaria italica*) provides insights into grass evolution and biofuel potential. *Nat. Biotechnol.* 30, 549–554. doi: 10.1038/nbt.2195

Zhou, Y., Lu, D., Li, C., Luo, J., Zhu, B.-F., Zhu, J., et al. (2012). Genetic control of seed shattering in rice by the APETALA2 transcription *factor SHATTERING ABORTION1*. *Plant Cell* 24, 1034–1048. doi: 10.1105/tpc.111.094383

Conflict of Interest Statement: The authors declare that the research was conducted in the absence of any commercial or financial relationships that could be construed as a potential conflict of interest.

frontiers in Plant Science

ORIGINAL RESEARCH
published: 30 July 2018
doi: 10.3389/fpls.2018.01103

SiSTL2 Is Required for Cell Cycle, Leaf Organ Development, Chloroplast Biogenesis, and Has Effects on C_4 Photosynthesis in *Setaria italica* (L.) P. Beauv.

Shuo Zhang†, Sha Tang†, Chanjuan Tang, Mingzhao Luo, Guanqing Jia, Hui Zhi and Xianmin Diao**

Institute of Crop Sciences, Chinese Academy of Agricultural Sciences, Beijing, China

Deoxycytidine monophosphate deaminase (DCD) is a key enzyme in the *de novo* dTTP biosynthesis pathway. Previous studies have indicated that DCD plays key roles in the maintenance of the balance of dNTP pools, cell cycle progression, and plant development. However, few studies have elucidated the functions of the DCD gene in Panicoideae plants. *Setaria* has been proposed as an ideal model of Panicoideae grasses, especially for C_4 photosynthesis research. Here, a *Setaria italica* stripe leaf mutant (*sistl2*) was isolated from EMS-induced lines of "Yugu1," the wild-type parent. The *sistl2* mutant exhibited semi-dwarf, striped leaves, abnormal chloroplast ultrastructure, and delayed cell cycle progression compared with Yugu1. High-throughput sequencing and map-based cloning identified the causal gene *SiSTL2*, which encodes a DCD protein. The occurrence of a single-base G to A substitution in the fifth intron introduced alternative splicing, which led to the early termination of translation. Further physiological and transcriptomic investigation indicated that *SiSTL2* plays an essential role in the regulation of chloroplast biogenesis, cell cycle, and DNA replication, which suggested that the gene has conserved functions in both foxtail millet and rice. Remarkably, in contrast to DCD mutants in C_3 rice, *sistl2* showed a significant reduction in leaf cell size and affected C_4 photosynthetic capacity in foxtail millet. qPCR showed that *SiSTL2* had a similar expression pattern to typical C_4 genes in response to a low CO_2 environment. Moreover, the loss of function of *SiSTL2* resulted in a reduction of leaf ^{13}C content and the enrichment of DEGs in photosynthetic carbon fixation. Our research provides in-depth knowledge of the role of DCD in the C_4 photosynthesis model *S. italica* and proposed new directions for further study of the function of DCD.

Keywords: dCMP deaminase, chloroplast biogenesis, cell cycle, cell expansion, C_4 photosynthesis, *Setaria italica*

OPEN ACCESS

Edited by:
Jianjun Chen,
University of Florida, United States

Reviewed by:
Xinguang Zhu,
University of Chinese Academy of Sciences (UCAS), China
Taniguchi Mitsutaka,
Nagoya University, Japan

****Correspondence:***
Hui Zhi
zhihui@caas.cn
Xianmin Diao
diaoxianmin@caas.cn

† These authors have contributed equally to this work.

Specialty section:
This article was submitted to Plant Breeding, a section of the journal Frontiers in Plant Science

Received: *26 February 2018*
Accepted: *09 July 2018*
Published: *30 July 2018*

Citation:
Zhang S, Tang S, Tang C, Luo M, Jia G, Zhi H and Diao X (2018) SiSTL2 Is Required for Cell Cycle, Leaf Organ Development, Chloroplast Biogenesis, and Has Effects on C_4 Photosynthesis in Setaria italica (L.) P. Beauv. Front. Plant Sci. 9:1103. doi: 10.3389/fpls.2018.01103

INTRODUCTION

Deoxycytidine monophosphate deaminase (DCD) is a key enzyme in the *de novo* deoxythymidine triphosphate (dTTP) synthesis pathway. DCD catalyzes the deamination of deoxycytidylate (dCMP) to produce deoxyuridine monophosphate (dUMP), the latter of which is the substrate that ultimately forms dTTP (Ellims et al., 1981). As described in previous studies, DCD contains two

conserved motifs, HXE and PCXXC, which reportedly function as a zinc-binding motif (Weiner et al., 1993). The DCD monomer is characterized to have between four and five α-helixes and six β-sheets, which are arranged in an α-β-α sandwich (Scortecci et al., 2017). Six DCD monomers combine to form a biologically active homohexamer in bacteria and animals (Hou et al., 2008). As an allosteric enzyme, DCD contains an allosteric site. dTTP and deoxycytidine triphosphate (dCTP) are the inhibitor and activator of DCD, respectively, which competitively bind to the allosteric site to control protein stability and further regulate the activity of DCD (Hou et al., 2008; Marx and Alian, 2015). This allosteric regulation depends on the participation of divalent metal ions, such as Ca^{2+} and Mg^{2+} (Scortecci et al., 2017). The pools of dTTP and deoxyribonucleoside triphosphates (dNTPs) are basic elements essential for DNA synthesis, replication, recombination, and repair (Kumar et al., 2011), which further guarantee the normal procession of these biological pathways. Two enzymes, the abovementioned DCD and ribonucleoside reductase (RNR), are mostly responsible for the maintenance of sufficient dTTP (Ke et al., 2005). RNR, which catalyzes the reduction reaction to produce deoxy-ribonucleotide diphosphate (dNDPs), is responsible for the *de novo* biosynthesis of four dNTPs to ensure the dNTP pools balance (Buckland et al., 2014). In addition to the *de novo* pathway, dTTP can be supplemented by the thymidine kinase (TK) salvage pathway in a majority of higher eukaryotes. TK, as the key enzyme in the salvage pathway, can catalyze the phosphorylation of deoxidized thymidine to form deoxythymidine monophosphate, the substrate to produce dTTP (Leija et al., 2016). When either of the *de novo* or salvage pathway is defective, the other can compensate for the loss of pyrimidine synthesis function (Leija et al., 2016). Thus, these pathways are mutually interrelated to maintain sufficient dTTP and the balance of the dNTP pools. In addition, the biosynthesis of dTTP is a highly coordinated process.

Deoxycytidine monophosphate deaminase defects always lead to the imbalance of the dNTP pools and further cause the abnormal synthesis of DNA. In the process of DNA synthesis, the accuracy of DNA polymerase depends on the supply of dNTPs (Buckland et al., 2014). When the correct dNTP inserts into a nucleotide chain, it competes with three other kinds of dNTPs. In addition, the fidelity of DNA replication also depends on the GC% in the dNTP pools. Thus, unbalanced dNTP pools increase the probability of the insertion of the wrong base (Gu and Li, 1994; Gawel et al., 2014). In addition, unbalanced dNTP pools can increase the frequencies of insertion/deletion mutations (Kumar et al., 2011). It has been reported that in fission yeast, the deletion of *DCD1* leads to drastic changes in the accumulations of dCTP and dTTP. The mutant strain becomes sensitive to DNA damage inducers, has a decreased capacity for DNA replication and repair, even appears the collapse of replication folk (Sanchez et al., 2012). Previous studies also reported that in budding yeast, *DCD* or *RNR* mutation could increase the mutation rates, slow down the DNA replication, and impact the genome integrity and stability (Kohalmi et al., 1991; Sanchez et al., 2012). In rice, the mutation of *OsDCD* results in DNA damage and leaf cell apoptosis (Niu et al., 2017).

In contrast, DCD decrease sometimes impaired cell cycle progression. The S-phase is the period in which the majority of DNA replication is established. Thus, the adequacy of dNTPs is a precondition of entrance into S-phase (McIntosh et al., 1986). Insufficient dNTPs or the imbalance of dNTP pools can activate the S-phase checkpoint, delay the progress of the cell cycle, decrease the cell proliferation rate, and even lead to cell apoptosis (Kumar et al., 2010). Previous studies have established that DCD or RNR deficiency in yeast resulted in cell cycle arrest in the S-phase (Elledge and Davis, 1990; Sanchez et al., 2012). The deficits of DCD in rice also cause cell cycle progression defects (Niu et al., 2017). DCD and other dNTPs biosynthetic genes are coordinated with cell cycle progression. Some cell cycle associated enzymes participate in the regulation of nucleotide metabolizing genes (Ke et al., 2005). In addition, the activities of most dTTP synthetic enzymes exhibit periodic fluctuations during the cell cycle (McIntosh et al., 1986). TK and thymidylate kinase (TMPK) are the targets of the cell cycle proteasome APC/C and can be degraded by APC/C during the G1-phase to maintain the balance of the dNTP pools in mammals (Ke et al., 2005). E2Fs, as important cell cycle associated transcription factors (TFs), can induce specific *RNR1a* expression in the G1/S-phase (Lincker et al., 2004). However, *DCD1* is reported to have a periodic expression level during the cell cycle in HeLa cells, but is transcribed at a constant level in *Saccharomyces cerevisiae* (McIntosh et al., 1986).

In higher plants, mutations of dNTPs synthesis genes always result in abnormal leaf development. For example, the phenotype of the *Arabidopsis thaliana RNR1* mutant has crinkled leaves with white pits. The mutant has fewer, larger, and dysplastic chloroplasts (Garton et al., 2007). Similarly, mutations in large and small submits of RNR in rice lead to dwarf plants, white stripe leaves, low chlorophyll contents, and undeveloped chloroplasts (Yoo et al., 2009; Qin et al., 2017). There are few reports on DCD gene functions in higher plants. A previous study showed that rice *OsDCD* mutant *st2* has white stripe leaves and reduced plant height. The chloroplast development and chlorophyll accumulation of *st2* are defected (Xu et al., 2014). In a recent study, another rice *DCD* mutant, *alr*, showed similar, but more severe phenotypes compared with *st2*, which had a small grain size and necrotic spots on the leaves. In addition, the cells of the *alr* mutant were increased in size, but decreased in number (Niu et al., 2017). Previous studies have proposed several explanations for these phenotypes in the *OsDCD* mutant. First, the unbalanced dNTP pools impaired the plastid genome replication and delayed chloroplast development. Second, the cell cycle progression and cell division were influenced, which resulted in small organs and dwarf plants (Niu et al., 2017).

Here, we isolated an *Setaria italica* mutant *sistl2* from EMS-induced lines of the Yugu1 cultivar. The mutant gene *SiSTL2* encodes a DCD protein. *sistl2* has similar phenotypes to those of *alr* and *st2* in rice. More interestingly, we found that *sistl2* was different to the rice *alr* mutant, including significantly reduced leaf cell size, normal second and third leaves, and uninfluenced grain size. It is worth noting that the C_4 photosynthetic character

of *sistl2* was affected, which has not been previously reported. In our study, we analyzed the mutant phenotypes, the expression of the causal genes, and expounded the function of *SiSTL2* in *S. italica*. Our research provides further insights into the role of DCD in the C_4 model *S. italica* and proposed new perspectives for further study of DCD functions.

MATERIALS AND METHODS

Plant Materials and Growth Condition

The *sistl2* mutant was obtained from the EMS-induced *S. italica* cultivar Yugu1. The identified mutant plants were backcrossed with Yugu1 three times before the characterization of the morphological and physical traits. To measure the agronomic traits and to determine the chlorophyll content and photosynthesis rate of Yugu1 and *sistl2*, the plants were grown in the experimental fields of the Institute of Crop Sciences, Chinese Academy of Agricultural Sciences, in Beijing (116.6° E, 40.1° N), China.

Chlorophyll Content, Photosynthetic Rate, and Chlorophyll Fluorescence

Setaria italica leaves harvested from the heading stage were cut into pieces and soaked in 95% alcohol for approximately 3 days until the leaf pieces were discolored completely. The supernatant was then collected and the absorbance values at 665 and 649 nm were measured by using a UV-1800 ultraviolet/visible light spectrophotometer. Chlorophyll *a* (Chl *a*) and chlorophyll *b* (Chl *b*) levels were then calculated by using the equation reported by Lichtenthaler (1987). The photosynthetic parameters were measured on fine mornings by using the Li-6400 portable photosynthesis system (LI-COR, Lincoln, NE, United States) to analyze mature leaves from five individual heading stage plants (6400-02B LED light source, ParIn = 1000 μmol m^{-2} s^{-1}). The $\Delta\Phi$PS II [(Fm′–Fs)/Fm′] was calculated from the equation mentioned by Hu et al. (2014).

Phenotypic Analysis of Leaf Venation Patterns

The leaves gained from the heading stage were observed and photographed by using an Anyty^{TM} 3R MSV500 portable digital microscope (3R Eddytek, Beijing, China). For the I_2–KI dye, the leaves were cut into pieces of 5 mm × 5 mm and fixed in FAA (3.7% formaldehyde, 50% ethanol, and 5.0% glacial acetic acid) overnight at 4°C, followed by a graded ethanol series and xylene series, and finally dyed in I_2–KI for 12 h. The samples were then observed and photographed by using a light microscope. For the cell size measurement, 20 medium-sized cells from three horizons were analyzed by using Image-Pro plus 6.0 (Media Cybernetics, Silver Spring, Georgia Avenue, United States).

Leaf Microstructure Observations

For the leaf cross section, the leaves of the seedling stage were cut into pieces of 2 mm × 1 mm, fixed, and treated as described above. After the treatment, the samples were embedded in resin. Microtome sections were stained with toluidine blue and photographed by using a light microscope.

For transmission electron microscopy (TEM) analysis, the leaf materials were obtained from seedlings of *Yugu1* and *sistl2* and cut into pieces of 2 mm × 1 mm. The materials were fixed overnight in 0.1 M phosphate buffer with 2.5% glutaraldehyde. Then the samples were washed three times with 0.2 M phosphate buffer and post-fixed in 1% osmium tetroxide for 1 h. After staining with uranyl acetate, the samples were further dehydrated in a gradient ethanol series and finally embedded into resin. Ultrathin sections were made and examined by using a JEM 1230 TEM.

Map-Based Cloning and High-Throughput Sequencing

For MutMap+ analysis (Fekih et al., 2013), the leaf samples were harvested from recessive individuals and dominant individuals, respectively. Then, two DNA pools contained the same amounts of DNA samples from 27 recessive/dominant individuals for whole genome resequencing were built. The resequencing was performed by using the Illumina HiSeq 2500 platform with a 150 bp paired-end strategy. The raw sequencing data was deposited at EMBL-EBI in the European Nucleotide Archive database under the accession number ERP106777. Data from the two sample pools were aligned to each other and analyzed in accordance with methods described in our previous study (Xiang et al., 2017).

To exclude irrelevant SNPs from the results of MutMap+ analysis, an F_2 population from the hybridization between *sistl2* and the SSR41 cultivar was used for mapping of the SiSTL2 locus. Three SSR markers based on earlier studies (Jia et al., 2009; Zhang et al., 2014) were adopted and an In-Del marker Ins9-1 was designed for gene cross positioning (**Supplementary Table S1**). To verify the change in transcript splicing, coding sequences of *Seita.9G511200* in WT and *sistl2* were amplified by using PCR primers (5′-ATGGCCTCGACGAGGGA-3′ and 5′-AAGGGCAAGGGAGTGAT-3′) and transformed into vectors by using the pEASY-Blunt cloning Kit (TRAN, Beijing, China). Four clones of each transformed cases were picked for sequencing by using the M13+/− universal primer.

Complementation Assay

The PCR reaction for the amplification of the promoter (primer with underlined in-fusion adaptor: 5′-GGCCAGTGCCAAGCTTCGTCGTTCCCTCCAAGTT-3′ and 5′-TCGAGGCCATGGATCCCGCGCTCGGGCGGTGGGGA-3′) and genome sequence (primer with in-fusion adaptor underlined: 5′-CCCGAGCGCGGGATCCATGGCCTCGACGAGGGA-3′ and 5′-GATCGGGGAAATTCGAGCTCAGAGGATCAAGCCATAGGACAC-3′) of *SiSTL2* were performed and transformed into the pTCK303 vector by using the In-Fusion HD Cloning Kit (Cat no. 072012, Clontech, United States) in two separate operations. The rice *Ubiquitin* gene was used as a reference for the RT-qPCR of transgenic lines in accordance with a previous report (Wang Y. et al., 2017).

Bioinformatics Analysis

The sequence, structure, and function annotation of the candidate genes were obtained from the *S. italica* V2.2 database of *Phytozome*[1]. The functional domains and motifs were predicted from the amino acid sequence by Conversed Domain search in *NCBI*[2]. The 3D structure analysis was produced by the *PDB* database[3]. Transcription factor binding sites were predicted by PlantRegMap[4].

Enzymatic Assays

For enzymatic assays, Wild-type *SiSTL2* cDNA and mutant *SiSTL2* cDNA (sequence before the mutant site) was subcloned into pCold vector and transformed into *E. coli* Transetta (DE3) for prokaryotic expression (sequences of primers with underlined in-fusion adaptor: for WT, 5′-TACCCTCGAGGGATCCATGGCCTCGACGAGGGA-3′ and 5′-GCTTGAATTCGGATCCTGGCTCCTGAAACTTGATCG-3′; for mutant, 5′-TACCCTCGAGGGATCCATGGCCTCGACGAGGGA-3′ and 5′-GCTTGAATTCGGATCCTAGGATTATTCCCTCTTGGCT-3′). Bacterial cultures (2 ml) were grown overnight at 37°C in LB medium, then transformed into 200 ml LB, and cultivate until OD_{600} = 0.6. Then the cells were induced using 0.3 mM isopropyl β-Dthiogalactopyranoside (IPTG) for 10 h at 15°C. Next, the cells were harvested by centrifugation and resuspended in 1 × PBS buffer, containing 1 mM PMSF and 100 unit/ml DNase. After disruption by sonication, the cell debris was removed by centrifugation at 16,100 *g* for 10 min. The soluble lysis fraction was purified by histidine specific Ni-NTA agarose resin and the target protein was eluted in elution buffer. Finally, the wild-type and mutant fusion protein with histidine tag were detected by SDS-PAGE, and used in enzyme assays.

Enzyme assays were conducted to measure the specific activity at 30°C in the buffer described previously with 100 μM dCTP and 0.2 mM $MgCl_2$ (Hou et al., 2008; Niu et al., 2017) by detecting the decrease in absorption at 290 nm using a UV-1800 ultraviolet/visible light spectrophotometer. The dCMP concentration varied from 0 to 3 mM with a grade of 0.5 mM. The enzyme concentration was fixed at 0.5 μg/ml. All measurements were performed three times, and average values and standard deviation were calculated.

qRT-PCR Analysis

The total RNA was gained from fresh plant tissues by using a Pure Link RNA Mini Kit (Cat no. 12183018, Invitrogen, United Kingdom). First-strand cDNA was prepared using a Primer Script First Strand cDNA Synthesis Kit (Cat no. 6210A, TaKaRa, Otsu, Japan). Quantitative-PCR (qPCR) was performed by using a Fast Start Universal SYBR Green Master (ROX) (Cat no. 04913914001, Roche, Mannheim, Germany). The specific primers for qPCR are listed in **Supplementary Table S2**. *Cullin* and the rice *Ubiquitin* gene were chosen as references for the RT-qPCR in *S. italica* tissues and the rice transgenic lines, respectively, according to the previous reports (Martins et al., 2016; Wang Y. et al., 2017). The data were analyzed by using an Applied Biosystems 7300 Analyzer (Applied Biosystems, Foster City, CA, United States).

Flow Cytometry

For flow cytometry, approximately 100 mg of proliferating first leaves were lacerated into 1 ml of cold nuclear isolation buffer (Lin et al., 2012) and then filtered with a 74 μm mesh. The suspension liquid was then stained with 2.5 mg ml^{-1} of 4′,6-diamidino-2-phenylindole (DAPI) for 10 min and analyzed on a MoFlo XDP cytometer (Beckman Coulter, CA, United States). For each test, 8000 nuclei were record to detect the ploidy level.

Yeast One-Hybrid Analysis

For the yeast one-hybrid analysis, the bait sequences containing adaptors and three tandem repeats of binding site sequence are listed in **Supplementary Table S3** (EBS, mEBS). The coding sequences of prey proteins were amplified with the primers listed in **Supplementary Table S3** (for *Seita.4G108100*: primer pairs "4G100"; for *Seita.1G314900*: primer pairs "1G900"). The yeast one-hybrid assay was operated by using a Matchmaker Gold Yeast one-hybrid system (Cat no. 630491, Clontech, Mountain View, CA, United States).

Transcriptome Sequencing Analysis

Yugu1 and *sistl2* plants were grown under the conditions of 16 h light and 8 h dark at 28°C for 4 weeks. The fourth extending leaves of *sistl2* and Yugu1 were harvested for total RNA extraction. The transcriptome sequencing was then performed and the cDNA libraries of *sistl2* and the WT were constructed in accordance with the Illumina sequencing manual and then sequenced on an Illumina HiSeq 2500 Genome Analyzer (Illumina, San Diego, CA, United States) with three independent biological replicates. Raw sequencing data were deposited with EMBL-EBI in the European Nucleotide Archive database under the accession number ERP106657. The qRT-PCR primers for the validation of the RNA-seq results are listed in **Supplementary Table S9**.

Carbon Isotope Determination and Low CO_2 Treatment

Approximately 50 mg of mature leaf samples at the heading stage of Yugu1 and *sistl2* were harvested. The samples were dried off at 80°C for 24 h. Pulverized samples were then disposed in accordance with a method described in a previous study (Cousins et al., 2008). The carbon isotopes were measured by using a Thermo Fisher Delta V isotope ratio mass spectrometer and calculated from a previously described equation (Stutz et al., 2014).

To verify how a low CO_2 environment impacts *SiSTL2* and photosynthesis-associated genes, 4-week-old plants of the WT and *sistl2* were grown in a CO_2 level control box. The CO_2 level was set to 40 ppm with 16 h of light and 8 h of dark at 28°C. To avoid the influence due to the daily fluctuation of the genes,

[1]https://phytozome.jgi.doe.gov/pz/portal.html

[2]https://www.ncbi.nlm.nih.gov/Structure/cdd/wrpsb.cgi

[3]http://www.rcsb.org/

[4]http://plantregmap.cbi.pku.edu.cn/binding_site_prediction.php

samples are harvested from the same parts of the leaves at the same time in each day (10 o'clock a.m.).

RESULTS

Phenotypic Characterization of the *S. italica sistl2* Mutant

The *S. italica* stripe leaf mutant *sistl2* was isolated from EMS-induced Yugu1 cultivar. Before the three-leaf stage, the phenotype of the mutant was normal, except for the white striped first leaf (**Figures 1A–D**). From the fourth leaf, *sistl2* begins to display white striped leaves (**Figure 1B**). At the shooting and heading stage, *sistl2* exhibited decreased plant height, impaired plant development, and notable narrow leaves covered with white stripes (**Figures 1F,G**). However, the grain size of the mutant was not affected (**Figure 1E**).

Several key agronomic traits of WT and *sistl2* were also surveyed. The results proved that the entire plant development of *sistl2* was arrested (**Supplementary Table S4**). It is worth noting that the leaf length and leaf width were clearly reduced; in addition, the panicle size, panicle weight, and seed setting percentage in *sistl2* also decreased extensively (**Figure 1H** and **Supplementary Table S4**). These results indicated that leaf extension and reproductive development were impaired in *sistl2*.

C_4 Typical Plant Leaf Structure and Development Was Seriously Defective

To investigate the changes in the leaf anatomy structure in *sistl2,* we observed the leaves by using a portable digital microscope. The results showed that the leaf veins of WT were complete. Bundle sheath (BS, contain more and larger chloroplasts), mesophyll tissue (M, contain less and smaller chloroplasts), and vascular bundles (VBs, without any chloroplasts) array neatly (**Figure 2A**). In contrast, some leaf veins of *sistl2* are misshapen and array in a disordered fashion (**Figure 2B**, red arrows). This result can also be confirmed by the I_2–KI staining on the leaves of WT and *sistl2* (**Figures 2C,D**). Because of different starch accumulation in chloroplast, BS and M can be dyed different color by I_2–KI. The BS and M of WT were dyed brown and yellow, respectively, and arrayed neatly. These results showed that the leaf veins of WT were intact and regular (**Figure 2C**). However, some veins of *sistl2* are discontinuous (**Figure 2D**, red arrows).

To further assess the anatomical traits, cross sections of the leaf were obtained (**Figures 2E,F**). In the leaves of Yugu1, the Kranz structure is regular; mesophyll cells (MCs) and bundle sheath cells (BSCs) contain many chloroplasts which are dyed purple (**Figure 2E**, yellow arrows). As a typical C_4 plant, *S. italica* has a constant leaf vein distance; between the two leaf veins (V) there are always two to three MCs in WT leaves (**Figure 2E**). Compared with the WT, the Kranz structure of *sistl2* was irregular. Although some BSCs and MCs are normal (**Figure 2F**, yellow arrows), many have fewer chloroplasts or even do not contain any chloroplast (**Figure 2F**, red arrows). In addition, for some leaf veins of *sistl2*, the BSCs appear to be undeveloped or absent (**Figure 2F**, gray polygons) and there is only one MC between the two veins (**Figure 2F**, blue arrow). In addition, it is worth noting that the sizes of BSCs and MCs in *sistl2* were decreased to 43.52 and 40.27% of that in the WT, respectively (**Figure 2G**). These results indicated that the chloroplast biogenesis and the leaf cell expansion of *sistl2* were inhibited and that the leaf anatomical structure was also impaired.

To further investigate the influences on *sistl2* chloroplast biogenesis, mature leaves of *sistl2* and WT were observed by TEM, as shown in **Figure 3**. The Kranz structures of the WT and the *sistl2* mutants are shown in **Figures 3A,B**, respectively. Normal and abnormal (red arrows in **Figure 3B**, these cells have less or no chloroplast) BSCs/MCs could be observed in *sistl2*. The chloroplasts in the normal MCs of *sistl2* were similar to the WT, containing fully developed stroma lamellas and granum lamellas (**Figures 3E,F**). As *S. italica* is an NADP-ME type C_4 plant, the BSCs contain only stroma lamellas. The chloroplasts in normal BSCs of *sistl2* also have well-developed stroma lamellas (**Figures 3C,D**). However, some BSC chloroplasts of *sistl2* contained fewer starch grains relative to the number found in Yugu1 (**Figures 3C,D**). In contrast, the chloroplasts in the abnormal BSCs/MCs of *sistl2* seem to be undeveloped (**Figures 3G,H**; red arrows). These results further clarify that the formation of Kranz structure, the leaf cell development, and chloroplast biogenesis in *sistl2* were significantly impaired.

Genetic Mapping of the *SiSTL2* Locus and Bioinformatics Analysis

Fine mapping was performed by the means of MutMap+ by using the M_4 population (Fekih et al., 2013). The *SiSTL2* locus was mapped to a 12 Mb genomic region from 46.8 to 58.9 Mb on chromosome 9 (**Figure 4A**, gray box). In accordance with the requirement for the index of homozygous recessive mutation should be greater than 0.9, four putative mutation sites were identified (**Supplementary Table S5**). In addition, an F_2 mapping population was generated from a cross between *sistl2* with the SSR41 cultivar. Through the use of this F_2 population (120 individuals with striped leaves), a 1 Mb genomic region between the In-Del marker Ins9-1 and the SSR marker b171 was defined (**Figure 4A**). Among those four putative mutations, only the mutant site of a G to A mutation at 54,317,059 on chromosome 9 is included in this region and it is predicted to lead a splice site alteration at *Seita.9G511200*. *Seita.9G511200* was assumed to have nine exons and eight introns, with the G to A mutation located at the last base of the third intron. The transcript sequence verified that this mutation caused the first base of the fourth exon to be altered to the last base of the upstream intron, which further leads to a single-base deletion of the coding sequence (**Figure 4B**) and resulted in a frame shift and a premature stop codon at the fifth exon.

Gene annotation revealed that *SiSTL2* encoded a putative *Setaria* deoxycytidylate (dCMP) deaminase. *SiSTL2* encoded a 228 amino acid peptide chain. The protein structure domain, as predicted by NCBI, showed that SiSTL2 comprised a dCMP deaminase (DCD) domain from amino acids 71 to 184. Six catalytic motifs and four Zn^{2+} binding sites were located in this domain, which were essential for catalytic function. However, the

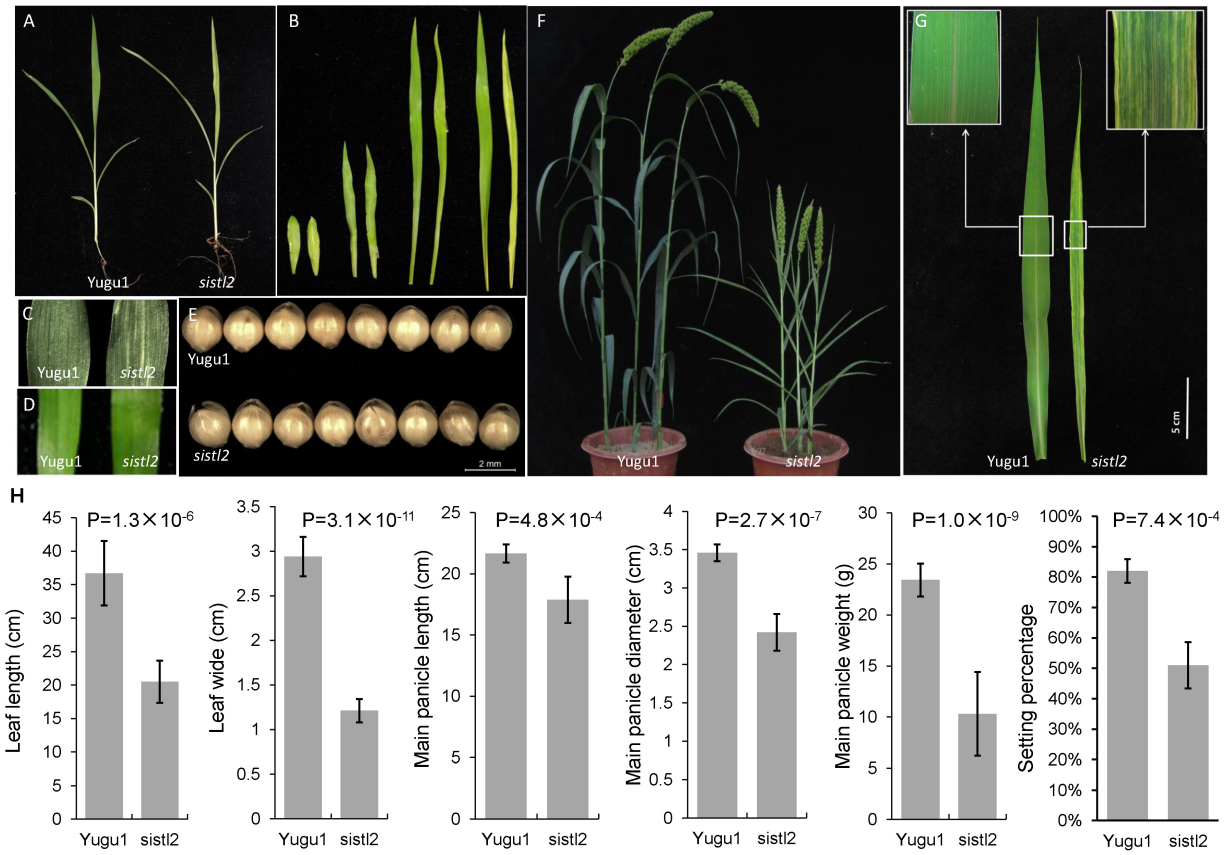

FIGURE 1 | Phenotypic characterization of *sistl2* mutant. **(A)** The four-leaf stage seedlings of Yugu1 and *sistl2*. **(B)** The first four leaves of Yugu1 and *sistl2* were placed in order from left to right. In each couple, the left one is Yugu1, and the right one is *sistl2*. **(C)** The first leaf of Yugu1 and the mutant. **(D)** The third leaf of Yugu1 and the mutant. **(E)** The seeds of Yugu1 and *sistl2*. **(F)** Heading stage phenotypes of Yugu1 and *sistl2*. **(G)** The mature leaves of Yugu1 and *sistl2* of heading stage. **(H)** The leaf length and leaf width were clearly reduced in addition to the panicle size, panicle weight, and the seed setting percentage of Yugu1 and *sistl2*. The leaves used for size measurement are mature top second leaves of Yugu1 and *sistl2* at heading stage, respectively. The means and standard deviations were obtained from five independent leaf samples. Statistical analysis was performed with the *t*-test.

mutation occurred at amino acid 107. As a result, the mutant SiSTL2 protein (ΔSiSTL2) lacks all the functional motifs and a large section of the DCD domain, which caused a defective protein function (**Figure 4C**). The SiSTL2 3D protein structure of the WT and *sistl2* were modeled (**Figure 4D**). These results showed that the SiSTL2 protein contained five alpha helixes and eight beta sheets, which functioned as a homo-hexamer, which forms a hexagon. However, ΔSiSTL2 loses four alpha helixes and six beta sheets, so that it cannot form any homo-multimer (**Figure 4D**).

SiSTL2 Can Complete the Phenotype of the *OsDCD* Mutant

The protein sequence BLAST showed that SiSTL2 was a homologous protein of *Oryza sativa* OsDCD. Owing to the difficulty of *S. italica* transformation, we choose the *OsDCD* mutant *st2*, which has a similar phenotype to *sistl2*, to perform the complementation assay. A fragment harboring a 6.75 kb genome sequence of *Seita.9G511200*, which contains a promoter and a 3′-UTR is introduced into *st2*. All five positive transgenic lines exhibited normal phenotypes. The phenotype and chlorophyll content of complemented T_0 (Com) was restored to WT (**Figures 5A,B**). The transcript of *SiSTL2* accumulated abundantly in transgenic lines, but did not exist in *st2* and the WT (**Figure 5C**). These results indicated that SiSTL2 had a similar function to OsDCD and was responsible for the stripe-leaf phenotype.

DCD Deamination Activity and Chloroplast Development Are Impaired in *sistl2*

To gain whether SiSTL2, the homolog of OsDCD, has DCD deamination activity, wild-type SiSTL2 protein with histidine tag (His-SiSTL2) and mutant SiSTL2 protein with histidine tag (His-ΔSiSTL2) were purified (**Supplementary Figure S1**). Then an *in vitro* assay was performed to test the deamination activity of SiSTL2 and ΔSiSTL2 (**Figure 6A**). The kinetic assay showed that with the substrate concentration increased, the deamination activity of the recombinant His-SiSTL2 rose and reached maximum. However, His-ΔSiSTL2 almost has no

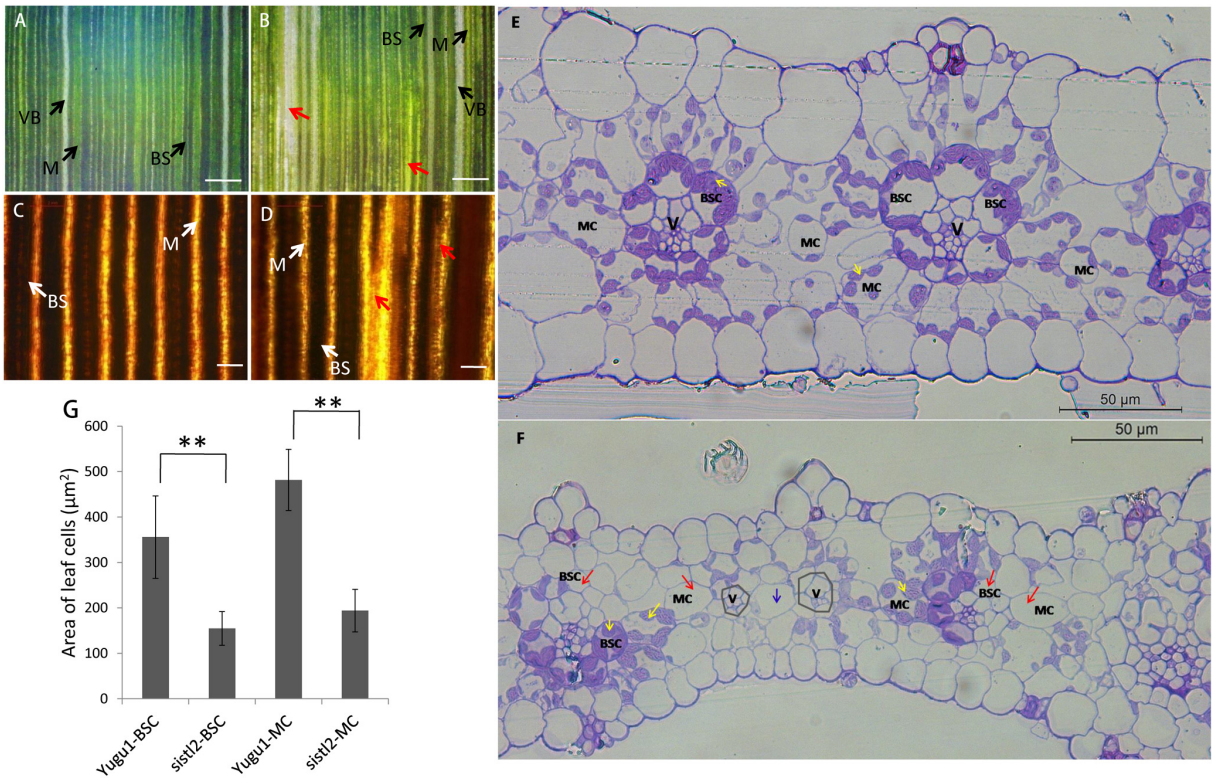

FIGURE 2 | Leaf structure of Yugu1 and *sistl2*. **(A,B)** The leaves of Yugu1 and *sistl2* observed by portable digital microscope. BS, bundle sheath. M, mesophyll tissue. Red arrows show abnormal leaf veins. Bars: 500 μm. **(C,D)** The leaves of Yugu1 and *sistl2* dyed by I_2–KI and viewed by using a light microscope. Red arrows show abnormal leaf veins. BS, bundle sheath; M, mesophyll tissue. Bars: 100 μm. **(E,F)** Leaf cross sections of Yugu1 and *sistl2*, respectively. Yellow arrows, chloroplasts in normal BSCs/MCs; Red arrows, BSCs/MCs contain no chloroplasts; Gray polygons show the leaf veins with undeveloped BSCs. Blue arrow, only one MC between two leaf veins (V). The type of the cell between two leaf veins was judged by the structure of its chloroplast as elucidated in **Supplementary Figure R1**. **(G)** The areas of BSCs and MCs in Yugu1 and *sistl2*. Twenty medium-sized cells from three horizons were calculated. The statistical analysis was performed by *t*-test. $^{**}P = 0.01$.

deamination activity (**Figure 6A** and **Supplementary Figure S1**, histidine tag protein as a negative control). This result indicate that SiSTL2 has deamination activity and can catalyze the deamination of dCMP. However, when the C terminal of the protein is deleted, ΔSiSTL2 lost the deamination activity.

To study the influence on transcription level caused by the mutation of *SiSTL2*, the relative expression levels of *SiSTL2* were verified in leaves at the seedling stage (**Figure 6C**). The results showed that the transcription levels of *SiSTL2* in the mutant was significantly reduced compared with Yugu1. This result indicated genes involved in *de novo* pathway and the salvage pathway of dTTP biosynthesis were affected. As the pyrimidine triphosphate salvage pathway is also essential for dTTP synthesis, the relative expression levels of several salvage pathway genes (*SiTK1*, *SiUDK*, *SiUDN*, and *SiCDA*) were also determined (**Figures 6B,C**). The results showed that the expression of salvage pathway genes in the mutant was also decreased. These results suggested that the mutation in *SiSTL2* influenced both the *de novo* pathway and the salvage pathway of dTTP biosynthesis.

To explain the white stripe formation in *sistl2*, the expression levels of chloroplast development associated genes were also detected. The results indicated that the transcription levels of most of these genes were significantly lower in *sistl2* (**Figure 6D**), which suggested that the chloroplast development was impaired at the transcriptome level. However, whether this transcription decline is result from the dTTP biosynthesis is still unclear.

SiSTL2 May Be Controlled by E2F and Is Involved in Cell Cycle Regulation

Deoxycytidine monophosphate deaminase decreases can sometimes impair the mitosis cell cycle progression (Niu et al., 2017). Thus, the DNA ploidy levels of leaf cells in the WT and *sistl2* were determined by using flow cytometric analysis. The first leaves of Yugu1 and *sistl2* were harvested at 48 h after germination sprout. The results displayed that *sistl2* has higher percentage of 2C cells, but less 4C and 8C cells than Yugu1 (**Figures 7A,B**). In other words, in *sistl2*, more cells were present in the G1/S-phase and fewer cells were in the G2/M-phase than those in the WT. This result indicated that the mitotic cell cycle of *sistl2* was delayed at the transition from the G1/S- to the G2/M- phase.

It has been reported that the expressions of DCD and many other nucleotide biosynthetic genes were coordinated with cell

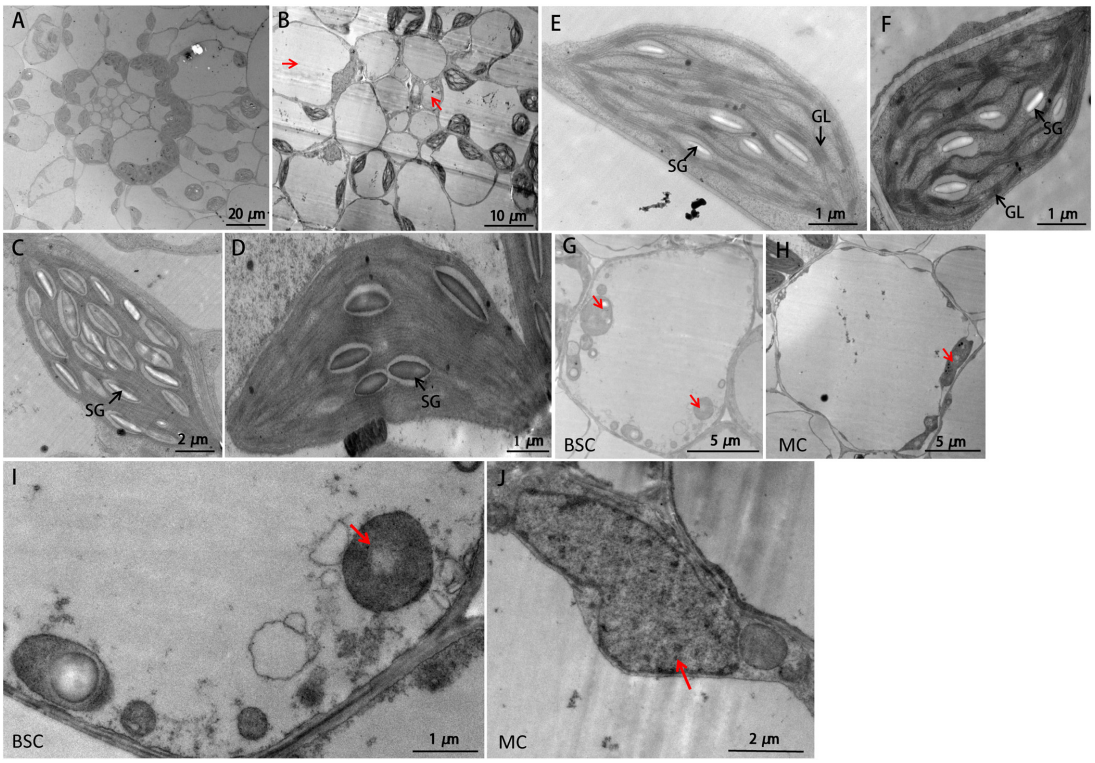

FIGURE 3 | TEM images of WT and *sistl2*. **(A,B)** Kranz structures of Yugu1 and *sistl2*, respectively. Red arrows, abnormal BSCs and MCs. **(C,E)** The chloroplasts in BSC and MC of Yugu1, respectively. The structure of an individual BSC chloroplast (WT) was shown in **Supplementary Figure R2**. **(D,F)** The chloroplasts in normal BSC and MC of *sistl2*, respectively. SG, starch granules; GL, grana lamella. Abnormal BSC **(G)** and MC **(H)** in *sistl2*. Red arrows show the undeveloped chloroplasts. **(I,J)** Undeveloped chloroplast in BSC and MC.

cycle progression and regulated by some cell cycle-associated enzymes (Ke et al., 2005). We also considered whether the expression of *SiSTL2* was controlled by any cell cycle-related proteins. Thus, the *cis*-acting elements in the *SiSTL2* promoter were predicted and an E2F transcription factor binding site (EBS) (CCCCAAAGTTTCCCGCGCTTA) was found at −99 to −119 bp upstream of the initiation codon of *SiSTL2*. A random sequence (mEBS) (TCGCATCTGCCACCTCAGTAC) of the same length as EBS was considered to represent a negative control. Then, we verified the interactions between the EBS element and the SiE2F proteins by using the yeast one-hybrid assay (**Figure 7C**). The results showed that *Seita.4G108100* and *Seita.1G314900*, which are homologs of E2Fe, could bind to the EBS of the *SiSTL2* promoter and activate the expression of the *Aureobasidin A* (AbA) resistance gene in yeast strains. E2F family members are TFs that are closely related to the regulation of cell cycle progression. Collectively, these results suggested that *SiSTL2* may be regulated by cell cycle-related E2Fe and impacted cell cycle progression. Defective *SiSTL2* resulted in blockage of the cell cycle.

Comparison of Genome-Wide Transcriptomes of WT and *sistl2*

Deoxycytidine monophosphate deaminase is a key enzyme in the regulation of the synthesis of dTTP. The lack of dTTP may impact DNA replication and further influence the other aspects of growth and development. The *sistl2* mutant showed comprehensive abnormal phenotypes of plant height, panicle size, seed-set rate, and especially leaf development. Thus, to reveal the signaling pathways and the regulatory networks that changed in the *sistl2* mutant, and to explain the relationships between SiSTL2 and leaf or chloroplast development, the genome-wide transcriptomes of leaves of Yugu1 and *sistl2* were compared. The fourth leaves during extension were chosen as the material for RNA sequencing.

The analysis detected 2694 different expressed genes (DEGs) between Yugu1 and *sistl2* (**Supplementary Table S6**). The enriched KEGG pathways of the top 10 DEGs are listed in **Table 1**. The data showed that the DEGs were most concentrated in photosynthesis associated pathways (photosynthesis, carbon fixation in photosynthetic organisms, and photosynthesis-antenna proteins) and DNA replication associated pathways (DNA replication and mismatch repair). Genes associated with carbon metabolism and secondary metabolite (fatty, glyoxylate, and phenylpropanoid) biosynthesis and metabolic pathways were also extensively changed. The results of Gene Ontology (GO) analysis showed that DEGs were enriched in GO terms related to photosynthesis, cell cycle progression, DNA replication, and microtubule (involved in spindle formation) (**Figure 8A**).

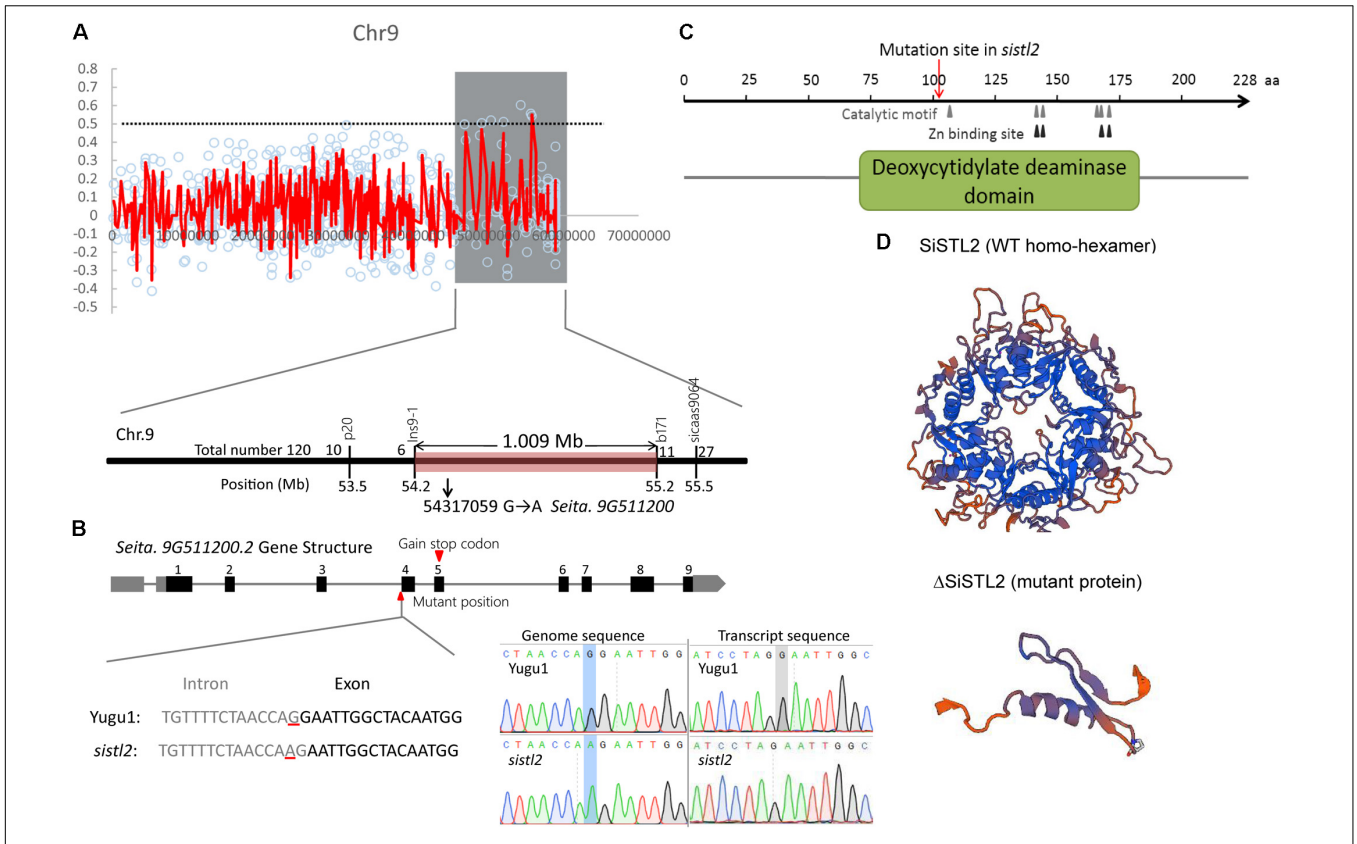

FIGURE 4 | (A) Genetic mapping of the *SiSTL2* locus. In top panel, Y-axis means the ΔSNP index, X-axis means physical location. Red lines show the ΔSNP indexes of different SNPs on chromosome. Gray box shows the candidate region obtained by MutMap+. The bottom panel indicates that the gene is narrowed to a 1.009 Mb region between Ins9-1 and b171 by 120 F_2 individuals. **(B)** The top of the figure shows the gene structure. Black boxes, exons; gray boxes, UTRs; gray lines, introns. The bottom of the figure shows the transcript variation proved by sequencing. Left bottom: gray text, intron; black text, exon; red lines, mutant position. Right bottom: the blue boxes and gray box show the mutant positions in genome sequence and transcript sequence, respectively. **(C)** The conserved functional domain and motifs of the SiSTL2 protein. Gray triangles show the six catalytic motifs, black triangles show the four Zn binding sites, and red arrows show the mutant position. **(D)** 3D protein structures of SiSTL2 (WT homo-hexamer) and ΔSiSTL2 (mutant protein).

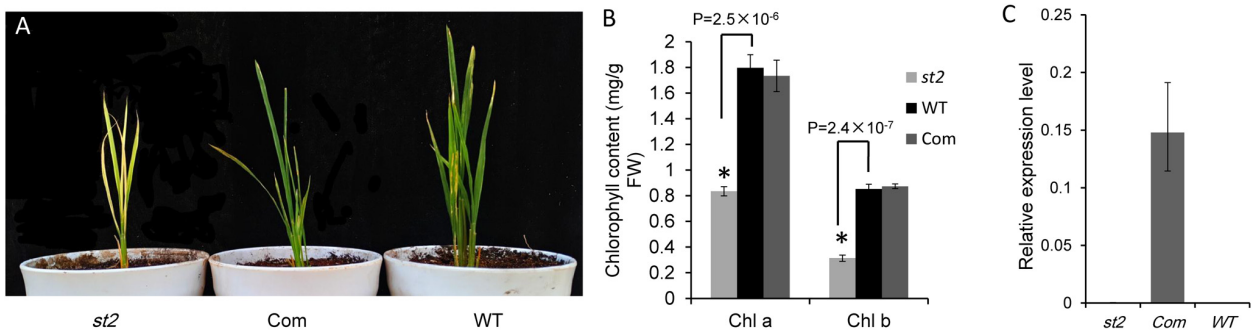

FIGURE 5 | (A) Phenotypic comparison of *st2*, complemented T_0 (Com), and the WT of *st2*. The *st2* mutant and WT were grown 28 days in the green house, and the completed T_0 was 14 days after transplant. **(B)** The chlorophyll content of *st2*, Com, and WT. The means and standard deviations were obtained from three independent leaf samples. Statistical analysis was performed with the *t*-test. $^*P = 0.05$. **(C)** The transcription levels of *SiSTL2* in *st2*, WT, and transgenic lines. The means and standard deviations are obtained from three independent leaf assays.

Given the function of SiSTL2 and the phenotypes of the *sistl2* mutant, we selected DEGs in the pathways associated with photosynthesis, DNA replication, chlorophyll metabolism, hormone signals, and carbon metabolism and analyzed the changes in expression (**Figure 8B** and **Supplementary Table S7**). Most of the DEGs in photosynthesis-associated pathways and chlorophyll metabolism were down-regulated, which was consistent with the decreased capacity of photosynthesis and

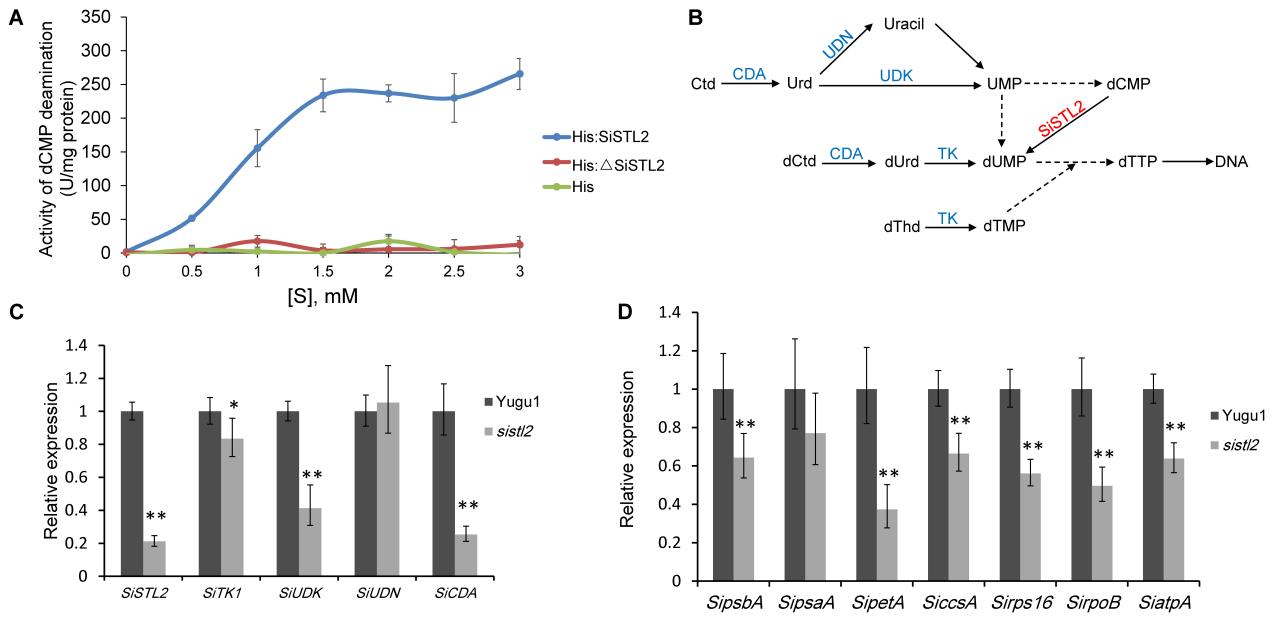

FIGURE 6 | (A) Enzyme activity assay of SiSTL2. One unit of activity refers to deamination of 1 μM dCMP per minute under the conditions of the assay. The activity of SiSTL2 was determined with increasing concentrations of dCMP. The standard deviations are obtained from three independent assays. **(B)**The *de novo* biosynthesis pathway and salvage pathway of dTTP according to previous study (Leija et al., 2016) with several changes based on *phytozome* database. The DCD homolog SiSTL2 is shown in red and enzymes in salvage pathway are shown in blue. TK, thymidine kinase; UDK, uridine kinase; UDN, uridine nucleosidase; CDA, cytidine deaminase. The dotted lines indicate the abbreviated multi-steps. **(C)** The relative expression levels of *SiSTL2* and pyrimidine triphosphate salvage-associated genes **(D)** The relative expression levels of chloroplast development-associated genes. *SipsbA*, encodes PS II protein D1; *SipsaA*, encodes PS I P700 apoprotein A1; *SipetA*, encodes cytochrome f; *SiccsA*, encodes cytochrome c heme attachment protein; *Sirps16*, encodes cytochrome c heme attachment protein; *SirpoB*, encodes RNA polymerase beta subunit; *SiatpA*, encodes ATP synthase CF1 alpha subunit. The means and standard deviations were obtained from three independent samples. Statistical analysis was performed with *t*-test. **P* = 0.05; ***P* = 0.01.

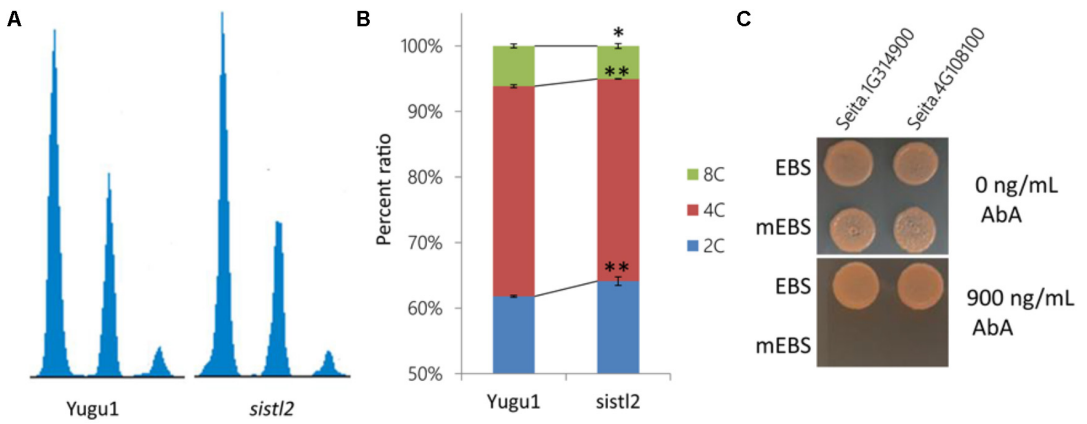

FIGURE 7 | (A) Ploidy distribution in the proliferating leaves of Yugu1 and *sistl2*. **(B)** Percentage ratios of 2C, 4C, and 8C cells in Yugu1 and *sistl2*. The means and standard deviations were obtained from three independent samples. **P* = 0.05; ***P* = 0.01. **(C)** The interactions between the *SiSTL2* promoter and two E2F family members. EBS means the E2F binding site in SiSTL2 promoter. mEBS is a random sequence used as a negative control. AbA, *Aureobasidin A*. 900 ng/ml is the lowest concentration of AbA that can avoid self-activating effects; 0 ng/ml AbA is the negative control.

chlorophyll content of *sistl2*. Almost all of the DEGs in nucleotide metabolism, DNA replication and mismatch repair pathways were up-regulated; this may be caused by feedback regulation of the SiSTL2 functional defect. DEGs in carbon metabolism and glyoxylate/dicarboxylate metabolism generally were down-regulated, indicating that energy conversion may be impaired in *sistl2*. DEGs in hormone signal pathways showed great changes, especially several auxin and cytokinin response regulator genes were sharply up-regulated (*SiIAA26*, 1.80 fold; *SiLAX2*, 1.74 fold; *SiARR12*, 2.14 fold; *SiARF5*, 2.31 fold; *SiDFL1*, 5.50 fold; *SiARR9*, 1.99 fold; *SiTGA9*, 2.58 fold). This suggested that hormone regulators that

promote growth respond positively to the development of plant retardation. Most DEGs that participate in cell cycle regulation were up-regulated, which was consistent with the results of flow cytometric analysis and the yeast one-hybrid assay.

The expression changes of some associated TFs are summarized in **Figure 8C** and **Supplementary Table S8**. It is noteworthy that some TFs families are generally up-regulated, such as Teosinte Branched 1/Cycloidea/Proliferating Cell Factor (TCP), E2F, Growth Regulating Factor (GRF), YABBY, and Auxin Response Factor (ARF). Among these TFs families, ARF, E2F, and GRF control the leaf growth and development by regulating cell proliferation (Kim et al., 2003; Horiguchi et al., 2005, 2006; Magyar et al., 2005; Guilfoyle and Hagen, 2007; Lim et al., 2010). TCP family members are responsible for the progress of leaf expansion and development (Martin-Trillo and Cubas, 2010; Efroni et al., 2013). YABBY can regulate the leaf axial development (Sarojam et al., 2010). Additionally, some members of ARF and GRF are speculated to be associated with C_4 photosynthesis in maize (Wang et al., 2013; Ding et al., 2015). However, some other TFs families also may be associated with leaf patterning, plastid biogenesis, and photomorphogenesis, such as MYB, GLK, bHLH, GRAS, and GATA (Wang et al., 2013). These TFs are also speculated to participate in C_4 photosynthesis (Wang et al., 2013; Wang P. et al., 2017). Members of these TFs families are numerous. In *sistl2* mutant, many members of these TFs up-regulated or down-regulated sharply compared with that in WT. This indicates that the expression of these TFs are influenced in the mutant (**Figure 8C**). Collectively, the leaf development and C_4 photosynthesis may be impaired because of the mutation of *SiSTL2*. In addition, to validate the RNA-seq, 13 genes were selected and detected by qRT-PCR (**Supplementary Figure S2**). These genes are associated with photosynthesis, DNA replication, and cell cycle, encoding PS I/II reaction center proteins (Seita.J018400, Seita.3G149000, Seita.3G184900, and Seita.6G032200), chlorophyll binding protein (Seita.6G158500), DNA polymerase subunits (Seita.6G050100 and Seita.5G394500), DNA replication licensing factor (Seita.1G352100), cycle division control proteins (Seita.4G045900 and Seita.2G283000), and cyclins (Seita.9G171000, Seita.5G005800, and Seita.5G352700). The consequences are correspond to that in RNA-seq.

SiSTL2 Affects C_4 Photosynthesis Capacity in Foxtail Millet

To investigate the influence of SiSTL2 on the capacity for C_4 photosynthesis, the photosynthetic index, chlorophyll fluorescence kinetic parameters, and chlorophyll (Chl) accumulation were detected in *sistl2*. The results showed that compared with Yugu1, the net photosynthetic rate of *sistl2* was decreased by 46.1%; the stomata conductance was decreased by 45.6%; the transpiration rate declined by 65.2%, whereas the intercellular CO_2 concentration showed no significant difference compared with that in Yugu1, concurrently. This suggested that the photosynthetic capacity of *sistl2* was impaired, which led to the accumulation of intercellular CO_2. The ΦPSII reflects the light absorbed by PS II that is used in photochemical reactions. Fv′/Fm′ indicates the excitation energy capture efficiency, which is also reflective of the light portion used in photochemistry. The significant decrease in these two indices of *sistl2* indicated that light-use efficiency was influenced by the mutation (**Figure 9A**). Interestingly, Chl *a* content was not influenced, whereas the Chl *b* content and total Chl content was significantly decrease in the *sistl2* mutant (by approximately 67 and 18%, respectively; **Figure 9B**). It has been reported that the degradation of Chl b is prior to Chl a, and can translate to Chl a (Schelbert et al., 2009). This is consist with our result.

As described in **Figure 3B**, the leaf Kranz structure of the *sistl2* mutant is defective. The results of RNA-seq also suggested that the C_4 photosynthesis of *sistl2* may be affected. To confirm this, the stable carbon isotopes of the *sistl2* mutant, Yugu1, and a rice *Japonica cultivar*, as a C_3 control, were measured. The atmosphere contains a small amount of ^{13}C. When C_3 plants fix CO_2, Rubisco prefers $^{12}CO_2$. However, the C_4 photosynthetic CO_2 fixation enzyme PEPC does not tend to function on $^{12}CO_2$. Rubisco of C_4 plants only exists in BSCs which segregates rubisco from air. As a result, ^{13}C accumulates to a greater extent in C_4 plants than in C_3 plants. It has been reported that C_3 plants and C_4 plants can be identified by the value of $\Delta^{13}C$ ‰ (C_3: −32 to −23‰; C_4: −19 to −6‰) (Bender, 1971). Our data show that $\Delta^{13}C$‰ in *sistl2* was significantly decreased by 4.87% (**Figure 9C**), although the value was still within the range of C_4. Then, we tested the expression of *SiSTL2* and certain C_4 photosynthesis-related genes that respond to the stress of low CO_2 environments. The results showed that in Yugu1, the expression level of *SiSTL2* was rapidly up-regulated until 12 h, decreased to the initial level, and remained stable. However, in *sistl2*, the transcription level remained at a low level until 24 h and started to increase after 36 h (**Figure 9D**). This suggested that the expression of *SiSTL2* can respond in a timely manner to the low CO_2 level. The mutation in *SiSTL2* resulted in a delayed response to the stress of a low CO_2 environment. The C_4 photosynthesis-related genes (Ding et al., 2015; Huang et al., 2017) showed a similar expression pattern to *SiSTL2* in low CO_2 conditions, which increased to a peak value at 12 h and then returned to the initial level (**Figure 9E**). In conclusion, we speculated that *SiSTL2* might indirectly regulated C_4 photosynthesis.

To further verify the connection between *SiSTL2* and C_4 photosynthesis, transcript levels of 102 previously reported *S. italica* C_4 candidate genes (Ding et al., 2015) in WT and *sistl2* are summarized from our RNA-seq data (**Supplementary Table S10**). According to the expression patterns differences between C_3 and C_4 species, these genes are divided into three types. Type I including genes that have higher expression levels in C_4 leaves compared with C_3 leaves. Type II genes show different expression patterns between C_4 and C_3 species. Type III genes have orthologs in C_4 species but absent in C_3 species (Ding et al., 2015). Comparison result showed that most of these genes (89 of 102; Type I, 18 of 20; Type II, 59 of 65; Type III, 12 of 17) also changed their

TABLE 1 | DEGs most enriched KEGG pathways.

Pathway	DEGs with pathway annotation (454)	All genes with pathway annotation (5291)	*P*-value	*Q*-value	Pathway ID
Photosynthesis	33 (7.27%)	82 (1.54%)	2.97×10^{-15}	3.09×10^{-13}	ko00195
Carbon fixation in photosynthetic organisms	31 (6.83%)	83 (1.56%)	2.40×10^{-13}	1.25×10^{-11}	ko00710
Photosynthesis – antenna proteins	13 (2.86%)	16 (0.3%)	4.69×10^{-12}	1.63×10^{-10}	ko00196
DNA replication	21 (4.63%)	67 (1.27%)	7.04×10^{-8}	1.83×10^{-6}	ko03030
Carbon metabolism	51 (11.23%)	293 (5.5%)	3.70×10^{-7}	0.000007	ko01200
Fatty acid elongation	15 (3.3%)	48 (0.91%)	5.64×10^{-6}	0.000106	ko00062
Mismatch repair	14 (3.08%)	49 (0.93%)	0.000039	0.000581	ko03430
Glyoxylate and dicarboxylate metabolism	18 (3.96%)	77 (1.46%)	0.000063	0.000815	ko00630
Phenylpropanoid biosynthesis	41 (9.03%)	264 (4.99%)	0.000106	0.001226	ko00940
Phenylalanine metabolism	12 (2.64%)	50 (0.95%)	0.000815	0.008471	ko00360

The English in this document has been checked and edited by two professional editors, both native speakers of English. For a certificate, please see the upload file "Certificate_of_editing-SRATA_1.pdf."

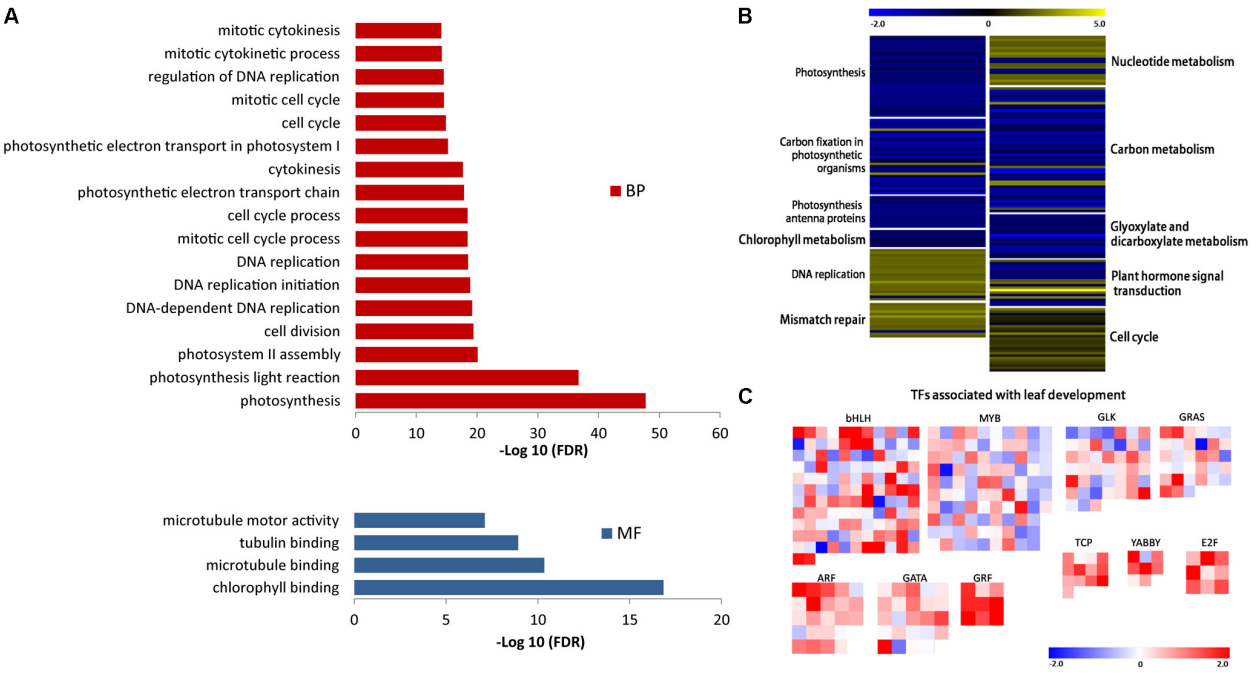

FIGURE 8 | (A) DEGs with enriched GO terms. BP, biological process; MF, molecular function. **(B)** Expression analysis of DEGs in KEGG pathways associated with mutant phenotype regulation. Each group of color-block represent a KEGG pathway. The pathways name are shown beside each block group. Color of each block represent the value of $\log_2$(RPKM-mutant/RPKM-WT), reflecting the expression pattern of each gene in the mutant compared with WT. Expression patterns are shown as the color bar ranging from –2.0 to 5.0. **(C)** Transcript abundance differences of DEGs in TFs families responsible for C_4 photosynthesis and leaf development. Color of each block represent the value of $\log_2$(RPKM-mutant/RPKM-WT), reflecting the expression pattern of each TF encoding gene in the mutant compared with WT. Expression patterns are shown as the color bar ranging from –2.0 to 2.0. Data are obtained from three independent biological replicates.

expression patterns in *sistl2* mutant (**Supplementary Table S10**). Moreover, expression of 25.5% of these genes decreased more than twofolds in *sistl2* compared with WT. According to the previous study (Ding et al., 2015), C_4 candidate genes which are associated with C_4 photosynthesis in leaves and C_4 evolution are also summarized, respectively (**Supplementary Figure S3**, right panel and **Supplementary Table S10**). The result showed that 87.8% C_4 photosynthesis associated genes (43 of 49) and 86.0% C_4 evolution associated genes (37 of 43) are down-regulated in *sistl2*. These results further indicated that the mutant in *SiSTL2* has some linkage with C_4 photosynthesis.

DISCUSSION

Comparison of DCD Mutant Characteristics in Foxtail Millet and Rice

In *sistl2*, the plant height and chlorophyll contents were significantly decreased, the leaves have white stripes (**Figure 1**).

Furthermore, some leaf cells in *sistl2* contain fewer chloroplasts or even have no chloroplast (**Figures 2E,F**). All these phenotypes were quite similar to the mutants of *OsDCD* (Xu et al., 2014; Niu et al., 2017). This suggested that the function of SiSTL2 is similar to that of OsDCD. What's more, similar phenotypes also exist in the mutants of other dNTP synthesis associated genes and other species (Yoo et al., 2009; Qin et al., 2017). Thus we speculate that there are some correlations between dNTPs synthesis and leaf/chloroplast development, which need more experiments and evidences to prove it. In our study, the cell cycle progression of *sistl2* was impaired (**Figures 7A,B**), DEGs were enriched in the cell cycle GO term (**Figure 8A**) and most of the cell cycle-associated genes were up-regulated (**Figure 8B**). In the *alr* mutant, the cell cycle progression was also delayed (Niu et al., 2017). This indicated that SiSTL2 played a similar role in cell cycle regulation to OsDCD. In addition, the dNTP pools in *alr* were unbalanced. This caused further defects in DNA replication and repair (Niu et al., 2017). Our results show that SiSTL2 also has deamination activity similar with OsDCD (**Figure 6A**). In *sistl2*, the results of RNA-seq showed that abundant DEGs were enriched in the DNA replication and mismatch repair pathways (**Table 1**). In addition, most DEGs associated with nucleotide metabolism, DNA replication, and mismatch repair were up-regulated, which may be caused by feedback control (**Figure 8B**). These results suggested that similar to OsDCD, SiSTL2 can regulate DNA replication and reparation. In addition, the expression levels of chloroplast development-associated genes in *sistl2* were significantly decreased relative to Yugu1 (**Figure 6C**). The same results were also obtained in *alr* mutant (Niu et al., 2017), indicating that SiSTL2 disruption can impair chloroplast development. In summary, SiSTL2 has a similar function to OsDCD, and has effects on DNA replication and reparation, cell cycle progression, and chloroplast development.

SiSTL2 Participates in the Regulation of Cell Division and Influences Cell Expansion

The leaves of the *sistl2* mutant were significantly smaller than that of Yugu1 (**Figure 1H** and **Supplementary Table S4**). The smaller sizes of organs usually from a reduction in cell number or cell size. These two parameters always depend on cell proliferation and cell expansion.

In our study, the ratios of 4C and 8C cells are significantly lower in *sistl2* compared with the level in Yugu1 (**Figures 7A,B**). We also found that in the vasculature of *sistl2*, the number of MCs and BSCs was reduced (**Figure 2F**). This indicated that the cell cycle progression in *sistl2* was delayed and that the cell proliferation may be defective. RNA-seq also showed that cell cycle-related genes (**Figure 8A**) and TFs (E2F; Heuvel and Dyson, 2008) suggesting that cell cycle of *sistl2* is influenced. Some reports indicated that many dNTP synthesis-associated genes were controlled by cell cycle regulating proteins (Ke et al., 2005). RNR, as an upstream gene of DCD and the S-phase check point, can active the cell cycle going into S-phase under the control of cell cycle regulating transcription factor E2F5 (Lincker et al., 2004). The promoter of *SiSTL2* also has binding sites of SiE2Fe (**Figure 7C**). Thus, we speculated that SiSTL2, similar to RNR,

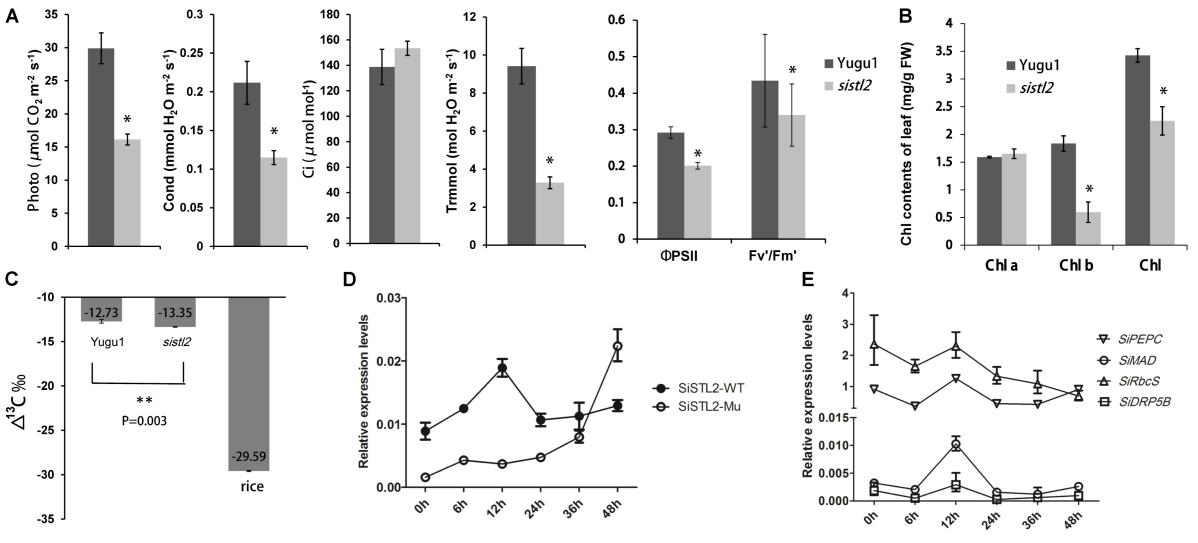

FIGURE 9 | (A) Photosynthetic parameters in WT and *sistl2*. Photo, net photosynthetic rate. Cond, stomata conductance. Ci, intercellular CO_2 concentration. Trmmol, transpiration rate. The means and standard deviations were obtained from five independent leaf samples. Statistical analysis was performed with the *t*-test. $^*P = 0.05$. **(B)** The chlorophyll contents of Yugu1 and sistl2. The means and standard deviations were obtained from five independent leaf samples. Statistical analysis is performed with the *t*-test. $^*P = 0.05$. **(C)** ^{13}C contents in leaves of WT, *sistl2*, and rice. $^{**}P = 0.01$. **(D)** The expression patterns of *SiSTL2* gene in Yugu1 and the mutant under low CO_2 treatment. **(E)** Expression patterns of the C_4 photosynthesis genes in low CO_2 conditions. PEPC, phosphoenolpyruvate carboxylase; MAD, malate dehydrogenase; RbcS, rubisco small submit; DRP5B, a dynamin-related family protein involved in chloroplast division and development (Pyke and Leech, 1994). The means and standard deviations were obtained from three independent samples.

maybe be correlated with cell cycle regulation. However, SiE2Fe is predicted to have the opposite function relative to E2F5 in cell cycle regulation. Therefore, the role of SiSTL2 in the cell cycle required further exploration.

However, the leaf cell sizes of both BSCs and MCs in *sistl2* were also significantly decreased (**Figures 2F,G**), which indicated that the cell expansion of *sistl2* was also impacted. The RNA-seq data showed that TFs associated with cell expansion, such as TCP and GRF (Kim et al., 2003; Martin-Trillo and Cubas, 2010), were up-regulated. This suggested that the mutation in SiSTL2 also impaired cell expansion. In addition, *sistl2* the decreases in cell sizes (by 43.52% in BSCs and 40.27% in MCs) were as strong as those in leaf length (44.1% reduction) and leaf width (58.8% reduction) relative to Yugu1 (**Figure 2G** and **Supplementary Table S4**). However, the cell cycle progression changes were not so strong (**Figure 7B**). Therefore, we surmised that SiSTL2 may participate in cell cycle regulation and influence the cell expansion. In *sistl2,* the smaller leaf size was mainly caused by defective cell expansion, with reduced cell proliferation a subordinate reason for the smaller leaf size.

SiSTL2 May Have an Impact on C_4 Photosynthesis

Chloroplast development is important for photosynthesis, and the Kranz leaf structure is a characteristic and precondition of C_4 photosynthesis. In *sistl2*, some BSCs and MCs have fewer or even no chloroplasts (**Figures 2E,F**) and the expression of chloroplast development genes are also decreased (**Figure 6D**). This suggested that the mutation in *SiSTL2* may affect the chloroplast development at transcription level. Considering that the chloroplast genes transcription depend on both nucleus-encoded RNA polymerase and plastid-encoded RNA polymerase, we speculate that the defect of SiSTL2 may have some influence on the nucleus or plastid transcription system. Additionally, *sistl2* displayed some abnormal phenotypes with respect to Kranz structure, such as undeveloped veins, reduced BSCs and decreased mesophyll cell number between vascular bundles (**Figures 2E,F**). This may be the result of the restraints in both cell expansion and cell division. However, many members of the TFs families that regulate leaf development and leaf cell differentiation, such as YABBY, bHLH, GRAS, and GATA (Siegfried et al., 1999; Wang et al., 2013) are differently expressed in *sistl2*. These suggested that mutations in *SiSTL2* influenced the leaf development and leaf structure. Meanwhile, most genes in the carbon fixation pathways in photosynthetic organisms were down-regulated (**Figure 8A**); the expression of TFs may regulate C_4 photosynthesis (ARF, MYB, and GLK) (Ding et al., 2015) changed extensively (**Figure 8B**). And most of the C_4 candidate genes were down-regulated after *SiSTL2* was defected (**Supplementary Figure S3**). These suggest that there are some linkage between C_4 photosynthesis and the mutation of *SiSTL2*. The ^{13}C accumulation in *sistl2* was also significantly reduced (**Figure 9C**). This suggested that the C_4 photosynthesis of the mutant was affected. Moreover, under the stress of a low CO_2 environment, *SiSTL2* can respond to the up-regulation in the similar pattern compared with C_4 photosynthesis genes (**Figures 9D,E**). Given that the regulation of dTTP synthesis by DCD is a relatively upstream biological pathway, we speculate that the effect of the *SiSTL2* mutation is global in plants, indirectly regulating the chloroplast development and C_4 photosynthesis. As the decrease in chloroplast biogenesis, the abilities of both photosynthesis and carbon fixation were impaired seriously. In the conditions of low CO_2, the mobilization of C_4 photosynthesis genes requires sufficient dNTPs to ensure that the expression levels of *SiSTL2* and C_4 photosynthesis genes are subsequently altered.

AUTHOR CONTRIBUTIONS

XD conceived the project. SZ and ST performed the data analysis and wrote the manuscript. SZ, CT, and ML conducted the experimental work. HZ provided the materials and performed the field trials. XD, ST, and GJ guided the experimental work. All authors read and approved the final manuscript.

FUNDING

This work was supported by the Fundamental Research Funds of CAAS (CAAS-XTCX2016002), the China Agricultural Research System (CARS06-13.5-A04), the National Natural Science Foundation of China (31501324), and the Agricultural Science and Technology Innovation Program of the Chinese Academy of Agricultural Sciences.

ACKNOWLEDGMENTS

We thank Zuhua He Ph.D., from the Institute of Plant Physiology and Ecology, SIBS, CAS, for providing the *OsDCD* mutant *st2*. We also thank Mei Niu Ph.D., from the Institute of Crop Science, CAAS, and Yihua Wang Ph.D., from the State Key Laboratory of Crop Genetics and Germplasm Enhancement, Nanjing Agricultural University, for providing technical guidance.

SUPPLEMENTARY MATERIAL

The Supplementary Material for this article can be found online at: https://www.frontiersin.org/articles/10.3389/fpls.2018.01103/full#supplementary-material

FIGURE S1 | Western blot of recombinant proteins His-SiSTL2, His-ΔSiSTL2 and His tag expressed in *E. coli*. Marker shows molecular mass in kilodaltons.

FIGURE S2 | The transcript levels of genes for validation of RNA-seq result.

FIGURE S3 | The expression analysis of the genes associated with C_4 photosynthesis in leaves and C_4 evolution. Color of each block represent the value of $\log_2$(RPKM-mutant/RPKM-WT), reflecting the expression pattern of each gene in the mutant compared with WT. Expression patterns are shown as the color bar ranging from −2.0 to 2.0.

TABLE S1 | SSR and In-Del markers for fine mapping.

TABLE S2 | Primers used for qRT-PCR.

TABLE S3 | Primers used for yeast one-hybrid.

TABLE S4 | Characterization of agronomic traits of *sistl2* mutant.

TABLE S5 | Putative mutation sites information.

TABLE S6 | Genes that were differentially expressed in *sistl2* compared with the wild-type.

TABLE S7 | DEGs in mutant phenotype-associated pathways.

TABLE S8 | DEGs in phenotype-associated TFs families.

TABLE S9 | The qRT-PCR primers for the validation of RNA-seq result.

TABLE S10 | Transcript levels of C_4 candidate genes.

FIGURE R1 | Top panel, the red cycles show two leaf veins of *sistl2*, the red box shows the cell between two leaf veins. The bottom panel shows the chloroplast (red arrow) of the cell in the red box in the top panel. The granum lamellas can be observed clearly in the chloroplast.

FIGURE R2 | (A) Kranz structure of Yugu1, the *S. italica* wild type. A chloroplast of BSC was pointed out by a blue cycle and magnified in **(B)**. **(B)** The red arrows show the structures like grana in BSC chloroplast.

REFERENCES

Bender, M. M. (1971). Variations in the 13C/12C rations of plants in relation to the pathway of photosynthetic carbon dioxide fixation. *Phytochemistry* 10, 1239–1244.

Buckland, R. J., Watt, D. L., Chittoor, B., Nilsson, A. K., Kunkel, T. A., and Chabes, A. (2014). Increased and imbalanced dNTP pools symmetrically promote both leading and lagging strand replication infidelity. *PLoS Genet.* 10:e1004846. doi: 10.1371/journal.pgen.1004846

Cousins, A. B., Badger, M. R., and Von Caemmerer, S. (2008). C4 photosynthetic isotope exchange in NAD-ME- and NADP-ME-type grasses. *J. Exp. Bot.* 59, 1695–1703. doi: 10.1093/jxb/ern001

Ding, Z., Weissmann, S., Wang, M., Du, B., Huang, L., Wang, L., et al. (2015). Identification of photosynthesis-associated C4 candidate genes through comparative leaf gradient transcriptome in multiple lineages of C3 and C4 Species. *PLoS One* 10:e0140629. doi: 10.1371/journal.pone.0140629

Efroni, I., Han, S. K., Kim, H. J., Wu, M. F., Steiner, E., and Birnbaum, K. D. (2013). Regulation of leaf maturation by chromatin-mediated modulation of cytokinin responses. *Dev. Cell* 24, 438–445. doi: 10.1016/j.devcel.2013.01.019

Elledge, S. J., and Davis, R. W. (1990). Two genes differentially regulated in the cell cycle and by DNA-damaging agents encode alternative regulatory subunits of ribonucleotide reductase. *Genes Dev.* 4, 740–751. doi: 10.1101/gad.4.5.740

Ellims, P. H., Kao, A. Y., and Chabner, B. A. (1981). Deoxycytidylate deaminase purification and some properties of the enzyme isolated from human spleen. *J. Biol. Chem.* 256, 6335–6340.

Fekih, R., Takagi, H., Tamiru, M., Abe, A., Natsume, S., Yaegashi, H., et al. (2013). MutMap plus: genetic mapping and mutant identification without crossing in rice. *PLoS One* 8:e68529. doi: 10.1371/journal.pone.0068529

Garton, S., Knight, H., Warren, G. J., Knight, M. R., and Thorlby, G. J. (2007). Crinkled leaves 8 - a mutation in the large subunit of ribonucleotide reductase - leads to defects in leaf development and chloroplast division in *Arabidopsis thaliana*. *Plant J.* 50, 118–127. doi: 10.1111/j.1365-313X.2007.03035.x

Gawel, D., Fijalkowska, I. J., Jonczyk, P., and Schaaper, R. M. (2014). Effect of dNTP pool alterations on fidelity of leading and lagging strand DNA replication in *E. coli*. *Mutat. Res.* 759, 22–28. doi: 10.1016/j.mrfmmm.2013.11.003

Gu, X., and Li, W. H. (1994). A model for the correlation of mutation rate with GC content and the origin of GC-rich isochores. *J. Mol. Evol.* 38, 468–475. doi: 10.1007/BF00178846

Guilfoyle, T. J., and Hagen, G. (2007). Auxin response factors. *Curr. Opin. Plant Biol.* 10, 453–460. doi: 10.1016/j.pbi.2007.08.014

Heuvel, S., and Dyson, N. J. (2008). Conserved functions of the Prb and E2F families. *Nat. Rev. Mol. Cell Biol.* 9, 713–724. doi: 10.1038/nrm2469

Horiguchi, G., Fujikura, U., Ferjani, A., Ishikawa, N., and Tsukaya, H. (2006). Large-scale histological analysis of leaf mutants using two simple leaf observation methods: identification of novel genetic pathways governing the size and shape of leaves. *Plant J.* 48, 638–644. doi: 10.1111/j.1365-313X.2006.02896.x

Horiguchi, G., Kim, G. T., and Tsukaya, H. (2005). The transcription factor AtGRF5 and the transcription coactivator AN3 regulate cell proliferation in leaf primordia of *Arabidopsis thaliana*. *Plant J.* 43, 68–78. doi: 10.1111/j.1365-313X.2005.02429.x

Hou, H. F., Liang, Y. H., Li, L. F., Su, X. D., and Dong, Y. H. (2008). Crystal structures of *Streptococcus mutans* 2′-deoxycytidylate deaminase and its complex with substrate analog and allosteric regulator dCTP center dot Mg^{2+}. *J. Mol. Biol.* 377, 220–231. doi: 10.1016/j.jmb.2007.12.064

Hu, H. Q., Wang, L. H., Wang, Q. Q., Jiao, L. Y., Hua, W. Q., and Zhou, Q. (2014). Photosynthesis, chlorophyll fluorescence, and chlorophyll content of soybean seedlings unde combined stress of bisphenol A and cadmium. *Environ. Toxicol. Chem.* 33, 2455–2462. doi: 10.1002/etc.2720

Huang, P., Studer, A. J., Schnable, J. C., Kellogg, E. A., and Brutnell, T. P. (2017). Cross species selection scans identify components of C4 photosynthesis in the grasses. *J. Exp. Bot.* 68, 127–135. doi: 10.1093/jxb/erw256

Jia, X., Zhang, Z., Liu, Y., Zhang, C., Shi, Y., Song, Y., et al. (2009). Development and genetic mapping of SSR markers in foxtail millet [*Setaria italica* (L.) P. Beauv.]. *Theor. Appl. Genet.* 118, 821–829. doi: 10.1007/s00122-008-0942-9

Ke, P. Y., Kuo, Y. Y., Hu, C. M., and Chang, Z. F. (2005). Control of dTTP pool size by anaphase promoting complex/cyclosome is essential for the maintenance of genetic stability. *Genes Dev.* 19, 1920–1933. doi: 10.1101/gad.1322905

Kim, J. H., Choi, D., and Kende, H. (2003). The AtGRF family of putative transcription factors is involved in leaf and cotyledon growth in *Arabidopsis*. *Plant J.* 36, 94–104. doi: 10.1046/j.1365-313X.2003.01862.x

Kohalmi, S. E., Glattke, M., Mcintosh, E. M., and Kunz, B. A. (1991). Mutational specificity of DNA precursor pool imbalances in yeast arising from deoxycytidylate deaminase deficiency or treatment with thymidylate. *J. Mol. Biol.* 220, 933–946. doi: 10.1016/0022-2836(91)90364-c

Kumar, D., Abdulovic, A. L., Viberg, J., Nilsson, A. K., Kunkel, T. A., and Chabes, A. (2011). Mechanisms of mutagenesis in vivo due to imbalanced dNTP pools. *Nucleic Acids Res.* 39, 1360–1371. doi: 10.1093/nar/gkq829

Kumar, D., Viberg, J., Nilsson, A. K., and Chabes, A. (2010). Highly mutagenic and severely imbalanced dNTP pools can escape detection by the S-phase checkpoint. *Nucleic Acids Res.* 38, 3975–3983. doi: 10.1093/nar/gkq128

Leija, C., Rijo-Ferreira, F., Kinch, L. N., Grishin, N. V., Nischan, N., Kohler, J. J., et al. (2016). Pyrimidine Salvage enzymes are essential for de novo biosynthesis of deoxypyrimidine nucleotides in *Trypanosoma brucei*. *PLoS Pathog.* 12:e1006010. doi: 10.1371/journal.ppat.1006010

Lichtenthaler, H. K. (1987). [34] Chlorophylls and carotenoids: pigments of photosynthetic biomembranes. *Methods Enzymol.* 148, 350–382. doi: 10.1016/0076-6879(87)48036-1

Lim, P. O., Lee, I. C., Kim, J., Kim, H. J., Ryu, J. S., and Woo, H. R. (2010). Auxin response factor 2 (ARF2) plays a major role in regulating auxin-mediated leaf longevity. *J. Exp. Bot.* 61, 1419–1430. doi: 10.1093/jxb/erq010

Lincker, F., Philipps, G., and Chaboute, M. E. (2004). UV-C response of the ribonucleotide reductase large subunit involves both E2F-mediated gene transcriptional regulation and protein subcellular relocalization in tobacco cells. *Nucleic Acids Res.* 32, 1430–1438. doi: 10.1093/nar/gkh310

Lin, Q., Wang, D., Dong, H., Gu, S., Cheng, Z., Gong, J., et al. (2012). Rice APC/C^{TE} controls tillering by mediating the degradation of MONOCULM 1. *Nat. Commun.* 3:752. doi: 10.1038/ncomms1716

Magyar, Z., De Veylder, L., Atanassova, A., Bakó, L., Inzé, D., and Bögre, L. (2005). The role of the *Arabidopsis* E2FB transcription factor in regulating auxin-dependent cell division. *Plant Cell* 17, 2527–2541. doi: 10.1105/tpc.105.033761

Martins, P. K., Mafra, V., De Souza, W. R., Ribeiro, A. P., Vinecky, F., Basso, M. F., et al. (2016). Selection of reliable reference genes for RT-qPCR analysis during developmental stages and abiotic stress in *Setaria viridis*. *Sci. Rep.* 6:28348. doi: 10.1038/srep28348

Martin-Trillo, M., and Cubas, P. (2010). TCP genes: a family snapshot ten years later. *Trends Plant Sci.* 15, 31–39. doi: 10.1016/j.tplants.2009.11.003

Marx, A., and Alian, A. (2015). The first crystal structure of a dTTP-bound deoxycytidylate deaminase validates and details the allosteric-inhibitor binding site. *J. Biol. Chem.* 290, 682–690. doi: 10.1074/jbc.M114.617720

McIntosh, E. M., Gadsden, M. H., and Haynes, R. H. (1986). Transcription of genes encoding enzymes involved in DNA synthesis during the cell cycle of *Saccharomyces cerevisiae*. *Mol. Gen. Genet.* 204, 363–366. doi: 10.1007/BF00331011

Niu, M., Wang, Y. H., Wang, C. M., Lyu, J., Wang, Y. L., Dong, H., et al. (2017). ALR encoding dCMP deaminase is critical for DNA damage repair, cell cycle progression and plant development in rice. *J. Exp. Bot.* 68, 5773–5786. doi: 10.1093/jxb/erx380

Pyke, K. A., and Leech, R. M. (1994). A genetic analysis of chloroplast division and expansion in *Arabidopsis thaliana*. *Plant Physiol.* 104, 201–207. doi: 10.1104/pp.104.1.201

Qin, R., Zeng, D. D., Liang, R., Yang, C. C., Akhter, D., Alamin, M., et al. (2017). Rice gene SDL/RNRS1, encoding the small subunit of ribonucleotide reductase, is required for chlorophyll synthesis and plant growth development. *Gene* 627, 351–362. doi: 10.1016/j.gene.2017.05.059

Sanchez, A., Sharma, S., Rozenzhak, S., Roguev, A., Krogan, N. J., Chabes, A., et al. (2012). Replication fork collapse and genome instability in a deoxycytidylate deaminase mutant. *Mol. Cell. Biol.* 32, 4445–4454. doi: 10.1128/Mcb.01062-12

Sarojam, R., Sappl, P. G., Goldshmidt, A., Efroni, I., Floyd, S. K., and Eshed, Y. (2010). Differentiating Arabidopsis shoots from leaves by combined YABBY activities. *Plant Cell* 22, 2113–2130. doi: 10.1105/tpc.110.075853

Schelbert, S., Aubry, S., Burla, B., Agne, B., Kessler, F., and Krupinska, K. (2009). Pheophytin pheophorbide hydrolase (Pheophytinase) is involved in chlorophyll breakdown during leaf senescence in *Arabidopsis*. *Plant Cell* 24, 507–518. doi: 10.1105/tpc.108.064089

Scortecci, J. F., Serrao, V. H. B., Cheleski, J., Torini, J. R., Romanello, L., Demarco, R., et al. (2017). Spectroscopic and calorimetric assays reveal dependence on dCTP and two metals (Zn^{2+} + Mg^{2+}) for enzymatic activity of *Schistosoma mansoni* deoxycytidylate (dCMP) deaminase. *Biochim. Biophys. Acta* 1865, 1326–1335. doi: 10.1016/j.bbapap.2017.07.015

Siegfried, K. R., Eshed, Y., Baum, S. F., Otsuga, D., Drews, G. N., and Bowman, J. L. (1999). Members of the YABBY gene family specify abaxial cell fate in Arabidopsis. *Development* 126, 4117–4128.

Stutz, S. S., Edwards, G. E., and Cousins, A. B. (2014). Single-cell C(4) photosynthesis: efficiency and acclimation of *Bienertia sinuspersici* to growth under low light. *New Phytol.* 202, 220–232. doi: 10.1111/nph.12648

Wang, P., Kelly, S., Fouracre, J. P., and Langdale, J. A. (2013). Genome-wide transcript analysis of early maize leaf development reveals gene cohorts associated with the differentiation of C-4 Kranz anatomy. *Plant J.* 75, 656–670. doi: 10.1111/tpj.12229

Wang, P., Khoshravesh, R., Karki, S., Tapia, R., Balahadia, C. P., and Bandyopadhyay, A. (2017). Re-creation of a key step in the evolutionary switch from C3 to C4 leaf anatomy. *Curr. Biol.* 27, 3278–3287. doi: 10.1016/j.cub.2017.09.040

Wang, Y., Ren, Y., Zhou, K., Liu, L., Wang, J., Xu, Y., et al. (2017). *WHITE STRIPE LEAF4* encodes a novel P-Type PPR protein required for chloroplast biogenesis during early leaf development. *Front. Plant Sci.* 8:1116. doi: 10.3389/fpls.2017.01116

Weiner, K. X., Weiner, R. S., Maley, F., and Maley, G. F. (1993). Primary structure of human deoxycytidylate deaminase and overexpression of its functional protein in *Escherichia coli*. *J. Biol. Chem.* 268, 12983–12989.

Xiang, J., Tang, S., Zhi, H., Jia, G., Wang, H., and Diao, X. (2017). *Loose Panicle1* encoding a novel WRKY transcription factor, regulates panicle development, stem elongation, and seed size in foxtail millet [*Setaria italica* (L.) P. Beauv.]. *PLoS One* 12:e0178730. doi: 10.1371/journal.pone.0178730

Xu, J., Deng, Y. W., Li, Q., Zhu, X. D., and He, Z. H. (2014). *STRIPE2* encodes a putative dCMP deaminase that plays an important role in chloroplast development in rice. *J. Genet. Genomics* 41, 539–548. doi: 10.1016/j.jgg.2014.05.008

Yoo, S. C., Cho, S. H., Sugimoto, H., Li, J. J., Kusumi, K., Koh, H. J., et al. (2009). Rice *Virescent3* and *Stripe1* encoding the large and small subunits of ribonucleotide reductase are required for chloroplast biogenesis during early leaf development. *Plant Physiol.* 150, 388–401. doi: 10.1104/pp.109.136648

Zhang, S., Tang, C. J., Zhao, Q., Li, J., Yang, L. F., Qie, L. F., et al. (2014). Development of highly polymorphic simple sequence repeat markers using genome-wide microsatellite variant analysis in Foxtail millet [*Setaria italica* (L.) P. Beauv.]. *BMC Genomics* 15:78. doi: 10.1186/1471-2164-15-78

Conflict of Interest Statement: The authors declare that the research was conducted in the absence of any commercial or financial relationships that could be construed as a potential conflict of interest.

frontiers in Plant Science

ORIGINAL RESEARCH
published: 21 August 2018
doi: 10.3389/fpls.2018.01183

Species-Associated Differences in the Below-Ground Microbiomes of Wild and Domesticated *Setaria*

Srinivasa Chaluvadi and Jeffrey L. Bennetzen**

Department of Genetics, University of Georgia, Athens, GA, United States

The rhizosphere microbiome is known to play a crucial role in promoting plant growth, partly by countering soil-borne phytoparasites and by improving nutrient uptake. The abundance and composition of the rhizosphere and root-associated microbiota are influenced by several factors, including plant species and genotype. We hypothesize that crop domestication might influence the composition and diversity of plant-associated microbiomes. We tested the contribution of domestication to the bacterial and archaeal root and soil composition associated with six genotypes of domesticated *Setaria italica* and four genotypes of its wild ancestor, *S. viridis*. The bacterial microbiome in the rhizoplane and root endophyte compartments, and the archaea in the endophyte compartment, showed major composition differences. For instance, members of the Betaproteobacteria and Firmicutes were overrepresented in *S. italica* root samples compared to *S. viridis*. Metagenomic analysis of samples that contained both root surface-bound (rhizoplane) and inside-root (endophytic) bacteria defined two unique microbial communities only associated with *S. italica* roots and one only associated with *S. viridis* roots. Root endophytic bacteria were found in six discernible communities, of which four were primarily on *S. italica* and two primarily on *S. viridis*. Among archaea, Methanobacteria, and Methanomicrobia exhibited species-associated differences in the rhizosphere and root compartments, but most detected archaea were not classified more specifically than at the level of phylum. These results indicate a host genetic contribution to the microbial composition in *Setaria*, and suggest that domestication has selected for specific associations in the root and in the rhizosphere.

Keywords: endophytes, Euryarchaeota, foxtail millet, metagenome, rhizosphere, root

OPEN ACCESS

Edited by:
Thomas P. Brutnell, Donald Danforth Plant Science Center, United States

Reviewed by:
Andrea Campisano, Edmund Mach Foundation, Italy
Collin M. Timm, Johns Hopkins University, United States

****Correspondence:***
Srinivasa Chaluvadi
src@uga.edu
Jeffrey L. Bennetzen
maize@uga.edu

Specialty section:
This article was submitted to Plant Breeding, a section of the journal Frontiers in Plant Science

Received: *17 January 2018*
Accepted: *24 July 2018*
Published: *21 August 2018*

Citation:
Chaluvadi S and Bennetzen JL (2018) Species-Associated Differences in the Below-Ground Microbiomes of Wild and Domesticated Setaria. Front. Plant Sci. 9:1183. doi: 10.3389/fpls.2018.01183

INTRODUCTION

Plants, like all other organisms, are surrounded by massive numbers of microbes from a huge diversity of taxa (Thompson et al., 2017). The critical associations between plants and their microbes is the result of millions of years of co-evolution. Even with more than three decades of DNA-based diagnostic tools (Pace et al., 1985; Handelsman et al., 1998; Hugenholtz et al., 1998; Muyzer and Smalla, 1998; Lundberg et al., 2012; Peiffer et al., 2013; Edwards et al., 2015), only a small percentage of microbial ecotypes have been identified and only a tiny fraction of these studied to any great depth. For example, a recent study of the earth's microbiome diversity indicated that >1/3 of metagenome reads from plant-associated microbial communities could not be mapped to existing rRNA databases (Thompson et al., 2017). This is not surprising, because sequence-based phylogenetic analysis of all of the ∼8000 prokaryotic genomes available in 2015 resulted in the identification of 79 bacterial phyla and 21 archaeal phyla (Parks et al., 2017), yet only four

bacterial phyla have been identified by whole genome sequence analysis in ∼1000 phytobacterial genomes analyzed so far (Levy et al., 2018). This could be an accurate reflection of host ranges and/or an indication of the dearth of plant-associated studies conducted to date. Perhaps because plants do not have mobile immune cells or circulating antibodies, many microbes have established durable relationships within plant tissues. In some cases, these microbes provide useful services to the plant, such as for nitrogen fixation (Werner et al., 2015; Coskun et al., 2017) or mineral uptake (Bonfante and Genre, 2010; Smith and Smith, 2011) in the root. Many microbes are pathogenic to the plant, but these constitute only a tiny percentage of the total microbiome in plant::microbe interactions, while the great majority of plant-associated microbes provide either no services or unknown services.

Because soils are the most diverse source of microbes on the planet (Roesch et al., 2007; Trevors, 2010; Delmont et al., 2011), with as many as 10^4 to 10^7 unique bacterial cells per gram of soil, every root of a field-grown plant is bathed in as many as 10^{11} microbial cells per gram of root and more than 30,000 prokaryotic species (Berendsen et al., 2012; Bulgarelli et al., 2015). Numerous studies have shown that the microbial compositions of soils are dramatically altered by root growth, with the diversity significantly lowered and some microbes immensely increased in abundance in the rhizosphere (Reinhold-Hurek et al., 2015;Niu et al., 2017). These root-adjacent microbes can reach abundances of $>10^9$ per gram of soil (Mendes et al., 2013) and are nurtured primarily by the exudates actively transported out of the plant root. These exudates, including organic acids, sugars, amino acids and many additional molecules, can amount to >50% of the energy/carbohydrate captured by the host plant through photosynthesis (Kuzyakov and Domanski, 2000; McNear, 2012). Hence, despite the fact that plants can be grown in sterile soils, these results suggest that soil microbes are of great importance for root and plant growth in real-world environments.

Many researchers believe that, like in the animal gut, a major role for microbial communities associated with the plant root is to physically displace pathogens and/or to generate antimicrobials against possible pathogenic microbes (Berendsen et al., 2012; Brader et al., 2017; Hacquard et al., 2017; Schlatter et al., 2017). This, of course, raises the issue of how plant::microbe interactions have co-evolved so that beneficial microbes are attracted and pathogenic microbes are discouraged. Part of the evolved plant component of this specificity is likely to involve specific signaling molecules, like the phenolics that attract and stimulate rhizobial (Cao et al., 2017) and mycorrhizal (Schmitz and Harrison, 2014) symbiosis. This signaling regimen creates a strong selection for pathogens, commensalists and mutualists (Hacquard et al., 2017) to also recognize these signals, similar to the case for the parasitic weed Striga that recognizes the same signal that attracts mycorrhizae (Lopez-Raez et al., 2017). Hence, an evolutionary arms race is expected between the host and pathogen in this process, as is also the case for specific recognition of pathogen effector molecules in plant disease resistance processes (Hacquard et al., 2017; Lopez-Raez et al., 2017).

Recent studies have shown that both host plant genetics and soil environment are major determinants of the microbial communities that abound in, on and/or near roots (Peiffer et al., 2013; Edwards et al., 2015; Goodrich et al., 2016). The plant genetic component is significant when different species are compared, but is also detected when different genotypes of the same plant species are investigated. This, then, opens the possibility that specific alleles of plant genes can be identified that determine which microbes are present in a plant::soil interaction. One dramatic variation in host plant genetics is associated with the suite of human-selected changes that are responsible for crop domestication (Wang et al., 2005; Doebley, 2006; Konishi et al., 2006; Cockram et al., 2007; Zhou et al., 2015). Most of the selected traits are for such agronomic properties as seed retention (shattering) and the day length dependence of flowering. However, there is some evidence that root traits might also be selected during domestication (Waines and Ehdaie, 2007). It makes sense that such factors as irrigation, monoculture or uniform plant spacing would put unique pressures on root development that might also affect root and rhizosphere microbial populations.

In the current study, we have chosen to use the *Setaria* model system, consisting of a developmentally plastic wild ancestor (*S. viridis*, green foxtail) and a domesticated descendant (*Setaria italica*, foxtail millet) (Brutnell et al., 2015). This study provides the first examination of possible effects of domestication upon the root and rhizosphere microbiomes in the genus *Setaria.* One previous study has investigated the rhizosphere microbiomes of several *S. italica* cultivars and in two locations (Jin et al., 2017). This investigation demonstrated that microhabitats and geographic location shape foxtail millet root microbial communities, but did not test for any possible role of host genetics on the root microbiome. The current study, in contrast, describes the different prokaryotic communities inside the root, on the root surface and in the surrounding rhizosphere. The results indicate that the domesticated and wild species differ in their microbes by plant genotype, but also show extensive variability in their microbiomes in replicated trials in the greenhouse and field. Six endophyte microbiome communities are identified in the greenhouse, of which four are primarily associated with *S. italica*.

MATERIALS AND METHODS

Plant Growth Conditions and Microbial Sampling

Seeds from six accessions of *S. italica* (Yugu1, B100, 129-86, 84-96, 15-96, and 130-96) and four accessions of *S. viridis* [A10, SV9-2 (PI212625), PI230135, and 4-V (UMDEL)] were obtained from Prof. Katrien Devos. These seeds were collected from various field locations and USDA GRIN and multiplied in the University of Georgia Plant Biology Greenhouse by standard methods used for self-pollinated crops (Devos et al., 1998; Bennetzen et al., 2012; Mauro-Herrera et al., 2013; Schroder et al., 2017). The seeds were surface sterilized with 8% sodium hypochlorite (Bioworld, United States) for 10 min, followed

by three rinses with sterile distilled water. Previous studies demonstrated that the disinfection of seed with 2-5% sodium hypochlorite solution eliminated any surface fungal or bacterial cells and spores (Sauer and Burroughs, 1986; Chun et al., 1997). Seed were germinated in circular-section pots (10″ in diameter and 10″ high) containing a 2:1 mixture of field soil collected from the University of Georgia farm in Bogart, GA and sand. The sand and soil mixture was steamed for 30 min. *Setaria* plants were grown in a greenhouse (with a 14 h photo-period and day-night temperatures of 26–20°C) and watered daily to approximately 70% soil water holding capacity. Each genotype was grown in three pots with each pot having three seedlings and the pots were randomly arranged. Neither pot location nor orientation were rotated on any specific schedule. Plants were grown for 30 days before the roots were harvested for metagenomic analyses.

Rhizosphere soil samples were taken from three individual plants (one per pot) of each genotype. Rhizosphere (Rh) was defined as the soil still attached to the roots after shaking the roots by hand, thus separating off soil not adhering tightly to the roots. Each root system with closely adhering soil was transferred to a 250 ml sterile flask containing 150 ml sterile distilled water. The bottles were shaken for 15 min. The rhizosphere soil fraction from the supernatant was precipitated after centrifugation of the extract for 30 min at 6,000 rpm and then stored at −80°C.

The washed roots were transferred to new 50 ml tubes and rinsed once again with sterile water and a portion of these roots was then stored at −80°C. This sample (from now on called REE) constitutes root surface-bound (ectophytic, i.e., rhizoplane) and inside-root (endophytic) bacteria. The other portion of the washed roots (∼2 g) was transferred to a 15 ml falcon tube with 5 ml phosphate buffer (pH 8.0), 50 μl lysozyme (100 mg/ml), 0.5 U Chitinase, 5 μl RNAseA (100 mg/ml), 2 g sterile 710–1180 micron beads, 2 g sterile 212–300 micron glass beads and shook at 250 rpm for 30 min @ 37°C. These roots were then washed gently with sterile water and stored at −80°C. This root sample, which is enriched for the root internal (endophytic) microbiome, is called REN.

Amplification and Pyrosequencing

Each DNA sample was subjected to PCR with two sets of primers, each specific for amplification of rRNA sequences from either bacteria or archaea. For Illumina Miseq analyses, each metagenomic DNA sample used dual-indexed (Kozich et al., 2013) 16S rRNA primers to PCR amplify the V3–V4 region (Peiffer et al., 2013). The forward primer (5′–3′) had adapter sequence necessary for binding to the Illumina flow cell (underlined), i5 index sequence (x), binding sites for the Illumina sequencing primers (bold), two maximally degenerate bases (N) and conserved microbial primer 515F (caps) (aatgatacggcgaccaccgagatctacactctttccctXXXXXXXX**acacgacgctcttccgatct**NNGTGCCAGCMGCCGCGGTAA). Similarly, the reverse primers (5′–3′) had adapter sequences necessary for binding to the flow cell (underlined), i7 index sequence (X) to distinguish each sample, the Illumina sequencing primers (bold), and bacterial primer 806R (CAP) (caagcagaagacggcatacgagatXXXXXX**gtgactggagttcagacgtgtgctcttccgatct**GGACTACHVGGGTWTCTAAT). A complete list of unique index sequences is provided in **Supplementary Table S1**. The forward primer (5′–3′) to PCR amplify archaeal 16S rRNA gene sequence contained 454 Life Sciences primer B and conserved primer 109F sequences (ACKGCTCAGTAACACGT), while the reverse primer (GCCTTGCCAGCCCGCT XXXXXXXXXX **ACCGCGGC KGCTGGC**) contained 454 Life Sciences primer A (underlined), a 11 base unique barcode (X) and the archaeal primer 529R (bold) for each sample. Further details regarding primers and barcodes used in bacterial and archaeal analysis are presented in **Supplementary Table S2**.

PCR reactions were performed in 50 μL with 100 ng of template DNA, 1 × Phusion High Fidelity Buffer (NEB, United States), 0.25 μM of each primer, 0.5 μM each dNTP, and 1U Phusion High-Fidelity Taq Polymerase (NEB, United States). Detailed information for primers and barcodes for each metagenomic sample is listed in **Supplementary Table S2**. PCR conditions were 98°C for 2 min; 26 cycles of 98°C for 10 s, 58°C for 10 s, 72°C for 30 s; with a final extension at 72°C for 10 min. Three replicate PCR reactions were performed for each sample with each primer pair. Replicate reactions were pooled and cleaned by using solid-phase reversible immobilization (SPRI) beads (Deangelis et al., 1995). DNA was quantified using a fluorometric kit (Quant-IT PicoGreen, Invitrogen). Equimolar quantities of each library (from 140 metagenomic sample libraries) were pooled. For Illumina Miseq, the 16S amplicon libraries were mixed up to 20% with Illumina-generated PhiX control libraries to artificially increase the genetic sequence diversity. The Illumina-MiSeq (PE250) run for the 16S amplicon library pool, and two runs of the Roche-454 sequencing of 16S archaeal amplicon libraries was performed at the Georgia Genomics and Bioinformatics Core (University of Georgia, Athens, GA, United States). Sequence data were submitted to Genbank under the Bioproject ID: PRJNA430270.

Sequence Analysis and Tree Construction

Illumina Miseq data were analyzed using MOTHUR MiSeq SOP[1], whereas Roche-454 data were analyzed with MOTHUR 454 SOP[2]. Briefly, sequence datasets were trimmed, clustered and classified in MOTHUR (Schloss et al., 2009) according to the following parameters: minimum length = 200 bp, maximum length = 500 bp, average quality score = 25, nucleotide mismatches in the primer sequence = 0, the maximum number of *N*s = 0. The trimmed sequences of bacterial and archaeal reads were further cleaned by removing chloroplast 16S rRNA reads and chimeric reads with remove.seq (using taxonomic classification) and UCHIME, respectively, in MOTHUR. Sequences were combined and aligned in MOTHUR using the full alignments of the rRNA small subunit sequences of the SILVA database as a template. The

[1]https://www.mothur.org/wiki/MiSeq_SOP
[2]https://www.mothur.org/wiki/454_SOP

MOTHUR program was also used for preclustering, rarefaction analysis, distance calculations, clustering, and further analysis based on OTUs. A distance matrix was generated from the resulting sequences. Sequences were clustered into OTUs using the farthest-neighbor algorithm. Illumina 16S OTUs were further analyzed by retaining only abundant OTUs, defined as occurring >100 times in the entire dataset. For instance, a sample could have 101 reads in one sample, and it would be considered abundant, or it could have 21 reads in each of five samples, and would still be considered abundant. We rarified and normalized the reads by randomly subsampling 10,000 abundant reads from each sample. That is, differences in total read numbers between samples was not a factor in our analysis, so that all final values of OTU counts represent a percentage of an identical 10,000 reads from each sample.

Data Analysis

Bacterial and archaeal data were analyzed separately using the phylogenetic framework provided within the suite of tools in the MOTHUR and Fast UniFrac program (Schloss et al., 2009; Hamady et al., 2010). Alpha diversity values for bacterial and archaeal sequence data were estimated using the Shannon diversity index and rarefaction curves. Principal Coordinate Analysis (PCoA) was performed using the Fast UniFrac metric (Hamady et al., 2010) and visualized as the clustering of samples from different treatments (e.g., *S. viridis* vs. *S. italica*) by using the JMP Pro. Both UniFrac and AMOVA were used to compare the microbial communities. These two methods test different hypotheses and can result in different *p*-values. Taxonomy-based classification of bacterial and archaeal 16S rRNA gene sequences was obtained using the RDP taxonomy and Bayesian classifier (Wang et al., 2007; Cole et al., 2014).

The color-coded Clustered Image Maps (CIMs) ("heat maps") were generated using CIMminer (Scherf et al., 2000). CIMminer utilizes a hierarchical clustering algorithm based on the average-linkage method of Sokal (1958). The OTU tables were represented graphically by coloring each cell on the basis of the abundance of a particular OTU across different samples. A dendrogram is appended to the colored table to indicate the nature of the computed relationship among OTU abundances in the table. Species- and root compartment-specific metagenomic biomarkers were identified using the linear discriminant analysis (LDA) effect size (LefSe) method (Segata et al., 2011). LefSe determines the OTUs most likely to explain differences between classes by coupling standard tests for statistical significance with additional tests that factor in biological constancy and relevance. LefSe first uses the non-parametric factorial Kruskal–Wallis (KW) sum-rank test to detect features with significant differential abundance with respect to the sample of interest. Biological consistency is subsequently investigated using a set of pairwise tests among species/compartments using the (unpaired) Wilcoxon rank-sum test (Wilcoxon, 1945; Mann and Whitney, 1947). As a last step, LEfSe employs LDA (Fisher, 1936) to estimate the effect size of each differentially abundant OTU.

RESULTS

In our greenhouse experiments investigating *Setaria* growth in sterile and non-sterile soils, we have routinely observed seedling growth and root development differences between treatments and between *S. italica* and *S. viridis* responses (**Supplementary Figure S1**). In order to investigate the microbiomes of these *Setaria*, metagenome analyses were pursued.

In order to differentiate between very different below-ground plant::microbe interactions, all harvested root samples were used to generate three DNA sources. The first source was from soil washed from a root that had been pulled from the greenhouse pot (see section "Materials and Methods"). We call this sample the rhizosphere (Rh). The roots were separated into two aliquots, one treated with lysozyme and chitinase and the other untreated. The wash from the enzyme-treated roots did not produce any bacterial colonies on four different media that we tested. Thus, the root sample treatment should have removed most or all microbes on the root surface, and is thus called the root endophytic microbiome (REN). The untreated root sample is a mixture of root endophytes and ectophytes (attached to the root surface), so this sample is called REE.

We have generated Rh, REE, and REN samples from 18 plants of *S. italica* and 12 plants of *S. viridis*. Thus, a total of 90 sample types were collected from the greenhouse experiments. After DNA extraction, each sample is expected to contain both microbial genomic DNA and plant genomic DNA. Metagenomic analyses were then performed with either bacterial 16S ribosomal DNA primers or archaeal 16S ribosomal DNA primers. These primers were chosen because they do not extensively amplify host plant ribosomal DNA from either the organelles or the nucleus. These ribosomal DNA sequences were grouped into specific microbial operational taxonomic units (OTUs), which are equated with unique ecotypes when the degree of OTU similarity is >97%, which is a commonly used rule to define species by the metagenome research community (Mysara et al., 2017). Our first analyses were with sequences generated with 454 technology, but we then switched to Illumina data generation in order to get larger numbers of reads. The results shown are only for the Illumina data, but independent analyses of the two data sets yielded the same conclusions (data not shown), although these conclusions were less robust when only using the 454 data. OTU tables obtained from a total of 89 bacterial samples and 71 archaeal samples were used in the final analyses. The bacterial and archaeal OTU tables are shown in **Supplementary Tables S3**, **S4**.

Bacterial diversity was higher in the Rh than in the REE or REN compartments (**Supplementary Table S5**). We did not find a significant difference in the microbial diversity between *S. italica* and *S. viridis* samples (**Supplementary Figure S2A**). Rh samples have the most OTU types that were not found in other compartments (**Supplementary Figures S2B,C**). The root endophytic (REN) results have extensive overlap (that is, are a subset of) the Rh and REE samples. The differences between REE and REN results are the microbes tightly affixed to the root surface, an understudied component of the microbial soil::root interaction. To determine the microbes unique to the rhizoplane ("ectophytes"), we determined the abundant OTUs in both REE

and REN compartments, and then found those that were unique to the REE. We found 25 abundant OTUs that are present only on the root surface (REE) of *S. italica* and 126 abundant OTUs that are present only in the REE compartment of *S. viridis* (**Supplementary Figures S2B,C**). We did not find any abundant genera in REN compartments of *S. italica* or *S. viridis* genotypes that were not also found in the REE samples. This was expected, given that OTUs in the REN samples (endophytes) should be a subset of the OTUs found in the REE (endophyte plus ectophyte) samples.

The PCoA graphs in **Figure 1** shows a comparison of bacterial communities between the *S. italica* and *S. viridis* hosts in Rh, REE and REN compartments. Multiple genotypes of each species were used in the analysis, and three replicates of each genotype in most cases, so these results indicate differences that separate the domesticated plants from the wild plants. PCoA showed root compartment-specific and species-dependent separation. REE samples and REN samples showed significant species-dependent separation (**Figure 1A**). A separate analysis of only Rh samples (**Figure 1B**), only REE samples (**Figure 1C**) and only REN samples (**Figure 1D**) confirmed that both REE and REN samples showed significant species-dependent separation. A non-parametric analysis of variance (AMOVA) was performed to verify whether the differences in bacterial diversity between the groups (i.e., genotype, species, and root compartment) were different than within the groups. The result showed that there were statistically significant differences in bacterial diversity between species for REE and REN compartments (p-value ~0.001). The analysis showed that the Rh compartment exhibits less significant host species-dependent microbial associations (p-value 0.046).

The presence and the abundances of different phyla and genera were assessed by taxonomic assignment of all the abundant sequences using the RDP classifier, and comparative

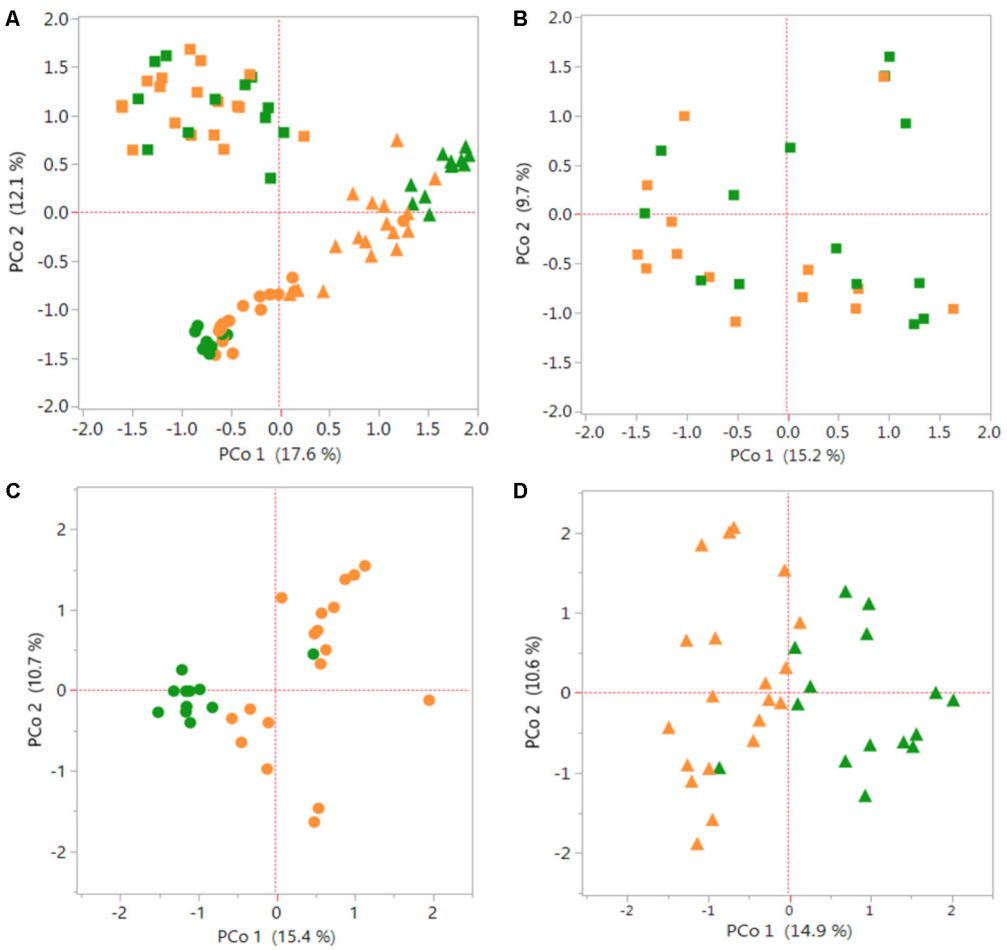

FIGURE 1 | Species-dependent colonization of rhizosphere and root microbiomes in *Setaria* species. Bacterial OTUs of *Setaria italica* (orange) and *S. viridis* (green) were analyzed using Principal Coordinates Analysis (PCoA) plots generated from distance matrices for the Jaccard indices sets. The plot shows the first two principal axes. Rhizosphere (Rh) samples are shown as squares, root external plus root endophytic (REE) samples are shown as circles and root endophytic (REN) samples are shown as triangles. **(A)** Comparison of the three compartments across both species. **(B–D)** Figures are comparisons between species of the Rh, REE, and REN compartments individually. Non-parametric AMOVA to find significant differences between *S. italica* and *S. viridis* samples for each compartment produced p-values 0.056, 0.001, and 0.001 for Rh, REE, and REN samples, respectively.

analysis was conducted using MOTHUR tools. A total of 693 bacterial genera belonging to 23 phyla were recognized by RDP taxonomy. Out of these, 366 genera from 23 phyla were represented by more than 100 reads in the entire Illumina dataset. The top three phyla of Proteobacteria (76%), Actinobacteria (11%) and Firmicutes (9%) contributed 96% of the total bacterial diversity. Among Proteobacteria, the subphylum Alphaproteobacteria were the most abundant in the rhizosphere soil. In contrast, Deltaproteobacteria were the most abundant in the REE samples and Gammaproteobacteria were most abundant in the REN samples. These general abundance characteristics are very similar to those seen with many other root::soil communities (Bulgarelli et al., 2015).

A comparative analysis of Rh samples from *S. italica* and *S. viridis* showed that Alphaproteobacteria were overrepresented in the *S. italica* rhizosphere, whereas Gammaproteobacteria, Deltaproteobacteria, and Firmicutes were overrepresented in the *S. viridis* rhizosphere soil (**Figure 2**). The REE fractions of *S. italica* roots were richer in Betaproteobacteria and Firmicutes than *S. viridis* roots. The REE fraction of *S. viridis* roots were found to be enriched with Deltaproteobacteria and Actinobacteria (**Figure 2**). The root endophyte compartment (REN) of *S. italica* was richer in Betaproteobacteria and Firmicutes compared to *S. viridis*. In contrast, the REN samples of *S. viridis* were enriched for Gammaproteobacteria (**Figure 2**). Sixteen genera (*Actinotalea, Algiphilus, Basilea, Caldivirga, Carnimonas, Ewingella, Hungatella, Mangrovibacter, Microvirga, Mitsuaria, Oxalicibacterium, Sphingobacterium, Succinivibrio, Taonella, Telmatocola, Xylophilus*), all abundantly present in rhizosphere soil, were completely absent in REE and REN compartments of both *S. italica* and *S. viridis*. Twelve genera (*Actinomyces, Desulfobaculum, Thiohalobacter, Polaromonas, Hamadaea, Edwardsiella, Peredibacter, Brevibacillus, Rivibacter, Thermocladium, Ochrobactrum, Mizugakiibacter*) that were abundant in REE compartments of both species were absent in the endophytic REN compartment.

In order to characterize and depict the specific bacterial communities that are dominating these microbiomes, a heat map analysis is presented for the most abundant OTUs in the Rh, REE, and REN samples (**Figure 3**). We have also analyzed significant OTUs in each cluster by the LefSe method that predicts OTUs that are statistically different among biological samples. The significant OTUs in each heat map community are listed in the **Supplementary Table S6**.

The heat map analyses indicated two highly separable species-dependent microbiome communities in Rh samples (**Figure 3A**). The ARH community predominantly has *S. italica* samples with three *S. viridis* samples. The BRH community, which is found on most of the *S. viridis* samples, is also found on five *S. italica* samples. The OTUs coded as 1 (*Sphingomonas*), 41 (*Stakelama*), 67 (*Sphingomonas*), 126 (*Mesoaciditoga*), 128 (*Stakelama*), and 171 (*Stakelama*) in our analysis are significantly enriched in the ARH community compared to the BRH community, whereas 2 (*Lawsonia*), 3 (*Leclercia*), 5 (*Bhargavaea*), 6 (*Pseudomonas*) and 7 (*Massilia*) are most abundant in the BRH community.

The REE samples demonstrate four highly separable microbiome community types (**Figure 3B**). Each REE microbial

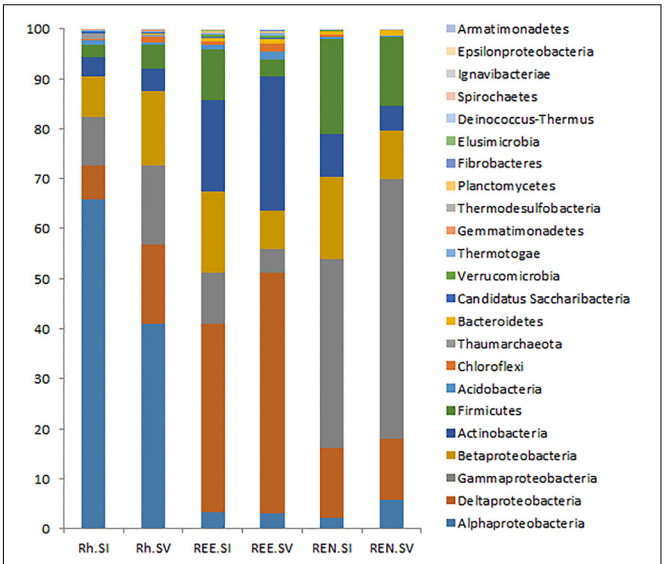

FIGURE 2 | Relative abundance of bacterial phyla in the rhizosphere microbes (Rh), root external and endophytic microbes (REE) and root endophytic microbes (REN). The averages of each phylum for all *S. italica* samples (SI) and all *S. viridis* samples (SV) were shown as two bars for Rh, REE, and REN.

community was completely species-dependent, with AREE and CREE communities only found with *S. italica* germplasm and BREE and DREE communities existing only with *S. viridis* roots. All of the replicates of four *S. italica* genotypes (Yugu1, B100, 84-96, and 129-96) were associated with the CREE community. All replicates of one *S. viridis* (A10) genotype were associated with the DREE community (**Figure 3B**). Some genotypes of *S. italica* and *S. viridis* associated with more than one type of microbial community. AREE has abundances of OTUs 27 (*Hathewaya*), 51 (*Rhizomicrobium*), 63 (*Clostridiaceae*), 111 (*Treponema*), and 142 (*Azospira*). BREE has a high proportion of OTUs 2 (*Lawsonia*), 220 (*Gimesia*), 776 (*Aquabacterium*), 1430 (*Aquabacterium*), and 1449 (*Pseudorhodoferax*), while CREE has high abundance of 46 (*Sporomusa*), 113 (*Succinivibrio*), 114 (*Anaerobacterium*), 159 (*Ideonella*) and 183 (*Anaerospora*). DREE contains high abundances of OTUs 9 (*Kitasatospora*), 35 (*Haliangium*), 492 (*Actinosynnema*), 614 (*Kallotenue*), and 786 (*Acidobacteria*).

The REN samples also have six distinct microbial communities, with AREN and CREN, DREN, and EREN within the roots of *S. italica* samples and BREN and FREN communities inside the roots of *S. viridis* samples (**Figure 3C**). All three replicates of Yugu1 had the AREN community and all the three replicates of SV4-2 and 9-2 have BREN communities, while A10 roots hosted the FREN microbial community. AREN exhibits over-representation of 6 (*Pseudomonas*), 10 (*Exiguobacterium*), 47 (*Pseudocitrobacter*), 62 (*Niastella*), and 72 (*Azorhizophilus*).BREN has overrepresentation of OTUs 1 (*Sphingomonas*), 3 (*Leclercia*), 73 (*Luteibacter*), 83 (*Achromobacter*), and 286 (*Siccibacter*), CREN has overrepresentation of 21 (*Tumebacillus*), 25 (*Janthinobacterium*), 37 (*Methylohalobius*), 318 (*Cedecea*), and 376 (*Massilia*), DREN

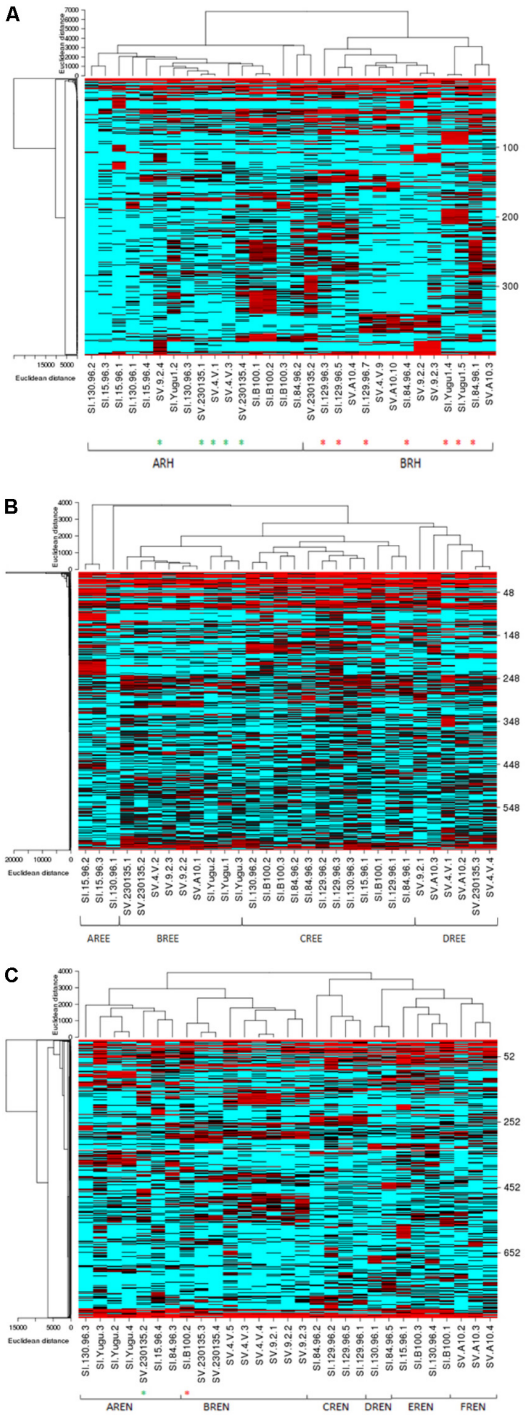

FIGURE 3 | Species-dependent colonization of the rhizosphere (Rh) microbiome in *Setaria* species. Heat maps showing relative abundances of the most abundant bacterial OTUs in the Rh **(A)**, REE **(B)**, and REN **(C)** compartments (*Y*-axis) versus the *Setaria* genotypes (*X*-axis) used in the current study. Red indicates high abundance and blue indicates low abundance. The *Setaria* sample designations are on the bottom. The green stars at the bottom indicate *S. viridis* samples in an otherwise *S. italica* cluster and red stars indicate *S. viridis* samples in an otherwise *S. viridis* cluster. The *p*-values based on the Analysis of Molecular Variation (AMOVA) are 0.046*, 0.001*, and 0.001* for Rh, REN, and REE, respectively.

has overrepresentation of 2 (*Lawsonia*), 4 (*Amycolatopsis*), 14 (*Byssovorax*), 17 (*Povalibacter*), 23 (*Mobilitalea*), EREN has significantly high proportion of OTUs 31 (*Serpens*), 86 (*Sulfuritalea*), 119 (*Acidobacteria*), 162 (*Serpens*), and 212 (*Leclercia*), while FREN has over abundance of OTUs 278 (*Enterobacter*), 674 (*Defluviitoga*), and 682 (*Puniceicoccus*).

The OTU results were further analyzed to identify species-specific and compartment-specific biomarkers using the LefSe method. Six distintive ("biomarker") OTUs were found for *S. italica* Rh, 14 for *S. viridis* Rh, 80 for *S. italica* REE, and 69 for *S. viridis* REE. In addition 51 biomarkers were found for the *S. italica* REN compartment, and 141 for the *S. viridis* REN compartment. The lists of significant OTUs are presented in **Supplementary Table S7**. The relative abundances of some of these exemplar biomarker OTUs are presented in **Figure 4**.

The archaeal diversity was estimated in the Rh, REE and REN compartments of *S. italica* and *S. viridis* genotypes (**Supplementary Table S8**). *S. italica* roots have more archaea than *S. viridis* roots in all the compartments (**Supplementary Figure S3**). **Figure 5** presents the archaeal analyses on these same Rh and REN samples. PCoA demonstrated that the separation by domesticated versus wild *Setaria* genotypes in these experiments is more distinct in REN samples (**Figure 5B**) than in Rh or REE compartments (**Figure 5A** and **Supplementary Figure S4A**). Analysis of Rh and REN samples also indicated that the archaea predominantly belong to the phylum Euryarchaeota, with lower quantities of Thaumarchaeota. Euryarchaeota classes Methanomicrobia, Methanobacteria and an unknown class of Euryarchaeota constituted 80–90% of the Rh and REN archaea of both *Setaria* species (**Figure 5C** and **Supplementary Figure S4B**). Thaumarchaeota classes were represented by Nitrososphaerales and Nitrosopumilales.

DISCUSSION

Domestication of monocotyledonous crops resulted in changes in several traits, including seed size, seed yield, seed dispersal, determinate growth, loss of seed dormancy, and changes in photoperiod sensitivity (Doebley et al., 2006; Cockram et al., 2007; Zhou et al., 2015). Although these were all knowingly selected, there are no reports of selecting root architecture during domestication. However, there is evidence for an unknowing selection for less root biomass in domesticated wheat (Waines and Ehdaie, 2007), and decreases in the capacity for root plasticity under selection pressures in barley and foxtail millet (Grossman and Rice, 2012; Sebastian et al., 2016). *Setaria italica* is believed to have been domesticated from *S. viridis* in Northern China around 6000 BC (Bettinger et al., 2010), probably prior to rice domestication. It has been shown that some types of roots, such as the crown roots that originate from the shoot, show reduced sensitivity to water deficit in *S. italica* than in *S. viridis*, suggesting that this response has been influenced by human selection (Sebastian et al., 2016). Hence, there is a precedent for the idea that domestication can influence root traits.

Many factors are known and/or expected to influence the microbial communities associated with plant roots. The

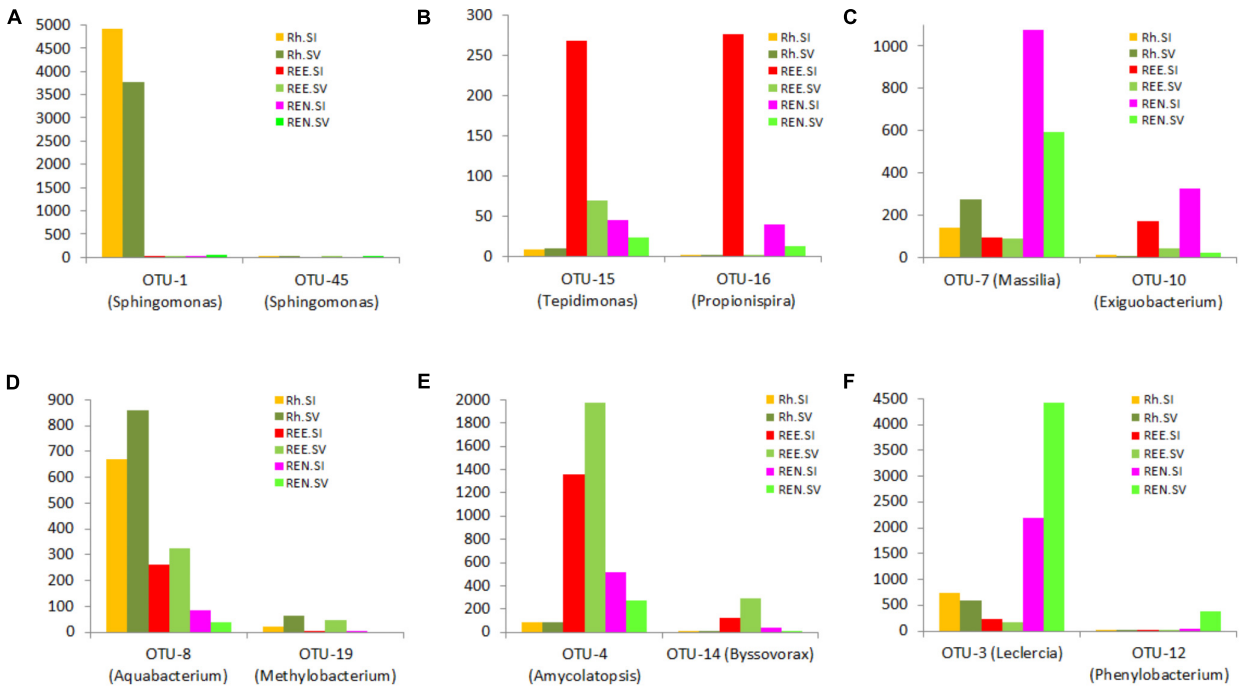

FIGURE 4 | Species- and root compartment-specific significant OTUs were identified using the linear discriminant analysis (LDA) effect size (LefSe) method. A list of significant OTUs is presented in the Supplementary Data. This figure shows relative abundance of some exemplar biomarkers for *S. italica* Rh **(A)**, REE **(B)**, and REN **(C)** compartments and *S. viridis* Rh **(D)**, REE **(E)**, and REN **(F)**.

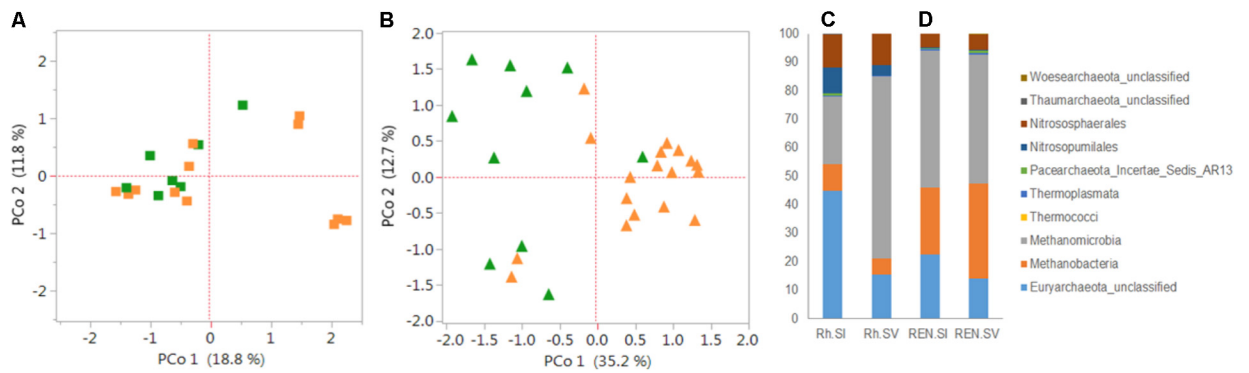

FIGURE 5 | Diversity and composition of archaea in the roots and rhizospheres of *S. italica* and *S. viridis*. PCoA plots were based on 16S archaeal rRNA gene sequences for **(A)** rhizosphere microbiome (Rh) and **(B)** root endophytic microbiome (REN). The distance matrices were calculated from the Jaccard coefficients using Bray–Curtis indices. *P*-values calculated for the significance of the differences between *S. italica* and *S. viridis* in there results were based on unweighted UniFrac distances. The *p*-values were 0.12 and 0.016 for Rh and REN samples, respectively. The composition of archaeal classes for Rh samples **(C)** and REN samples **(D)** of *S. italica* and *S. viridis*.

environment plays a major factor, especially soil chemical, structural and organic composition (Girvan et al., 2003; Fierer and Jackson, 2006). Cultivation history is also known to influence subsequent microbial communities, as simply exemplified by the abundance of rhizobiales and suppression of nitrifying microbial communities that are observed in a field that has recently supported a crop of legumes (Sugiyama et al., 2014; Paungfoo-Lonhienne et al., 2017). Soil composition can vary across very small scales, due to topographic issues like slope and altitude (Robertson et al., 1993; Kravchenko et al., 2005; Garcia-Palacios et al., 2012; Tamme et al., 2016). Hence, greenhouse experiments with controlled growth, soil and microbial composition conditions should offer substantial advantages for the generation of reproducible results. However, greenhouses are not as uniform as often assumed, particularly regarding edge issues of shading, distance to ventilation, local humidity variation and distances to exterior walls (and, thus, temperature variation), although these

issues can be minimized by frequent pot translocation (Brien et al., 2013; Kutta and Hubbart, 2014). The greenhouse pot experiments in this study exhibited substantial environmental variation, as shown by differences in the replicates, but still yielded consistent signals regarding the differences between the microbiomes of domesticated versus wild *Setaria* prokaryotic ectophytes and endophytes. The higher abundance of Betaproteobacteria and Firmicutes in the REE and REN compartments of *S. italica* compared to *S. viridis* are clear examples. In addition, many significant species-specific OTUs belonging to these phyla were identified in the LefSe analyses.

Some of the different Rh, REE, and REN communities generated in this project show little to no overlap in their predominant community members, despite initiation of the community by identical microbial community inocula. Hence, the observed communities do not represent continuums, but rather the establishment of a defined community that show varying degrees of preference for a particular host genotype.

The microbial diversity in the REE and REN compartments showed substantial OTU overlap with the microbial communities in the Rh compartment, confirming the expectation that the REE and REN communities arising from a soil inoculation will be a subsample of Rh communities. Though seeds of all the genotypes in the current study were multiplied in the same potting mix in the same greenhouse, we cannot rule out the possibility that seed-transmitted microbes may have founded differences in the endophytic communities that were represented in the seedling root. However, previous work indicated that seed endophytic communities are distinctly different from rhizosphere or root microbial communities (Philippot et al., 2013; Leff et al., 2017).

There are several studies that have shown that the plant host genotype has a small but significant impact on the composition of an associated microbiome (Peiffer et al., 2013; Edwards et al., 2015). The host plant acquires its microbiome from the surrounding environments, but selects only a tiny subset of available species for associated growth. Soil type, biological history, water quality, water abundance and several other factors have important impacts on the microbes present as well. Establishing a novel microbiome takes time, so that greenhouse experiments on seedlings, especially on tiny seedlings like those of *S. viridis* and *S. italica*, are likely to show the smallest differentiation from the inoculum and the smallest host-specific effects. For instance, the host genotype-dependence of the microbiome was less apparent in a tiny annual such as Arabidopsis (Lundberg et al., 2012) than in a larger perennial plant, *Boechera stricta* (Wagner et al., 2016). Hence, we believe that the differences seen in our experiments would be more dramatic with larger and older plants than in these seedlings.

There are few studies that have directly assessed the possible effects of human agricultural intervention on the microbial communities in the roots. It was shown in wheat and maize that the root and rhizosphere bacterial communities are more diverse in land races than in the modern cultivars (Germida and Siciliano, 2001; Szoboszlay et al., 2015). However, it was shown in sunflower that there was less fungal diversity in the wild germplasm compared to domesticated genotypes (Leff et al., 2017). Leff et al. (2017) argued that the domestication of sunflowers may have decreased the prevalence of pathogens associated with the plants and may have increased the prevalence of symbionts. Our results suggest that the Betaproteobacteria, which include most of the nitrogen fixers in nature (Chen et al., 2003; Santi et al., 2013), are more abundant in the REE and REN compartments of the domesticated species, *S. italica*. Though we did not observe dramatic difference in the over-all microbial diversity between *S. italica* and *S. viridis*, we observed more microbial phylotypes specific to *S. viridis* than to *S. italica*. This could be a reflection of the broader adaptability of *S. viridis*, one of the two or three most widely distributed weeds on the planet, than seen for *S. italica*, which was domesticated and primarily grown in only one region of China. All crop domestication and improvement are expected to be associated with the narrowing of germplasm, so this phenomenon would also predict less diversity of all kinds (including the associated microbiome) in an elite crop.

Previous studies have postulated that ancient cultivars and their wild relatives were generally exposed to more marginal soils before the invention of synthetic fertilizer–driven agricultural production, and their gene pools might have a different adaptive capacity to engage in novel microbial associations with rhizosphere microbes compared with the gene pools of present-day cultivars (Wissuwa et al., 2009; Bulgarelli et al., 2015). These observations suggest that identification of the alleles in *S. viridis* that promote root::soil microbe diversity might also contribute to improved adaptation of the crop foxtail millet to diverse environments. Mapping and introgression of the *Setaria* genes responsible for these root::soil microbe differences will be needed to test this hypothesis.

CONCLUSION

This study demonstrates that host genetics, including the outcomes of crop domestication, can play an important role in selecting the prokaryotes present in the plant::soil interaction network. The communities established in the rhizosphere, root surface and endophytic space are very different, but are all affected by both host genetics and the plant microenvironment. Now that these differences have been observed, future field experiments and experiments with controlled innocula can be used to determine the contributions of individual microbial species to the community and to plant performance.

AUTHOR CONTRIBUTIONS

JB designed the experiments, analyzed the data, and wrote the manuscript. SC designed and conducted the experiments, analyzed the data, and wrote the manuscript.

FUNDING

This research was funded by The BioEnergy Science Center (Department of Energy, United States), endowment funds from the University of Georgia Giles Professorship and the Georgia Research Alliance.

ACKNOWLEDGMENTS

The authors thank Prof. Katrien Devos for providing *Setaria* seed. They also thank Jeff Wagner and Myriam Belanger at the Georgia Genomics Facility at the University of Georgia for assistance with 454 and Illumina sequencing. Roche 454 and Illumina sequence data are deposited in the NCBI Genbank (Bioproject ID. PRJNA430270).

SUPPLEMENTARY MATERIAL

The Supplementary Material for this article can be found online at: https://www.frontiersin.org/articles/10.3389/fpls.2018.01183/full#supplementary-material

REFERENCES

Bennetzen, J. L., Schmutz, J., Wang, H., Percifield, R., Hawkins, J., Pontaroli, A. C., et al. (2012). Reference genome sequence of the model plant *Setaria*. *Nat. Biotechnol.* 30, 555–561. doi: 10.1038/nbt.2196

Berendsen, R. L., Pieterse, C. M. J., and Bakker, P. A. (2012). The rhizosphere microbiome and plant health. *Trends Plant Sci.* 17, 478–486. doi: 10.1016/j.tplants.2012.04.001

Bettinger, R. L., Barton, L., and Morgan, C. (2010). The origins of food production in North China: a different kind of agricultural revolution. *Evol. Anthropol.* 19, 9–21. doi: 10.1002/evan.20236

Bonfante, P., and Genre, A. (2010). Mechanisms underlying beneficial plant-fungus interactions in mycorrhizal symbiosis. *Nat. Commun.* 1:48. doi: 10.1038/ncomms1046

Brader, G., Compant, S., Vescio, K., Mitter, B., Trognitz, F., Ma, L. J., et al. (2017). Ecology and genomic insights into plant-pathogenic and plant-nonpathogenic endophytes. *Annu. Rev. Phytopathol.* 55, 61–83. doi: 10.1146/annurev-phyto-080516-035641

Brien, C. J., Berger, B., Rabie, H., and Tester, M. (2013). Accounting for variation in designing greenhouse experiments with special reference to greenhouses containing plants on conveyor systems. *Plant Methods* 9:5. doi: 10.1186/1746-4811-9-5

Brutnell, T. P., Bennetzen, J. L., and Vogel, J. P. (2015). *Brachypodium distachyon* and *Setaria viridis*: model genetic systems for the grasses. *Annu. Rev. Plant Biol.* 66, 465–485. doi: 10.1146/annurev-arplant-042811-105528

Bulgarelli, D., Garrido-Oter, R., Munch, P. C., Weiman, A., Droge, J., Pan, Y., et al. (2015). Structure and function of the bacterial root microbiota in wild and domesticated barley. *Cell Host Microbe* 17, 392–403. doi: 10.1016/j.chom.2015.01.011

Cao, Y., Halane, M. K., Gassmann, W., and Stacey, G. (2017). The role of plant innate immunity in the legume-rhizobium symbiosis. *Annu. Rev. Plant Biol.* 68, 535–561. doi: 10.1146/annurev-arplant-042916-041030

Chen, W.-M., Moulin, L., Bontemps, C., Vandamme, P., Béna, G., and Boivin-Masson, C. (2003). Legume symbiotic nitrogen fixation by β-proteobacteria is widespread in nature. *J. Bacteriol.* 185, 7266–7272. doi: 10.1146/annurev-arplant-042916-041030

Chun, S. C., Schneider, R. W., and Cohn, M. A. (1997). Sodium hypochlorite: effect of solution pH on rice seed disinfestation and its direct effect on seedling growth. *Plant Dis.* 81, 821–824. doi: 10.1128/JB.185.24.7266-7272.2003

Cockram, J., Jones, H., Leigh, F. J., O'sullivan, D., Powell, W., Laurie, D. A., et al. (2007). Control of flowering time in temperate cereals: genes, domestication, and sustainable productivity. *J. Exp. Bot.* 58, 1231–1244. doi: 10.1094/PDIS.1997.81.7.821

Cole, J. R., Wang, Q., Fish, J. A., Chai, B. L., Mcgarrell, D. M., Sun, Y. N., et al. (2014). Ribosomal database project: data and tools for high throughput rRNA analysis. *Nucleic Acids Res.* 42, D633–D642. doi: 10.1093/nar/gkt1244

Coskun, D., Britto, D. T., Shi, W. M., and Kronzucker, H. J. (2017). How plant root exudates shape the nitrogen cycle. *Trends Plant Sci.* 22, 661–673. doi: 10.1016/j.tplants.2017.05.004

Deangelis, M. M., Wang, D. G., and Hawkins, T. L. (1995). Solid-phase reversible immobilization for the isolation of PCR products. *Nucleic Acids Res.* 23, 4742–4743. doi: 10.1016/j.tplants.2017.05.004

Delmont, T. O., Robe, P., Cecillon, S., Clark, I. M., Constancias, F., Simonet, P., et al. (2011). Accessing the soil metagenome for studies of microbial diversity. *Appl. Environ. Microbiol.* 77, 1315–1324. doi: 10.1128/AEM.01526-10

Devos, K. M., Wang, Z. M., Beales, J., Sasaki, Y., and Gale, M. D. (1998). Comparative genetic maps of foxtail millet (*Setaria italica*) and rice (*Oryza sativa*). *Theor. Appl. Genet.* 96, 63–68. doi: 10.1111/tpj.12842

Doebley, J. (2006). Plant science - Unfallen grains: how ancient farmers turned weeds into crops. *Science* 312, 1318–1319. doi: 10.1111/tpj.12842

Doebley, J. F., Gaut, B. S., and Smith, B. D. (2006). The molecular genetics of crop domestication. *Cell* 127, 1309–1321. doi: 10.1126/science.1128836

Edwards, J., Johnson, C., Santos-Medellin, C., Lurie, E., Podishetty, N. K., Bhatnagar, S., et al. (2015). Structure, variation, and assembly of the root-associated microbiomes of rice. *Proc. Natl. Acad. Sci. U.S.A.* 112, E911–E920. doi: 10.1073/pnas.1414592112

Fierer, N., and Jackson, R. B. (2006). The diversity and biogeography of soil bacterial communities. *Proc. Natl. Acad. Sci. U.S.A.* 103, 626–631. doi: 10.1128/AEM.00358-07

Fisher, R. A. (1936). The use of multiple measurements in taxonomic problems. *Ann. Hum. Genet.* 7, 179–188. doi: 10.1073/pnas.0507535103

Garcia-Palacios, P., Maestre, F. T., Bardgett, R. D., and De Kroon, H. (2012). Plant responses to soil heterogeneity and global environmental change. *J. Ecol.* 100, 1303–1314. doi: 10.1111/j.1469-1809.1936.tb02137.x

Germida, J., and Siciliano, S. (2001). Taxonomic diversity of bacteria associated with the roots of modern, recent and ancient wheat cultivars. *Biol. Fert. Soils* 33, 410–415. doi: 10.1111/j.1365-2745.2012.02014.x

Girvan, M. S., Bullimore, J., Pretty, J. N., Osborn, A. M., and Ball, A. S. (2003). Soil type is the primary determinant of the composition of the total and active bacterial communities in arable soils. *Appl. Environ. Microbiol.* 69, 1800–1809. doi: 10.1007/s003740100343

Goodrich, J. K., Davenport, E. R., Waters, J. L., Clark, A. G., and Ley, R. E. (2016). Cross-species comparisons of host genetic associations with the microbiome. *Science* 352, 532–535. doi: 10.1126/science.aad9379

Grossman, J. D., and Rice, K. J. (2012). Evolution of root plasticity responses to variation in soil nutrient distribution and concentration. *Evol. Appl.* 5, 850–857. doi: 10.1111/j.1752-4571.2012.00263.x

Hacquard, S., Spaepen, S., Garrido-Oter, R., and Schulze-Lefert, P. (2017). Interplay between innate immunity and the plant microbiota. *Annu. Rev. Phytopathol.* 55, 565–589. doi: 10.1146/annurev-phyto-080516-035623

Hamady, M., Lozupone, C., and Knight, R. (2010). Fast UniFrac: facilitating high-throughput phylogenetic analyses of microbial communities including analysis of pyrosequencing and PhyloChip data. *ISME J.* 4, 17–27. doi: 10.1038/ismej.2009.97

Handelsman, J., Rondon, M. R., Brady, S. F., Clardy, J., and Goodman, R. M. (1998). Molecular biological access to the chemistry of unknown soil microbes: a new frontier for natural products. *Chem. Biol.* 5, R245–R249. doi: 10.1038/ismej.2009.97

Hugenholtz, P., Goebel, B. M., and Pace, N. R. (1998). Impact of culture-independent studies on the emerging phylogenetic view of bacterial diversity. *J. Bacteriol.* 180, 4765–4774. doi: 10.1016/S1074-5521(98)90108-9

Jin, T., Wang, Y., Huang, Y., Xu, J., Zhang, P., Wang, N., et al. (2017). Taxonomic structure and functional association of foxtail millet root microbiome. *Gigascience* 6, 1–12. doi: 10.1093/gigascience/gix089

Konishi, S., Izawa, T., Lin, S. Y., Ebana, K., Fukuta, Y., Sasaki, T., et al. (2006). An SNP caused loss of seed shattering during rice domestication. *Science* 312, 1392–1396. doi: 10.1126/science.1126410

Kozich, J. J., Westcott, S. L., Baxter, N. T., Highlander, S. K., and Schloss, P. D. (2013). Development of a dual-index sequencing strategy and curation pipeline for analyzing amplicon sequence data on the MiSeq Illumina sequencing platform. *Appl. Environ. Microbiol.* 79, 5112–5120. doi: 10.1128/AEM.01043-13

Kravchenko, A. N., Robertson, G. P., Thelen, K. D., and Harwood, R. R. (2005). Management, topographical, and weather effects on spatial variability of crop grain yields. *Agron. J.* 97, 514–523. doi: 10.2134/agronj2005.0514

Kutta, E., and Hubbart, J. (2014). Improving understanding of microclimate heterogeneity within a contemporary plant growth facility to advance climate control and plant productivity. *J. Plant Sci.* 2, 167–178. doi: 10.11648/j.jps.20140205.14

Kuzyakov, Y., and Domanski, G. (2000). Carbon input by plants into the soil. *J. Plant Nutr. Soil Sci.* 163, 421–431. doi: 10.1002/1522-2624(200008)163:4<421::AID-JPLN421>3.0.CO;2-R

Leff, J. W., Lynch, R. C., Kane, N. C., and Fierer, N. (2017). Plant domestication and the assembly of bacterial and fungal communities associated with strains of the common sunflower. *Helianthus annuus*. *New Phytol.* 214, 412–423. doi: 10.1111/nph.14323

Levy, A., Gonzalez, I. S., Mittelviefhaus, M., Clingenpeel, S., Paredes, S. H., Miao, J. M., et al. (2018). Genomic features of bacterial adaptation to plants. *Nat. Genet.* 50, 138–150. doi: 10.1038/s41588-017-0012-9

Lopez-Raez, J. A., Shirasu, K., and Foo, E. (2017). Strigolactones in plant interactions with beneficial and detrimental organisms: the yin and yang. *Trends Plant Sci.* 22, 527–537. doi: 10.1016/j.tplants.2017.03.011

Lundberg, D. S., Lebeis, S. L., Paredes, S. H., Yourstone, S., Gehring, J., Malfatti, S., et al. (2012). Defining the core *Arabidopsis thaliana* root microbiome. *Nature* 488, 86–90. doi: 10.1038/nature11237

Mann, H. B., and Whitney, D. R. (1947). On a test of whether one of two random variables is stochastically larger than the other. *Ann. Math. Stat.* 18, 50–60. doi: 10.1214/aoms/1177730491

Mauro-Herrera, M., Wang, X. W., Barbier, H., Brutnell, T. P., Devos, K. M., and Doust, A. N. (2013). Genetic control and comparative genomic analysis of flowering time in *Setaria* (Poaceae). *G3* 3, 283–295. doi: 10.1534/g3.112.005207

McNear, D. H. (2012). The rhizosphere - roots, soil and everything in between. *Nat. Educ. Knowl.* 4:14. doi: 10.1093/aob/mcs061

Mendes, R., Garbeva, P., and Raaijmakers, J. M. (2013). The rhizosphere microbiome: significance of plant beneficial, plant pathogenic, and human pathogenic microorganisms. *FEMS Microbiol. Rev.* 37, 634–663. doi: 10.1111/1574-6976.12028

Muyzer, G., and Smalla, K. (1998). Application of denaturing gradient gel electrophoresis (DGGE) and temperature gradient gel electrophoresis (TGGE) in microbial ecology. *Antonie Van Leeuwenhoek* 73, 127–141. doi: 10.1023/A:1000669317571

Mysara, M., Vandamme, P., Props, R., Kerckhof, F. M., Leys, N., Boon, N., et al. (2017). Reconciliation between operational taxonomic units and species boundaries. *FEMS Microbiol. Ecol.* 93:fix029. doi: 10.1093/femsec/fix029

Niu, B., Paulson, J. N., Zheng, X. Q., and Kolter, R. (2017). Simplified and representative bacterial community of maize roots. *Proc. Natl. Acad. Sci. U.S.A.* 114, E2450–E2459. doi: 10.1073/pnas.1616148114

Pace, N. R., Stahl, D. A., Lane, D. J., and Olsen, G. J. (1985). Analyzing natural microbial populations by rRNA sequences. *ASM News* 51, 4–12.

Parks, D. H., Rinke, C., Chuvochina, M., Chaumeil, P. A., Woodcroft, B. J., Evans, P. N., et al. (2017). Recovery of nearly 8,000 metagenome-assembled genomes substantially expands the tree of life. *Nat. Microbiol.* 2, 1533–1542. doi: 10.1038/s41564-017-0012-7

Paungfoo-Lonhienne, C., Wang, W., Yeoh, Y. K., and Halpin, N. (2017). Legume crop rotation suppressed nitrifying microbial community in a sugarcane cropping soil. *Sci. Rep.* 7:16707. doi: 10.1038/s41598-017-17080-z

Peiffer, J. A., Spor, A., Koren, O., Jin, Z., Tringe, S. G., Dangl, J. L., et al. (2013). Diversity and heritability of the maize rhizosphere microbiome under field conditions. *Proc. Natl. Acad. Sci. U.S.A.* 110, 6548–6553. doi: 10.1073/pnas.1302837110

Philippot, L., Raaijmakers, J. M., Lemanceau, P., and Van Der Putten, W. H. (2013). Going back to the roots: the microbial ecology of the rhizosphere. *Nat. Rev. Microbiol.* 11, 789–799. doi: 10.1038/nrmicro3109

Reinhold-Hurek, B., Bunger, W., Burbano, C. S., Sabale, M., and Hurek, T. (2015). Roots shaping their microbiome: global hotspots for microbial activity. *Annu. Rev. Phytopathol.* 53, 403–424. doi: 10.1146/annurev-phyto-082712-102342

Robertson, G. P., Crum, J. R., and Ellis, B. G. (1993). The spatial variability of soil resources following long-term disturbance. *Oecologia* 96, 451–456. doi: 10.1007/BF00320501

Roesch, L. F., Fulthorpe, R. R., Riva, A., Casella, G., Hadwin, A. K. M., Kent, A. D., et al. (2007). Pyrosequencing enumerates and contrasts soil microbial diversity. *ISME J.* 1, 283–290. doi: 10.1038/ismej.2007.53

Santi, C., Bogusz, D., and Franche, C. (2013). Biological nitrogen fixation in non-legume plants. *Ann. Bot.* 111, 743–767. doi: 10.1093/aob/mct048

Sauer, D., and Burroughs, R. (1986). Disinfection of seed surfaces with sodium hypochlorite. *Phytopathology* 76, 745–749. doi: 10.1371/journal.ppat.1005914

Scherf, U., Ross, D. T., Waltham, M., Smith, L. H., Lee, J. K., Tanabe, L., et al. (2000). A gene expression database for the molecular pharmacology of cancer. *Nat. Genet.* 24, 236–244. doi: 10.1038/73439

Schlatter, D., Kinkel, L., Thomashow, L., Weller, D., and Paulitz, T. (2017). Disease suppressive soils: new insights from the soil microbiome. *Phytopathology* 107, 1284–1297. doi: 10.1094/PHYTO-03-17-0111-RVW

Schloss, P. D., Westcott, S. L., Ryabin, T., Hall, J. R., Hartmann, M., Hollister, E. B., et al. (2009). Introducing MOTHUR: open-source, platform-independent, community-supported software for describing and comparing microbial communities. *Appl. Environ. Microbiol.* 75, 7537–7541. doi: 10.1128/AEM.01541-09

Schmitz, A. M., and Harrison, M. J. (2014). Signaling events during initiation of arbuscular mycorrhizal symbiosis. *J. Integr. Plant Biol.* 56, 250–261. doi: 10.1111/jipb.12155

Schroder, S., Bahri, B. A., Eudy, D. M., Layton, D. J., Kellogg, E. A., and Devos, K. M. (2017). Genetic diversity and origin of North American green foxtail [*Setaria viridis* (L.) Beauv.] accessions. *Genet. Resour. Crop Evol.* 64, 367–378. doi: 10.1007/s10722-016-0363-6

Sebastian, J., Yee, M. C., Viana, W. G., Rellan-Alvarez, R., Feldman, M., Priest, H. D., et al. (2016). Grasses suppress shoot-borne roots to conserve water during drought. *Proc. Natl. Acad. Sci. U.S.A.* 113, 8861–8866. doi: 10.1073/pnas.1604021113

Segata, N., Izard, J., Waldron, L., Gevers, D., Miropolsky, L., Garrett, W. S., et al. (2011). Metagenomic biomarker discovery and explanation. *Genome Biol.* 12:R60. doi: 10.1186/gb-2011-12-6-r60

Smith, S. E., and Smith, F. A. (2011). Roles of arbuscular mycorrhizas in plant nutrition and growth: new paradigms from cellular to ecosystem scales. *Annu. Rev. Plant Biol.* 62, 227–250. doi: 10.1146/annurev-arplant-042110-103846

Sokal, R. R. (1958). A statistical method for evaluating systematic relationship. *Univ. Kansas Sci. Bull.* 28, 1409–1438.

Sugiyama, A., Ueda, Y., Zushi, T., Takase, H., and Yazaki, K. (2014). Changes in the bacterial community of soybean rhizospheres during growth in the field. *PLoS One* 9:e100709. doi: 10.1371/journal.pone.0100709

Szoboszlay, M., Lambers, J., Chappell, J., Kupper, J. V., Moe, L. A., and Mcnear, D. H. Jr. (2015). Comparison of root system architecture and rhizosphere microbial communities of Balsas teosinte and domesticated corn cultivars. *Soil Biol. Biochem.* 80, 34–44. doi: 10.1016/j.soilbio.2014.09.001

Tamme, R., Gazol, A., Price, J. N., Hiiesalu, I., and Pärtel, M. (2016). Co-occurring grassland species vary in their responses to fine-scale soil heterogeneity. *J. Veg. Sci.* 27, 1012–1022. doi: 10.1111/jvs.12431

Thompson, L. R., Sanders, J. G., Mcdonald, D., Amir, A., Ladau, J., Locey, K. J., et al. (2017). A communal catalogue reveals Earth's multiscale microbial diversity. *Nature* 551, 457–463. doi: 10.1038/nature24621

Trevors, J. T. (2010). One gram of soil: a microbial biochemical gene library. *Antonie Van Leeuwenhoek* 97, 99–106. doi: 10.1007/s10482-009-9397-5

Wagner, M. R., Lundberg, D. S., Del Rio, T. G., Tringe, S. G., Dangl, J. L., and Mitchell-Olds, T. (2016). Host genotype and age shape the leaf and root microbiomes of a wild perennial plant. *Nat. Commun.* 7:12151. doi: 10.1038/ncomms12151

Waines, J. G., and Ehdaie, B. (2007). Domestication and crop physiology: roots of green-revolution wheat. *Ann. Bot.* 100, 991–998. doi: 10.1093/aob/mcm180

Wang, H., Nussbaum-Wagler, T., Li, B. L., Zhao, Q., Vigouroux, Y., Faller, M., et al. (2005). The origin of the naked grains of maize. *Nature* 436, 714–719. doi: 10.1038/nature03863

Wang, Q., Garrity, G. M., Tiedje, J. M., and Cole, J. R. (2007). Naive Bayesian classifier for rapid assignment of rRNA sequences into the new bacterial taxonomy. *Appl. Environ. Microbiol.* 73, 5261–5267. doi: 10.1128/AEM.00062-07

Werner, G. D. A., Cornwell, W. K., Cornelissen, J. H. C., and Kiers, E. T. (2015). Evolutionary signals of symbiotic persistence in the legume-rhizobia mutualism. *Proc. Natl. Acad. Sci. U.S.A.* 112, 10262–10269. doi: 10.1073/pnas.1424030112

Wilcoxon, F. (1945). Individual comparisons by ranking methods. *Biom. Bull.* 1, 80–83. doi: 10.2307/3001968

Wissuwa, M., Mazzola, M., and Picard, C. (2009). Novel approaches in plant breeding for rhizosphere-related traits. *Plant Soil* 321, 409–430. doi: 10.1007/s11104-008-9693-2

Zhou, Z. K., Jiang, Y., Wang, Z., Gou, Z. H., Lyu, J., Li, W. Y., et al. (2015). Resequencing 302 wild and cultivated accessions identifies genes related to domestication and improvement in soybean. *Nat. Biotechnol.* 33, 408–416. doi: 10.1038/nbt.3096

Conflict of Interest Statement: The authors declare that the research was conducted in the absence of any commercial or financial relationships that could be construed as a potential conflict of interest.

frontiers in Plant Science

ORIGINAL RESEARCH
published: 04 September 2018
doi: 10.3389/fpls.2018.01308

SiYGL2 Is Involved in the Regulation of Leaf Senescence and Photosystem II Efficiency in *Setaria italica* (L.) P. Beauv.

*Shuo Zhang, Hui Zhi, Wen Li, Jianguo Shan, Chanjuan Tang, Guanqing Jia, Sha Tang and Xianmin Diao**

Institute of Crop Sciences, Chinese Academy of Agricultural Sciences, Beijing, China

A yellow-green leaf mutant was isolated from EMS-mutagenized lines of *Setaria italica* variety Yugu1. Map-based cloning revealed the mutant gene is a homolog of *Arabidopsis thaliana AtEGY1*. EGY1 (ethylene-dependent gravitropism-deficient and yellow-green 1) is an ATP-independent metalloprotease (MP) that is required for chloroplast development, photosystem protein accumulation, hypocotyl gravitropism, leaf senescence, and ABA signal response in *A. thaliana*. However, the function of EGY1 in monocotyledonous C_4 plants has not yet been described. The *siygl2* mutant is phenotypically characterized by chlorotic organs, premature senescence, and damaged PS II function. Sequence comparisons of the AtEGY1 and SiYGL2 proteins reveals the potential for SiYGL2 to encode a partially functional protein. Phenotypic characterization and gene expression analysis suggested that SiYGL2 participates in the regulation of chlorophyll content, leaf senescence progression, and PS II function. Additionally, our research will contribute to further characterization of the mechanisms regulating leaf senescence and photosynthesis in *S. italica*, and in C_4 plants in general.

Keywords: EGY1, *Setaria italica*, chlorotic mutant, leaf senescence, PS II efficiency

OPEN ACCESS

Edited by:
Thomas P. Brutnell, Shandong Agricultural University, China

Reviewed by:
Ru Zhang, Donald Danforth Plant Science Center, United States
Yan Lu, Western Michigan University, United States

****Correspondence:***
Xianmin Diao
diaoxianmin@caas.cn

Specialty section:
This article was submitted to Plant Breeding, a section of the journal Frontiers in Plant Science

Received: *29 November 2017*
Accepted: *20 August 2018*
Published: *04 September 2018*

Citation:
Zhang S, Zhi H, Li W, Shan J, Tang C, Jia G, Tang S and Diao X (2018) SiYGL2 Is Involved in the Regulation of Leaf Senescence and Photosystem II Efficiency in Setaria italica (L.) P. Beauv. Front. Plant Sci. 9:1308. doi: 10.3389/fpls.2018.01308

INTRODUCTION

AtEGY1 is an ATP-independent metalloprotease (MP) belonging to the M50 family (van der Hoorn, 2008). Members of the M50 family typically contain four to eight transmembrane helices (TMHs), three adjacent ones of which can form a conserved three-TMH core structure. The conversed motifs HEXXH and NPDG are located in the first TMH and the third TMH of the core structure, respectively (Kinch et al., 2006; Feng et al., 2007; Koussis et al., 2017). M50 family members contain three metal ligand-binding sites required for protease activity. Two of the ligand-binding sites reside in the HEXXH motif and the third is coordinated by the Asp residue in NPDG motif (Yu and Kroos, 2000; Feng et al., 2007). As MPs, M50 family proteins participate in multiple cellular processes by cleaving substrates such as membrane-tethered proteins, transcription factors, and signal peptides (Bölter et al., 2006; Kinch et al., 2006; Mukherjee et al., 2009; Che et al., 2010; Saito et al., 2011). AtEGY1 is targeted to chloroplasts and can be upregulated by both light and ethylene treatment in *A. thaliana* (Chen et al., 2005). The function of AtEGY1 has been characterized in a number of different studies. AtEGY1 has three conversed motifs: GNLR, HEXXH, and NPDG. The first is a signature motif unique to EGY family

proteins (Chen et al., 2005); the function of this motif has not yet been clarified. The latter two motifs are metal-chelating motifs unique to M50 family members. AtEGY1 was shown to play a role in many biological processes including the regulation of chloroplast development, ethylene-dependent hypocotyl gravitropism, the accumulation of membrane-bound chlorophyll *a*/*b* binding (CAB) proteins, and responding to ammonium and phosphate stress (Chen et al., 2005; Guo et al., 2008; Li et al., 2012; Yu et al., 2016). In addition, AtEGY1 was reported to be involved in leaf senescence. The T-DNA insertion mutant of *AtEGY1*, *Ategy1*, had yellow rosette leaves and reduced chlorophyll content, leaf survival, and Fv/Fm. Mutants also showed decreased soluble protein content and increased ion leakage compared with WT. The expression of senescence-associated genes were increased in *Ategy1*. Under dark treatment, the aging phenotype in *Ategy1* was more obvious than that in WT. These data indicated that the loss of AtEGY1 function accelerated leaf aging and decreased photosystem II (PS II) efficiency. In addition, exogenously applied glucose could rescue these mutant phenotypes (Chen et al., 2016).

Leaf senescence is an important plant developmental process that is associated with a range of unique physiological and biochemical characteristics. During leaf senescence, leaves turn yellow; chlorophyll is degraded; proteins, fatty acids, nucleic acids, and other macromolecules are metabolized; plastids disintegrate rapidly; and nitrogen and nutrients are efficiently transferred into growing tissues and sink organs (Yang and Ohlrogge, 2009; Sakamoto and Takami, 2014; Diaz-Mendoza et al., 2016). Concurrently, thousands of senescence-associated genes are upregulated or downregulated at the transcriptional or post-transcriptional level as senescence is a well-controlled process that transfers nutrients from source to sink (Gupta et al., 2016; Wu et al., 2016). Crop yield and quality are, therefore, closely related to the timing of senescence. Proteins in old organs are extensively degraded into amino acids, amides, and ammoniums. For cereal crops, leaf senescence provides most of the nitrogen in grains. It has been reported that delayed senescence could lead to high yields (Lu et al., 2017) because the filling period is prolonged and sugar and nitrogen accumulation is increased (Egli, 2011; Gregersen et al., 2013). Conversely, grain quality has negative correlations with senescence progression. Because delayed senescence could cause inefficient nitrogen remobilization. The grain quality parameters such as proteins and micronutrients are diluted by carbohydrates, thereby leading to a low grain quality (Gregersen et al., 2008). There is a balance between grain yield and quality. Thus, the better understanding of the senescence process could help improve crop production and seed quality (Diaz-Mendoza et al., 2016).

Metalloproteases (MPs) are one type of plant proteases, which plays important roles in leaf senescence. There are approximately 100 MPs in plants, belonging to 19 families which are classified by the similarity in amino acid sequence. Although they are involved in many biological processes, the roles of MPs in leaf senescence are poorly understood (van der Hoorn, 2008). The most studied senescence-associated MPs are FtsH (filamentation temperature sensitive H) proteases that belong to the M41 family. FtsH1, 2, 5, and 8 can form a hexameric ring in the chloroplast thylakoid to regulate the thylakoid structure and remove photodamaged D1 protein in PS II under light stress (Yoshioka-Nishimura et al., 2014). Changes in the expression of *FtsH1*, *2*, and *5* observed in senescing and aging leaves was found to be associated with light stress, dark conditions, or nitrogen stress (Roberts et al., 2012). FtsH6 is reportedly involved in detached leaf senescence and dark-induced leaf senescence. Other proteases including members of the M10 and M17 MP families have also been reported associated with leaf senescence. Matrix MPs (MMPs) belong to the M10 family and are reportedly upregulated during senescence (Roberts et al., 2012). A mutant of At2-MMP shows a late flowering and early senescence phenotype, suggesting that MMPs are responsible for senescence regulation (Golldack et al., 2002). Leucine aminopeptidase 2 (LAP2) is a member of the M17 family. In *A. thaliana*, a mutant of LAP2 displays an early-senescence phenotype, suggesting that LAPs are involved in leaf longevity (Waditee-Sirisattha et al., 2011). EGY1 belongs to M50 family. To date, seven M50 family members have been identified in *A. thaliana*, *Oryza sativa*, and *Zea mays*. These proteases play roles in chloroplast development, hypocotyl elongation and gravitropism, stress response, nuclear plastid signaling pathway, and plant development, respectively (Nishimura et al., 2016).

Setaria italica is a new model C_4 monocotyledonous species that promises to accelerate functional genomics studies in the grasses (Doust et al., 2009). In this study, a pale green mutant *siygl2* was isolated from EMS-mutagenized lines of the *S. italica* Yugu1 cultivar. Map-based cloning indicated that the mutant gene encoded SiYGL2, a homolog of AtEGY1. Phenotypic surveys showed that *siygl2*, such as *Ategy1*, is characterized by chlorotic organs, premature senescence, and damaged PS II function. Unlike *Ategy1*, however, chloroplast development is not impaired in *siygl2*. Our study focused on the function of SiYGL1 in regulating senescence and photosynthesis in *S. italica* to supplement the existing functional gene knowledge available for this C_4 model plant. Additionally, our research provides further insight into the mechanisms underlying the regulation of leaf senescence.

MATERIALS AND METHODS

Plant Materials and Growth Condition

The *siygl2* mutant was identified in screens of EMS mutagenized populations of *S. italica* cultivar Yugu1. To determine the chlorophyll content and the photosynthetic rate, plants were planted under natural conditions in the experimental field of institute of Crop Sciences, Chinese Academy of Agricultural Sciences, in Beijing (116.6°E, 40.1°N) in summer season. For dark-induced senescence, detached leaves were incubated in water at 28°C.

Chlorophyll Content, Photosynthetic Rate, and Chlorophyll Fluorescence

For analysis of photosynthetic pigments, leaves were cut into pieces and soaked in 95% alcohol for approximately 72 h until leaf pieces were completely transparent. The absorbance values of the supernatant were measured at 665 and 649 nm with

UV-1800 ultraviolet/visible light. Chlorophyll *a* (Chl *a*) and chlorophyll *b* (Chl *b*) levels were then calculated as described by Lichtenthaler (1987). Statistics analysis was conducted using Welch's two-sample *t* test. Multiple comparisons were made with LSD by IBM SPSS Statistics 23.0. The photosynthetic rate and chlorophyll fluorescence were measured on sunny days using a Li-6400 portable photosynthesis system (LI-COR, Lincoln, NE, United States) using mature leaves from five individuals. The light source used for measuring the photosynthetic parameters is 6400-02B LED light source, the ParIn parameter was set to 1000 μmol m^{-2} s^1. The equations for the photosynthetic parameters are calculated as follows (Hu et al., 2014).

$$\Delta \Phi \text{PS II} = (\text{Fm}' - \text{Fs})/\text{Fm}'$$

$$\Delta \text{ETR} = \text{PAR (photosynthetic active radiation)} \times \Delta \Phi \text{PS II} \times 0.84 \times 0.5$$

Transmission Electron Microscopy

The second leaf and seventh leaf were obtained from plants that were at the eight-leaf stage. Leaf material was cut into 2 mm × 1 mm pieces and fixed overnight in 0.1 M phosphate buffer with 2.5% glutaraldehyde. The samples were then washed with 0.2 M phosphate buffer three times and post-fixed in 1% osmium tetroxide for 1 h. After staining with uranyl acetate, samples were further dehydrated in a gradient ethanol series and finally embedded into resin. Ultrathin sections were made and examined by JEM 1230 transmission electron microscopy (TEM). The areas of plastoglobulis are calculated by Image-Pro plus 6.0 (Media Cybernetics, Silver Spring, Georgia Avenue, United States). Statistics treatment was made with Welch's two-sample *t* test.

Map-Based Cloning

An F2 population generated from a cross between *siygl2* and the SSR41 cultivar was used for mapping of the *SiYGL2* locus. Sixty-five SSR markers based on earlier studies (Jia et al., 2009; Zhang et al., 2014) were adopted for gene cross positioning. Thirteen cleaved amplified polymorphism sequences (CAPS) markers were newly designed for fine mapping based on the single-nucleotide polymorphism information between Yugu1 and SSR41 (Jia et al., 2013) (**Supplementary Table S1**). To identify mutant locations, 40 sequencing primers were developed that covered the whole candidate region based on the genome sequence information from the *S. italica* genome project V2.2[1] database (**Supplementary Table S2**).

RNA Preparation and Transcript Analysis

RNA was isolated from wild-type (WT) and *siygl2* stems, panicles, and 1st and 10th leaves from the top of the plant at the heading stage from fresh plant tissues using a Pure Link RNA Mini Kit (Cat no. 12183018, Invitrogen, United Kingdom). First-srtand cDNA was synthesized with a PrimerScript 1st Strand cDNA Synthesis Kit (Cat no. 6210A, TaKaRa, Otsu Shiga, Japan). Quantitative PCR was conducted using a Fast Start Universal SYBR Green Master (ROX) (Cat no. 04913914001, Roche, Mannheim, Germany) using the specific primers listed in **Supplementary Table S3**. *Cullin* was selected as the reference gene according to a previous study (Martins et al., 2016). The data were detected and analyzed using an Applied Biosystems 7300 Analyzer (Applied Biosystems, Foster City, CA, United States). Statistics treatment was made with Welch's two-sample *t* test.

Bioinformatics Analysis

The sequences and structures of the candidate genes were obtained from the *S. italica* genome project V2.2. For phylogenetic analysis, homologs were obtained by NCBI Protein Blast[2]. Sequence alignments and cladograms were produced using MEGA 5.0 software. Protein TMHs were calculated using TMHMM_v.2[3].

Subcellular Localization

The full-length cDNA of *SiYGL2*, excluding the stop code, was amplified from Yugu1 using the following primers: 5′ TATCTCTAGAGGATCCCTATCCTCCTTCGGTCCTTCCCATT 3′ and 5′ TGCTCACCATGGATCCGAACGAAGTAACAAGCCCTACACCT 3′ [the underlined sequences are adaptors for In-fusion® PCR cloning system (Cat no. 072012, Clontech, United States) and contain *Bam*HI cleavage sites]. The cDNA sequences were cloned into the p16318hGFP vector to form fusion proteins with the C-terminus of GFP. These vectors were then transfected into foxtail millet protoplasts by PEG-mediated transformation and detected by confocal microscopy (LSM700, Carl Zeiss, Germany).

RESULTS

The Chlorotic Mutant *siygl2* Has Reduced Chlorophyll Accumulation and Poor Agronomic Traits

The *S. italica* chlorotic mutant *siygl2* was generated from the Yugu1 cultivar by EMS treatment. The *siygl2* mutant showed a relatively normal phenotype in the seedling stage (**Figure 1A**). Throughout development, however, these plants gradually became chlorotic, and in the late developmental stages, *siygl2* produced chlorotic leaves, stems, and panicles (**Figures 1B–E**). Additionally, the lower leaves of *siygl2* had more abnormal phenotypes than the upper leaves (**Figure 1F**). Senescence appeared to be accelerated in *siygl2* as the basal leaves of *siygl2* were tip burned. Several key agronomic traits of *siygl2* and WT plants were analyzed. The results showed that some yield characteristics, such as floret grain number and panicle weight, are significantly reduced compared to WT (**Table 1**).

Analysis of the Chlorophyll Content and Photosynthetic Rate

To further characterize the chlorotic phenotype of the *siygl2* mutant, we measured the chlorophyll content of leaf, sheath,

[1]https://phytozome.jgi.doe.gov/

[2]https://blast.ncbi.nlm.nih.gov/

[3]http://www.cbs.dtu.dk/services/TMHMM/

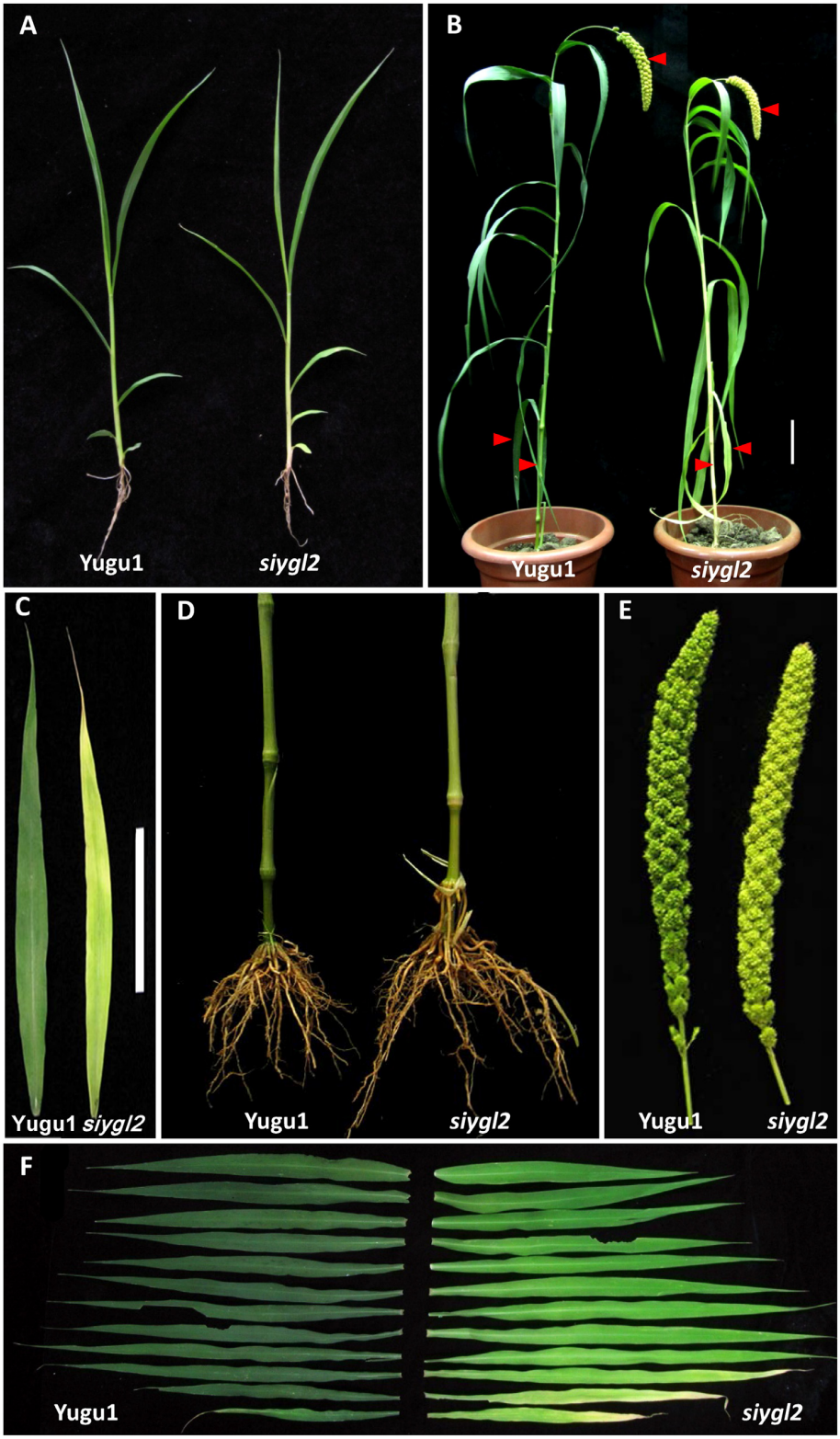

FIGURE 1 | Phenotypic characteristics of the *siygl2* mutant. **(A)** Five-week-old seedling phenotypes of the wild-type (WT) cultivar Yugu1 and the *siygl2* mutant. **(B)** Heading stage phenotypes of Yugu1 and *siygl2*. The red bars point out the significant abnormal phenotypes in panicles, stems, and bottom leaves. **(C–E)** Lower leaves, stems, and panicles of heading stage plants. **(F)** Leaf color comparison of the WT (left) and *siygl2* (right) at the heading stage. Leaves from the top of the plant to the bottom are arranged accordingly.

TABLE 1 | Agronomic traits in wild-type Yugu1 and mutant *siygl2* plants.

Trait		Yugu1	*siygl2*	*P*-value
Plant height (cm)		139.6 ± 7.8	136.1 ± 5.7	0.117
Tiller number		2.8 ± 1.1	2 ± 0.7	0.212
Main panicle length (cm)	*	18.4 ± 1.3	15.2 ± 1.8	0.013
Main panicle diameter (cm)	*	28.8 ± 1.5	17.8 ± 6.4	0.021
Floret number		109.2 ± 13.2	124.6 ± 22.4	0.222
Floret grain number	**	94.6 ± 26.1	41.6 ± 18.3	0.006
Panicle weight per plant (g)	**	30.2 ± 9.5	10.8 ± 4.0	0.003
Main panicle weight (g)	**	17.8 ± 1.4	9.0 ± 3.2	0.001
Thousand seed weight (g)		2.6 ± 0.1	2.7 ± 0.2	0.309

*Means and standard deviations were obtained from ten independent leaf samples grown under normal growth conditions. Means and standard deviations are obtained from 10 independent samples. Statistics treatment was made with Welch's two-sample t test. **Significantly different at P = 0.01. *Significantly different at P = 0.05.*

panicle, and stem at the heading stage (**Figure 2A**), and found them to have 71, 35, 28, and 28% the chlorophyll content of WT tissues, respectively. Both Chl *a* and Chl *b* levels were reduced in *siygl2*, with the reduction in Chl *b* being more severe in leaves.

As reductions in chlorophyll may be associated with changes of the photosynthetic capacity, the photosynthetic parameters of the newly emerging leaves (from the top of the plant) were measured (**Figure 2B**). Surprisingly, *siygl2* photosynthetic capacity was not significantly affected at the seedling stage, the elongation stage, or the heading stage. The stomatal conductance of *siygl2* decreased about 22% in the elongation stage concurrent with a decrease in the intercellular carbon dioxide concentration of approximately 40%. Overall, the decrease in chlorophyll accumulation in *siygl2* did not significantly affect photosynthesis in the newly developed leaves. Variations in the intercellular carbon dioxide concentration and stomatal conductance may be caused by other effects of the mutant gene or environmental factors. Further study in investigating the ACi curve of both WT and mutants would help to reveal the effects of EGY1 in photosynthesis.

SiYGL2 May Be Involved in the Regulation of Leaf Senescence and PS II Efficiency

As the basal leaves of *siygl2* had a more obvious chlorotic phenotype than the top leaves and showed accelerated senescence

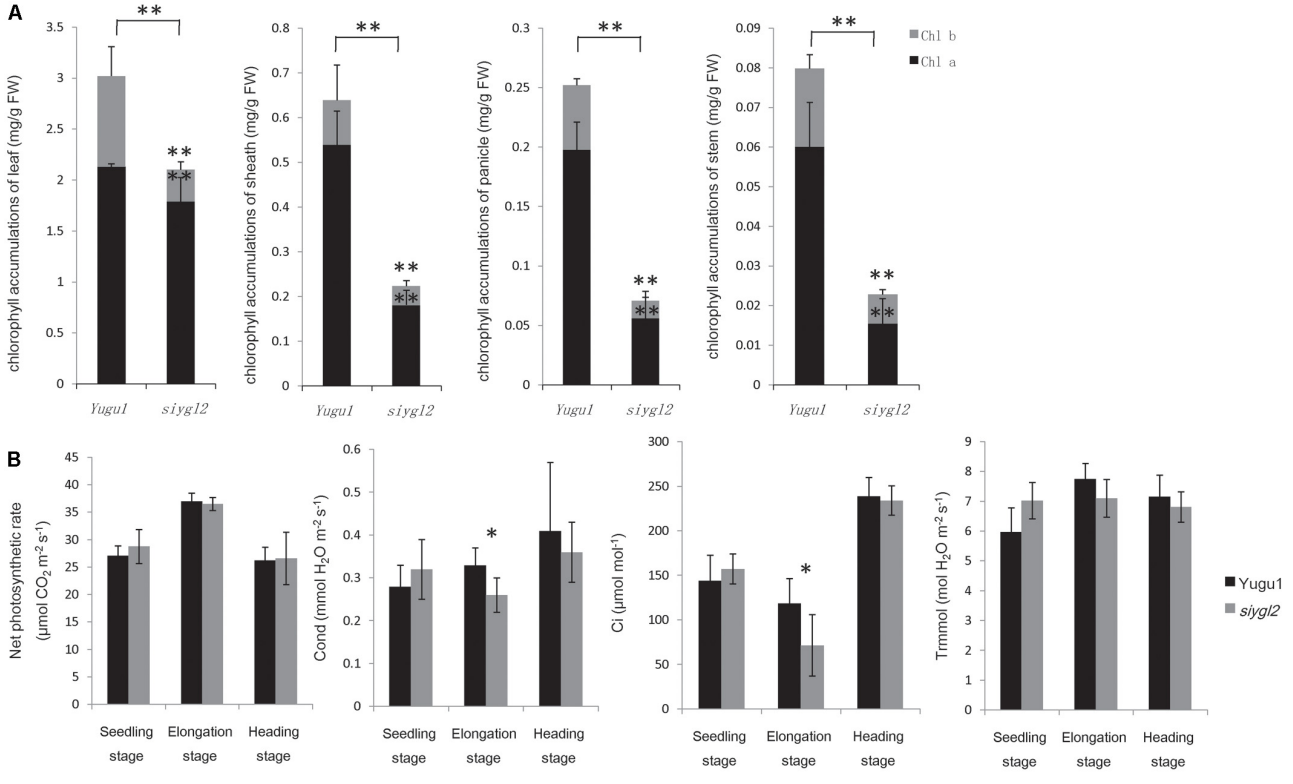

FIGURE 2 | (A) Chlorophyll content of leaves, sheaths, panicles, and stems at the heading stage of wild-type cultivar Yugu1 and the *siygl2* mutant. Black and gray boxes show the amount of chlorophyll *a* and chlorophyll *b*, respectively. FW, fresh weight; Chl *a*, chlorophyll *a*; Chl *b*, chlorophyll *b*. Means and standard deviations were obtained from five independent leaf samples grown under normal growth conditions. **(B)** Photosynthetic parameters in different developmental stages. Means and standard deviations were obtained from five independent leaf samples grown under normal growth conditions. Photo, photosynthetic rate; Cond, stomatal conductance; Ci, intercellular carbon dioxide concentration; Trmmol, transpiration rate. Means and standard deviations are obtained from five independent samples. *Significantly different at *P* = 0.05. **Significantly different at *P* = 0.01.

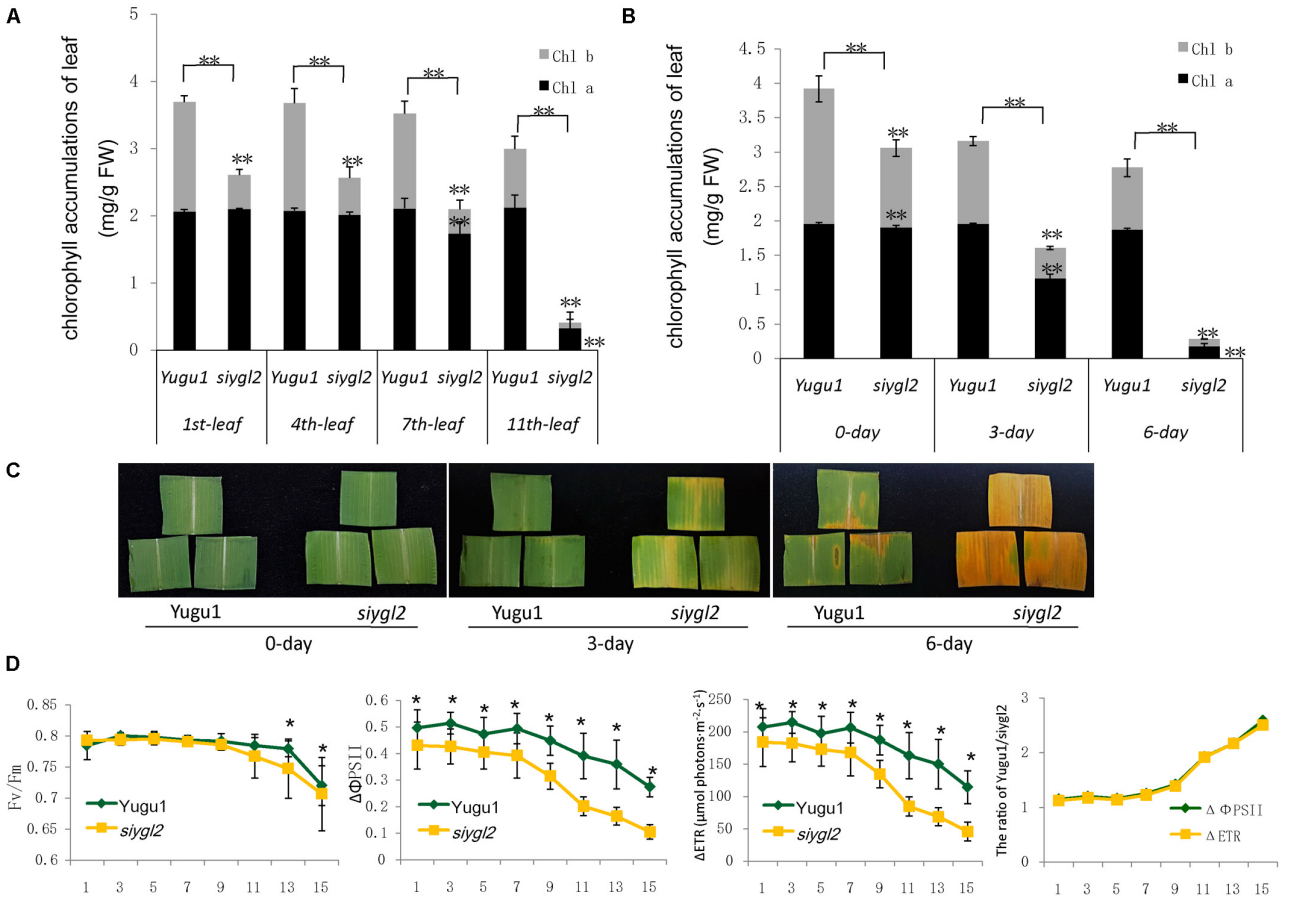

FIGURE 3 | (A) Chlorophyll accumulation in different leaves at the heading stage (mg/g FW). Black and gray boxes represent Chl *a* and Chl *b*, respectively. **(B)** Chlorophyll accumulations after different durations of dark treatment. **(C)** Leaves of Yugu1 and *siygl2* after different durations of dark treatment. **(D)** Chlorophyll fluorescence in different leaves of Yugu1 and *siygl2*. The *X* axis shows the leaf position from the top of plants. For measuring the chlorophyll content and chlorophyll fluorescence, means and standard deviations are obtained from five independent plants for each genotype. *Significantly different at $P = 0.05$. **Significantly different at $P = 0.01$.

(**Figures 1B,F**), the chlorophyll pigment levels of the 1st, 4th, 7th, and 11th leaves from the top of *siygl2* and WT Yugu1 plants were examined (**Figure 3A**). Chlorophyll accumulation in the first leaves of *siygl2* declined by approximately 30% compared with Yugu1. However, in basal leaves, *siygl2* only contained one-third of the chlorophyll of the WT leaves at the same position. This suggests that chlorophyll levels decline earlier in the old leaves of *siygl2* than in Yugu1. We also noticed that in the first and fourth leaves of *siygl2*, the Chl *b* levels decreased while Chl *a* levels did not. In the 11th leaves, both Chl *a* and Chl *b* in *siygl2* are sharply decreased compared with Yugu1 (**Figure 3A**). Anyhow, the accelerated leaf senescence of *siygl2* could be associated with changes in the function of SiYGL2.

To verify the changes in leaf aging in *siygl2*, we first conducted a detached leaf senescence assay using dark treatments (**Figures 3B,C**). After 3 days of dark treatment, first leaves of WT and *siygl2* were compared. The leaves of *siygl2* began turning yellow, while the leaves of the WT remained green (**Figure 3C**). After 6 d of dark treatment, *siygl2* leaves were completely yellow, whereas only the cut ends of the WT leaves showed yellowing (**Figure 3C**). The chlorophyll content also reflected the changes induced by dark treatment (**Figure 3B**). These results suggest that SiYGL2 helps to negatively regulate dark-induced leaf senescence, with senescence promoted by the loss of SiYGL2 function. In addition, we noticed that at the beginning of dark treatment, the effect on the reduction of Chl *b* levels are stronger than on the reduction of Chl *a* levels (**Figure 3B**).This is similar with the phenomenon showed in **Figure 3A**.

The maximum photochemical efficiency (Fv/Fm) is a senescence-associated index. We measured the Fv/Fm values of the 1st, 3rd, 5th, 7th, 11th, 13th, and 15th leaves of WT and *siygl2* plants. The Fv/Fm values of the WT Yugu1 plants decreased gradually from the upper to the lower leaves. The Fv/Fm values of the mutant *siygl2* leaves displayed a similar decreasing tendency, with levels declining more sharply than in the WT in the 13th and 15th leaves (**Figure 3D**). This suggests that the basal leaves of *siygl2* enter senescence earlier than Yugu1. We further tested effective PSII quantum yield (ΔΦPS II) and photosynthetic electron transport rate (ΔETR) to describe the changes PS II light-use efficiency (**Figure 3D**). Both ΔΦPS II and

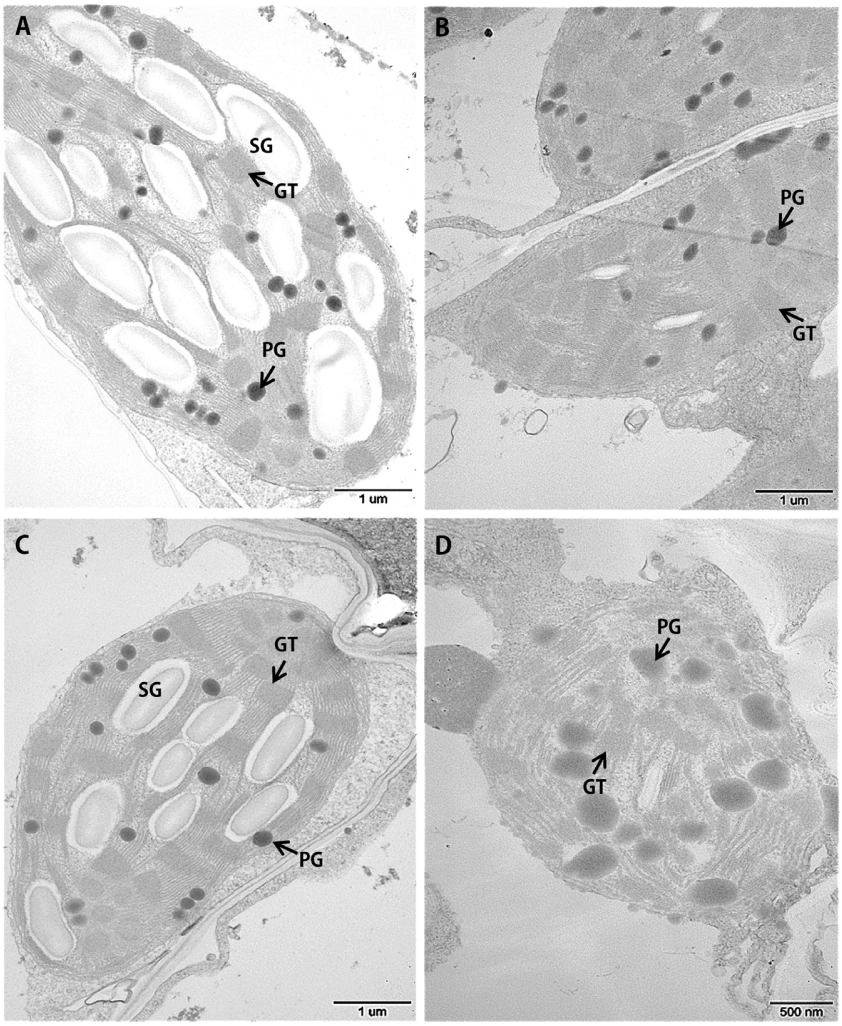

FIGURE 4 | Transmission electron microscopic images of chloroplasts in the WT Yugu1 cultivar **(A,B)** and *siygl2* mutant **(C,D)**. **(A,C)** Chloroplasts in tender leaves. **(B,D)** Chloroplasts in tender aging leaves. SG, starch granules; PG, plastoglobuli; GT, grana thylakoid stacks.

ΔETR declined generally in leaves when moving from the top to the bottom of the plant, indicating that PS II photosynthesis capacity decreases with aging. In the whole-plant leaves, both ΔΦPS II and ΔETR of *siygl2* were lower than in Yugu1. From the 11th leaf, the ratio of both ΔΦPS II and ΔETR of Yugu1/*siygl2* significantly increased compared with that in the upper leaves, indicating that these two indices drop more acutely than in *siygl2* (**Figure 3D**). These results verify that PS II photosynthesis capacity is decreased and senescence is premature in *siygl2*.

Leaf senescence is always accompanied by changes in chloroplast ultrastructure. We obtained entirely expanded young leaves and basal leaves of plants at the elongating stage (eight leaf-stage) and surveyed the mesophyll cell-chloroplasts of these leaves. TEM observations showed that in the young leaves of *siygl2*, the chloroplasts were similar to those of Yugu1 (**Figures 4A,C**), indicating that thylakoid and chloroplast development were not impaired. However, in the basal leaves of *siygl2*, the chloroplasts were seriously disintegrated. The size of the plastoglobuli increased by 57.4% in *siygl2* (**Supplementary Figure S1**), and irregular grana thylakoid stacks were also be observed in the chloroplasts of the mutant (**Figure 4D**). In *siygl2* leaves at the same position as in Yugu1, chloroplasts retained their normal state (**Figure 4B**). This result indicates that chloroplast degradation of *siygl2* is advanced.

Taken together, the above results suggest that the *SiYGL2* gene may play a role in maintaining chlorophyll accumulation and chloroplast structure in aging leaves, and may delay the onset of leaf senescence. Suppression of SiYGL2 function could, therefore, lead to early senescence of basal leaves.

Map-Based Cloning of the *SiYGL2* Locus and Bioinformatic Analysis

For genetic analysis of the *siygl2* mutant, we constructed an F_2 population by hybridizing *siygl2* with the Yugu1 cultivar. The F_2 progeny showed a segregation ratio of 3:1 (266:80,

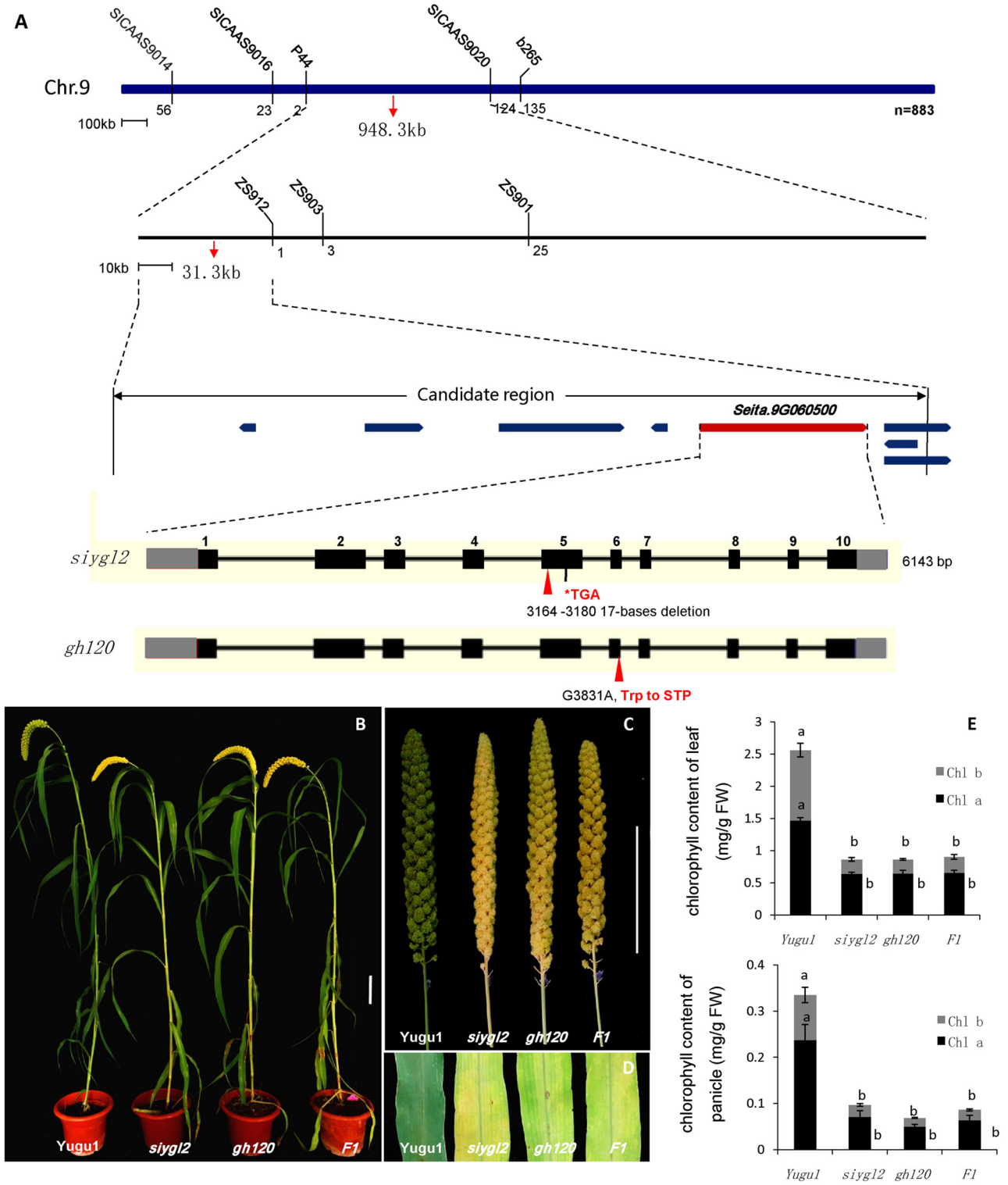

FIGURE 5 | (A) Map-based cloning, gene structure of *Seita.9G060500*, and the mutant positions of *siygl2* and *gh120*. **(B–D)** are phenotypes of WT Yugu1 plants and mutants. **(E)** Chlorophyll content of *siygl2*, *gh120*, and F1 individuals. Means and standard deviations are obtained from five independent samples. Values connected by same letters are not statistically different; values not connected by same letters are statistically different at $P = 0.05$.

$\chi^2 = 0.56 < \chi^2_{0.05} = 3.84$), suggesting that this chlorotic phenotype was controlled by a single recessive gene.

To map the *siygl2* locus, an F_2 mapping population was generated from a cross between *siygl2* and the cultivar SSR41. Using this F_2 population (883 yellow leaf plants), we generated a DNA pool of 40 individual mutant plants and preliminarily mapped the *siygl2* gene to a 948.3-kb genomic region on chromosome 9 by bulked segregation analysis. On this basis, a 31.3-kb genomic region between the SSR marker P44 and the CAPS marker zs912 was then defined. Within this region, eight open reading frames (ORFs) were predicted from the data on *phytozome*[4] (**Figure 5A**). These ORFs were amplified and sequenced and only the fifth ORF (*Seita.9G060500*) was found to carry a 17-bp deletion (AATGTTTGACATATCAA) at the position 3,478,889–3,478,905 of chromosome 9. The gene structure of *Seita.9G060500* is predicted to contain 11 exons and 10 introns. The identified deletion in this gene leads to a frameshift that results in a termination codon at the fifth exon (**Figure 5A**).

We also identified another leaf chlorotic mutant, *gh120*, that shows the same phenotypes as *siygl2* (**Figures 5B–E**). Genome sequencing indicated that there is a single base change (G 3831 A) at the sixth exon of *Seita.9G060500* that leads to the alteration of Trp to a termination codon. The F_1 individuals of a cross between *siygl2* and *gh120* are hemizygous at both the mutation sites of their parents (**Supplementary Figure S2**) and display similar phenotypes to their parents (**Figures 5B,D**). The chlorophyll content of F_1 plants is consistent with that of *siygl2* and *gh120* mutant (**Figure 5E**). These results suggest that the mutations in *Seita.9G060500* indeed cause the abnormal phenotype in the *siygl2* and *gh120*.

Amino acid sequence comparison indicated that SiYGL2 is most closely related to AtEGY1, with these proteins sharing 77.3% amino acid sequence identity. SiYGL2 was, therefore, proposed to be a homolog of AtEGY1, a S2P-like chloroplast membrane-located MP. Phylogenetic analysis further confirmed this relationship (**Figure 6**). In *Arabidopsis,* there are three EGY proteins: AtEGY1, AtEGY2, and AtEGY3 (Chen et al., 2005). Similarly, two homologs of SiYGL2, Seita.5G097600 (SiEGY2) and Seita.9G108100 (SiEGY3), were identified in *S. italica* (**Figure 6**).

SiYGL2 is predicted to encode a 548-aa protein, with a peptide chain that contains three conversed motifs, GNLR (aa 169–178), HEXXH (aa 311–315), and NPDG (aa 442–454) (**Figure 7A**), that reportedly also occur in AtEGY1 (Chen et al., 2005). However, the mutant SiYGL2 protein (ΔSiYGL2) was predicted to lack 165 amino acid residues from the carboxyl terminus. Furthermore, frameshift mutation caused changes in the sequence from 362–383 aa, leading to the loss of NPDG motif. This suggests that the protein structure and function of ΔSiYGL2 is likely to differ significantly from that of SiYGL2.

Hydropathy analysis revealed that the AtEGY1 protein is highly hydrophobic as it contains six predicted transmembrane (tm) helices in its C-terminus (tm1, aa 340–362; tm2, aa 369–387; tm3, aa 402–424; tm4, aa 462–484; tm5, aa 516–538; tm6, aa 559–576). Conversely, ΔSiYGL2 lost four of these tm helices (**Figure 7B**).

Expression Analysis of *SiYGL2*

As the *siygl2* mutant showed chlorotic leaves, stems, and panicles, with this phenotype more apparent in older leaves, the expression pattern of *SiYGL2* was investigated in different organs and leaves at different developmental stages by qRT-PCR (**Figure 8**). *SiYGL2* was more highly expressed in panicles and young leaves (1st leaves) than in stems and old leaves (10th leaves), suggesting that SiYGL2 is typically more active in young organs. However, *SiYGL2* expression in *siygl2* organs differed significantly; in panicle, stem, and the 10th leaf in *siygl2*, *SiYGL2* expression decreased to 27.7, 43.5, and 20.0% of those in WT, respectively. In the 10th leaf, in particular, transcript accumulation was very low. However, the expression *SiYGL2* in the first leaf of *siygl2* was higher (1.25-fold) than in the WT. These results suggest that the expression of *SiYGL2* in *siygl2* is not dependent on the function of the SiYGL2 protein.

Subcellular Location Analysis of SiYGL2 Protein

To explore the subcellular location of SiYGL2, we generated a *SiYGL2-GFP* fusion gene. The fusion gene was placed under the control of the CaMV 35S promoter and introduced into protoplasts of Yugu1. The results obtained from confocal laser microscopy show that SiYGL2 is localized to the chloroplast (**Figure 9A**). This result is similar to that of AtEGY1 (Chen et al., 2005). In the GFP transgenic control line, GFP fluorescence was found in the cytomembrane, the plasma, and the nucleus (**Figure 9B**).

Complicated Regulation of Senescence-Related Genes in the *siygl2* Mutant

To further verify the influence of the *SiYGL2* mutation on leaf senescence, several senescence-related genes examined using qRT-PCR (**Figure 10**). *AtSAG12*, encoding a putative cysteine protease, is a negative regulator of senescence. In *A. thaliana*, expression of *AtSAG12* is strictly associated with senescence progression, with expression levels increasing throughout leaf aging before decreasing at the end of the aging process (Weaver et al., 1998). We used *SiSAG12*, a homolog of *AtSAG12* as a reporter to follow the progression of leaf senescence. In old 10th leaves of Yugu1, the expression level of *SiSAG12* was upregulated dramatically (approximately sevenfold), consistent with the reported expression of AtSAG12. While *SiSAG12* expression levels in both young and old leaves of *siygl2* were lower than those in the corresponding leaves of Yugu1. *SiSAG12* expression did increase by approximately threefold in 10th leaf than that in young leaf of *siygl2* (**Figure 10**). These results suggest that the expression of senescence-associated genes in *siygl2* is impaired, reflecting the variations in aging processes between *siygl2* and WT.

SGR1 and NYC1 are reportedly involved in chlorophyll degradation and disassembly of the light-harvesting complex

[4]http://phytozome.jgi.doe.gov/pz/portal.html

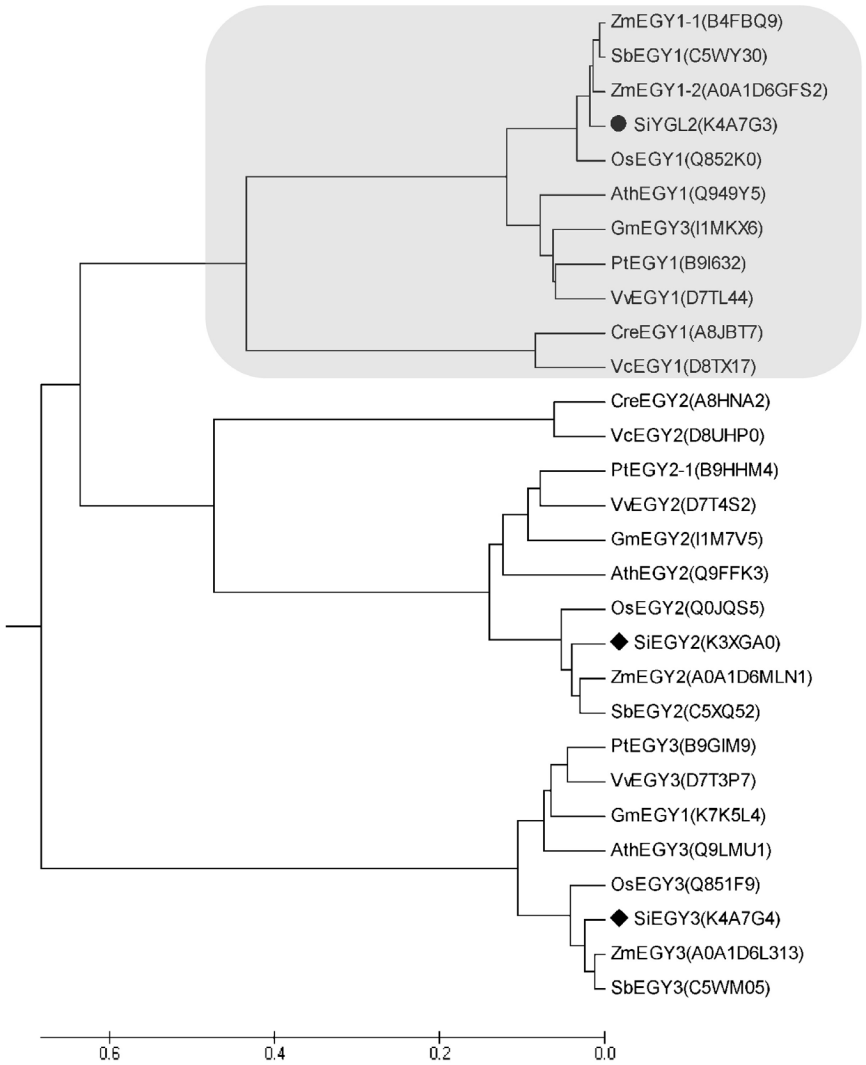

FIGURE 6 | Phylogenetic analysis of EGY proteins in diverse species. Ath, *A. thaliana*; Cre, *Chlamydomonas reinhardtii*; Gm, *Glycine max*; Os, *Oryza sativa*; Pt, *Populus trichocarpa*; Sb, *Sorghum bicolor*; Si, *S. italica*; Vv, *Vitis vinifera*; Zm, Zea mays. Protein IDs are listed in brackets and are archived in the UNIPROT database (http://www.uniprot.org/). SiEGY2, Seita.5G097600. SiEGY3, Seita.9G108100.

of PS II (LHC II) during leaf senescence (Kusaba et al., 2007; Sakuraba et al., 2012). In the young leaves of *siygl2*, the expression of these two genes was higher than in the young WT leaves. Furthermore, the transcript accumulation of these two genes in mutant old leaves also differed significantly from their expression in WT. These results indicate that chlorophyll metabolism and LHC II stability during the aging process may be affected in the mutant. Two other senescence-associated genes, RCCR and PAO, also reportedly participate in chlorophyll degradation (Sakuraba et al., 2016). These two genes were upregulated in old WT leaves. In *siygl2*, however, the expression of these two genes differed significantly from the WT in both the 1st and 10th leaves. This suggests that chlorophyll degradation in *siygl2* is affected.

In summary, we conclude that changes in SiYGL2 function affects the regulation of several senescence-associated genes, with chlorophyll degradation and leaf senescence also affected.

DISCUSSION

SiYGL2 Is Associated With the Regulation of Leaf Senescence, Chlorophyll Metabolism, and PS II Efficiency

Our study has shown that *SiYGL2* gene expression levels are higher in panicles and first leaves than in stems and old leaves (**Figure 8**). The flag leaf and panicle are the most important source and sink organs, respectively, and should retain high chlorophyll levels and photosynthetic capacities to avoid premature aging and ensure their continued output. The high expression of *SiYGL2* in these organs suggests that *SiYGL2* may play a role in maintaining the physiological state of the leaf and its photosynthetic capacity. Mutation of *SiYGL2* results in

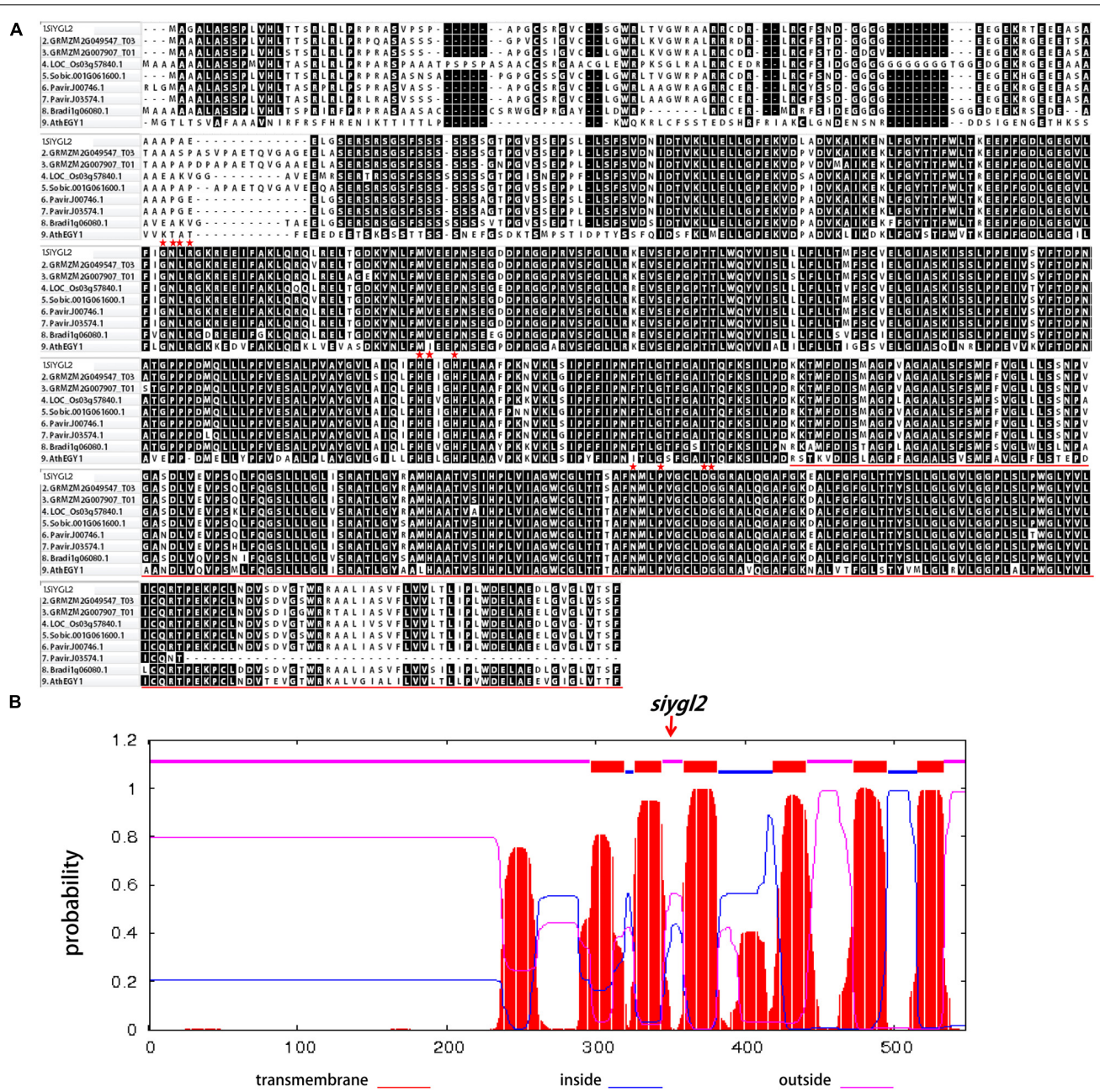

FIGURE 7 | (A) Amino acid sequence alignment of the homologous proteins. Red stars show the position of the conserved motifs GNLR, HEXXH, and NPDG, respectively. The red lines show lost amino acid sequence of ΔSiYGL2. **(B)** Hydropathy plot of SiYGL2 and ΔSiYGL2. Red boxes show the transmembrane helices. Blue lines and pink lines at the top of the figure indicate the inside and outside peptide chains, respectively. The arrow indicates the mutated position of *siygl2*.

premature chlorophyll degradation, chloroplast disintegration, and leaf senescence in the basal leaves (**Figures 3A**, **4**). Furthermore, aging of the leaves of the *siygl2* mutant can be induced more easily by dark than in the WT (**Figures 3B,C**). Taken together, these results suggest that SiYGL2 may be involved in delaying the onset of leaf senescence. This is consistent with the results reported for the SiYGL2 homolog AtEGY1 in *Arabidopsis* (Chen et al., 2016).

The chlorophyll content of *siygl2* was lower than in WT in both the top and basal leaves (**Figure 3A**), indicating that SiYGL2 may be related to chlorophyll metabolism. The chlorophyll degradation-associated genes SiNYC1, SiSGR1, and SiRCCR were expressed more highly in young leaves of *siygl2* than in Yugu1 (**Figure 10**), suggesting that chlorophyll degradation is mobilized early in young *siygl2* leaves. We also find that the effects on Chl *b* caused by *SiYGL2* mutant, natural senescence, and dark

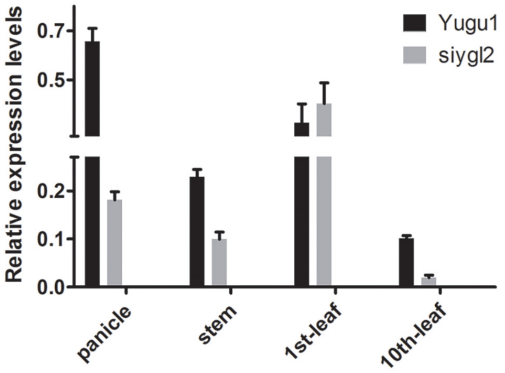

FIGURE 8 | Transcript accumulation of *SiYGL2* in panicle, stem, and leaves. Black boxes, Yugu1; gray boxes, *siygl2*. Means and standard deviations are obtained from three independent samples and three independent assays. Statistics treatment was made with Welch's two-sample *t* test. *Significantly different at $P = 0.05$.

treatment are stronger than that on Chl *a* (**Figures 2A**, **3A,B**). First, this may be explained by that the degradation of Chl *b* is prior to Chl *a*. And Chl *b* can converted into Chl *a* when undergoing degradation (Schelbert et al., 2009). Thus, at the preliminary stage of senescence, Chl *b* is sharply decreased while Chl *a* seems to be not impaired. With the aging process, Chl *a* is also degraded. Therefore, both the Chl *a* and Chl *b* contents are reduced in later period of senescence. Second, the reduction in Chl *b* content but not Chl *a* suggesting that the light harvesting is altered. The mutant may not grow well under low light condition, but would be fine under moderately high light. Shading and light deficiency may be one of the reasons the bottom leaf had earlier senescence. This hypothesis could be tested with a light response curve in further study.

In all leaves at different ages, both ΔΦPS II and ΔETR were lower in *siygl2* than in WT (**Figure 3D**), indicating that the PS II function was impaired in *siygl2*. Thus, we propose that SiYGL2 plays a role in the regulation of PS II function. In conclusion, in monocotyledonous *S. italica*, SiYGL2 is associated with the regulation of leaf senescence, chlorophyll metabolism, and PS II efficiency. As described in previous studies, AtEGY1 participates in chlorophyll accumulation, leaf senescence, and PS II function (Chen et al., 2005, 2016). This indicates that the function of SiYGL2 in monocotyledonous *S. italica* is quite similar to that its homolog AtEGY1 in dicotyledonous *Arabidopsis*.

The HEXXH Motif May Be Essential for the Function of SiYGL2 in Chloroplast Development

The *Arabidopsis* mutant *egy1-1* displayed a defective chloroplast development phenotype (Chen et al., 2005). However, the *S. italica EGY1* mutant *siygl2* has relatively normal chloroplasts (**Figure 4C**). Further analysis of the function of SiYGL2 in chloroplast development is therefore required. We compared the peptide chains of these two mutants and found that the mutant AtEGY1 protein lacks the HEXXH and NPDG motifs, while the mutant SiYGL2 protein lacks only the NPDG motif. Thus, we propose two hypotheses for the differences in chloroplast development between the *egy1-1* and *siygl2* mutants. First, it has been reported that for S2P family members in *Bacillus subtilis*, HEXXH and NPDG together form the catalytic center required for protease function (Rudner et al., 1999). Furthermore, two other MPs, AtVAR2 and AtVIR3, which have the HEXXH motif but lack the NPDG motif, could regulate chloroplast development (Chen et al., 1999; Qi et al., 2016). We, therefore, speculate that HEXXH is essential for chloroplast development-related function of EGY1 and alone can guarantee normal chloroplast development, but requires NPDG to regulate leaf senescence. Second, SiYGL2 and AtEGY1 share 77.3% amino acid sequence similarity, so the differences between remaining amino acids may lead to differences in function. Homologous

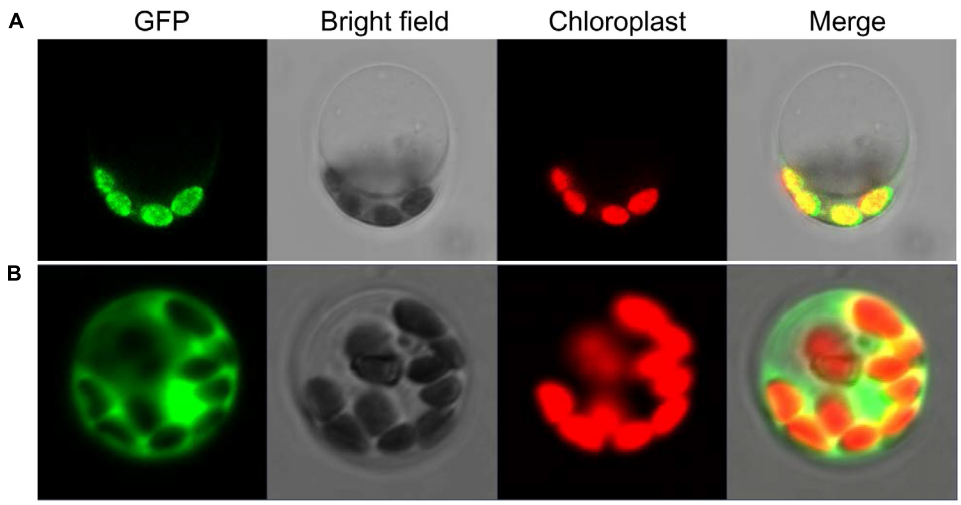

FIGURE 9 | Subcellular localization of SiYGL2. **(A)** SiYGL2:GFP signal. **(B)** Empty GFP vector as a control.

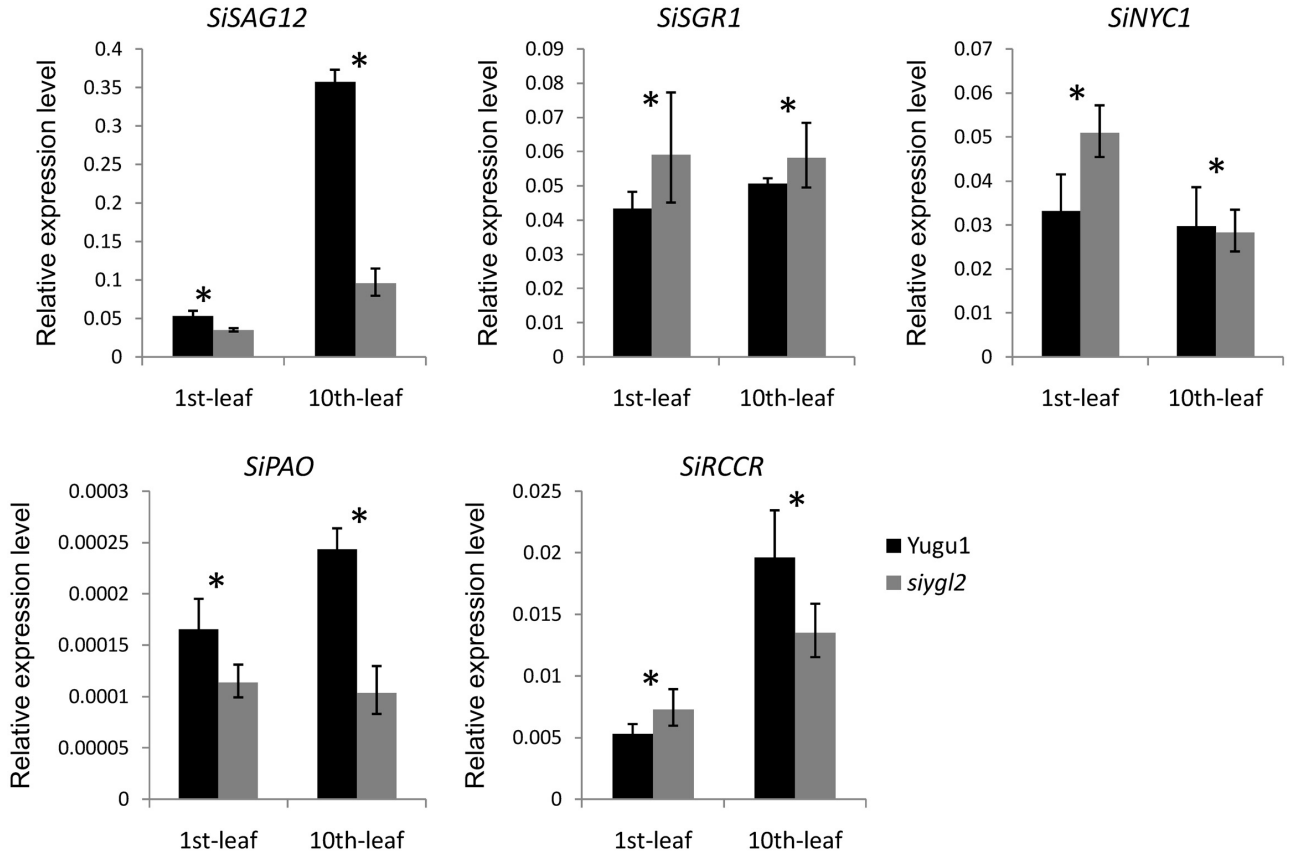

FIGURE 10 | Relative expression levels of chlorophyll degradation- and leaf senescence-associated genes.

proteins commonly show different functions in different species; EGY1 may potentially have changed its chloroplast development-related function in dicotyledonous C_3 *Arabidopsis* relative to the monocotyledonous C_4 plant *S. italica* during evolution. These two hypotheses could be verified in future by removing the HEXXH motif of SiYGL2 and observing the chloroplast structure of the resulting plants.

Chlorophyll Content and PS II Efficiency May Be Not the Limiting Factors of Photosynthesis Capacity

Chlorophylls functions as the antenna pigment in the photosynthesis and as such is an essential component to PS II function (Stirbet et al., 2014; Kato et al., 2016). However, while chlorophyll content, ΔΦPS II, and ΔETR were lower in *siygl2* than in WT (**Figures 10B,C**), net photosynthetic rate of *siygl2* remained the same as in the WT (**Figure 2B**). Similar results have been reported in the *S. italica ygl1* mutant and rice *ygl7* mutant, which are two mutants of D submit of Mg-chelatase encoding gene, that show decreased chlorophyll levels and defective chloroplasts and, yet display increased photosynthetic rates and photosynthetic reaction center activity (Deng et al., 2014; Li et al., 2016). A previous report has stated that plants contain an abundance of light-harvesting pigments and absorb more light than they can use (Ort et al., 2015). Following this, we speculate that in the *siygl2* mutant leaves, even though chlorophyll accumulation is reduced, photosynthesis can still be maintained at the same level as in the WT because sufficient light is still harvested by the chlorophyll present. The fact that a reduction in PS II efficiency does not impair the photosynthetic rate of the mutant may suggest that the *siygl2* mutant may have improvements in other photosynthesis-related components that compensate for the decrease in PS II efficiency. In addition, the induction of alternative electron transport (water–water cycle, etc.) may be also a reason leading to the alteration in ΔETR but not photosynthetic rate. These should be confirmed by further experiments.

Accelerated Leaf Senescence and Panicle Chlorosis May Be Associated With Yield Decreases in *siygl2* Mutants

Despite the conserved photosynthetic rate, the yield of *siygl2* was significantly reduced when compared with WT plants. We propose two explanations for this phenomenon. On the one hand, yield is closely related to leaf senescence, so accelerated leaf senescence could influence the mobilization of nutrients to reproductive organs and reduce the grain yield. Alternatively, the panicle has photosynthetic carbon assimilation capabilities

and plays an important role in grain formation. Glumes can ensure remobilization of nutrients to grains as a vital part of crop source–sink translocation. Compared with the flag leaf, glumes are more crucial in the later period of grain filling (Kong et al., 2015). In our study, the *siygl2* mutant panicle contained only 28% of the chlorophyll contained in the WT panicle at the heading stage (**Figure 2**). This suggests that the low chlorophyll content and impaired photosynthetic capability of the glume may be associated with the reduced yield in the *siygl2* mutant.

AUTHOR CONTRIBUTIONS

XD conceived the project. SZ, WL, JS, and CT carried out the experimental work. HZ provided the materials and did the field trials. SZ did the data analysis and wrote the manuscript. XD, GJ, and ST guided the experimental work. All authors read and approved the final manuscript.

FUNDING

This work was supported by Fundamental Research Funds of CAAS (CAAS-XTCX2016002), China Agricultural Research System (CARS06-13.5-A04), the National Natural Science Foundation of China (31501324 and 31522040), and the Agricultural Science and Technology Innovation Program of the Chinese Academy of Agricultural Sciences.

ACKNOWLEDGMENTS

We thank Emma Tacken, Ph.D., from Liwen Bianji, Edanz Group China (www.liwenbianji.cn/ac), for editing the English text of a draft of this manuscript.

SUPPLEMENTARY MATERIAL

The Supplementary Material for this article can be found online at: https://www.frontiersin.org/articles/10.3389/fpls.2018.01308/full#supplementary-material

FIGURE S1 | The plastoglobulis areas of the young leaves and old leaves in Yugu1 and *siygl2*. Means and standard deviations are obtained from 10 plastoglobulis. Statistics treatment was made with Welch's two-sample *t* test. **Significantly different at $P = 0.01$.

FIGURE S2 | Sequences at the mutation sites of Yugu1, *siygl2*, *gh120*, and F_1 individuals. The red boxes and arrow show the mutant sites.

TABLE S1 | CAPS markers for fine mapping.

TABLE S2 | Sequencing primers for the candidate region.

TABLE S3 | Primers used for qRT-PCR analysis.

REFERENCES

Bölter, B., Nada, A., Fulgosi, H., and Soll, J. (2006). A chloroplastic inner envelope membrane protease is essential for plant development. *FEBS Lett.* 580, 789–794. doi: 10.1016/j.febslet.2005.12.098

Che, P., Bussell, J. D., Zhou, W., Estavillo, G. M., Pogson, B. J., and Smith, S. M. (2010). Signaling from the endoplasmic reticulum activates brassinosteroid signaling and promotes acclimation to stress in Arabidopsis. *Sci. Signal.* 3:ra69. doi: 10.1126/scisignal.2001140

Chen, C. Y., Wang, J., and Zhao, X. (2016). Leaf senescence induced by EGY1 defection was partially restored by glucose in *Arabidopsis thaliana*. *Bot. Stud.* 57:5. doi: 10.1186/s40529-016-0120-3

Chen, G., Bi, Y. R., and Li, N. (2005). EGY1 encodes a membrane-associated and ATP-independent metalloprotease that is required for chloroplast development. *Plant J.* 41, 364–375. doi: 10.1111/j.1365-313X.2004.02308.x

Chen, M., Jensen, M., and Rodermal, S. (1999). The yellow variegated mutant of Arabidopsis is plastid autonomous and delayed in chloroplast biogenesis. *J. Heredity* 90, 207–214. doi: 10.1093/jhered/90.1.207

Deng, X. J., Zhang, H. Q., Wang, Y., He, F., Liu, J. L., and Xiao, X. (2014). Mapped clone and functional analysis of leaf-color gene Ygl7 in a rice hybrid (*Oryza sativa* L. ssp. indica). *PLoS One* 9:e99564. doi: 10.1371/journal.pone.00

Diaz-Mendoza, M., Velasco-Arroyo, B., Santamaria, M. E., Gonzalez-Melendi, P., Martinez, M., and Diaz, I. (2016). Plant senescence and proteolysis: two processes with one destiny. *Genet. Mol. Biol.* 39, 329–338. doi: 10.1590/1678-4685-GMB-2016-0015

Doust, A. N., Kellogg, E. A., Devos, K. M., and Bennetzen, J. L. (2009). Foxtail millet: a sequence-driven grass model system. *Plant Physiol.* 149, 137–141. doi: 10.1104/pp.108.129627

Egli, D. B. (2011). Time and the productivity of agronomic crops and cropping systems. *Agron. J.* 103, 743–750. doi: 10.2134/agronj2010.0508

Feng, L., Yan, H., Wu, Z., Yan, N., Wang, Z., and Jeffrey, P. D. (2007). Structure of a site-2 protease family intramembrane metalloprotease. *Science* 38, 1608–1612. doi: 10.1126/science.1150755

Golldack, D., Popova, O. V., and Dietz, K. J. (2002). Mutation of the matrix metalloproteinase At2-MMP inhibits growth and causes late flowering and early senescence in Arabidopsis. *J. Biol. Chem.* 277, 5541–5547. doi: 10.1074/jbc.M106197200

Gregersen, P. L., Culetic, A., Boschian, L., and Krupinska, K. (2013). Plant senescence and crop productivity. *Plant Mol. Biol.* 82, 603–622. doi: 10.1007/s11103-013-0013-8

Gregersen, P. L., Holm, P. B., and Krupinska, K. (2008). Leaf senescence and nutrient remobilization in barley and wheat. *Plant Biol* 10, 37–49. doi: 10.1111/j.1438-8677.2008.00114.x

Guo, D., Gao, X. R., Li, H., Zhang, T., Chen, G., Huang, P. B., et al. (2008). EGY1 plays a role in regulation of endodermal plastid size and number that are involved in ethylene-dependent gravitropism of light-grown Arabidopsis hypocotyls. *Plant Mol. Biol.* 66, 345–360. doi: 10.1007/s11103-007-9273-5

Gupta, R., Lee, S. J., Min, C. W., Kim, S. W., Park, K. H., and Bae, D. W. (2016). Coupling of gel-based 2-DE and 1-DE shotgun proteomics approaches to dig deep into the leaf senescence proteome of Glycine max. *J. Proteom.* 148, 65–74. doi: 10.1016/j.jprot.2016.07.025

Hu, H. Q., Wang, L. H., Wang, Q. Q., Jiao, L. Y., Hua, W. Q., and Zhou, Q. (2014). Photosynthesis, chlorophyll fluorescence, and chlorophyll content of soybean seedlings unde combined stress of bisphenol a and cadmium. *Environ. Toxicol. Chem.* 33, 2455–2462. doi: 10.1002/etc.2720

Jia, G. Q., Huang, X. H., Zhi, H., Zhao, Y., Zhao, Q., and Li, W. J. (2013). A haplotype map of genomic variations and genome-wide association studies of agronomic traits in foxtail millet (*Setaria italica*). *Nat. Genet.* 45, 957–U167. doi: 10.1038/ng.2673

Jia, X. P., Zhang, Z. H., Liu, Y. H., Zhang, C. W., Shi, Y. S., and Song, Y. C. (2009). Development and genetic mapping of SSR markers in foxtail millet [*Setaria italica* (L.) P. Beauv.]. *Theor. Appl. Genet.* 118, 821–829. doi: 10.1007/s00122-008-0942-9

Kato, Y., Nagao, R., and Noguchi, T. (2016). Redox potential of the terminal quinone electron acceptor QB in photosystem II reveals the mechanism of electron transfer regulation. *Proc. Natl. Acad. Sci. U.S.A.* 113, 620–625. doi: 10.1073/pnas.1520211113

Kinch, L. N., Ginalski, K., and Grishin, N. V. (2006). Site-2 protease regulated intramembrane proteolysis: sequence homologs suggest an ancient signaling cascade. *Protein Sci.* 15, 84–93. doi: 10.1110/ps.051766506

Kong, L. G., Sun, M. Z., Xie, Y., Wang, F. H., and Zhao, Z. D. (2015). Photochemical and antioxidative responses of the glume and flag leaf to seasonal senescence in wheat. *Front. Plant Sci.* 6:358. doi: 10.3389/fpls.2015.00358

Koussis, K., Goulielmaki, E., Chaliri, A., Withers-Martinez, C., Siden-Kiamos, I., and Matuschewski, K. (2017). Targeted deletion of a plasmodium site-2 Protease impairs life cycle progression in the mammalian host. *PLoS One* 12:e0170260. doi: 10.1371/journal.pone.0170260

Kusaba, M., Ito, H., Morita, R., Iida, S., Sato, Y., and Fujimoto, M. (2007). Rice non-yellow coloring1 is involved in light-harvesting complex II and grana degradation during leaf senescence. *Plant Cell* 19, 1362–1375. doi: 10.1105/tpc.106.042911

Li, B., Li, Q., Xiong, L., Kronzucker, H. J., Kramer, U., and Shi, W. (2012). Arabidopsis plastid AMOS1/EGY1 integrates abscisic acid signaling to regulate global gene expression response to ammonium stress. *Plant Physiol.* 160, 2040–2051. doi: 10.1104/pp.112.206508

Li, W., Tang, S., Zhang, S., Shan, J. G., Tang, C. J., and Chen, Q. N. (2016). Gene mapping and functional analysis of the novel leaf color gene siygl1 in foxtail millet [*Setaria italica* (L.) P. Beauv]. *Physiol. Plant.* 157, 24–37. doi: 10.1111/ppl.12405

Lichtenthaler, H. K. (1987). Chlorophylls and carotenoids: pigments of photosynthetic biomembranes. *Methods Enzymol.* 148, 350–382. doi: 10.1016/0076-6879(87)48036-1

Lu, G., Casaretto, J. A., Ying, S., Mahmood, K., Liu, F., Bi, Y. M., et al. (2017). Overexpression of OsGATA12 regulates chlorophyll content, delays plant senescence and improves rice yield under high density planting. *Plant Mol. Biol.* 94, 215–227. doi: 10.1007/s11103-017-0604-x

Martins, P. K., Mafra, V., De Souza, W. R., Ribeiro, A. P., Vinecky, F., and Basso, M. F. (2016). Selection of reliable reference genes for RT-qPCR analysis during developmental stages and abiotic stress in Setaria viridis. *Sci. Rep.* 6:28348. doi: 10.1038/srep28348

Mukherjee, P., Sureka, K., Datta, P., Hossain, T., Barik, S., and Das, K. P. (2009). Novel role of Wag31 in protection of mycobacteria under oxidative stress. *Mol. Microbiol.* 73, 103–119. doi: 10.1111/j.1365-2958.2009.06750.x

Nishimura, K., Kato, Y., and Sakamoto, W. (2016). Chloroplast Proteases: updates on proteolysis within and across suborganellar compartments. *Plant Physiol.* 171, 2280–2293. doi: 10.1104/pp.16.00330

Ort, D. R., Merchant, S. S., Alric, J., Barkan, A., Blankenship, R. E., and Bock, R. (2015). Redesigning photosynthesis to sustainably meet global food and bioenergy demand. *Proc. Natl. Acad. Sci. U.S.A.* 112, 8529–8536. doi: 10.1073/pnas.1424031112

Qi, Y. F., Liu, X. Y., Liang, S., Wang, R., Li, Y. F., and Zhao, J. (2016). A putative chloroplast thylakoid metalloprotease VIRESCENT3 regulates chloroplast development in *Arabidopsis thaliana*. *J. Biol. Chem.* 291, 3319–3332. doi: 10.1074/jbc.M115.681601

Roberts, I. N., Caputo, C., Criado, M. V., and Funk, C. (2012). Senescence-associated proteases in plants. *Physiol. Plant.* 145, 130–139. doi: 10.1111/j.1399-3054.2012.01574.x

Rudner, D., Fawcett, P., and Losick, R. (1999). A family of membrane-embedded metalloproteases involved in regulated proteolysis of membrane-associated transcription factors. *Proc. Natl. Acad. Sci. U.S.A.* 96, 14765–14770. doi: 10.1073/pnas.96.26.14765

Saito, A., Hizukuri, Y., Matsuo, E., Chiba, S., Mori, H., and Nishimura, O. (2011). Post-liberation cleavage of signal peptides is catalyzed by the site-2 protease (S2P) in bacteria. *Proc. Natl. Acad. Sci. U.S.A.* 108, 13740–13745. doi: 10.1073/pnas.1108376108

Sakamoto, W., and Takami, T. (2014). Nucleases in higher plants and their possible involvement in DNA degradation during leaf senescence. *J. Exp. Bot.* 65, 3835–3843. doi: 10.1093/jxb/eru091

Sakuraba, Y., Han, S.-H., Lee, S.-H., Hörtensteiner, S., and Paek, N.-C. (2016). *Arabidopsis* NAC016 promotes chlorophyll breakdown by directly upregulating *STAYGREEN1* transcription. *Plant Cell Rep.* 35, 155–166. doi: 10.1007/s00299-015-1876-8

Sakuraba, Y., Schelbert, S., Park, S. Y., Han, S. H., Lee, B. D., and Andres, C. B. (2012). STAY-GREEN and chlorophyll catabolic enzymes interact at light-harvesting complex II for chlorophyll detoxification during leaf senescence in Arabidopsis. *Plant Cell* 21, 767–785. doi: 10.1105/tpc.111.089474

Schelbert, S., Aubry, S., Burla, B., Agne, B., Kessler, F., and Krupinska, N.-C. (2009). Pheophytin pheophorbide hydrolase (Pheophytinase) is involved in chlorophyll breakdown during leaf senescence in Arabidopsis. *Plant Cell* 24, 507–518. doi: 10.1105/tpc.108.064089

Stirbet, A., Riznienko, G. Y., Rubin, A. B., and Goindjee, P. (2014). Modeling chlorophyll a fluorescence transient: relation to photosynthesis. *Biochem. Moscow* 79, 291–323. doi: 10.1134/S0006297914040014

van der Hoorn, R. A. (2008). Plant proteases: from phenotypes to molecular mechanisms. *Annu. Rev. Plant Biol.* 59, 191–223. doi: 10.1146/annurev.arplant.59.032607.092835

Waditee-Sirisattha, R., Shibato, J., Rakwal, R., Sirisattha, S., Hattori, A., and Nakano, T. (2011). The Arabidopsis aminopeptidase LAP2 regulates plant growth, leaf longevity and stress response. *New Phytol.* 191, 958–969. doi: 10.1111/j.1469-8137.2011.03758.x

Weaver, L. M., Gan, S. S., Quirino, B., and Amasino, R. M. (1998). A comparison of the expression patterns of several senescence-associated genes in response to stress and hormone treatment. *Plant Mol. Biol.* 37, 455–469. doi: 10.1023/A:1005934428906

Wu, X. Y., Hu, W. J., Luo, H., Xia, Y., Zhao, Y., and Wang, L. D. (2016). Transcriptome profiling of developmental leaf senescence in sorghum (Sorghum bicolor). *Plant Mol. Biol* 92, 555–580. doi: 10.1007/s11103-016-0532-1

Yang, Z., and Ohlrogge, J. B. (2009). Turnover of fatty acids during natural senescence of Arabidopsis, Brachypodium, and switchgrass and in Arabidopsis beta-oxidation mutants. *Plant Physiol.* 150, 1981–1989. doi: 10.1104/pp.109.140491

Yoshioka-Nishimura, M., Nanba, D., Takaki, T., Ohba, C., Tsumura, N., and Morita, N. (2014). Quality control of photosystem II: direct imaging of the changes in the thylakoid structure and distribution of FtsH proteases in spinach chloroplasts under light stress. *Plant Cell Physiol.* 55, 1255–1265. doi: 10.1093/pcp/pcu079

Yu, F. W., Zhu, X. F., Li, G. J., Kronzucker, H. J., and Shi, W. M. (2016). The chloroplast protease AMOS1/EGY1 affects phosphate homeostasis under phosphate stress. *Plant Physiol.* 172, 1200–1208. doi: 10.1104/pp.16.00786

Yu, Y. T., and Kroos, L. (2000). Evidence that SpoIVFB is a novel type of membrane metalloprotease governing intercompartmental communication during Bacillus subtilis sporulation. *J. Bacteriol.* 182, 3305–3309. doi: 10.1128/JB.182.11.3305-3309.2000

Zhang, S., Tang, C. J., Zhao, Q., Li, J., Yang, L. F., and Qie, L. F. (2014). Development of highly polymorphic simple sequence repeat markers using genome-wide microsatellite variant analysis in foxtail millet [*Setaria italica* (L.) P. Beauv.]. *BMC Genomics* 15:78. doi: 10.1186/1471-2164-15-78

Conflict of Interest Statement: The authors declare that the research was conducted in the absence of any commercial or financial relationships that could be construed as a potential conflict of interest.

The reviewer RZ and handling editor declared their shared affiliation at the time of the review.

frontiers in Plant Science

ORIGINAL RESEARCH
published: 12 September 2018
doi: 10.3389/fpls.2018.01309

A Dynamic Co-expression Map of Early Inflorescence Development in *Setaria viridis* Provides a Resource for Gene Discovery and Comparative Genomics

*Chuanmei Zhu†, Jiani Yang†, Mathew S. Box, Elizabeth A. Kellogg and Andrea L. Eveland**

Donald Danforth Plant Science Center, St. Louis, MO, United States

The morphological and functional diversity of plant form is governed by dynamic gene regulatory networks. In cereal crops, grain and/or pollen-bearing inflorescences exhibit vast architectural diversity and developmental complexity, yet the underlying genetic framework is only partly known. *Setaria viridis* is a small, rapidly growing grass species in the subfamily Panicoideae, a group that includes economically important cereal crops such as maize and sorghum. The *S. viridis* inflorescence displays complex branching patterns, but its early development is similar to that of other panicoid grasses, and thus is an ideal model for studying inflorescence architecture. Here we report a detailed transcriptional resource that captures dynamic transitions across six sequential stages of *S. viridis* inflorescence development, from reproductive onset to floral organ differentiation. Co-expression analyses identified stage-specific signatures of development, which include homologs of previously known developmental genes from maize and rice, suites of transcription factors and gene family members, and genes of unknown function. This spatiotemporal co-expression map and associated analyses provide a foundation for gene discovery in *S. viridis* inflorescence development, and a comparative model for exploring related architectural features in agronomically important cereals.

Keywords: inflorescence development, *Setaria*, panicoid grasses, transcriptome profiling, meristem, spikelet

OPEN ACCESS

Edited by:
Prem Bhalla,
The University of Melbourne, Australia

Reviewed by:
Michael J. Scanlon,
Cornell University, United States
Andrea Gallavotti,
Rutgers University, The State University of New Jersey, United States

***Correspondence:**
Andrea L. Eveland
aeveland@danforthcenter.org

† These authors have contributed equally to this work

Specialty section:
This article was submitted to Plant Breeding, a section of the journal Frontiers in Plant Science

Received: *01 May 2018*
Accepted: *20 August 2018*
Published: *12 September 2018*

Citation:
Zhu C, Yang J, Box MS, Kellogg EA and Eveland AL (2018) A Dynamic Co-expression Map of Early Inflorescence Development in Setaria viridis Provides a Resource for Gene Discovery and Comparative Genomics. Front. Plant Sci. 9:1309. doi: 10.3389/fpls.2018.01309

INTRODUCTION

Extensive morphological diversity is exhibited by inflorescences across grass species, family Poaceae. Since the inflorescences bear grain, understanding the genetic and molecular bases for this variation can accelerate the generation of higher yielding crops through breeding or precision engineering. Grasses encompass the world's important cereal crops; e.g., maize, sorghum, and millets in the subfamily Panicoideae, wheat, oats, and barley in subfamily Pooideae, and rice in subfamily Oryzoideae (Soreng et al., 2017). Many genes that regulate aspects of inflorescence architecture in grasses have been discovered and characterized, largely in maize and rice (Zhang and Yuan, 2014; Bommert and Whipple, 2017). In many cases gene function is conserved across species (Whipple et al., 2010; Bommert and Whipple, 2017), whereas in others, it varies between species or clades (McSteen, 2006; Whipple, 2017; Bommert and Whipple, 2017). Relatively little is known about how these genes interact in the larger context of a developmental network to control inflorescence form and how these networks are rewired across species.

All inflorescence structures are ultimately derived from a group of pluripotent cells called the inflorescence meristem (IM). The IM is indeterminate and transitions from the shoot apical meristem (SAM) during the shift from vegetative to reproductive growth (Bartlett and Thompson, 2014; Kyozuka et al., 2014). In grasses, the terminal reproductive structure is the spikelet, which bears one or more flowers that produce the seeds. The different routes that the IM takes to form a determinate spikelet meristem (SM) largely determine the morphology of the mature inflorescence (Kyozuka et al., 2014; Whipple, 2017). For example, the IM can produce SMs directly on its flanks, as in wheat, or it can produce few to many indeterminate branch meristems (BMs), which is typical for most grasses. Like the IM, BMs can produce SMs directly, as in finger millet, or can initiate higher order branches, as in rice. The IM and BM may ultimately convert to a terminal SM or simply cease development. Eventually, SMs initiate sterile bracts (glumes) and floral meristems (FMs), which produce lateral organs that differentiate into floral structures including lemma, palea, anthers, and ovary.

In species of the Andropogoneae tribe, which includes maize and sorghum, spikelets are borne in pairs where two SMs arise from a spikelet pair meristem (SPM). Paired spikelets also arose independently in some other closely related groups. In the "bristle clade" of grasses, which includes *Setaria* species and other members of the subtribe Cenchrinae (see Doust and Kellogg, 2002 and references therein), BMs can alternatively differentiate into sterile branches called bristles. While spikelets are not paired in these species, morphological analyses suggest that spikelets may be paired with bristles (Doust and Kellogg, 2002). Recent work in *Setaria viridis* showed that BMs poised to form bristles first initiate an SM identity program before the homeotic shift to bristle formation. This developmental switch is dependent on proper spatiotemporal synthesis of growth-promoting brassinosteroids (BRs) during SM development (Yang et al., 2017).

Despite this variation in inflorescence morphology among grasses, the core underlying developmental processes are shared, and often leverage common regulatory modules. Pathways that regulate IM size (Somssich et al., 2016), SM identity (Bommert and Whipple, 2017), and flower development (Hirano et al., 2014), for instance, are largely conserved across those grass species studied. However, these processes can vary by the spatiotemporal expression of certain factors, functional divergence of gene family members, and/or co-option of novel factors all together. For example, the RAMOSA1 (RA1) transcription factor (TF) is expressed at the base of SPMs in Andropogoneae species and acts to suppress branching by conferring determinacy on the SPM. The timing and degree of RA1 expression dictates inflorescence branching patterns; i.e., during maize tassel development *ra1* is induced early and suppresses higher order branching whereas in sorghum and *Miscanthus*, delayed *ra1* expression leads to highly branched inflorescences (Vollbrecht et al., 2005). By leveraging comparative transcriptome analyses across grasses, we can gain invaluable insight into the core components that regulate these processes, and what variations are associated with species-specific morphologies.

Transcriptome studies of early inflorescence development have been reported for a few important cereal crops, including maize (Eveland et al., 2014), rice (Furutani et al., 2006; Harrop et al., 2016), barley (Digel et al., 2015), and wheat (Feng et al., 2017), leading to systematic discovery of underlying regulatory modules. To our knowledge, maize is the only panicoid grass with existing transcriptome data across early inflorescence development (Eveland et al., 2014). Given the variation in architectures among important cereals in the Panicoideae, comparative expression maps from additional species will help determine conserved and species-specific components. Here, we present a comprehensive developmental and transcriptomics analysis of inflorescence development in *S. viridis,* a model panicoid grass with a rapid life cycle, sequenced genome, and emerging genetics and genomics toolkit (Doust et al., 2009; Brutnell et al., 2010; Bennetzen et al., 2012; Huang et al., 2016; Zhu et al., 2017). We profiled six sequential stages of inflorescence development that captured key events from the reproductive transition to floral organ differentiation and identified stage-specific co-expression signatures. Our detailed characterization of *S. viridis* inflorescence development at both morphological and molecular levels provides an invaluable resource for the community as a foundation for gene discovery and a comparative platform for studying diverse architectures in agronomically important cereal crops.

MATERIALS AND METHODS

Plant Growth Conditions

The reference *S. viridis* genotype A10.1 was used for this study. A10.1 seeds from 2-year-old stocks were used to ensure full loss of dormancy and promote synchronized germination. Seeds were planted in MetroMix 360 soil (Sun Gro Horticulture company) and grown in a controlled growth chamber with the following conditions: temperature of 31°C/23°C (day/night), light intensity of 200 μmol/sq.meter/s for 12 h (6am–6pm) and 50% relative humidity, at the Donald Danforth Plant Science Center's Integrated Plant Growth Facility. Plants were fertilized with Jack's 15-16-17 (Hummert International) twice a week.

Scanning Electron Microscopy

In our controlled conditions, the transition from a vegetative to IM occurred after 8 days after sowing (DAS) and before 10 DAS. Accordingly, vegetative SAMs were hand-dissected from plants at 8 DAS, and IMs from plants at 10, 11, 12, 13, 14, 15, 16, and 18 DAS. Samples were fixed immediately in FAA solution (3.75% formaldehyde, 50% ethanol, and 5% glacial acetic acid) and left overnight. They were then dehydrated using 50% ethanol for a minimum of 1 h and then shifted to 70% ethanol. For critical point drying, samples were dehydrated in an ethanol series (80, 95, 100, 100% ethanol) for at least 1 h for each step; they were then left in 100% ethanol overnight and then moved to fresh 100% ethanol from a newly opened bottle the next day.

Samples were then critical point dried using a Tousimis Samdri-780a, mounted on stubs and sputter coated using a Tousimis Samsputter-2a. Images were taken with a Hitachi S2600 SEM at 20 kV at Washington University's Central Institute for the Deaf.

RNA Extraction, RNA-seq Library Construction, Sequencing, and Analysis

Inflorescences were hand-dissected into fresh 100% acetone on dry ice from *S. viridis* seedlings at 10, 12, 14, 15, 16, and 18 DAS. Depending on the representative size at a given stage, 10–30 individual inflorescence primordia were pooled per biological replicate; three to four biological replicates were collected for each stage. All sampling was performed within a 2-h window in the morning to control for circadian effects. Acetone was removed and samples were flash-frozen in liquid nitrogen and ground into a fine powder using 3 mm tungsten-carbide beads (Qiagen) in a Tissue Lyser-II. Total RNA was isolated using the PicoPure RNA Isolation Kit (Thermo Fisher Scientific) with in-column DNase I treatment following manufacturer's protocols. RNA-seq libraries were generated from 1 μg total RNA using the NEBNext Ultra Directional RNA Library Prep Kit for Illumina (New England BioLabs Inc.) and size-selected for 200 bp inserts. Libraries were quantified on a Bioanalyzer (Agilent 2100) using a DNA 1000 chip to confirm the insert size and quantified again on a Qubit 3.0 Fluorometer (Life Technologies) to ensure different libraries were equally loaded, and then sequenced using standard Illumina protocols (Illumina, Inc.) for either paired-end (PE) or single-end (SE) sequencing at 100 bp on the Illumina HiSeq 2500 platform at the University of Illinois at Urbana-Champaign W.M. Keck Center.

Sequenced reads were quality-checked using fastQC with Phred scores all above 30. For read mapping and transcript quantification, we used *Salmon* (v0.8.1) (Patro et al., 2017) in a quasi-mapping mode for indexing reference transcripts from the *S. viridis* primary transcript file (Sviridis_311_v1; Phytozome[1] v12.1) (**Supplementary Table S1**). Transcripts were quantified using the option numBootstraps 30. Parameters not specified were run as default. *Salmon* outputs were imported into R with the Bioconductor package *tximport* (v1.0.3). Raw counts and transcripts per million (TPM) were extracted for 35,214 *S. viridis* primary transcripts (**Supplementary Table S2**). All subsequent analyses were conducted using TPM (Soneson et al., 2015).

Gene Co-expression Analyses

To reduce noise from genes with ubiquitously low expression or that do not change expression during development, we applied a set of criteria to filter genes that: (1) showed more than twofold change in expression between at least two of the stages, and (2) collectively had an expression value of at least 1 TPM across all stages. This resulted in 11,425 dynamically expressed genes during inflorescence development (**Supplementary Table S3**). To determine the optimal number of clusters to use for fuzzy c-means (FCM) cluster analysis, we used two functions in the R Bioconductor package, *Mfuzz* (Kumar and Futschik, 2007): (1) Dmin, which calculates the minimum centroid distance for a range of cluster numbers and (2) cselection, which reports the cluster number where empty clusters are detected in the repeated soft clustering. Cluster number was chosen for FCM analysis based on the centroids of each cluster being well separated based on Dmin and there were no empty clusters based on cselection. FCM was performed using *Mfuzz*. The 11,425 genes were clustered into groups based on their standardized mean expression profiles (for each transcript, average expression is 0 and the standard deviation across 6 stages is 1). Each gene was assigned to the cluster with its highest membership score. Heatmaps and hierarchical clustering using Euclidean distances and complete linkage clusters were generated using MeV[2] (version 4.8) (Saeed et al., 2003).

Gene Annotation and Homology Searches

The *S. viridis* genome (v1.1) and annotation files were downloaded from Phytozome v12.1. Functional annotations were assigned to *S. viridis* genes based on these files and information extracted from EnsemblPlants Biomart[3]. To determine homologs of *S. viridis* genes in other grass species [maize (v3 and v4 genomes), sorghum (v3.1.1), *Brachypodium* (v3.1), and *Setaria italica* (v2.2)], blastp[4] was used with two as the maximum target sequence for each gene. All genome sequence data were downloaded from Phytozome v12.1, except for maize v4, which was downloaded from MaizeGDB[5].

Phylogenetic Analysis of MADS-Box Family TFs

An HMM (Hidden Markov Model[6], HMMER 3.1b2) was used to classify genes encoding MADS-Box proteins in the proteome database of *S. viridis* (v1.1) and coding sequences of the primary transcripts were retrieved from Phytozome[1]. Previously identified MIKC type MADS-box genes from Arabidopsis, rice and maize genomes (Parenicová et al., 2003; Arora et al., 2007; Zhao et al., 2011) were included in building the phylogenetic tree. All protein coding sequences were manually checked for the presence of a MADS domain and were aligned using MUSCLE (Edgar, 2004) to construct a maximum likelihood tree by RAxML (Edgar, 2004; Stamatakis, 2014), with 1,000 bootstrap replicates. The final trees were drawn with the R Bioconductor package, *phytools* (Revell, 2011).

Weighted Gene Co-expression Network Analysis

The R Bioconductor package *wgcna* was used to perform weighted gene co-expression network analysis (WGCNA) on the same set of 11,425 genes used in FCM analysis (Langfelder and Horvath, 2008). A matrix of all genes with their TPM values across 23 samples (including individual biological replicates)

[1] phytozome.jgi.doe.gov

[2] http://mev.tm4.org/

[3] http://plants.ensembl.org

[4] https://blast.ncbi.nlm.nih.gov/

[5] https://www.maizegdb.org/assembly

[6] hmmer.org

was used as input. An adjacency matrix was generated to determine similarity between genes (i.e., correlation for every gene pair across the 23 samples) and transformed through a soft-thresholding procedure using the function "pickSoftThreshold," where a soft power of 18 was chosen for module detection. A topological overlap measure (TOM) was then calculated from the adjacency matrix to estimate network interconnectedness. The dissimilarity of TOM (1-TOM) was used as the input for average linkage hierarchical clustering to identify co-expression modules. Module eigengenes (MEs), the first principal component of a given module, was used as a representative gene expression profile for that module. Modules were further merged based on their MEs (using cutHeight = 0.25) and the module membership (MM) for each gene indicated the degree of similarity between its expression profile and each ME. The entire network including WGCNA-calculated weights for each edge between genes (nodes) is available on NCBI GEO. Gene-to-gene connections were filtered if the weight of interaction was <0.02. Sub-networks were visualized using Cytoscape[7] v3.4.10.

RESULTS AND DISCUSSION

Morphological Characterization of Inflorescence Development in *S. viridis*

To characterize the developmental progression of the *S. viridis* inflorescence, we used scanning electron microscopy (SEM) to examine sequential stages from floral transition to floral organ development. At 8 DAS, the SAM had not yet transitioned, but had emerged from surrounding leaf primordia (**Figure 1A**). By 10 DAS, the SAM had transitioned to the IM and BMs were initiated but barely visible (**Figure 1B**). By 11 DAS, primary BMs had initiated at the base of the developing inflorescence and continued to form in a helical pattern at 12 DAS (**Figures 1C,D**). From 12 to 14 DAS, secondary and tertiary BMs developed sequentially in a distichous pattern (**Figures 1D–F**). By 15 DAS, the IM had ceased to produce new BMs and those at the inflorescence tip were the first to differentiate into SMs or bristles (**Figures 1G,J**). At 16 DAS, differentiation of SMs and bristles continued basipetally and the two developing structures became morphologically distinguishable. SMs then initiated glumes and FMs, while bristles started to elongate and form an indented ring below the meristem tip (**Figures 1H,K**), which often later detached (Doust and Kellogg, 2002; Yang et al., 2017). By 18 DAS, floral organs such as lemma, palea, and anther primordia formed in the spikelets, and bristles further elongated and produced prickle hairs (Doust and Kellogg, 2002; **Figures 1I,L**).

Transcriptome Profiling and Stage-Specific Expression of TF Families

To establish a dynamic transcriptome map of *S. viridis* inflorescence development, we used RNA-seq to link global changes in gene expression with developmental transitions. Based on our detailed morphological characterization, we selected six stages that captured key events in inflorescence development for transcriptome profiling by RNA-seq: the initiation of the IM (10 DAS), primary and secondary (12 DAS), and higher order (14 DAS) branching events, transition to SMs (15 DAS), differentiation of spikelets and bristles (16 DAS), and development of floral organs (18 DAS) (**Figure 1**). For each of these six stages, inflorescence primordia were hand-dissected and RNA-seq libraries prepared for three to four biological replicates as described in the Section "Materials and Methods" (**Supplementary Table S1**). Transcript abundance was quantified in TPM at each of the six stages; these analyses showed strong correlations among biological replicates and dynamic patterns of gene expression across developmental stages (**Supplementary Figures S1**, **S2** and **Supplementary Table S2**). Based on our filtering criteria described in the section "Materials and Methods," all analyses in this manuscript were performed using a subset of 11,425 dynamically expressed genes (**Supplementary Table S3**).

We explored developmental dynamics of TF families across the six stages. Spatiotemporal expression and combinatorial action of TF family members fine-tune developmental decisions, and knowledge of their individual expression profiles can provide insight into underlying regulatory mechanisms. We annotated several TF families in *S. viridis* based on annotations of functional TF domains from various sources. Specifically, we focused on families with multiple members previously implicated in plant development and plotted relative expression of family members across the six stages: MADS-box, TCP, SBP (**Figure 2**), AP2/ERF, bHLH, C2H2_Zinc, bZIP, LOB, and NAC families (**Supplementary Figure S3**; see abbreviations in **Box 1**). Individual TF family members showed dynamic expression profiles during early inflorescence development in *S. viridis* (**Figures 2**, **Supplementary Figures S3**, **S4** and **Supplementary Table S4**). These included orthologs of previously characterized developmental regulators from maize and rice, as well as many uncharacterized family members with potential functions in inflorescence development based on their co-expression patterns. For example, we identified a set of 21 candidate TFs that were highly expressed and showed large fold changes in expression that peaked at specific stages of inflorescence development (**Supplementary Figure S4** and **Supplementary Table S4**).

In addition, we performed a detailed phylogenetic analysis for the MIKC type MADS-box family based on these annotations to determine homology between the *S. viridis* genes and those in maize, rice and/or Arabidopsis (**Supplementary Figure S5**).

BOX 1 | Abbreviations and names of TF families annotated in this study.

	Transcription factor (TF) family
AP2/ERF	AP2/ethylene-responsive factor
bHLH	Basic helix-loop-helix
bZIP	Basic-leucine zipper protein
C2H2_Zinc	C2H2-zinc finger protein
LOB	Lateral organ boundary domain proteins
NAC	NAM, ATAF1/2, and CUC2 domain proteins
SBP	Squamosa promoter-binding protein
TCP	Teosinte branched 1/CYCLOIDEA/PROLIFERATING CELL FACTOR1

[7]http://www.cytoscape.org

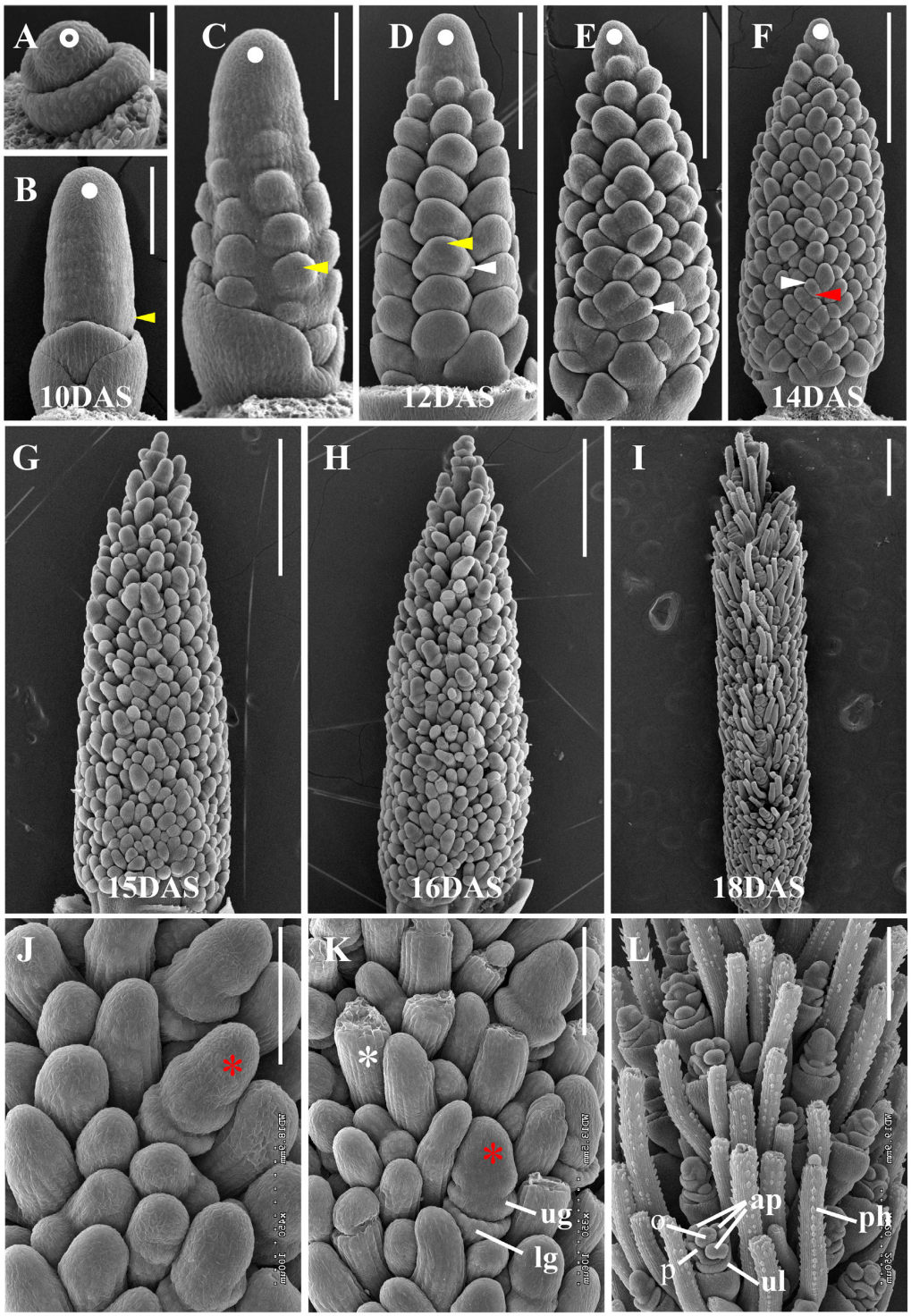

FIGURE 1 | Key developmental stages of *Setaria viridis* inflorescence development by SEM. **(A)** At 8 DAS, the *S. viridis* SAM (*white open circle*) had not yet transitioned to reproductive development. **(B)** By 10 DAS, the SAM had transitioned to an indeterminate IM (*white dot*) and primary BMs (*yellow arrow*) were initiated. As development proceeds through **(C)** 11 DAS, **(D)** 12 DAS, **(E)** 13 DAS, and **(F)** 14 DAS stages, primary, secondary, and higher order branching was progressively initiated (white dot, IM; yellow arrow, primary BM; white arrow, secondary BM; red arrow, tertiary BM). **(G**, **J)** At 15 DAS, SMs (*red asterisk*) had begun to differentiate and by 16 DAS **(H**, **K)**, were distinguishable from developing bristles (*white asterisk*) and initiated glume primordia (lg, lower glume; ug, upper glume). **(I**, **L)** At 18 DAS, bristles were elongated and developed prickle hairs (ph) and SMs further differentiated floral organs (ul, upper lemma; p, palea; ap, anther primordium; o, ovary). Developmental stages that were used for RNAseq-based transcript profiling are labeled. Scale bars = 50 μm in **(A)**, 100 μm in **(B**, **C**, **J**, and **K)**, 250 μm in **(D**–**F** and **L)**, and 500 μm in **(G**–**I)**.

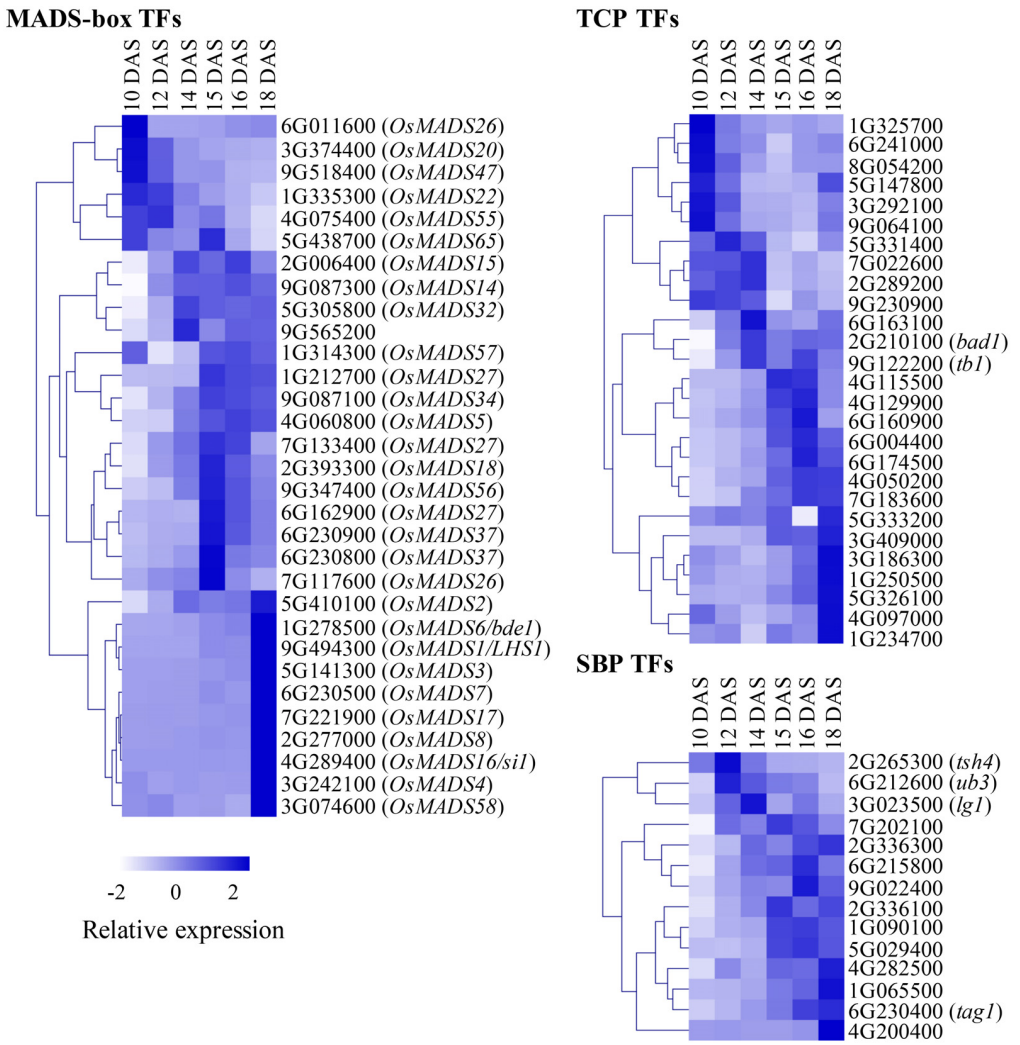

FIGURE 2 | Transcription factor (TF) family members show dynamic expression profiles across inflorescence development. Individual members of MADS-box, TCP and SBP TF families were annotated, TPM values for each were normalized based on a Z-scale and plotted as a heatmap across the six stages of *Setaria viridis* inflorescence development. For MADS-box genes, names of orthologous genes from rice are included. For TCP and SBP families, orthologs of classical maize genes are indicated. *White-to-dark* shading represents low-to-high relative expression level.

This phylogenetic framework enables comparative analyses among MADS-box family members that have been shown in multiple systems to work in a combinatorial manner to regulate development (Theißen et al., 2016; Bartlett, 2017).

Modules of Co-expressed Genes During *S. viridis* Inflorescence Development

To define signatures of gene expression across this developmental trajectory, we used an FCM clustering approach (Kumar and Futschik, 2007) and our filtered set of 11,425 dynamically expressed genes. Based on simulations and selection criteria as described in the Section "Materials and Methods," we determined 25 as an optimal number of clusters to use for the FCM analyses (**Supplementary Figure S6A**). FCM was used to assign a membership score for each gene to each cluster, and based on the highest score for each gene, 25 clusters with unique expression profiles were defined ranging from 290 to 608 genes per cluster (**Supplementary Figure S6B** and **Supplementary Table S3**).

The mean relative expression value across the six developmental stages was determined for each of the 25 clusters and hierarchical clustering on these values revealed four groups (**Figure 3A**), each representing a distinct developmental expression pattern: (1) floral transition and IM identity, (2) BM initiation and determinacy, (3) SM differentiation and FM initiation, and (4) floral organ development. We first located orthologs of known developmental genes; expression profiles of representative genes within each group were comparable to those of their orthologs in maize and rice, consistent with their predicted roles in development (**Figure 3B** and **Supplementary Table S3**). In the following four subsections, we describe expression of these and other key developmental regulators

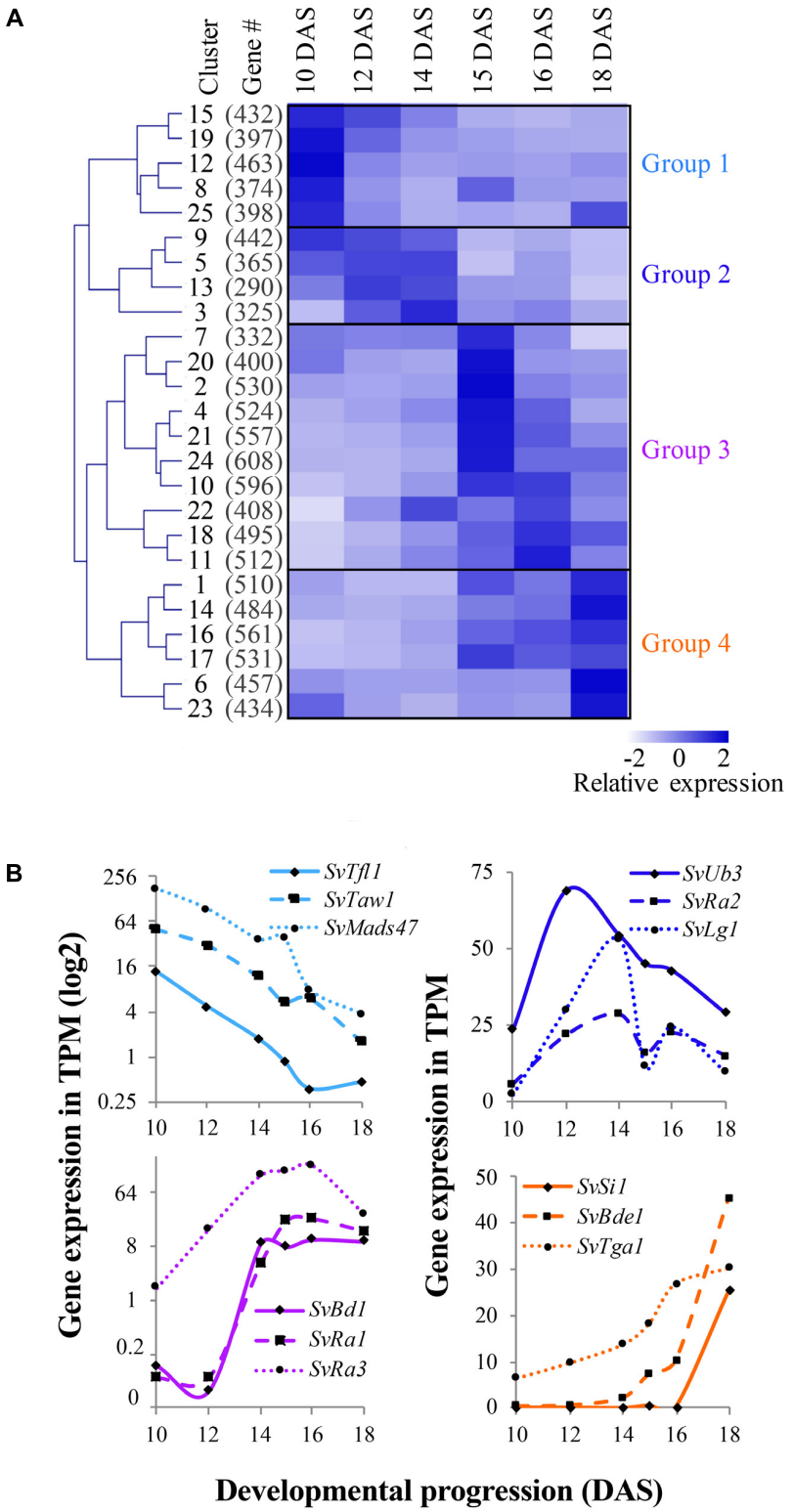

FIGURE 3 | Co-expression analysis revealed distinct gene expression signatures during *Setaria viridis* inflorescence development. **(A)** FCM clustering of 11,425 dynamically expressed genes identified 25 co-expression clusters. The mean relative expression value of genes in each cluster across development was used for hierarchical clustering and is displayed by the heatmap. Overall clusters organized into four general groups of expression associated with key developmental transitions. *White-to-dark* shading represents low-to-high relative expression level. **(B)** Within each of the four expression groups, homologs of known developmental genes from other species showed expected expression patterns.

during *S. viridis* inflorescence development compared to other grasses and highlight some key findings from each of the major expression groups. For simplicity, we listed full names and abbreviations of genes discussed in **Table 1**.

Group 1: Floral Transition and IM Identity

Genes in Group 1 (including clusters 8, 12, 15, 19, and 25) showed highest expression at 10 DAS as the IM was initiated and decreased at later stages of development (**Figure 3A**, **Supplementary Figure S6** and **Supplementary Table S3**). We inferred that genes involved in regulating the transition to reproductive growth, IM identity, and/or primary branch initiation would be included in these clusters. For example, *SvTfl1* (Sevir.8G033800), an ortholog of *TERMINAL FLOWER1,* a general repressor of flowering in many species including maize, rice, and Arabidopsis (Nakagawa et al., 2002; Danilevskaya et al., 2010; Hanano and Goto, 2011), was grouped in cluster 19 (**Figure 3B**). Three other *TFL1*-like homologs clustered in Group 1; Sevir.7G334800, a closely related paralog of *SvTfl1*, Sevir.7G097700 and Sevir.1G183200. The latter gene, which we named *SvTfl1-like,* was expressed markedly higher than the other two at 10–12 DAS in cluster 15 (**Supplementary Table S3**). Co-expressed in cluster 15 was *SvLg2* (Sevir.5G394700), the ortholog of *liguleless 2* (*lg2*) from maize, which encodes a bZIP TF responsible for early establishment of lateral organ boundary positioning (Harper and Freeling, 1996; Walsh et al., 1998).

TABLE 1 | *Setaria viridis* genes, short name descriptions and homologs in maize, rice, and Arabidopsis.

S. viridis		Maize	Rice	Arabidopsis
Sevir.8G033800	*SvTfl1*	*Zea centroradialis*	*RICE CENTRORADIALIS*	*TERMINAL FLOWER 1*
Sevir.5G394700	*SvLg2*	*Liguleless 2*		
Sevir.9G221800	*SvTaw1*		*TAWAWA 1*	
Sevir.4G229000	*SvMoc1*		*MONOCULM 1*	
Sevir.3G028500	*SvWus*		*TILLERS ABSENT 1*	*WUSCHEL*
Sevir.7G234000	*SvLfy*	*Zea floricaula*	*ABERRANT PANICLE ORGANIZATION 2*	*LEAFY*
Sevir.6G212600	*SvUb3*	*Unbranched 3*	*WEALTHY FARMER'S PANICLE*	
Sevir.2G265300	*SvTsh4*	*Tassel shealth 4*		
Sevir.3G136200	*SvTsh1*	*Tassel sheath 1*	*NECK LEAF 1*	*HANABA TARANU*
Sevir.3G023500	*SvLg1*	*Liguleless 1*		
Sevir.5G116100	*SvRa2*	*Ramosa 2*		
Sevir.4G025200	*SvBaf1*	*Barren stalk fastigiate 1*	*DEPRESSED PALEA 1*	*AT-HOOK NUCLEAR LOCALIZED 22*
Sevir.5G116300	*SvVt2*	*Vanishing tassel 2*		
Sevir.3G410700	*SvBif2*	*Barren inflorescence 2*		
Sevir.2G302300	*SvDfl1*	*Delayed flower 1*		
Sevir.9G259300	*SvPla1*			*PLASTOCHRON 1*
Sevir.5G251100	*SvSpi1*	*Sparse inflorescence 1*		
Sevir.5G374100	*SvBa1*	*Barren stalk 1*	*LAX PANICLE 1*	
Sevir.2G437800	*SvBd1*	*Branched silkless 1*	*FRIZZY PANICLE*	
Sevir.2G209800	*SvRa1*	*Ramosa 1*		
Sevir.2G407500	*SvRa3*	*Ramosa 3*		
Sevir.4G119100	*SvFea4*	*Fasciated ear 4*		*PERIANTHIA*
Sevir.4G294000	*SvTd1*	*Thick tassel dwarf 1*		*CLAVATA 1*
Sevir.8G183800	*SvFon2*		*FLORAL ORGAN NUMBER 2*	*CLAVATA 3*
Sevir.9G107600	*SvKn1*	*Knotted 1*		*BREVIPEDICELLUS*
Sevir.2G029800	*SvRs1*	*Rough sheath 1*		
Sevir.2G237500	*SvBrm*			*BRAHMA*
Sevir.4G112300	*SvSyd*			*SPLAYED*
Sevir.4G124400	*SvCuc2*			*CUP-SHAPED COTYLEDON 2/3*
Sevir.6G213600	*SvCuc3*			
Sevir.2G210100	*SvBad1*	*Branch angle defective 1/wavy auricle in blade 1*	*RETARDED PALEA 1*	
Sevir.9G122200	*SvTb1*	*Teosinte branched 1*		
Sevir.4G289400	*SvSi1*	*Silky 1*	*SUPERWOMAN1*	
Sevir.1G278500	*SvBde1*	*Bearded ear 1*		
Sevir.9G494300	*SvLhs1*		*LEAFY HULL STERILE1*	
Sevir.6G230400	*SvTga1*	*Teosinte glume architecture 1*		
Sevir.5G086100	*SvSl1*		*STAMENLESS 1*	
Sevir.1G255900	*SvTob1*	*Yabby 15*	*TONGARI-BOUSHI 1*	
Sevir.9G265300	*SvAn1*	*Anther ear 1*		
Sevir.9G439800	*SvTs2*	*Tassel seed 2*		

Loss-of-function *lg2* mutants in maize produce few to no tassel branches. Consistent with its expression profile in *S. viridis* (**Supplementary Figure S4**), *lg2* in maize has been implicated in the transition from vegetative to reproductive growth (Walsh and Freeling, 1999).

In rice, *TAWAWA1* (*TAW1*) encodes a nuclear protein belonging to the *ALOG* (*ARABIDOPSIS LSH1 and ORYZA G1*) gene family that is highly expressed in the IM and BMs early in inflorescence development, and decreases during the phase change to SM identity (Yoshida et al., 2013). *TAW1* promotes indeterminate IM and BM activity by suppressing acquisition of SM identity, and thus is a major regulator of inflorescence architecture (Yoshida et al., 2013). The *S. viridis* ortholog, *SvTaw1* (Sevir.9G221800), was found in cluster 19 (**Figures 3A,B**), which shows a very similar expression profile to cluster 15, consistent with *TAW1* expression in rice. Five other *ALOG* genes were found in Group 1 and shared similar expression profiles (Table S3); Sevir.7G17600 and Sevir.1G244200, which we named *SvTaw1-like 1* and *SvTaw1-like 2,* respectively, shared highest homology with *SvTaw1* and were co-expressed in cluster 15 (**Figure 4**). Functional studies of other *ALOG* genes in various species indicate that they generally share a role in developmental phase changes and organ identity, and their spatiotemporal expression patterns determine their specificity (Yoshida et al., 2009; Cho and Zambryski, 2011; Takeda et al., 2011). Notably, three genes belonging to a subfamily of MADS-box TFs called *SHORT VEGETATIVE PHASE* (*SVP*), were also co-expressed in Group 1 (**Figures 3B**, **4** and **Supplementary Table S3**). In rice, homologs of these *SVP* genes (*OsMADS47*, *OsMADS55*, and *OsMADS22*) suppress FM initiation and were positively regulated by *TAW1* to promote indeterminacy (Yoshida et al., 2013; Kyozuka et al., 2014).

Group 2: BM Initiation and Determinacy

Genes in Group 2 (clusters 3, 5, 9, and 13) tended to show highest expression at 12 and 14 DAS, decreasing by 15 DAS and into later stages (**Figure 3A** and **Supplementary Figure S6**). This expression pattern coincides with the initiation, maintenance and patterning of BMs, which occurs mostly between 10 and 14 DAS, and is largely completed by 15 DAS. Among genes in this group were those with putative roles in axillary meristem initiation and maintenance. For example, *SvMoc1* (Sevir.4G229000), a GRAS family protein homologous to *MONOCULM 1* (*MOC1*) from rice, was found in cluster 3. This expression pattern is consistent with a possible role for *SvMoc1* in axillary meristem initiation, analogous to how it controls tiller outgrowth in rice (Li et al., 2003). The rice *WUSCHEL* (*WUS*) ortholog, *TILLERS ABSENT 1* (*TAB1*/*OsWUS*), was also shown to play a role in initiating axillary meristems (Tanaka et al., 2015). Consistent with this, the *S. viridis* ortholog, *SvWus* (Sevir.3G028500), was co-expressed in cluster 3 (**Supplementary Table S3**). Also co-expressed with these developmental regulators was *SvLfy*, the *S. viridis* ortholog of *zea floricaula1/2/ABERRANT PANICLE ORGANIZATION 2 (APO2)/LEAFY* (*SvLfy,* Sevir.7G234000). These genes play universal roles in regulation of meristem determinacy, but with some species-specific differences; *LFY* and *zfl1/2* promote meristem determinacy and FM identity in Arabidopsis and maize, respectively (Schultz and Haughn, 1991; Bomblies et al., 2003), but *APO2* promotes meristem indeterminacy as well as BM initiation in rice (Kyozuka et al., 1998; Ikeda-Kawakatsu et al., 2012).

Among the SBP TFs annotated in developing *S. viridis* inflorescences (**Figure 2**), three were associated with Group 2. *SvUb3* (Sevir.6G212600), the ortholog of *unbranched 3 (ub3)* from maize and *WEALTHY FARMERS PANICLE (WFP)* from rice, was expressed in cluster 3. The function of this gene is generally conserved in both species in controlling partitioning of cells between lateral organ formation and meristem maintenance (Jiao et al., 2010; Miura et al., 2010; Chuck et al., 2014; Li et al., 2016). In maize, *ub3* shares redundant roles with *tassel sheath 4* (*tsh4*), another SPB TF that functions also to suppress formation of leaves in the inflorescence (Chuck et al., 2010, 2014). *SvTsh4* (Sevir.2G265300) was also found in Group 2, and was co-expressed in cluster 13 with *SvTsh1* (Sevir.3G136200), which encodes a GATA TF that functions in the same pathway (Wang et al., 2009; Whipple et al., 2010; **Figures 2**, **3A**).

Initiation of lateral organs involves the formation of boundaries, regions of decreased cell division that separate the growing organ primordia from meristematic signals to promote proper organ identity. Genes implicated in setting up lateral organ boundaries were identified in Group 2. *SvLg1* (Sevir.3G023500), the third SBP TF in this group and orthologous to *liguleless 1* (*lg1*) from maize (Moreno et al., 1997; Lewis et al., 2014) and *OsLG1* from rice (Lee et al., 2007), was found in cluster 3 (**Figures 2**, **3B**). In maize, *lg1* is classically known for its role in setting up the proximal-distal boundary that separates leaf blade from sheath and, along with *lg2*, is required for ligule and auricle development, thus controlling leaf angle. Recently, *lg1* was also shown to regulate inflorescence architecture by controlling tassel branch number in maize (Lewis et al., 2014) and branch angle in rice (Ishii et al., 2013; Zhu et al., 2013). Consistent with our data from *S. viridis*, *lg2* was proposed to act upstream of *lg1* in maize, with *lg2* expression initiated earlier in development to specify boundary position (Harper and Freeling, 1996; Lewis and Hake, 2016).

Also co-expressed with *lg1* in cluster 3 was *SvRa2* (Sevir.5G116100), ortholog of the maize *ramosa 2* (*ra2*) gene, which encodes a *LATERAL ORGAN BOUNDARY* (*LOB*) domain TF that is expressed transiently in positions where axillary meristems will form on the inflorescence (Moreno et al., 1997; Bortiri et al., 2006; **Figure 3B** and **Supplementary Figure S3**). In maize, *ra2* and *lg1* were shown to act in parallel pathways to control branch number and angle during early inflorescence development (Bai et al., 2012). The *S. viridis* ortholog of maize *barren stalk fastigiate 1* (*baf1*), *SvBaf1* (Sevir.4G025200), was also co-expressed in cluster 3 (**Figure 4** and **Supplementary Table S3**). In maize, *baf1* encodes an AT-hook protein that is involved in demarcating the boundary region of axillary meristems and plays a role in their initiation (Gallavotti et al., 2011).

The positioning of axillary meristems is strongly influenced by transport and function of the phytohormone auxin. As auxin flows in and out of emerging primordia, localized auxin

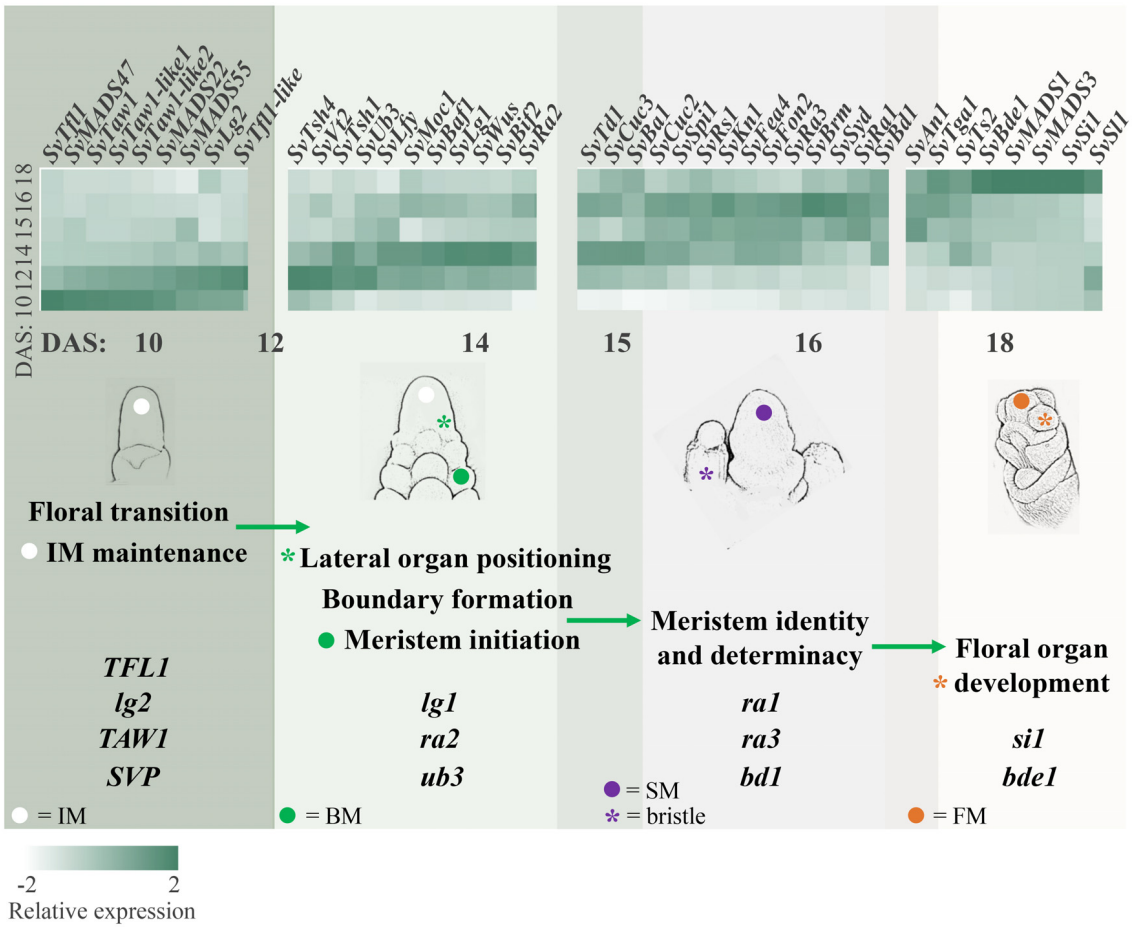

FIGURE 4 | Orthologs of genes known to regulate inflorescence architecture in maize and rice showed expected expression patterns during *Setaria viridis* inflorescence development and transitions between meristem types. The schematic diagrams sequential developmental transitions captured by the RNA-seq data and shows relative expression of genes predicted to control these transitions. For example, consistent with the initiation of BMs from the IM between 10 and 14 DAS, positive regulators of lateral meristem formation (e.g., *SvBif2* and *SvUb3)* showed increased expression between 10 and 14 DAS, and negative regulators of axillary meristem formation (e.g., *SvTd1* and *SvFea4*) increased later at 14–16 DAS. Genes displayed in the heatmap are divided by group and developmental processes can transition across groups. *Light-to-dark* color indicates low-to-high relative expression.

response maxima arise at places of lateral meristem initiation, and this mechanism is generally conserved in maize inflorescence development (Barazesh and McSteen, 2008; Gallavotti, 2013; Eveland et al., 2014). Therefore, we would expect suites of auxin-related genes to be dynamically expressed between 12 and 15 DAS in *S. viridis* while branching occurs; i.e., in Groups 2 and 3. We annotated genes in these groups based on homology to those implicated in synthesis, transport, signaling and/or response of auxin, and plotted their expression profiles (**Supplementary Figure S7** and **Supplementary Table S5**). The expression of *SvVt2* (Sevir.5G116300), the ortholog of maize *vanishing tassel 2* (*vt2*), was initiated early in development and associated with cluster 13, while expression of *SvBif2* (Sevir.3G410700), the ortholog of *barren inflorescence 2* (*bif2*), peaked slightly later and was in cluster 3. *Vt2* encodes a tryptophan aminotransferase that regulates an early step of auxin biosynthesis (Phillips et al., 2011), and *bif2* encodes a PINOID serine/threonine kinase that regulates auxin transport (McSteen et al., 2007; **Supplementary Figure S7**).

Other key genes implicated in auxin-mediated lateral branching in maize and rice inflorescence development were expressed slightly later and in Group 3 (**Figure 3A** and **Supplementary Figure S7**). For example, genes in cluster 22 increased expression between 10 and 14 DAS, but expression was stable after 15 DAS unlike Group 2 clusters that decreased expression between 15 and 18 DAS (**Figure 3A** and **Supplementary Figure S6**). These included *S. viridis* orthologs of maize *sparse inflorescence 1* (*spi1*; *SvSpi1*; Sevir.5G251100), encoding a *YUCCA-like* gene involved in a late step of auxin biosynthesis (Gallavotti et al., 2008), and *barren stalk 1* (*ba1*)/*LAX PANICLE 1* (*LAX1*) (*SvBa1;* Sevir.5G374100), a bHLH protein involved in auxin signaling (Komatsu et al., 2003a; Gallavotti et al., 2004; **Supplementary Figure S7**). In maize, functional BA1 is required for creation of auxin maxima at the meristem anlagen to promote lateral meristem initiation. Our expression data from *S. viridis* are consistent with expression and genetics analyses in maize

that show *ba1* acts downstream of *baf1* (Gallavotti et al., 2011).

Group 3: SM Differentiation and FM Initiation

Clusters 10, 11, 18, and 22 in Group 3 have similar expression signatures that show a progressive increase during early stages of development, peaking around 16 DAS, and decreasing slightly by 18 DAS (**Figure 3A** and **Supplementary Figure S6**). Among these clusters were a number of genes related to axillary meristem identity and determinacy. For example, *SvBd1* (Sevir.2G437800), a marker of SM identity in *S. viridis* (Yang et al., 2017), was found in cluster 18 (**Figure 3B** and **Supplementary Table S3**). Orthologs of this AP2/ERF TF across grass species, e.g., *branched silkless 1 (bd1)* in maize, *FRIZZY PANICLE* (*FZP)* in rice, and *MORE SPIKELETS 1* (*MOS1*) in *Brachypodium distachyon,* share a conserved function in specifying SM identity (Chuck et al., 2002; Komatsu et al., 2003b; Derbyshire and Byrne, 2013).

Genes in the maize RAMOSA pathway regulate meristem determinacy prior to SM identity (Vollbrecht et al., 2005). Among these genes, *ra2* is widely conserved across grasses and its expression comes on early during axillary meristem initiation. Consistent with genetics and expression data from maize (Bortiri et al., 2006; Satoh-Nagasawa et al., 2006), the *S. viridis* orthologs of *ra1* (*SvRa1;* Sevir.2G209800) and *ramosa 3* (*ra3*) (*SvRa3*; Sevir.2G407500), which encodes a trehalose-phosphate phosphatase (Satoh-Nagasawa et al., 2006), were expressed after initiation of *SvRa2* and were found in clusters 10 and 11, respectively, their expression peaking at 15–16 DAS (**Figures 3A,B**).

Genetic interactions among genes controlling meristem determinacy and meristem size pathways in maize indicated these processes interface generally (Bommert and Whipple, 2017). Interestingly, many genes orthologous to known players in meristem size pathways were also co-expressed in Group 3. For example, *SvFea4* (Sevir.4G119100), the ortholog of *fasciated ear 4* (*fea4*) from maize and *PERIANTHIA (PAN)* from Arabidopsis encoding a bZIP TF that negatively regulates meristem size (Maier et al., 2009; Pautler et al., 2015), was found in cluster 22 (**Figure 3A** and **Supplementary Figure S3**). Regulatory components of the CLAVATA-WUSCHEL negative feedback signaling pathway central to meristem maintenance (Somssich et al., 2016) were also co-expressed in cluster 22. Among these were *SvTd1* (Sevir.4G294000) and *SvFon2* (Sevir.8G183800), orthologs of maize *thick tassel dwarf 1 (td1)/CLAVATA1*, encoding a leucine-rich repeat receptor-like kinase (Bommert et al., 2005), and rice *FLORAL ORGAN NUMBER 2/CLV3*, encoding a CLV3/ESR related peptide (Chu et al., 2006; Goad et al., 2017), respectively (**Supplementary Figure S2** and **Supplementary Table S3**). Both *td1/CLV1* and *FON2/CLV3* negatively control meristem size.

Certain Class I KNOX homeodomain TFs also function in pathways to maintain meristem cell identity and size. Orthologs of the maize *knotted 1 (kn1)* and *rough sheath 1* (*rs1*) genes, *SvKn1* (Sevir.9G107600) and *SvRs1* (Sevir.2G029800), respectively, both homologs of the Arabidopsis *BREVIPEDICELLUS* (*BP*) gene, were co-expressed in cluster 11 (**Figure 3A** and **Supplementary Figure S6**). In maize, *kn1* is a key marker of meristem maintenance (Kerstetter et al., 1997; Bolduc et al., 2012), and the localized expression of *rs1* predicted and subtended the initiation of axillary meristems on the flanks of the IM (Schneeberger et al., 1995). Interestingly, the *S. viridis* homologs of the BP interaction partner, *BRAHMA* (*BRM*), and a closely related gene, *SPLAYED* (*SYD*), both encoding SWI/SNF chromatin remodeling ATPases in Arabidopsis (Wagner and Meyerowitz, 2002; Zhao et al., 2015), Sevir.2G237500 and Sevir.4G112300, respectively, were also found cluster 11 (**Supplementary Table S3**). In Arabidopsis, *BRM* upregulates *CUC* genes (Kwon et al., 2006), which are essential players in lateral meristem establishment and proper boundary formation; *SvCuc2* (Sevir.4G124400) and *SvCuc3* (Sevir.6G213600) were co-expressed in cluster 22. In addition, two class II TCP TFs orthologous to *branch angle defective 1* (*bad1*)/*wavy auricle blade 1* (*wab1*) (Bai et al., 2012; Lewis et al., 2014) and *teosinte branched 1* (*tb1*) (Doebley et al., 1997) were co-expressed in cluster 22 [*SvBad1* (Sevir.2G210100) and *SvTb1* (Sevir.9G122200), respectively]. Consistent with their expression profiles during *S. viridis* inflorescence development (**Figure 2**), their localized expression overlaps in axillary meristems of young maize tassels and both genes contribute to the regulation of branch outgrowth (Bai et al., 2012).

Group 4: Floral Organ Development

Genes in Group 4 (clusters 1, 6, 14, 16, 17, and 23) progressively increased in expression after 14 DAS and peaked largely at 18 DAS, coinciding with floral organ formation and differentiation (**Figure 3A** and **Supplementary Figure S6**). A number of genes encoding MIKC-type MADS-box TFs were found in this group, which was expected given their conserved roles as master regulators of floral organ identity across species (Theißen et al., 2016; **Figures 2** and **Supplementary Figure S5**). Among them were two B-class function TFs known to regulate lodicule identity and stamen development and co-expressed in cluster 6; an ortholog of the maize *silky1 (si1)* gene (*SvSi1*; Sevir.4G289400) and homolog of *OsMADS4* from rice (*SvMADS4*; Sevir.3G242100) (Ambrose et al., 2000; Nagasawa et al., 2003; Yao et al., 2008). A number of C-class, *AGAMOUS*-like genes were also co-expressed in cluster 6, including *SvBde1* (Sevir.1G278500), orthologous to the maize *bearded ear 1* (*bde1*) gene (Thompson et al., 2009), and homologs of rice *OsMADS17*, *OsMADS3*, and *OsMADS58*, Sevir.7G221900, Sevir.5G141300, and Sevir.3G074600, respectively (Yamaguchi et al., 2006). Also, three *SEPALLATA*-like E-class genes were expressed in cluster 6 including homologs of rice *OsMADS1/LEAFY HULL STERILE 1* (*LHS1*), *OsMADS7*, and *OsMADS8,* Sevir.9G494300, Sevir.6G230500, and Sevir.2G277000, respectively, which all presumably function in specifying floral organ identity (Jeon, 2000; Zahn et al., 2005; Cui et al., 2010).

Additional genes that function in floral organ specification were also found in Group 4. Among these, *SvTga1* (Sevir.6G230400), the ortholog of *teosinte glume architecture 1* (*tga1)* encoding an SBP TF that regulates glume development and was a key domestication locus in maize (Dorweiler and Doebley, 1997; Preston et al., 2012), was found in cluster 16 (**Figure 3B** and **Supplementary Figure S3**). In addition, orthologs of the C2H2 TF *STAMENLESS 1* from rice (Sevir.5G086100; *SvSl1*)

(Xiao et al., 2009) and maize *yabby 15*/rice *TONGARI-BOUSHI 1* (*TOB1*) (Sevir.1G255900; *SvTob1*) (Tanaka et al., 2012), were expressed in clusters 6 and 14, respectively (Tanaka et al., 2012). *TOB1* and close homologs regulate maintenance and fate of reproductive meristems whereas *OsSL1* regulates floral organ identity. Sex determination genes from maize were also associated with Group 4, including orthologs of maize *anther ear 1* (*an1*), a terpenoid synthase involved in the gibberellic acid biosynthesis (Sevir.9G265300; *SvAn1*) (Bensen et al., 1995) and *tassel seed 2* (*ts2*) (Sevir.9G439800; *SvTs2*) (DeLong et al., 1993) in cluster 17 and 16, respectively (**Figure 3A** and **Supplementary Table S3**).

Co-expression Network Analysis Using WGCNA

To extend our co-expression analyses, we also performed a WGCNA (Langfelder and Horvath, 2008). We used WGCNA to independently define modules of co-expressed genes and to construct a co-expression network for early *S. viridis* inflorescence development (**Supplementary Table S6**). WGCNA produced 14 co-expression modules based on parameters detailed in the Section "Materials and Methods," which were highly consistent with our FCM results; i.e., each WGCNA module largely corresponded to the sum of several FCM clusters (**Supplementary Figure S8**). In addition to grouping genes into co-expression modules, WGCNA was used to determine the interconnectedness of genes within and between modules. A strength value (i.e., weight) was assigned to the connection (edge) between each gene (node) and every other gene in the network. An integrated co-expression network was generated after filtering gene-to-gene connections with very low connectivity (weight >0.02; available in NCBI GEO).

To define sub-networks related to specific developmental processes and potentially identify new regulatory factors, we filtered the co-expression network for genes with strong connections to known genes of interest within a module. For example, we explored a co-expression module that included *SvLg1*, *SvBaf1*, and *SvBif2,* which are known players in boundary formation and axillary meristem initiation ("Plum" module; **Supplementary Figure S8** and **Supplementary Table S6**). To reduce complexity in visualization and

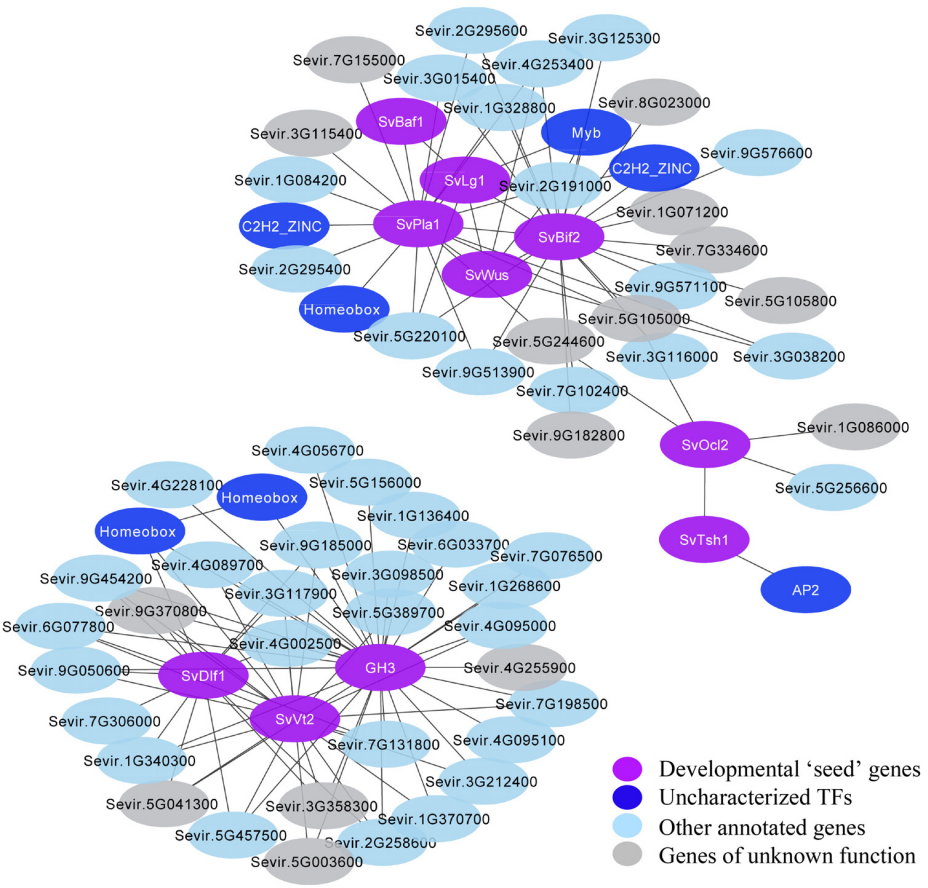

FIGURE 5 | Two sub-networks extracted from the WGCNA were defined based on gene connectivity to a set of co-expressed regulators of inflorescence development (shown in *purple*). Genes (or nodes) were included if they were connected to these developmental genes by edges with a weight >0.2. Developmental regulators within these sub-networks either show high connectivity (e.g., *SvVt2*, *SvBif2*) or low connectivity (e.g., *SvTsh1*, *SvBaf1*). Uncharacterized TFs are indicated in *dark blue*, other genes with assigned functional annotations in *light blue*, and genes of unknown function in gray.

interpretation of this module, we included only genes with strong interactions (edges between genes having a weight >0.2) to a set of ten predicted developmental genes (**Figure 5** and **Supplementary Table S7**). One sub-network was defined that included strong co-expression "interactions" among *SvDfl1* (Sevir.2G302300), a homolog of maize *delayed flower 1* (Muszynski et al., 2006), *SvVt2* and a GH3 IAA-amido synthase (Sevir.9G364900) (**Supplementary Figure S7**), homologous to Arabidopsis *YADOKARI 1* (*YDK1*) and predicted to regulate auxin levels (Staswick et al., 2005), via a common set of genes. In another sub-network, *SvPla1* (Sevir.9G259300), a cytochrome P450 homologous to Arabidopsis *PLASTOCHRON1* (Miyoshi et al., 2004; Sun et al., 2017), was identified as a hub gene directly or indirectly connected to *SvBaf1*, *SvLg1*, and *SvBif2*, consistent with its conserved role in lateral organ initiation (**Figure 5** and **Supplementary Table S7**). Within these subnetworks, some developmental regulators showed high connectivity to many other genes, while others showed relatively low connectivity (**Figure 5**).

Setaria viridis as a Comparative Model for Panicoid Grass Inflorescence Development

Our transcriptomics analysis in *S. viridis* identified homologs of known developmental regulators as well as uncharacterized genes with putative roles in panicoid grass inflorescence development. Based on spatiotemporal expression profiles, we showed that genes controlling transitions in meristem types during inflorescence development are largely conserved between *S. viridis* and maize (**Figure 4**). Since the diversity of inflorescence architectures found across grasses are largely determined by subtle regulatory variation on common developmental processes, it is not surprising that suites of genes have conserved functions across grasses, and often analogous functions in more distantly related species. For example, *tsh1/NL1* genes share conserved functions in boundary establishment and bract suppression in maize and rice (Wang et al., 2009; Whipple et al., 2010), whereas the close Arabidopsis homolog, *HANABA TARANU,* functions in floral organ development (Zhao et al., 2004). However, in some cases orthologous genes can take on context-specific functional roles. The rice ortholog of *baf1*, *DEPRESSED PALEA 1* (*DP1*), regulates palea formation, and floral organ number (Jin et al., 2011), while its close homolog in Arabidopsis, *AHL22,* functions in the floral transition (Yun et al., 2012).

We anticipate that species-specific expression differences underlie the variation in inflorescence form in *Setaria* spp. compared to maize and other closely related grasses. While we are beginning to elucidate some of the genes responsible for these morphological differences through mutant screens and experimental analyses (Yang et al., 2017), identifying subtle variation in gene regulation at the network level will require parallel transcriptomics resources from other species. In addition, using co-expression analyses to prioritize novel candidate genes as having previously undefined functions in development will also be most powerful when evaluated in the context of comparable datasets. Thus, a detailed knowledgebase of how the expression of individual genes shift during development and how co-expressed gene modules are rewired across grass species, is invaluable to understanding the genetic basis for morphological diversity in grass inflorescence architecture.

The apparent similarity between maize and *S. viridis* at the transcriptome level supports its use as a functional model for panicoid cereals, especially when paired with rapid advances in gene editing and transformation technologies (Zhu et al., 2017). Our transcriptomics analyses provide a platform for gene discovery in *S. viridis* inflorescence development and a comparative model for studying diverse architectures of agronomically important cereal crops. With respect to the former, it is anticipated that these data will help uncover novel expression patterns associated with the unique features of *S. viridis* inflorescence morphology, which can be translated to other millets (Huang et al., 2016), including subsistence crops in many developing countries that remain largely untapped for genetic improvement.

ACCESSION NUMBERS

RNA-seq data (raw sequence reads and processed data files) generated in this study and the WGCNA gene co-expression matrix are available from the NCBI Gene Expression Omnibus (GEO; www.ncbi.nlm.nih.gov/geo/) under accession number GSE118673.

AUTHOR CONTRIBUTIONS

AE and EK conceptualized and supervised the work. MB established the developmental sampling scheme. JY and MB performed SEM and RNA-seq experiments. JY and CZ performed bioinformatics analyses and data visualization. CZ, JY, EK, and AE wrote the paper. All authors read and approved the final manuscript.

FUNDING

CZ and MB were supported by National Science Foundation (NSF) grant IOS-1413824 to EK. JY was supported by PGRP-NSF grant IOS-1733606 to AE.

ACKNOWLEDGMENTS

We thank Drs. Edoardo Bertolini, Michael McKain, and Indrajit Kumar at the Donald Danforth Plant Science Center (DDPSC) for advice on bioinformatics analyses, and Kevin Reilly and his team at the DDPSC Integrated Growth Facility for growth chamber maintenance. We also thank the U.S.

Department of Energy (DOE) Joint Genome Institute for use of the *S. viridis* genome prior to publication, which is supported by the Office of Science of the U.S. DOE under Contract No. DE-AC02-05CH11231.

SUPPLEMENTARY MATERIAL

The Supplementary Material for this article can be found online at: https://www.frontiersin.org/articles/10.3389/fpls.2018.01309/full#supplementary-material

FIGURE S1 | Correlations of global gene expression profiles across all samples.

FIGURE S2 | Expression profiles of orthologs of known developmental genes across six stages of *Setaria viridis* inflorescence development showing standard deviation among biological replicates.

FIGURE S3 | Dynamic expression profiles of TF families during inflorescence development in *Setaria viridis*: LOB, NAC, AP2/ERF, C2H2, bZIP, and bHLH families.

FIGURE S4 | Expression profiles of uncharacterized TFs with highly dynamic changes during inflorescence development.

FIGURE S5 | Phylogenetic relationship of *Setaria viridis* MIKC-type MADS-box TFs with homologous genes in rice, maize, and Arabidopsis.

FIGURE S6 | Cluster number selection for FCM and developmental trajectories of 25 clusters.

FIGURE S7 | Expression profiles of auxin-related genes from Groups 2 and 3.

FIGURE S8 | Assignment of genes to co-expression modules using WGCNA and comparison to FCM analyses.

TABLE S1 | RNA-seq library sequencing and mapping statistics.

TABLE S2 | Gene expression values for all *S. viridis* genes, their closest orthologs in other species, and available functional annotations.

TABLE S3 | Cluster assignment of 11,425 dynamically expressed genes and associated functional annotation.

TABLE S4 | Expression values and annotations of selected transcriptional factor (TF) families.

TABLE S5 | Expression values and functional annotations of auxin-related genes from Groups 2 and 3.

TABLE S6 | Output from WGCNA using 11,425 dynamically expressed genes showing the relative connectivity of each gene to each of 14 modules.

TABLE S7 | Genes (or nodes) and their connections (edges) to each other within the two sub-networks depicted in **Figure 5**.

REFERENCES

Ambrose, B. A., Lerner, D. R., Ciceri, P., Padilla, C. M., Yanofsky, M. F., and Schmidt, R. J. (2000). Molecular and genetic analyses of the *silky1* gene reveal conservation in floral organ specification between eudicots and monocots. *Mol. Cell* 5, 569–579. doi: 10.1016/S1097-2765(00)80450-5

Arora, R., Agarwal, P., Ray, S., Singh, A. K., Singh, V. P., Tyagi, A. K., et al. (2007). MADS-box gene family in rice: genome-wide identification, organization and expression profiling during reproductive development and stress. *BMC Genomics* 8:242. doi: 10.1186/1471-2164-8-242

Bai, F., Reinheimer, R., Durantini, D., Kellogg, E. A., and Schmidt, R. J. (2012). TCP transcription factor, BRANCH ANGLE DEFECTIVE 1 (BAD1), is required for normal tassel branch angle formation in maize. *Proc. Natl. Acad. Sci. U.S.A.* 109, 12225–12230. doi: 10.1073/pnas.1202439109

Barazesh, S., and McSteen, P. (2008). Hormonal control of grass inflorescence development. *Trends Plant Sci.* 13, 656–662. doi: 10.1016/j.tplants.2008.09.007

Bartlett, M. E. (2017). Changing MADS-box transcription factor protein–protein interactions as a mechanism for generating floral morphological diversity. *Integr. Comp. Biol.* 57, 1312–1321. doi: 10.1093/icb/icx067

Bartlett, M. E., and Thompson, B. (2014). Meristem identity and phyllotaxis in inflorescence development. *Front. Plant Sci.* 5:508. doi: 10.3389/fpls.2014.00508

Bennetzen, J. L., Schmutz, J., Wang, H., Percifield, R., Hawkins, J., Pontaroli, A. C., et al. (2012). Reference genome sequence of the model plant Setaria. *Nat. Biotechnol.* 30, 555–561. doi: 10.1038/nbt.2196

Bensen, R. J., Johal, G. S., Crane, V. C., Tossberg, J. T., Schnable, P. S., Meeley, R. B., et al. (1995). Cloning and characterization of the maize *An1* gene. *Plant Cell* 7, 75–84. doi: 10.1105/tpc.7.1.75

Bolduc, N., Yilmaz, A., Mejia-Guerra, M. K., Morohashi, K., O'Connor, D., Grotewold, E., et al. (2012). Unraveling the KNOTTED1 regulatory network in maize meristems. *Genes Dev.* 26, 1685–1690. doi: 10.1101/gad.193433.112

Bomblies, K., Wang, R.-L., Ambrose, B. A., Schmidt, R. J., Meeley, R. B., and Doebley, J. (2003). Duplicate FLORICAULA/LEAFY homologs *zfl1* and *zfl2* control inflorescence architecture and flower patterning in maize. *Development* 130, 2385–2395. doi: 10.1242/dev.00457

Bommert, P., Lunde, C., Nardmann, J., Vollbrecht, E., Running, M., Jackson, D., et al. (2005). *thick tassel dwarf1* encodes a putative maize ortholog of the *Arabidopsis CLAVATA1* leucine-rich repeat receptor-like kinase. *Development* 132, 1235–1245. doi: 10.1242/dev.01671

Bommert, P., and Whipple, C. (2017). Grass inflorescence architecture and meristem determinacy. *Semin. Cell Dev. Biol.* 79, 37–47. doi: 10.1016/j.semcdb.2017.10.004

Bortiri, E., Chuck, G., Vollbrecht, E., Rocheford, T., Martienssen, R., and Hake, S. (2006). *ramosa2* encodes a LATERAL ORGAN BOUNDARY domain protein that determines the fate of stem cells in branch meristems of maize. *Plant Cell* 18, 574–585. doi: 10.1105/tpc.105.039032

Brutnell, T. P., Wang, L., Swartwood, K., Goldschmidt, A., Jackson, D., Zhu, X.-G., et al. (2010). *Setaria viridis*: a model for C4 photosynthesis. *Plant Cell* 22, 2537–2544. doi: 10.1105/tpc.110.075309

Cho, E., and Zambryski, P. C. (2011). *ORGAN BOUNDARY1* defines a gene expressed at the junction between the shoot apical meristem and lateral organs. *Proc. Natl. Acad. Sci. U.S.A.* 108, 2154–2159. doi: 10.1073/pnas.1018542108

Chu, H., Qian, Q., Liang, W., Yin, C., Tan, H., Yao, X., et al. (2006). The *FLORAL ORGAN NUMBER4* gene encoding a putative ortholog of Arabidopsis CLAVATA3 regulates apical meristem size in rice. *Plant Physiol.* 142, 1039–1052. doi: 10.1104/pp.106.086736

Chuck, G., Muszynski, M., Kellogg, E., Hake, S., and Schmidt, R. J. (2002). The control of spikelet meristem identity by the *branched silkless1* gene in maize. *Science* 298, 1238–1241. doi: 10.1126/science.1076920

Chuck, G., Whipple, C., Jackson, D., and Hake, S. (2010). The maize SBP-box transcription factor encoded by *tasselsheath4* regulates bract development and the establishment of meristem boundaries. *Development* 137, 1243–1250. doi: 10.1242/dev.048348

Chuck, G. S., Brown, P. J., Meeley, R., and Hake, S. (2014). Maize *SBP-box* transcription factors *unbranched2* and *unbranched3* affect yield traits by regulating the rate of lateral primordia initiation. *Proc. Natl. Acad. Sci. U.S.A.* 111, 18775–18780. doi: 10.1073/pnas.1407401112

Cui, R., Han, J., Zhao, S., Su, K., Wu, F., Du, X., et al. (2010). Functional conservation and diversification of class E floral homeotic genes in rice (*Oryza sativa*). *Plant J.* 61, 767–781. doi: 10.1111/j.1365-313X.2009.04101.x

Danilevskaya, O. N., Meng, X., and Ananiev, E. V. (2010). Concerted modification of flowering time and inflorescence architecture by ectopic expression of *TFL1*-like genes in maize. *Plant Physiol.* 153, 238–251. doi: 10.1104/pp.110.154211

DeLong, A., Calderon-Urrea, A., and Dellaporta, S. L. (1993). Sex determination gene *TASSELSEED2* of maize encodes a short-chain alcohol dehydrogenase required for stage-specific floral organ abortion. *Cell* 74, 757–768. doi: 10.1016/0092-8674(93)90522-R

Derbyshire, P., and Byrne, M. E. (2013). *MORE SPIKELETS1* is required for spikelet fate in the inflorescence of *Brachypodium*. *Plant Physiol.* 161, 1291–1302. doi: 10.1104/pp.112.212340

Digel, B., Pankin, A., and von Korff, M. (2015). Global transcriptome profiling of developing leaf and shoot apices reveals distinct genetic and environmental control of floral transition and inflorescence development in barley. *Plant Cell* 27, 2318–2334. doi: 10.1105/tpc.15.00203

Doebley, J., Stec, A., and Hubbard, L. (1997). The evolution of apical dominance in maize. *Nature* 386, 485–488. doi: 10.1038/386485a0

Dorweiler, J. E., and Doebley, J. (1997). Developmental analysis of *Teosinte glume architecture1*: a key locus in the evolution of maize (Poaceae). *Am. J. Bot.* 84:1313. doi: 10.2307/2446130

Doust, A. N., and Kellogg, E. A. (2002). Inflorescence diversification in the panicoid "bristle grass" clade (Paniceae, Poaceae): evidence from molecular phylogenies and developmental morphology. *Am. J. Bot.* 89, 1203–1222. doi: 10.3732/ajb.89.8.1203

Doust, A. N., Kellogg, E. A., Devos, K. M., and Bennetzen, J. L. (2009). Foxtail millet: a sequence-driven grass model system. *Plant Physiol.* 149, 137–141. doi: 10.1104/pp.108.129627

Edgar, R. C. (2004). MUSCLE: multiple sequence alignment with high accuracy and high throughput. *Nucleic Acids Res.* 32, 1792–1797. doi: 10.1093/nar/gkh340

Eveland, A. L., Goldshmidt, A., Pautler, M., Morohashi, K., Liseron-Monfils, C., Lewis, M. W., et al. (2014). Regulatory modules controlling maize inflorescence architecture. *Genome Res.* 24, 431–443. doi: 10.1101/gr.166397.113

Feng, N., Song, G., Guan, J., Chen, K., Jia, M., Huang, D., et al. (2017). Transcriptome profiling of wheat inflorescence development from spikelet initiation to floral patterning identified stage-specific regulatory genes. *Plant Physiol.* 174, 1779–1794. doi: 10.1104/pp.17.00310

Furutani, I., Sukegawa, S., and Kyozuka, J. (2006). Genome-wide analysis of spatial and temporal gene expression in rice panicle development. *Plant J.* 46, 503–511. doi: 10.1111/j.1365-313X.2006.02703.x

Gallavotti, A. (2013). The role of auxin in shaping shoot architecture. *J. Exp. Bot.* 64, 2593–2608. doi: 10.1093/jxb/ert141

Gallavotti, A., Barazesh, S., Malcomber, S., Hall, D., Jackson, D., Schmidt, R. J., et al. (2008). *sparse inflorescence1* encodes a monocot-specific YUCCA-like gene required for vegetative and reproductive development in maize. *Proc. Natl. Acad. Sci. U.S.A.* 105, 15196–201. doi: 10.1073/pnas.0805596105

Gallavotti, A., Malcomber, S., Gaines, C., Stanfield, S., Whipple, C., Kellogg, E., et al. (2011). BARREN STALK FASTIGIATE1 is an AT-hook protein required for the formation of maize ears. *Plant Cell* 23, 1756–1771. doi: 10.1105/tpc.111.084590

Gallavotti, A., Zhao, Q., Kyozuka, J., Meeley, R. B., Ritter, M. K., Doebley, J. F., et al. (2004). The role of *barren stalk1* in the architecture of maize. *Nature* 432, 630–635. doi: 10.1038/nature03148

Goad, D. M., Zhu, C., and Kellogg, E. A. (2017). Comprehensive identification and clustering of CLV3/ESR-related (CLE) genes in plants finds groups with potentially shared function. *New Phytol.* 216, 605–616. doi: 10.1111/nph.14348

Hanano, S., and Goto, K. (2011). *Arabidopsis* TERMINAL FLOWER1 is involved in the regulation of flowering time and inflorescence development through transcriptional repression. *The Plant Cell* 23, 3172–3184. doi: 10.1105/tpc.111.088641

Harper, L., and Freeling, M. (1996). Interactions of *liguleless1* and *liguleless2* function during ligule induction in maize. *Genetics* 144, 1871–1882.

Harrop, T. W. R., Ud Din, I., Gregis, V., Osnato, M., Jouannic, S., Adam, H., et al. (2016). Gene expression profiling of reproductive meristem types in early rice inflorescences by laser microdissection. *Plant J.* 86, 75–88. doi: 10.1111/tpj.13147

Hirano, H.-Y., Tanaka, W., and Toriba, T. (2014). Grass flower development. *Methods Mol. Biol.* 1110, 57–84. doi: 10.1007/978-1-4614-9408-9_3

Huang, P., Shyu, C., Coelho, C. P., Cao, Y., and Brutnell, T. P. (2016). *Setaria viridis* as a model system to advance millet genetics and genomics. *Front. Plant Sci.* 7:1781. doi: 10.3389/fpls.2016.01781

Ikeda-Kawakatsu, K., Maekawa, M., Izawa, T., Itoh, J.-I., and Nagato, Y. (2012). ABERRANT PANICLE ORGANIZATION 2/RFL, the rice ortholog of Arabidopsis LEAFY, suppresses the transition from inflorescence meristem to floral meristem through interaction with APO1. *Plant J.* 69, 168–180. doi: 10.1111/j.1365-313X.2011.04781.x

Ishii, T., Numaguchi, K., Miura, K., Yoshida, K., Thanh, P. T., Htun, T. M., et al. (2013). OsLG1 regulates a closed panicle trait in domesticated rice. *Nat. Genet.* 45, 465e1–462e1. doi: 10.1038/ng.2567

Jeon, J.-S. (2000). *leafy hull sterile1* is a homeotic mutation in a rice MADS box gene affecting rice flower development. *Plant Cell* 12, 871–884. doi: 10.1105/tpc.12.6.871

Jiao, Y., Wang, Y., Xue, D., Wang, J., Yan, M., Liu, G., et al. (2010). Regulation of *OsSPL14* by OsmiR156 defines ideal plant architecture in rice. *Nat. Genet.* 42, 541–544. doi: 10.1038/ng.591

Jin, Y., Luo, Q., Tong, H., Wang, A., Cheng, Z., Tang, J., et al. (2011). An AT-hook gene is required for palea formation and floral organ number control in rice. *Dev. Biol.* 359, 277–288. doi: 10.1016/j.ydbio.2011.08.023

Gallavotti, A., Barazesh, S., Malcomber, S., Hall, D., Jackson, D., Schmidt, R. J., et al. (2008). sparse *inflorescence1* encodes a monocot-specific *YUCCA*-like gene required for vegetative and reproductive development in maize. *Proc. Natl. Acad. Sci. U.S.A.* 105, 15196–15201. doi: 10.1073/pnas.0805596105

Kerstetter, R. A., Laudencia-Chingcuanco, D., Smith, L. G., and Hake, S. (1997). Loss-of-function mutations in the maize homeobox gene, *knotted1*, are defective in shoot meristem maintenance. *Development* 124, 3045–3054.

Komatsu, K., Maekawa, M., Ujiie, S., Satake, Y., Furutani, I., Okamoto, H., et al. (2003a). LAX and SPA: major regulators of shoot branching in rice. *Proc. Natl. Acad. Sci. U.S.A.* 100, 11765–11770.

Komatsu, M., Chujo, A., Nagato, Y., Shimamoto, K., and Kyozuka, J. (2003b). FRIZZY PANICLE is required to prevent the formation of axillary meristems and to establish floral meristem identity in rice spikelets. *Development* 130, 3841–3850.

Kumar, L., and Futschik, M. E. (2007). Mfuzz: a software package for soft clustering of microarray data. *Bioinformation* 2, 5–7. doi: 10.6026/97320630002005

Kwon, C. S., Hibara, K.-I., Pfluger, J., Bezhani, S., Metha, H., Aida, M., et al. (2006). A role for chromatin remodeling in regulation of CUC gene expression in the Arabidopsis cotyledon boundary. *Development* 133, 3223–3230. doi: 10.1242/dev.02508

Kyozuka, J., Konishi, S., Nemoto, K., Izawa, T., and Shimamoto, K. (1998). Down-regulation of RFL, the FLO/LFY homolog of rice, accompanied with panicle branch initiation. *Proc. Natl. Acad. Sci. U.S.A.* 95, 1979–1982. doi: 10.1073/pnas.95.5.1979

Kyozuka, J., Tokunaga, H., and Yoshida, A. (2014). Control of grass inflorescence form by the fine-tuning of meristem phase change. *Curr. Opin. Plant Biol.* 17, 110–115. doi: 10.1016/j.pbi.2013.11.010

Langfelder, P., and Horvath, S. (2008). WGCNA: an R package for weighted correlation network analysis. *BMC Bioinformatics* 9:559. doi: 10.1186/1471-2105-9-559

Lee, J., Park, J.-J., Kim, S. L., Yim, J., and An, G. (2007). Mutations in the rice *liguleless* gene result in a complete loss of the auricle, ligule, and laminar joint. *Plant Mol. Biol.* 65, 487–499. doi: 10.1007/s11103-007-9196-1

Lewis, M. W., Bolduc, N., Hake, K., Htike, Y., Hay, A., Candela, H., et al. (2014). Gene regulatory interactions at lateral organ boundaries in maize. *Development* 141, 4590–4597. doi: 10.1242/dev.111955

Lewis, M. W., and Hake, S. (2016). Keep on growing: building and patterning leaves in the grasses. *Curr. Opin. Plant Biol.* 29, 80–86. doi: 10.1016/j.pbi.2015.11.008

Li, M., Li, X., Zhou, Z., Wu, P., Fang, M., Pan, X., et al. (2016). Reassessment of the four yield-related genes *Gn1a*, *DEP1*, *GS3*, and *IPA1* in rice using a CRISPR/Cas9 system. *Front. Plant Sci.* 7:377. doi: 10.3389/fpls.2016.00377

Li, X., Qian, Q., Fu, Z., Wang, Y., Xiong, G., Zeng, D., et al. (2003). Control of tillering in rice. *Nature* 422, 618–621. doi: 10.1038/nature01518

Maier, A. T., Stehling-Sun, S., Wollmann, H., Demar, M., Hong, R. L., Haubeiss, S., et al. (2009). Dual roles of the bZIP transcription factor PERIANTHIA in the control of floral architecture and homeotic gene expression. *Development* 136, 1613–1620. doi: 10.1242/dev.033647

McSteen, P. (2006). Branching out: the ramosa pathway and the evolution of grass inflorescence morphology. *Plant Cell* 18, 518–522. doi: 10.1105/tpc.105.040196

McSteen, P., Malcomber, S., Skirpan, A., Lunde, C., Wu, X., Kellogg, E., et al. (2007). *barren inflorescence2* encodes a co-ortholog of the *PINOID* serine/threonine kinase and is required for organogenesis during inflorescence and vegetative development in maize. *Plant Physiol.* 144, 1000–1011. doi: 10.1104/pp.107.098558

Miura, K., Ikeda, M., Matsubara, A., Song, X.-J., Ito, M., Asano, K., et al. (2010). OsSPL14 promotes panicle branching and higher grain productivity in rice. *Nat. Genet.* 42, 545–549. doi: 10.1038/ng.592

Miyoshi, K., Ahn, B.-O., Kawakatsu, T., Ito, Y., Itoh, J.-I., Nagato, Y., et al. (2004). PLASTOCHRON1, a timekeeper of leaf initiation in rice, encodes cytochrome P450. *Proc. Natl. Acad. Sci. U.S.A.* 101, 875–880. doi: 10.1073/pnas.2636936100

Moreno, M. A., Harper, L. C., Krueger, R. W., Dellaporta, S. L., and Freeling, M. (1997). *liguleless1* encodes a nuclear-localized protein required for induction of ligules and auricles during maize leaf organogenesis. *Genes Dev.* 11, 616–628. doi: 10.1101/gad.11.5.616

Muszynski, M. G., Dam, T., Li, B., Shirbroun, D. M., Hou, Z., Bruggemann, E., et al. (2006). *delayed flowering1* encodes a basic leucine zipper protein that mediates floral inductive signals at the shoot apex in maize. *Plant Physiol.* 142, 1523–1536. doi: 10.1104/pp.106.088815

Nagasawa, N., Miyoshi, M., Sano, Y., Satoh, H., Hirano, H., Sakai, H., et al. (2003). *SUPERWOMAN1* and *DROOPING LEAF* genes control floral organ identity in rice. *Development* 130, 705–718. doi: 10.1242/dev.00294

Nakagawa, M., Shimamoto, K., and Kyozuka, J. (2002). Overexpression of *RCN1* and *RCN2*, rice *TERMINAL FLOWER 1/CENTRORADIALIS* homologs, confers delay of phase transition and altered panicle morphology in rice. *Plant J.* 29, 743–750. doi: 10.1046/j.1365-313X.2002.01255.x

Parenicová, L., de Folter, S., Kieffer, M., Horner, D. S., Favalli, C., Busscher, J., et al. (2003). Molecular and phylogenetic analyses of the complete MADS-box transcription factor family in Arabidopsis: new openings to the MADS world. *Plant Cell* 15, 1538–1551. doi: 10.1105/tpc.011544

Patro, R., Duggal, G., Love, M. I., Irizarry, R. A., and Kingsford, C. (2017). *Salmon* provides fast and bias-aware quantification of transcript expression. *Nat. Methods* 14, 417–419. doi: 10.1038/nmeth.4197

Pautler, M., Eveland, A. L., LaRue, T., Yang, F., Weeks, R., Lunde, C., et al. (2015). *FASCIATED EAR4* encodes a bZIP transcription factor that regulates shoot meristem size in maize. *Plant Cell* 27, 104–120. doi: 10.1105/tpc.114.132506

Phillips, K. A., Skirpan, A. L., Liu, X., Christensen, A., Slewinski, T. L., Hudson, C., et al. (2011). *vanishing tassel2* encodes a grass-specific tryptophan aminotransferase required for vegetative and reproductive development in maize. *Plant Cell* 23, 550–566. doi: 10.1105/tpc.110.075267

Preston, J. C., Wang, H., Kursel, L., Doebley, J., and Kellogg, E. A. (2012). The role of *teosinte glume architecture* (*tga1*) in coordinated regulation and evolution of grass glumes and inflorescence axes. *New Phytol.* 193, 204–215. doi: 10.1111/j.1469-8137.2011.03908.x

Revell, L. J. (2011). phytools: an R package for phylogenetic comparative biology (and other things). *Methods Ecol. Evol.* 3, 217–223. doi: 10.1111/j.2041-210X.2011.00169.x

Saeed, A. I., Sharov, V., White, J., Li, J., Liang, W., Bhagabati, N., et al. (2003). TM4: a free, open-source system for microarray data management and analysis. *Biotechniques* 34, 374–378.

Satoh-Nagasawa, N., Nagasawa, N., Malcomber, S., Sakai, H., and Jackson, D. (2006). A trehalose metabolic enzyme controls inflorescence architecture in maize. *Nature* 441, 227–230. doi: 10.1038/nature04725

Schneeberger, R. G., Becraft, P. W., Hake, S., and Freeling, M. (1995). Ectopic expression of the knox homeo box gene *rough sheath1* alters cell fate in the maize leaf. *Genes Dev.* 9, 2292–2304. doi: 10.1101/gad.9.18.2292

Schultz, E. A., and Haughn, G. W. (1991). *LEAFY*, a homeotic gene that regulates inflorescence development in Arabidopsis. *Plant Cell* 3, 771–781. doi: 10.1105/tpc.3.8.771

Somssich, M., Je, B. I., Simon, R., and Jackson, D. (2016). CLAVATA-WUSCHEL signaling in the shoot meristem. *Development* 143, 3238–3248. doi: 10.1242/dev.133645

Soneson, C., Love, M. I., and Robinson, M. D. (2015). Differential analyses for RNA-seq: transcript-level estimates improve gene-level inferences. *F1000Res.* 4:1521. doi: 10.12688/f1000research.7563.2

Soreng, R. J., Peterson, P. M., Romaschenko, K., Davidse, G., Teisher, J. K., Clark, L. G., et al. (2017). A worldwide phylogenetic classification of the Poaceae (Gramineae) II: an update and a comparison of two 2015 classifications. *J. Syst. Evol.* 55, 259–290. doi: 10.1111/jse.12262

Stamatakis, A. (2014). RAxML version 8: a tool for phylogenetic analysis and post-analysis of large phylogenies. *Bioinformatics* 30, 1312–1313. doi: 10.1093/bioinformatics/btu033

Staswick, P. E., Serban, B., Rowe, M., Tiryaki, I., Maldonado, M. T., Maldonado, M. C., et al. (2005). Characterization of an Arabidopsis enzyme family that conjugates amino acids to indole-3-acetic acid. *Plant Cell* 17, 616–627. doi: 10.1105/tpc.104.026690

Sun, X., Cahill, J., Van Hautegem, T., Feys, K., Whipple, C., Novák, O., et al. (2017). Altered expression of maize *PLASTOCHRON1* enhances biomass and seed yield by extending cell division duration. *Nat. Commun.* 8:14752. doi: 10.1038/ncomms14752

Takeda, S., Hanano, K., Kariya, A., Shimizu, S., Zhao, L., Matsui, M., et al. (2011). CUP-SHAPED COTYLEDON1 transcription factor activates the expression of *LSH4* and *LSH3*, two members of the ALOG gene family, in shoot organ boundary cells. *Plant J.* 66, 1066–1077. doi: 10.1111/j.1365-313X.2011.04571.x

Tanaka, W., Ohmori, Y., Ushijima, T., Matsusaka, H., Matsushita, T., Kumamaru, T., et al. (2015). Axillary meristem formation in rice requires the WUSCHEL ortholog TILLERS ABSENT1. *Plant Cell* 27, 1173–1184. doi: 10.1105/tpc.15.00074

Tanaka, W., Toriba, T., Ohmori, Y., Yoshida, A., Kawai, A., Mayama-Tsuchida, T., et al. (2012). The YABBY gene TONGARI-BOUSHI1 is involved in lateral organ development and maintenance of meristem organization in the rice spikelet. *Plant Cell* 24, 80–95. doi: 10.1105/tpc.111.094797

Theißen, G., Melzer, R., and Rümpler, F. (2016). MADS-domain transcription factors and the floral quartet model of flower development: linking plant development and evolution. *Development* 143, 3259–3271. doi: 10.1242/dev.134080

Thompson, B. E., Bartling, L., Whipple, C., Hall, D. H., Sakai, H., Schmidt, R., et al. (2009). *bearded-ear* encodes a MADS box transcription factor critical for maize floral development. *Plant Cell* 21, 2578–2590. doi: 10.1105/tpc.109.067751

Vollbrecht, E., Springer, P. S., Goh, L., Buckler, E. S. IV, and Martienssen, R. (2005). Architecture of floral branch systems in maize and related grasses. *Nature* 436, 1119–1126. doi: 10.1038/nature03892

Wagner, D., and Meyerowitz, E. M. (2002). SPLAYED, a novel SWI/SNF ATPase homolog, controls reproductive development in Arabidopsis. *Curr. Biol.* 12, 85–94. doi: 10.1016/S0960-9822(01)00651-0

Walsh, J., and Freeling, M. (1999). The *liguleless2* gene of maize functions during the transition from the vegetative to the reproductive shoot apex. *Plant J.* 19, 489–495. doi: 10.1046/j.1365-313X.1999.00541.x

Walsh, J., Waters, C. A., and Freeling, M. (1998). The maize gene *liguleless2* encodes a basic leucine zipper protein involved in the establishment of the leaf blade-sheath boundary. *Genes Dev.* 12, 208–218. doi: 10.1101/gad.12.2.208

Wang, L., Yin, H., Qian, Q., Yang, J., Huang, C., Hu, X., et al. (2009). NECK LEAF 1, a GATA type transcription factor, modulates organogenesis by regulating the expression of multiple regulatory genes during reproductive development in rice. *Cell Res.* 19, 598–611. doi: 10.1038/cr.2009.36

Whipple, C. J. (2017). Grass inflorescence architecture and evolution: the origin of novel signaling centers. *New Phytol.* 216, 367–372. doi: 10.1111/nph.14538

Whipple, C. J., Hall, D. H., DeBlasio, S., Taguchi-Shiobara, F., Schmidt, R. J., and Jackson, D. P. (2010). A conserved mechanism of bract suppression in the grass family. *Plant Cell* 22, 565–578. doi: 10.1105/tpc.109.073536

Xiao, H., Tang, J., Li, Y., Wang, W., Li, X., Jin, L., et al. (2009). STAMENLESS 1, encoding a single C2H2 zinc finger protein, regulates floral organ identity in rice. *Plant J.* 59, 789–801. doi: 10.1111/j.1365-313X.2009.03913.x

Yamaguchi, T., Lee, D. Y., Miyao, A., Hirochika, H., An, G., and Hirano, H.-Y. (2006). Functional diversification of the two C-class MADS box genes *OSMADS3* and *OSMADS58* in *Oryza sativa*. *Plant Cell* 18, 15–28. doi: 10.1105/tpc.105.037200

Yang, J., Thames, S., Best, N. B., Jiang, H., Huang, P., Dilkes, B. P., et al. (2017). Brassinosteroids modulate meristem fate and differentiation of unique inflorescence morphology in *Setaria viridis*. *Plant Cell* 30, 48–66. doi: 10.1105/tpc.17.00816

Yao, S.-G., Ohmori, S., Kimizu, M., and Yoshida, H. (2008). Unequal genetic redundancy of rice PISTILLATA orthologs, OsMADS2 and OsMADS4, in lodicule and stamen development. *Plant Cell Physiol.* 49, 853–857. doi: 10.1093/pcp/pcn050

Yoshida, A., Sasao, M., Yasuno, N., Takagi, K., Daimon, Y., Chen, R., et al. (2013). TAWAWA1, a regulator of rice inflorescence architecture, functions through

the suppression of meristem phase transition. *Proc. Natl. Acad. Sci. U.S.A.* 110, 767–772. doi: 10.1073/pnas.1216151110

Yoshida, A., Suzaki, T., Tanaka, W., and Hirano, H.-Y. (2009). The homeotic gene *long sterile lemma* (*G1*) specifies sterile lemma identity in the rice spikelet. *Proc. Natl. Acad. Sci. U.S.A.* 106, 20103–20108. doi: 10.1073/pnas.0907896106

Yun, J., Kim, Y.-S., Jung, J.-H., Seo, P. J., and Park, C.-M. (2012). The AT-hook motif-containing protein AHL22 regulates flowering initiation by modifying flowering LOCUS T chromatin in Arabidopsis. *J. Biol. Chem.* 287, 15307–15316. doi: 10.1074/jbc.M111.318477

Zahn, L. M., Kong, H., Leebens-Mack, J. H., Kim, S., Soltis, P. S., Landherr, L. L., et al. (2005). The evolution of the *SEPALLATA* subfamily of MADS-box genes: a preangiosperm origin with multiple duplications throughout angiosperm history. *Genetics* 169, 2209–2223. doi: 10.1534/genetics.104.037770

Zhang, D., and Yuan, Z. (2014). Molecular control of grass inflorescence development. *Annu. Rev. Plant Biol.* 65, 553–578. doi: 10.1146/annurev-arplant-050213-040104

Zhao, M., Yang, S., Chen, C.-Y., Li, C., Shan, W., Lu, W., et al. (2015). Arabidopsis BREVIPEDICELLUS interacts with the SWI2/SNF2 chromatin remodeling ATPase BRAHMA to regulate KNAT2 and KNAT6 expression in control of inflorescence architecture. *PLoS Genet.* 11:e1005125. doi: 10.1371/journal.pgen.1005125

Zhao, Q., Weber, A. L., McMullen, M. D., Guill, K., and Doebley, J. (2011). MADS-box genes of maize: frequent targets of selection during domestication. *Genet. Res.* 93, 65–75. doi: 10.1017/S0016672310000509

Zhao, Y., Medrano, L., Ohashi, K., Fletcher, J. C., Yu, H., Sakai, H., et al. (2004). HANABA TARANU is a GATA transcription factor that regulates shoot apical meristem and flower development in Arabidopsis. *Plant Cell* 16, 2586–2600. doi: 10.1105/tpc.104.024869

Zhu, C., Yang, J., and Shyu, C. (2017). Setaria comes of age: meeting report on the Second International *Setaria* Genetics Conference. *Front. Plant Sci.* 8:1562. doi: 10.3389/fpls.2017.01562

Zhu, Z., Tan, L., Fu, Y., Liu, F., Cai, H., Xie, D., et al. (2013). Genetic control of inflorescence architecture during rice domestication. *Nat. Commun.* 4:2200. doi: 10.1038/ncomms3200

Conflict of Interest Statement: The authors declare that the research was conducted in the absence of any commercial or financial relationships that could be construed as a potential conflict of interest.

frontiers in Plant Science

ORIGINAL RESEARCH
published: 31 October 2018
doi: 10.3389/fpls.2018.01585

Neural Net Classification Combined With Movement Analysis to Evaluate *Setaria viridis* as a Model System for Time of Day of Anther Appearance

Jigar S. Desai[1], *Erin Slabaugh*[1], *Donna J. Liebelt*[1], *Jacob D. Fredenberg*[1], *Benjamin N. Gray*[2], *S. V. Krishna Jagadish*[3], *Olivia Wilkins*[4] *and Colleen J. Doherty*[1]*

[1] Department of Molecular and Structural Biochemistry, North Carolina State University, Raleigh, NC, United States, [2] Benson Hill Biosystems, Inc., Saint Louis, MO, United States, [3] Department of Agronomy, Kansas State University, Manhattan, KS, United States, [4] Department of Plant Science, McGill University, Sainte-Anne-de-Bellevue, QC, Canada

In many plant species, the time of day at which flowers open to permit pollination is tightly regulated. Proper time of flower opening, or Time of Day of Anther Appearance (**TAA**), may coordinate flowering opening with pollinator activity or may shift temperature sensitive developmental processes to cooler times of the day. The genetic mechanisms that regulate the timing of this process in cereal crops are unknown. To address this knowledge gap, it is necessary to establish a monocot model system that exhibits variation in TAA. Here, we examine the suitability of *Setaria viridis*, the model for C4 photosynthesis, for such a role. We developed an imaging system to monitor the temporal regulation of growth, flower opening time, and other physiological characteristics in Setaria. This system enabled us to compare Setaria varieties Ames 32254, Ames 32276, and PI 669942 variation in growth and daily flower opening time. We observed that TAA occurs primarily at night in these three Setaria accessions. However, significant variation between the accessions was observed for both the ratio of flowers that open in the day vs. night and the specific time of day where the rate is maximal. Characterizing this physiological variation is a requisite step toward uncovering the molecular mechanisms regulating TAA. Leveraging the regulation of TAA could provide researchers with a genetic tool to improve crop productivity in new environments.

Keywords: flower opening time, spikelet opening time, timing of anthesis, setaria, developmental stage, image analysis of plants, biological image classification

OPEN ACCESS

Edited by:
Andrew Doust,
Oklahoma State University,
United States

Reviewed by:
Christian Dominik Kappel,
Universität Potsdam, Germany
Noah Fahlgren,
Donald Danforth Plant Science Center, United States

***Correspondence:**
Colleen J. Doherty
colleen_doherty@ncsu.edu

Specialty section:
This article was submitted to Plant Breeding, a section of the journal Frontiers in Plant Science

Received: *11 February 2018*
Accepted: *11 October 2018*
Published: *31 October 2018*

Citation:
Desai JS, Slabaugh E, Liebelt DJ, Fredenberg JD, Gray BN, Jagadish SVK, Wilkins O and Doherty CJ (2018) Neural Net Classification Combined With Movement Analysis to Evaluate Setaria viridis as a Model System for Time of Day of Anther Appearance. Front. Plant Sci. 9:1585. doi: 10.3389/fpls.2018.01585

INTRODUCTION

Most crops have been bred for maximum productivity in specific geographical locations and under particular management practices. In a time when weather patterns are changing the ranges in which many staple crops are grown, management practices such as planting dates and watering regimes that were optimized for one region, must be re-optimized for growth at new latitudes (Walthall et al., 2013; Challinor et al., 2014). One mechanism by which plants coordinate their activity with the local environment is through the temporal control of developmental transitions (Harmer, 2010; Bendix et al., 2015; Greenham and McClung, 2015; Nakamichi, 2015). The coordinated timing between developmental stages and environmental conditions is controlled by

the endogenous circadian clock and provides an adaptive advantage (Dodd, 2005; Yerushalmi and Green, 2009; Shrestha et al., 2014; Brambilla et al., 2017). The regulation of the developmental transition to flowering in response to photoperiod has been well characterized in Arabidopsis and has provided targets for agricultural selection and biotechnological advances (Blümel et al., 2015; Greenham and McClung, 2015; Hill and Li, 2016; Brambilla et al., 2017; Okada et al., 2017). The appropriate timing of many other developmental transitions is important for optimal coordination with the local environment, yet little is known about the molecular control of these transitions, particularly in monocot species.

The time of day of anther appearance (**TAA**), or the time of day at which flowers open in preparation for pollination, is a developmentally regulated process in dicots and monocots. Also known as time of day of flower opening time, it has been best studied in dicot species, where TAA often must coincide with pollinator activity (van Doorn and Kamdee, 2014). Many monocots, however, are wind or self-pollinated, and so TAA is constrained by other factors. TAA may be genetically and/or environmentally controlled to coincide or avoid particular environmental conditions (De Vries, 1974; Ichimura and Suto, 1998; Kobayasi et al., 2010; Colquhoun et al., 2011; Julia and Dingkuhn, 2012; Lukac et al., 2012; van Doorn and Kamdee, 2014; Aiqing et al., 2018). For example, heat-sensitive reproductive events, including anther dehiscence, pollination, and fertilization could be damaged by exposure to the hottest parts of the day resulting in spikelet sterility and corresponding decrease in agricultural yield (Jagadish et al., 2007; Kobayasi et al., 2010; Bita and Gerats, 2013; Prasad et al., 2017). Unlike the well-studied transitions between vegetative and reproductive phases of development, little is known about the molecular control of TAA in any species; some molecular controls have been identified in dicots (van Doorn and van Meeteren, 2003; Colquhoun et al., 2011; van Doorn and Kamdee, 2014), but much less is known in monocots.

The majority of cultivated rice varieties show little variation in TAA, which almost exclusively occurs within 5 h after dawn (Nishiyama and Blanco, 1981; Prasad et al., 2006; Sheehy et al., 2007; Cattivelli et al., 2008; Bheemanahalli et al., 2017). In contrast, wild rice varieties tend to show wide variation of TAA, ranging from early morning until after dusk. An early morning flowering (**EMF**) introgression line was identified (EMF20) from a cross between a wild accession of rice (*O. officinalis*) and a highly productive cultivated variety (*O. sativa, IR64*). In the EMF20 introgression line, the TAA was advanced by 1.5 h. Because the flowers opened at an earlier and cooler time of the day, the effect of high temperature on spikelet sterility during anthesis was greatly reduced in the greenhouse (Ishimaru et al., 2010) and field conditions (Bheemanahalli et al., 2017). Additionally, two EMF near isogenic lines (NILs) were generated in the Nanjing 11 and IR64 background. Both EMF NILs retained the ability to advance TAA and this earlier flowering resulted in significantly lower levels of spikelet sterility when exposed to heat stress during the day, demonstrating the effectiveness of the trait in both temperate and tropical indica backgrounds (Ishimaru et al., 2012; Hirabayashi et al., 2015; Bheemanahalli et al., 2017). A second EMF introgression line was also developed by crossing *O. rufipogon* and *O. sativa* cv Nipponbare, advancing TAA by about 3 h indicating that this control of TAA can extend to japonica cultivars of rice as well (Thanh et al., 2010). Although genetic control of TAA in rice has been confirmed by these studies, the molecular mechanisms have not been identified. Nor has this been expanded to determine if TAA is genetically controlled in other cereal species.

There are only a handful of TAA studies in other cereal species. In spring wheat, TAA occurs most often either in the early morning or the late evening coinciding with cooler atmospheric temperatures (de Vries, 1972; Aiqing et al., 2018). Unlike in rice, TAA in wheat appears to be strongly affected by environmental conditions; for example, high temperature stress during the day shifts TAA to later evening periods, resulting in flowers opening after the heat stress was released (Aiqing et al., 2018). Variability in TAA and the duration of flowering has been observed for many different wheat accessions (de Vries, 1972; De Vries, 1974). In a study of two northern European wheat varieties, the majority of TAA took place at midday within a span of 2–3 h (Lukac et al., 2012). Lukac et al. hypothesized that a wider range of TAA may improve heat resilience of wheat spikelets compared to varieties that exhibit narrow TAA characteristics.

The narrow range of TAA in domesticated rice cultivars and observed variability in wheat raises the question of whether TAA may have been a selected trait during domestication of some grasses. Identifying the mechanisms that control TAA will offer strategies to adjust TAA to regional environments. Yet, evaluation in controlled conditions will be necessary to fully distinguish between environmental and genetic influences on TAA. *Setaria viridis*, an emerging model for C4 grasses (Brutnell et al., 2010, 2015; Li and Brutnell, 2011; Bennetzen et al., 2012), may provide the opportunity to interrogate TAA in a rapidly growing, smaller stature, transformable plant system with increasing genetic resources. Three studies report observations on TAA in *Setaria* species. Siles et al. (2001) reported that for seven *Setaria italica* cultivars, TAA spanned most of the day for cultivars with elliptical seeds, and was restricted to between just before dawn and just after dusk for cultivars with round seeds (Siles et al., 2001). In a study that developed a crossing method for the common lab variety of *S viridis*, A10, Jiang et al. showed that TAA was primarily restricted to 1 h after dawn (Jiang et al., 2013). Another study analyzed TAA in the A10 variety, imaging of panicles at 1 min intervals over the course of 3 days and concluded that the majority of TAA in A10 takes place at night (Rizal et al., 2013). However, light and touch may induce flower opening (Kobayasi, 2012). In these previous studies fluorescent lights were used to take the night images or the number of open flowers was determined manually which may have interfered with the natural pattern of TAA.

To evaluate the feasibility of Setaria as a model for TAA we established a means for automating TAA analysis, so that the measurement itself does not influence the rate of flower opening. We developed an imaging system and processing pipeline that can track and classify flower opening events in both day and night conditions. We applied our pipeline to three Setaria accessions grown in identical environmental conditions and

determined that there are significant variations in TAA between the accessions. Using our imaging conditions, we also evaluated other temporal traits in these accessions and determined that leaf emergence also shows time of day variation between accessions.

MATERIALS AND METHODS

Plant Materials and Growth Conditions

Ames 32254, Ames 32276, and A10 (PI 669942) *S. viridis* seeds were obtained from GRIN (www.ars-grin.gov). A10 is a commonly used laboratory variety (Brutnell et al., 2010; Bennetzen et al., 2012). Although originating from Manitoba, Canada, A10 has been propagated in laboratory conditions for several generations. Ames 32254 and Ames 32276 originate from Manitoba, Canada and Bordeaux, France, respectively (**Supplementary Figure 1**). To break seed dormancy, 10–20 seeds from each accession were incubated with 1 mL concentrated sulfuric acid (Fisher, Hampton, NH) for 10 min, with gentle agitation. Seeds were rinsed four times with 1 mL sterile water. Sulfuric acid did not break dormancy in A10 seeds, therefore these were incubated in 1 mL 0.1% KNO_3 (Fisher, Hampton, NH) overnight at room temperature. The following day, the seeds were rinsed three times with water, then treated the same as the other varieties. Treated seeds were then placed in wet paper towels in a clear plastic container covered with plastic wrap to maintain moisture, and then placed in a growth chamber for 5–7 days. Seedlings were transplanted to soil that was composed of three parts MetroMix360 and 1-part vermiculite. Plants were fertilized three times a week with Peter's solution (NPK: 20-20-20). Chamber conditions were set to 12 h light: 12 h dark, under 4500–6500 K fluorescent lights, with a daytime temperature of 28°C and nighttime temperature of 23°C. During imaging, plants were grown in the presence of IR light at night (880 nm). Every 3 weeks 10–20 seeds were imbibed for these three Setaria accessions. When the plants transitioned to flowering the panicles were imaged using the platform described below.

Raspberry Pi Imaging Platform

Raspberry Pi single-board computers (https://www.raspberrypi.org/) were affixed with a NoIR Camera Board for infrared (IR) imaging capabilities. An IR light source was built according to the protocol developed by the Maker Group at the Danforth Center (http://maker.danforthcenter.org/). The camera and IR light source were mounted on ring stands. The focal length of the camera was manually adjusted to 10.2 cm. One image was taken every minute and images were immediately uploaded to a server using the sshpass function. Panicles were imaged for 3–4 days until flowering was complete. The image acquisition parameters for nighttime images are sensitive to the distance of IR source to object and the IR signature of the object. The optimal image acquisition parameters for night images were determined using the raspistill function and a custom optimization loop (https://github.com/DohertyLab/Setaria-Flower-Opening-Time). This loop tested all combinations of each camera option. The best camera option combination was scored by number of edges detected in night images. "–drc high –br 45" were added to night image options based on optimization scores. A sample dataset for the A10 images in both the day and night has been uploaded to https://dataverse.harvard.edu/dataverse/doherty.

Quantification of Open and Closed Flowers

Flower opening time was determined by two classification methods depending on light source. In the day the visible light spectrum provides (RGB) features to help classification of open and closed spikelets. In these conditions, neural network classification approaches excel at image classification and successfully classify open flowers for images taken in light. To apply these approaches, individual spikelets were monitored. Day time panicle images with a variety of spikelet flowering stages were used to subset spikelets into images of closed spikelets, open spikelets, and background images using LabelImg (https://github.com/tzutalin/labelImg, version 1.4.3). LabelImg was used to create an xml file of coordinates within images that indicate a location with either closed spikelets, open spikelets, or background points. An xml file was created for every panicle image used in the training set. Using the xml file and the original panicle image, all labeled xml coordinates were cropped out and converted to a list of small cropped images of closed spikelets, open spikelets, and background. This was accomplished using R package raster (version 2.58) to upload and store images in R and R package XML (version 3.98) to read the xml file into R. The images were then scaled to 34 × 34 images to meet the dimension input of Inception V3 neural network structure, the classifier we used (Szegedy et al., 2016). The list of images was converted to a 4-dimensional array. Where the 3rd dimension held RGB values and the 4th dimension held the picture order, which indicates the order of the images in the training set as they were used for learning. To summarize the input training set array had a structure of [1:34,1:34,1:3,1:6500], 1:34 is the image dimensions, 1:3 are the RBG values, and 1:6500 is the order of the images. Of the 6,500 training images 5,000 were background images, 1,000 were closed spikelets, and 500 were open spikelets. A separate vector contained label information (closed, open, and background) of the 6,500 training images. A validation set was created containing 600 images which included 500 background images, 50 closed spikelets, and 50 open spikelets. For training, mxnet's mx.model.FeedFoward.create was used to create a classification model. For the neural network configuration Inception V3 34 × 34 was used, for train.x input the described array from above was used, and for train.y the vector containing image labels was used. Other modified parameters include: num.rounds = 250, learning.rate = 0.0001, and momentum = 0.9). The validation set was scored with the eval.data option. After 250 rounds, the model reached 100% classification accuracy on the training set and 99.5% accuracy on the validation set, and 98% accuracy on the open vs. closed spikelet images (**Supplementary Figure 2**). The training phase took approximately 8 h per fifty iterations and the 250 rounds took 42 hours.

The saved model was loaded using mx.model.load. Each daytime image was segmented into 34 × 34 images as described above. If an image's dimension was not divisible by 34, it was then resized using the raster package to the closest dimension that would evenly divided by 34. For example, a 1000 × 500

panicle image would be resized to 986 × 476. Using the base R function, predict, classification probabilities of each image as closed, open, or background was determined using the same structure as the training set. The classification with the highest probability is used for the image call. To reduce processing time per image, background area was cropped from the panicle image. Raster select was used on an image stack to crop each image to the panicle region. A function was created to integrate this workflow for day time image classification. Both the function and the model can be found at https://github.com/DohertyLab/Setaria-Flower-Opening-Time.

Imaging Flower Opening Time in the Dark

All images from the 12 h night period were extracted and combined with the last image taken in the light. The last light image was used to identify the location of every spikelet as described above. The 34 × 34 images were then run through the day time flower neural network and used to identify open and closed spikelets. For the spikelets identified as closed, each spikelet image stack was cropped out to create a time series of images per spikelet (**Supplementary Videos 1–3**). Each spikelet imaged was analyzed independently and segmented into 30-min sections. The first image in each 30-min section was then subtracted from each image in the 30-min series. If at least 5% of the pixels in a spikelet image showed a change in pixel intensity that was greater than 50% of the max pixel intensity the time point of that image was considered the TAA. Often the movement associated with flower opening spanned several minutes, therefore, if a spikelet had more than one time segment with enough movement to be classified as opening, the change at the earliest time point was considered the TAA. To adjust for movement due to random vibrations or growth of the panicle the whole image was adjusted by change in the center of pixel intensity. Each consecutive image was adjusted by the previous center of pixel intensity at the previous time point so that the center of intensity was equal in all images. Validation of TAA calls for night images were confirmed by comparison to flower opening calls in the light period, that is a flower cannot open both at night and in the day, and by human assessment.

The rate of TAA was determined by calculating the total number of open flowers in a given time segment over the number of spikelets identified. For night images, the flowering time for all spikelets is combined and cumulatively summed. The cumulatively summed flowering time represents the increasing number of open flowers over the night period. This vector was then scaled to the ratio of open and closed spikelets of the previous day image and the first day image of the next day. This ratio is plotted over several day and night periods (**Supplementary Figure 3**). To find the rate of flower opening, R's smooth.spline was used to fit a function to the ratio of open and closed spikelets over time. R's deriv function was then used to find the rate of flower over time.

The *post hoc* test of the variance of the rate of TAA between accessions in the 1.5 h after dusk was performed using pairwise.t.test from the R stats package using Holm's adjustment for controlling Type I error.

Bristle Density Classifier

Bristle density was calculated by dividing the number of bristles by the total height of the panicle in the image. Bristles were identified by classifying the base pixels of the bristles and the tip pixel of the bristle. If the base of a bristle was able to be connected to a tip by continuous white pixels, then the bristle was counted. The panicle dimensions were calculated from the classified bases of each bristle. Regression lines were plotted through the bases and used to estimate the panicle dimensions. The total height of the panicle was determined by using the bottom of the image and the top intersection point of the regression lines. If the regression lines never intersect, then the row of the first white pixel not classified as a bristle from the top of the image was used. The bristle density was then calculated for each image in a set. All day time images after panicle emergence were averaged to determine the final bristle density for that panicle. Scripts are available at https://github.com/DohertyLab/Setaria-Flower-Opening-Time.

Quantification of Growth

ImageJ Fiji (https://imagej.net/Fiji/Downloads) was used to analyze the daily growth pattern of seedlings from 3 to 10 days after emergence. Dawn and dusk images at 8 a.m. and 8 p.m. were imported as an image sequence. In three replicates of each variety the second and/or third leaves were isolated first through manual cropping using the freehand selection tool and edit->clear function followed by applying a color threshold. The color threshold was adjusted and applied to the stacked images with the following parameters: hue range 39–113, saturation range 30–187, brightness range 0–255, thresholding method default, threshold color B&W, and color space HSB. Image color was then inverted and a script was applied to calculate the midpoint and length along the midpoint.

The setaria_growth_midpoint script inputs the jpeg image files, calculates the midpoint at all points along the leaf, then determines the length of the leaf from this midpoint. The total length is reported in a csv file. The leaf image is oriented vertically and the script iterates over the image, pairing white pixels across the width of the image for each row containing pixels. The pair of pixels of interest was then selected to calculate the midpoint. For all image analysis here, the leaf was oriented to be vertical in the image and we selected the left- and right-most white pixels in each row to calculate the midpoint. However, the provided script allows the user to specify this choice to adapt to different images. After the midpoints are determined along the length of the leaf, the length of this midline is calculated using the distance formula. If the line of midpoints is broken, then the distance is calculated from the two closest midpoints determined.

Quantification of Time of Leaf Emergence

The time and date of each emergence event was recorded manually using hourly images of 3- to 22-day-old seedlings. The number of emergence events at each hour was calculated using the "COUNTIF" excel function. Varieties were scaled using the number of emergence events for any given hour divided by total emergence events. The data was then graphed using the smooth.spline function in R with a degree of freedom of 3 as confirmed by a cross validation.

A

	True Positive	True Negative	False Positive	False Negative	Total
Day	48	50	0	2	100
Night	10	15	0	5	30

B

	Day 1	Day 2	Day 3
Open:Total Spikelets	0.24	0.667	0.95
			

FIGURE 1 | Evaluation of accuracy in flower opening analysis in A10 accession against human classification of images. **(A)** Table of results from the validation of day and night classification models. Validation of daytime classification was tested against 600 hold-out images. Validation of flower opening calls in IR images (Night) was tested against 30 time-lapse videos. True positive and true negative are flowers that were correctly called as "open" or "closed," respectively. **(B)** Table of the progression of the ratio of open spikelets to total spikelets for three daytime images based on the classification model for the daytime.

RESULTS

Determining TAA During Light Periods

Using the A10 accession of Setaria, we optimized our image capture and analysis platform. Images were taken every minute after panicle emergence until plants showed no more flower opening for a 24 h period using a Raspberry PI camera system. An IR light source (http://maker.danforthcenter.org/) was constructed and used for nighttime imaging. For each spikelet, the TAA for daytime images was quantified using Inception V3 convolutional neural network structure (**InceptionV3cnn**) (Szegedy et al., 2016). The training set consisted of 5,000 background images (e.g., leaf, stem, bristles, or other non-panicle images), 1,000 closed spikelets, and 500 open spikelets classified by two researchers. The model was trained until the prediction accuracy for the holdout validation set of 600 images (500 background, 50 closed spikelets, and 50 open spikelets) exceeded 99% (**Figure 1A**). Images of the A10 accession taken at 10-min intervals were then evaluated using this trained classifier. Each spikelet was classified as background, closed spikelet, or open spikelet. Each analysis was evaluated to ensure that the percent of open panicles increased with time (**Figure 1B**) and the initiation of flower opening and full flower opening agreed with human assessment as verified independently by two individuals.

Determining TAA in Night Images

We were unable to train the InceptionV3cnn classifier to correctly distinguish between open and closed flowers in the nighttime images. Images taken of plants illuminated by the IR light lacked the visible spectrum features the classifier used to distinguish between open and closed flowers. Therefore, we developed an approach to detect flower opening in nighttime images based on the movement of the flowers as they open (**Figure 2**, **Supplementary Videos 1–6**). A time series image stack was made for each spikelet that remained unopened in the last image of the day. The movement of each spikelet was monitored in 30-min intervals throughout the night images. A spikelet was determined to be flowering in the 30-min window if 5% of pixels showed a change in intensity greater than 50% of the total intensity value in the 30-min window. To account for background movement of the spikelet, the center of pixel intensity was used to adjust the frame around the whole panicle image. That is, as the center of pixel intensity for a spikelet moved relative to the frame, the entire frame was adjusted with the same change in intensity. The 30-min window with the earliest movement was classified as the TAA for that spikelet. The correct classification of TAA at night was validated by manually viewing 30 spikelets time series and identifying spikelets that were correctly called as transitioning to an open flower. Accuracy of nighttime flower opening was 83.3% (**Figure 1A**). Error in flower opening classification exclusively came from false negative calls (**Figure 1A**). Lowering the sensitivity for flower opening introduced more false positives. As our objective was to identify the rate of flower opening, we elected to proceed with the approach that used the higher sensitivity and calculate TAA as the rate of the detected flowers that open. The established night time flowering protocol was efficiently detecting flower opening time and could address variability in TAA across different accessions. Once the imaging setup and analysis pipeline was successfully established for the A10 accession, we then assessed its performance on other accessions.

Variation in Bristle Density Impacts Daytime Classification of Flower Opening

We imaged panicles for three accessions of *Setaria viridis:* Ames 32254, Ames 32276, and A10. We selected these lines because they consistently produced panicles in our chamber conditions and spanned a range of latitudes (49.64306000, 44.82616900). We tested both our day and nighttime TAA classification pipeline on these three accessions and found that while our nighttime movement algorithm performed equally well for all accessions, the variation in bristle density affected the performance of the daytime image analysis (**Figure 3**). Our early versions of the InceptionV3cnn reached peak performance only when trained with a data set of similar bristle density. Therefore, in anticipation of evaluating multiple accessions, we developed a classifier to categorize bristle density from a given training set (**Figure 3**). However, when properly trained with panicle images from each of the three accessions the InceptionV3cnn classifier performed equally well on all three accessions, and only one model was required.

Setaria Accessions Show Variation in TAA

The TAA was determined for three independent panicles for each accession. The rate of flowering was determined by taking

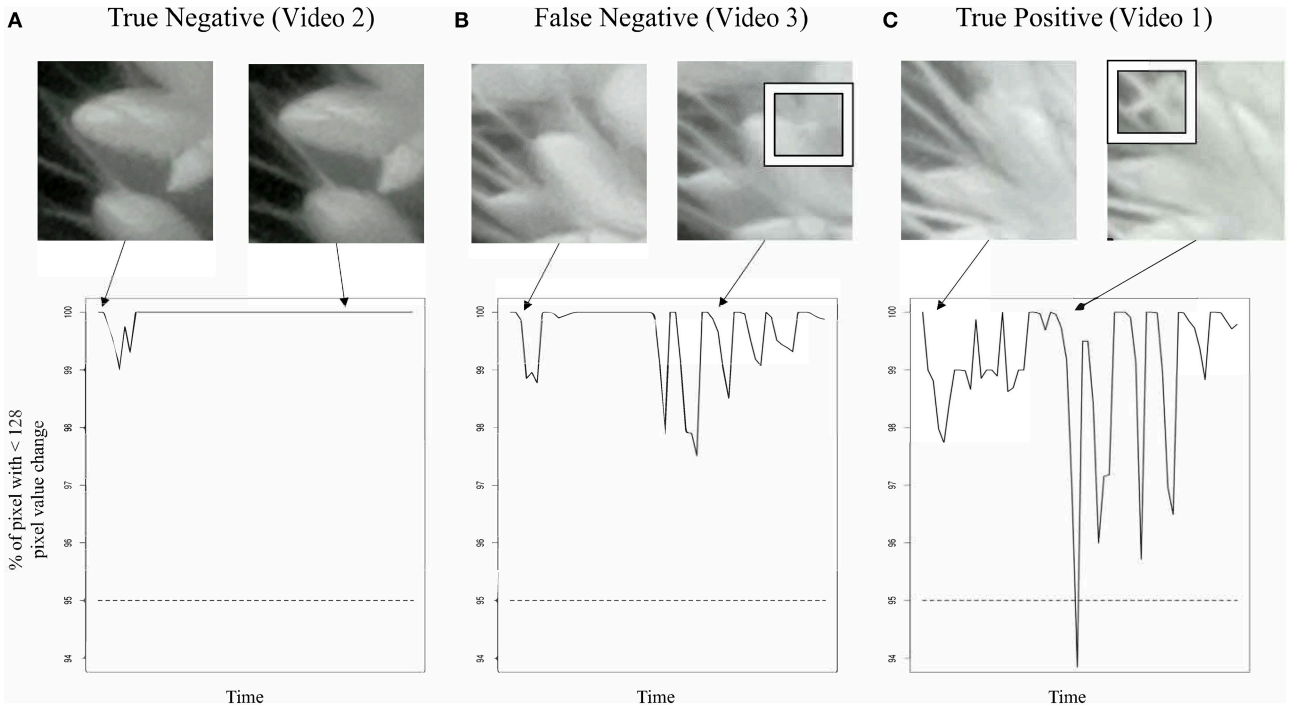

FIGURE 2 | Classification of TAA in nighttime images. Snapshots from nighttime image set (top row) and graph of movement detection (bottom row) for three selected spikelet nighttime image sets. **(A)** A true negative example. A spikelet classified as not opening that is validated as not opening in this 12 h time series, corresponds to Video 2. **(B)** A false negative example, a spikelet classified as not opening that does open. Inset box highlights anther appearance, corresponds to Video 3. **(C)** A true positive example, a spikelet classified as opening that does open in the 12 h time series. Inset box highlights anther appearance, corresponds to Video 1.

FIGURE 3 | Dot plot of the bristle density of A10, Ames 32254, and Ames 32276 (Student's *t*-test * < 0.05, $N = 3$) bar indicates mean for each accession.

the derivative of the ratio of open to closed spikelets over time. We normalized the rate of flower opening by the maximum rate of flowering per panicle. For all three accessions the rate of TAA was highest at night (**Figures 4**, **5**). To ensure that this was not due to differences between the classifiers, we evaluated the calls of the InceptionV3cnn classifier of the first and last image in the light, which confirmed that of the flowers identified as opened during the night. This observation is in agreement with a previous report that flower opening is predominantly restricted to the nighttime hours in *S. viridis* (Rizal et al., 2013). Further evaluation of the specific period in the night when the highest rate of TAA occurs indicates unique temporal differences between the varieties (**Figure 5**). A10 panicles show a low rate of flowering throughout the first half of the night, and then the flowering rate peaks after midnight and maintains this rate until dawn. Ames 32254 and Ames 32276 show almost no flower opening during the majority of the day period. These accessions appear to initiate flowering before dusk and the peak of flowering rate occurs just after dusk. Flowering rate drops off in Ames 32254 before midnight while the peak rate of flower opening for Ames 32276 occurs in the middle of the night. The variation between accessions indicates that select time intervals can be subset and examined to identify differences in TAA between accessions. For example, the rate of flower opening can be distinguished between the three accessions in the 1.5 h after dusk, but not in the 1.5 h after dawn (**Figure 5**). An analysis of variance was performed at these two times and showed that the effect of accession type was significant at dusk, but not at dawn [$F_{Dusk\ (2,6)} = 11.68$, $p\text{-value}_{Dusk} < 0.01$ $F_{Dawn\ (2,6)} = 1.43$, $p\text{-value}_{Dawn} > 0.1$). *Post hoc* test results of the 1.5 h after dusk time interval indicated that there is a significant difference between all three accessions (Holm's adjusted p-value < 0.05).

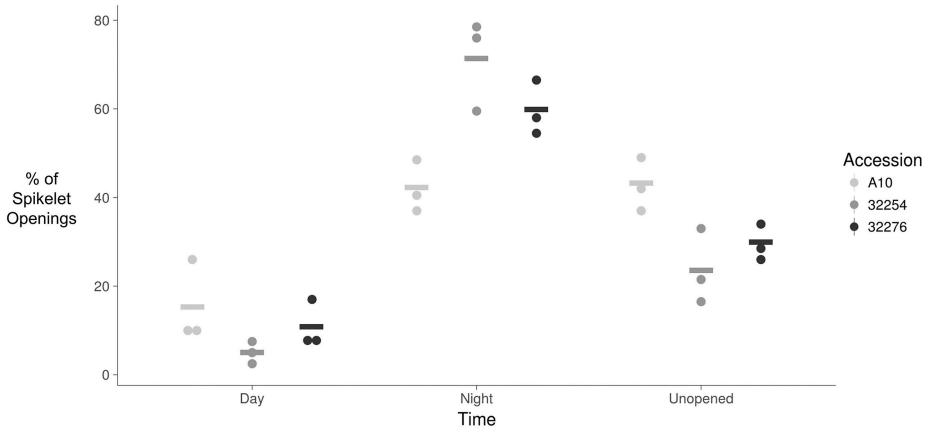

FIGURE 4 | Dot plot of percent of flower opening that occurs during the day, night, or remains unopened for A10, Ames 32254, and Ames 32276. Data represents all flowering opening events that were captured over a 3 day period ($N = 3$) bar indicates mean for each accession.

Time of Leaf Emergence Varies Between the Three Setaria Accessions

Time of leaf emergence has been reported to be under circadian control in Arabidopsis (Kim et al., 2016). To evaluate the potential for variation in time of day of leaf emergence in Setaria between accessions, leaf emergence was evaluated hourly. The time of emergence for accessions A10, Ames 32276 and Ames 32254 were graphed as a fraction of total emergence events observed for each variety (**Figure 6**). Leaf emergence in accession Ames 32254 begins prior to dawn, with the leaf emergence rate peaking in the period around dawn. In contrast, accessions A10 and Ames 32276 show very low rates of leaf emergence before dawn and the highest rate of leaf emergence in the period just after dawn. Little difference is observed between accessions A10 and Ames 32276. The period prior to dawn provides a clear distinction in leaf emergence rates between accessions A10 and Ames 32254.

Timing of Leaf Growth Varies Between the Three Setaria Accessions

We evaluated leaf growth, broadly distinguishing between how much the leaf grew in the 12 h between dawn and dusk and how much it grew in the night period. The majority of the growth for all three accessions in our conditions occurred in the light period (**Figure 7**). This is consistent with a previous analysis of *Brachypodium distachyon*, where growth rate was not constrained to a specific time of day, but was primarily responsive to temperature changes (Matos et al., 2014). We observed little variation in the amount of growth between these three accessions during the daytime. A more detailed analysis will be necessary to determine if there is variation in the specific time during the day when growth occurs.

DISCUSSION

Advantages of Identifying the Molecular Mechanisms of TAA

Little is known about the genetic regulators of TAA, particularly in monocot species (van Doorn and Kamdee, 2014). Heat escape mechanisms can be used by plants particularly field crops, to avoid high temperature stress by moving heat-sensitive processes, such as TAA and pollination related events to cooler times of the day (Jagadish et al., 2015; Ohama et al., 2017). Pollen development and anthesis have been shown to be highly sensitive to heat stresses in multiple crops including rice, wheat, and sorghum (Satake and Yoshida, 1978; Jagadish et al., 2007; Jain et al., 2007, 2010; Oliver et al., 2007; Ji et al., 2010, 2011). In rice, altering TAA through introgression of genomic regions from earlier flowering wild accessions results in higher spikelet fertility and grain yield under high temperatures (Ishimaru et al., 2012; Hirabayashi et al., 2015; Bheemanahalli et al., 2017). Although the effectiveness of this trait has been demonstrated at the agronomic scale, the molecular components that drive this change are unknown. Yet, without knowing the molecular components driving TAA, the full opportunities for optimizing TAA in rice and other monocot species cannot be achieved. Hence, identifying the molecular mechanisms that alter TAA in monocot species will enable more precise control of TAA in economically important crop species through breeding and/or biotechnology.

Efforts to identify the genetic regulators of TAA could be affected by environmental variation. Characterization of the environmental factors that influence TAA have revealed differences between rice genotypes, which has been reported as impervious to environmental perturbations (Kobayasi et al., 2010) and wheat where TAA is altered by high temperature (Aiqing et al., 2018). Evaluation of TAA in controlled conditions will reduce the potential confounding effects of environmental variables. *Setaria viridis*, with its small stature and rapid generation time (Li and Brutnell, 2011) could serve as a model for TAA in monocot species if genetic variation in TAA exists between Setaria varieties and this could help unravel the relationship between genotype and environment that may influence TAA by controlling environmental conditions in the greenhouse. We developed an image capture and analysis pipeline to classify TAA in *Setaria viridis*, demonstrated that the approach functions well in three different accessions, and identified variation in TAA between the three accessions. With

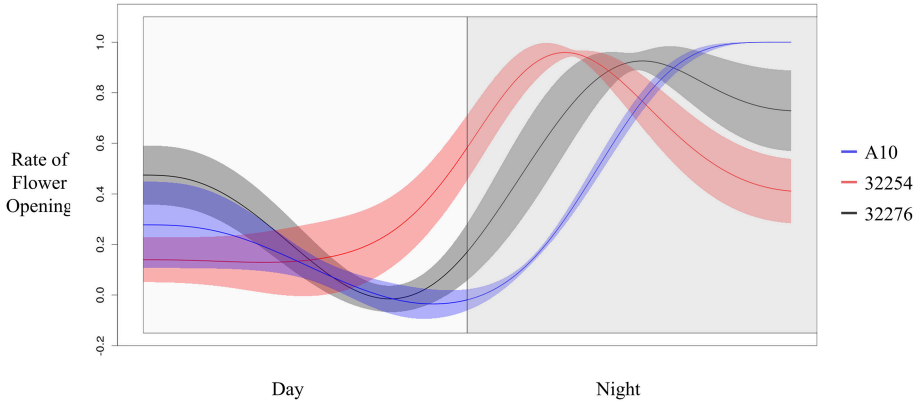

FIGURE 5 | Rate of flower opening of A10 (blue), Ames 32254 (red), and Ames 32276 (black). Rate of flower was normalized by the max rate of each variety. Shading represents the standard error at each timepoint ($N = 3$).

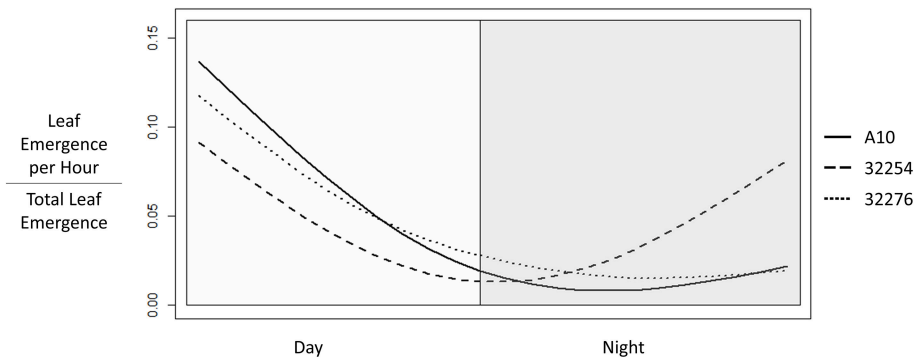

FIGURE 6 | Time of Leaf Emergence events for *Setaria viridis* varieties A10, Ames 32254, and Ames 32276 were determined from hourly images of 3 to 22 day old seedlings. The graph was constructed using the smooth.spline function in R with three degrees of freedom to show the fraction of emergence events at each hour in a 24 h period with day hours being from 8 a.m. to 8 p.m.

this imaging pipeline, the larger genetic resources available in *Setaria viridis* can be exploited to determine the mechanisms regulating TAA.

Potential for High-Throughput Analysis of TAA in Setaria

This approach was completed with a single imaging system. Given the low-cost of the Raspberry Pi, NoIR Camera, and IR light system, the throughput of this analysis can be increased. Higher throughput temporal imaging of multiple accessions will face two major challenges: the storage requirements for images and the processing time required for identifying TAA in IR-lit images based on movement. For the daytime images, the InceptionV3cnn approach was able to classify open spikelets in a computationally efficient manner that is suitable for adaptation to high-throughput analysis. The movement-based analysis was also able to classify spikelet opening in daytime images; however, this approach took about ten times longer than the InceptionV3cnn to apply and would not be suitable for large high-throughput datasets. In the IR-images, the InceptionV3cnn approach was not able to distinguish between open and closed spikelets. For these images, the challenge of the amount of time required for processing could be reduced by identifying specific times where differences are greatest between accessions. Additionally, we have not fully explored the effects of image compression or reducing the image quality on the ability to accurately determine TAA. If lower quality images perform as well, this could reduce the storage requirements. Reduced image size may also improve the feasibility of parallelizing the nighttime image analysis. Evaluating options for improving the distribution of individual processes for parallel processing will also enhance the throughput of the nighttime image analysis. Perhaps the most promising approach to improving the throughput is to first screen for differences in the percent of flowers that open in the day vs. night. This evaluation would reduce the required images to two per day and since the first and last image in the light could be used to determine this ratio, the InceptionV3cnn classifier could be used to identify open flowers.

Additional Improvements for Image Analysis

One challenge in the image analysis pipeline was identifying the spikelets themselves. Our approach, sectioning the panicle image, is appropriate for identifying when the detected flowers

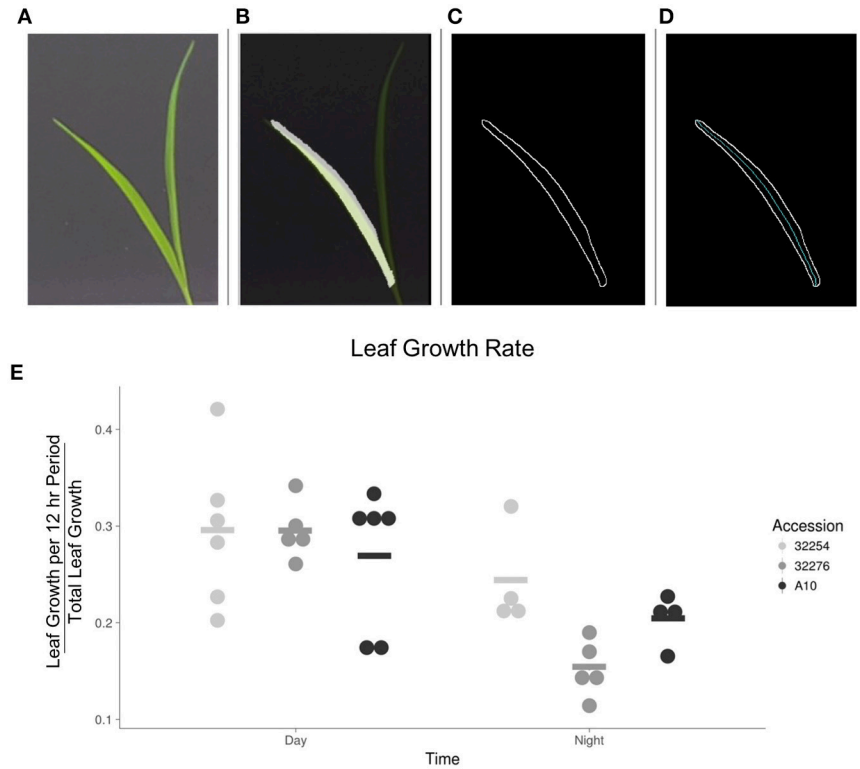

FIGURE 7 | Image analysis of leaf growth. **(A)** Original leaf image (leaf 3, 48 h after emergence). **(B)** Cropped image with a transparent original image overlaid. **(C)** Visualization of edge detection results. **(D)** Visualization of the calculation of the midline used to determine length of leaf. **(E)** Graph of the rate of growth as a percentage of the total growth for the three accessions in the day vs. the night ($N = 3$), bar indicates mean for each accession.

open since we only evaluated TAA based on the total spikelets detected. However, this approach may miss individual spikelets and therefore would not be sufficient for quantifying the number of flowers per panicle, size of individual spikelets, and other characteristics of interest for comparing between varieties. This is an area that requires further investigation to identify successful algorithms.

Setaria viridis as a Model for TAA

Similar to previously published reports in rice and wheat, in identical growth conditions genetic variation in TAA exists in Setaria. In our growth conditions, the three accessions we evaluated showed the majority of flowers opening at night. Overall TAA was restricted to the nighttime and the period just after dawn. Yet differences in the TAA could be distinguished between the accessions (**Figures 4**, **5**). From 3 to 6 h after dusk, and in the 3 h prior to dawn TAA rates in A10 could be distinguished from Ames 32276 and Ames 32254. The 2 h prior to dusk through 3 h after dusk provided the best time to distinguish between Ames 32276 and Ames 32254. For two Setaria accessions that show variation in TAA, the highest resolution of image acquisition could be concentrated to the time period where there is the greatest difference in the rate of TAA, thus reducing the number of images needed. For some accession comparisons, the total difference in the percent of spikelets that open in the day vs. the night can be distinguished. This difference could be tracked by measuring only the first and last image in the light. For such comparisons, this would greatly reduce the number of images that need to be captured and the analysis could be performed only on daytime images, which are not as computationally expensive for determining TAA.

The environmental plasticity of TAA in Setaria has not yet been examined, but this imaging system can provide the opportunity to determine if Setaria accessions show sensitivity in TAA similar to wheat or are reticent to changes in TAA like rice. This imaging system and platform will enable the evaluation of the effects of temperature, photoperiod, humidity, and stresses on TAA. The role of the circadian clock in regulation of TAA can be evaluated. Furthermore, Setaria cultivars can be examined to evaluate if there is genetic variation in the plasticity of the response to TAA.

We speculate that TAA may be a trait that is under selective pressure during domestication. In rice an evaluation of TAA across multiple wild accessions and domestic cultivars indicated that the domesticated cultivars typically completed TAA within a 1–2 h window (Nishiyama and Blanco, 1981; Prasad et al., 2006; Sheehy et al., 2007; Cattivelli et al., 2008; Bheemanahalli et al., 2017). In contrast, most wild varieties showed a much broader range of TAA (Sheehy et al., 2007). Efforts to reduce outcrossing and genetic variation in domesticated cultivars may inadvertently select for a narrow TAA. Alternatively, a narrow range of TAA may be linked to beneficial yield traits. It is

important to note that the A10 accession has been lab-grown for several generations, while the Ames 32276 and Ames 32254 accessions were more recently collected. The differences we observe here could be due to the selection of A10 under growth conditions distinct from the other accessions, perhaps indicating an early stage of domestication. Alternatively, there could be epigenetic differences in A10 due to the continued growth in laboratory conditions. The Setaria model system provides the opportunity to examine the sources of variation in TAA between wild *Setaria viridis* accessions and domesticated *Setaria italica* cultivars (Bennetzen et al., 2012; Mauro-Herrera et al., 2013; Qie et al., 2014).

AUTHOR CONTRIBUTIONS

ES, BG, SVKJ, OW, and CD conceived of the original concept. ES optimized Setaria growth and cultivation conditions to acquire healthy panicles for imaging. ES and JD optimized camera imaging. JD developed the script for optimizing camera parameters. JD identified, tested, and optimized the image processing and analysis algorithms for detecting TAA. JD and ES performed manual validation of TAA calls. JD and DL optimized image acquisition of setaria seedlings. JF developed the analysis of bristle density, leaf growth, and panicle growth. JF and DL optimized image processing and analysis of seedling growth. JD, ES, DL, JF, BG, SVKJ, OW, and CD contributed to the manuscript preparation including figure production, writing, and editing.

FUNDING

This project was supported by the North Carolina Biotechnology Center #2015-CFG-8006, the Agriculture and Food Research Initiative grant # 20156701322814 of the USDA National Institute of Food and Agriculture and the USDA National Institute of Food and Agriculture project 1002035. Contribution no. 19-073-J of the Kansas Agricultural Experiment Station.

ACKNOWLEDGMENTS

We sincerely thank GRIN for the seeds and advice on plant cultivation, and the setaria community for advice and on-line resources for working with setaria. In addition, we would like to specifically thank Ryan Sartor for the helpful discussion and advice on implementing and optimizing the numerous and approaches and machine learning algorithms we tested to determine FOT in IR-lit images, Gretchen Spiess, and Mallory Schlechte for assistance with optimizing Setaria growth conditions.

SUPPLEMENTARY MATERIAL

The Supplementary Material for this article can be found online at: https://www.frontiersin.org/articles/10.3389/fpls.2018.01585/full#supplementary-material

REFERENCES

Aiqing, S., Somayanda, I., Sebastian, S. V., Singh, K., Gill, K., Prasad, P. V. V., et al. (2018). Heat stress during flowering affects time of day of flowering, seed set, and grain quality in spring wheat. *Crop Sci.* 58:380. doi: 10.2135/cropsci2017.04.0221

Bendix, C., Marshall, C. M., and Harmon, F. G. (2015). Circadian clock genes universally control key agricultural traits. *Mol. Plant* 8, 1135–1152. doi: 10.1016/j.molp.2015.03.003

Bennetzen, J. L., Schmutz, J., Wang, H., Percifield, R., Hawkins, J., Pontaroli, A. C., et al. (2012). Reference genome sequence of the model plant Setaria. *Nat. Biotechnol.* 30, 555–561. doi: 10.1038/nbt.2196

Bheemanahalli, R., Sathishraj, R., Manoharan, M., Sumanth, H. N. H., Muthurajan, R., Ishimaru, T., et al. (2017). Is early morning flowering an effective trait to minimize heat stress damage during flowering in rice? *F. Crop. Res.* 203, 1–6. doi: 10.1016/j.fcr.2016.11.011

Bita, C. E., and Gerats, T. (2013). Plant tolerance to high temperature in a changing environment: scientific fundamentals and production of heat stress-tolerant crops. *Front. Plant Sci.* 4, 1–18. doi: 10.3389/fpls.2013.00273

Blümel, M., Dally, N., and Jung, C. (2015). Flowering time regulation in crops-what did we learn from Arabidopsis? *Curr. Opin. Biotechnol.* 32, 121–129. doi: 10.1016/j.copbio.2014.11.023

Brambilla, V., Gomez-Ariza, J., Cerise, M., and Fornara, F. (2017). The importance of being on time: regulatory networks controlling photoperiodic flowering in cereals. *Front. Plant Sci.* 8:665. doi: 10.3389/fpls.2017.00665

Brutnell, T. P., Bennetzen, J. L., and Vogel, J. P. (2015). Brachypodium distachyon and setaria viridis: model genetic systems for the grasses. *Annu. Rev. Plant Biol.* 66, 465–485. doi: 10.1146/annurev-arplant-042811-105528

Brutnell, T. P., Wang, L., Swartwood, K., Goldschmidt, A., Jackson, D., Zhu, X.-G., et al. (2010). Setaria viridis: a model for C4 photosynthesis. *Plant Cell Online* 22, 2537–2544. doi: 10.1105/tpc.110.075309

Cattivelli, L., Rizza, F., Badeck, F.-W., Mazzucotelli, E., Mastrangelo, A. M., Francia, E., et al. (2008). Drought tolerance improvement in crop plants: an integrated view from breeding to genomics. *F. Crop. Res.* 105, 1–14. doi: 10.1016/j.fcr.2007.07.004

Challinor, A. J., Watson, J., Lobell, D. B., Howden, S. M., Smith, D. R., and Chhetri, N. (2014). A meta-analysis of crop yield under climate change and adaptation. *Nat. Clim. Chang.* 4, 287–291. doi: 10.1038/nclimate2153

Colquhoun, T. A., Schwieterman, M. L., Wedde, A. E., Schimmel, B. C. J., Marciniak, D. M., Verdonk, J. C., et al. (2011). EOBII controls flower opening by functioning as a general transcriptomic switch. *Plant Physiol.* 156, 974–984. doi: 10.1104/pp.111.176248

de Vries, A. P. (1972). Some aspects of cross-pollination in wheat (*Triticum aestivum* L.) 1. Pollen concentration in the field as influenced by variety, diurnal pattern, weather conditions and level as compared to the height of the pollen donor. *Euphytica* 21, 185–203. doi: 10.1007/BF00036759

De Vries, A. P. (1974). Some aspects of cross-pollination in wheat (*Triticum aestivum* L.). 4. Seed set on male sterile plants as influenced by distance from the pollen source, pollinator: male sterile ratio and width of the male sterile strip. *Euphytica* 23, 601–622. doi: 10.1007/BF00022483

Dodd, A. N. (2005). Plant circadian clocks increase photosynthesis, growth, survival, and competitive advantage. *Science* 309, 630–633. doi: 10.1126/science.1115581

Greenham, K., and McClung, C. R. (2015). Integrating circadian dynamics with physiological processes in plants. *Nat. Rev. Genet.* 16, 598–610. doi: 10.1038/nrg3976

Harmer, S. (2010). Plant biology in the fourth dimension. *Plant Physiol.* 154, 467–470. doi: 10.1104/pp.110.161448

Hill, C. B., and Li, C. (2016). Genetic architecture of flowering phenology in cereals and opportunities for crop improvement. *Front. Plant Sci.* 7:1906. doi: 10.3389/fpls.2016.01906

Hirabayashi, H., Sasaki, K., Kambe, T., Gannaban, R. B., Miras, M. A., Mendioro, M. S., et al. (2015). QEMF3, a novel QTL for the early-morning flowering trait

from wild rice, Oryza officinalis, to mitigate heat stress damage at flowering in rice, *O. sativa*. *J. Exp. Bot.* 66, 1227–1236. doi: 10.1093/jxb/eru474

Ichimura, K., and Suto, K. (1998). Environmental factors controlling flower opening and closing in a portulaca hybrid. *Ann. Bot.* 82, 67–70. doi: 10.1006/anbo.1998.0642

Ishimaru, T., Hirabayashi, H., Ida, M., Takai, T., San-Oh, Y. A., Yoshinaga, S., et al. (2010). A genetic resource for early-morning flowering trait of wild rice *Oryza officinalis* to mitigate high temperature-induced spikelet sterility at anthesis. *Ann. Bot.* 106, 515–520. doi: 10.1093/aob/mcq124

Ishimaru, T., Hirabayashi, H., Kuwagata, T., Ogawa, T., and Kondo, M. (2012). The early-morning flowering trait of rice reduces spikelet sterility under windy and elevated temperature conditions at anthesis. *Plant Prod. Sci.* 15, 19–22. doi: 10.1626/pps.15.19

Jagadish, S. V., Craufurd, P. Q., and Wheeler, T. R. (2007). High temperature stress and spikelet fertility in rice (*Oryza sativa* L.). *J. Exp. Bot.* 58, 1627–1635. doi: 10.1093/jxb/erm003

Jagadish, S. V., Murty, M. V., and Quick, W. P. (2015). Rice responses to rising temperatures-challenges, perspectives and future directions. *Plant Cell Environ.* 38, 1686–1698. doi: 10.1111/pce.12430

Jain, M., Chourey, P. S., Boote, K. J., and Allen, L. H. (2010). Short-term high temperature growth conditions during vegetative-to-reproductive phase transition irreversibly compromise cell wall invertase-mediated sucrose catalysis and microspore meiosis in grain sorghum (Sorghum bicolor). *J. Plant Physiol.* 167, 578–582. doi: 10.1016/j.jplph.2009.11.007

Jain, M., Prasad, P. V. V., Boote, K. J., Hartwell, A. L., and Chourey, P. S. (2007). Effects of season-long high temperature growth conditions on sugar-to-starch metabolism in developing microspores of grain sorghum (Sorghum bicolor L. Moench). *Planta* 227, 67–79. doi: 10.1007/s00425-007-0595-y

Ji, X., Dong, B., Shiran, B., Talbot, M. J., Edlington, J. E., Hughes, T., et al. (2011). Control of abscisic acid catabolism and abscisic acid homeostasis is important for reproductive stage stress tolerance in cereals. *Plant Physiol.* 156, 647–662. doi: 10.1104/pp.111.176164

Ji, X., Shiran, B., Wan, J., Lewis, D. C., Jenkins, C. L. D., Condon, A. G., et al. (2010). Importance of pre-anthesis anther sink strength for maintenance of grain number during reproductive stage water stress in wheat. *Plant. Cell Environ.* 33, 926–942. doi: 10.1111/j.1365-3040.2010.02130.x

Jiang, H., Barbier, H., and Brutnell, T. (2013). Methods for performing crosses in *Setaria viridis*, a new model system for the grasses. *J. Vis. Exp.* 80:e50527. doi: 10.3791/50527

Julia, C., and Dingkuhn, M. (2012). Variation in time of day of anthesis in rice in different climatic environments. *Eur. J. Agron.* 43, 166–174. doi: 10.1016/j.eja.2012.06.007

Kim, H., Kim, Y., Yeom, M., Lim, J., and Nam, H. G. (2016). Age-associated circadian period changes in Arabidopsis leaves. *J. Exp. Bot.* 67, 2665–2673. doi: 10.1093/jxb/erw097

Kobayasi, K. (2012). "Effects of solar radiation on fertility and the flower opening time in rice under heat stress conditions," in *Solar Radiation*, ed E. B. Babatunde (Rijeka: In Tech Open), 245–266. doi: 10.5772/35393

Kobayasi, K., Matsui, T., Yoshimoto, M., and Hasegawa, T. (2010). Effects of temperature, solar radiation, and vapor-pressure deficit on flower opening time in rice. *Plant Prod. Sci.* 13, 21–28. doi: 10.1626/pps.13.21

Li, P., and Brutnell, T. P. (2011). *Setaria viridis* and *Setaria italica*, model genetic systems for the Panicoid grasses. *J. Exp. Bot.* 62, 3031–3037. doi: 10.1093/jxb/err096

Lukac, M., Gooding, M. J., Griffiths, S., and Jones, H. E. (2012). Asynchronous flowering and within-plant flowering diversity in wheat and the implications for crop resilience to heat. *Ann. Bot.* 109, 843–850. doi: 10.1093/aob/mcr308

Matos, D. A., Cole, B. J., Whitney, I. P., MacKinnon, K. J. M., Kay, S. A., and Hazen, S. P. (2014). Daily changes in temperature, not the circadian clock, regulate growth rate in Brachypodium distachyon. *PLoS ONE* 9:e100072. doi: 10.1371/journal.pone.0100072

Mauro-Herrera, M., Wang, X., Barbier, H., Brutnell, T. P., Devos, K. M., and Doust, A. N. (2013). Genetic control and comparative genomic analysis of flowering time in setaria (Poaceae). *G3 Genes Genomes Genet.* 3, 283–295. doi: 10.1534/g3.112.005207

Nakamichi, N. (2015). Adaptation to the local environment by modifications of the photoperiod response in crops. *Plant Cell Physiol.* 56, 594–604. doi: 10.1093/pcp/pcu181

Nishiyama, I., and Blanco, L. (1981). Artificial control of flower opening time during the day in rice plants. *Japan J. Crop Sci.* 50, 59–66. doi: 10.1626/jcs.50.59

Ohama, N., Sato, H., Shinozaki, K., and Yamaguchi-Shinozaki, K. (2017). Transcriptional regulatory network of plant heat stress response. *Trends Plant Sci.* 22, 53–65. doi: 10.1016/j.tplants.2016.08.015

Okada, R., Nemoto, Y., Endo-Higashi, N., and Izawa, T. (2017). Synthetic control of flowering in rice independent of the cultivation environment. *Nat. Plants* 3:17039. doi: 10.1038/nplants.2017.39

Oliver, S. N., Dennis, E. S., and Dolferus, R. (2007). ABA regulates apoplastic sugar transport and is a potential signal for cold-induced pollen sterility in rice. *Plant Cell Physiol.* 48, 1319–1330. doi: 10.1093/pcp/pcm100

Prasad, P. V. V., Bheemanahalli, R., and Jagadish, S. V. K. (2017). Field crops and the fear of heat stress—opportunities, challenges and future directions. *F. Crop. Res.* 200, 114–121. doi: 10.1016/j.fcr.2016.09.024

Prasad, P. V. V., Boote, K. J., Allen Jr, L. H., Sheehy, J. E., and Thomas, J. M. G. (2006). Species, ecotype and cultivar differences in spikelet fertility and harvest index of rice in response to high temperature stress. *F. Crop. Res.* 95, 398–411. doi: 10.1016/j.fcr.2005.04.008

Qie, L., Jia, G., Zhang, W., Schnable, J., Shang, Z., Li, W., et al. (2014). Mapping of Quantitative Trait Locus (QTLs) that contribute to germination and early seedling drought tolerance in the interspecific cross *Setaria italica* x *Setaria viridis*. *PLoS ONE* 9:e0101868. doi: 10.1371/journal.pone.0101868

Rizal, G., Acebron, K., Mogul, R., Karki, S., Larazo, N., and Quick, W. P. (2013). Study of flowering pattern in *Setaria viridis*, a proposed model species for c4 photosynthesis research. *J. Bot.* 2013, 1–7. doi: 10.1155/2013/592429

Satake, T., and Yoshida, S. (1978). High temperature-induced sterility in indica rices at flowering. *Jap. J. Crop Sci.* 47, 6–17. doi: 10.1626/jcs.47.6

Sheehy, J. E., Mabilangan, A. E., Dionora, M. J. A., and Pablico, P. P. (2007). Time of day of flowering in wild species of the genus Oryza. *Int. Rice Res. Notes* 32, 12–13.

Shrestha, R., Gómez-Ariza, J., Brambilla, V., and Fornara, F. (2014). Molecular control of seasonal flowering in rice, arabidopsis and temperate cereals. *Ann. Bot.* 114, 1445–1458. doi: 10.1093/aob/mcu032

Siles, M. M., Baltensperger, D. D., and Nelson, L. A. (2001). Technique for artificial hybridization of foxtail millet [*Setaria italica* (L.) Beauv.]. *Crop Sci.* 41, 1408–1412. doi: 10.2135/cropsci2001.4151408x

Szegedy, C., Vanhoucke, V., Ioffe, S., Shlens, J., and Wojna, Z. (2016). "Rethinking the inception architecture for computer vision," in *Proceedings of the IEEE Conference on Computer Vision and Pattern Recognition*, 2818–2826.

Thanh, P. T., Phan, P. D. T., Ishikawa, R., and Ishii, T. (2010). QTL analysis for flowering time using backcross population between *Oryza sativa* Nipponbare and *O. rufipogon*. *Genes Genet. Syst.* 85, 273–279. doi: 10.1266/ggs.85.273

van Doorn, W. G., and Kamdee, C. (2014). Flower opening and closure: an update. *J. Exp. Bot.* 65, 5749–5757. doi: 10.1093/jxb/eru327

van Doorn, W. G., and van Meeteren, U. (2003). Flower opening and closure: a review. *J. Exp. Bot.* 54, 1801–1812. doi: 10.1093/jxb/erg213

Walthall, C. L., Anderson, C. J., Baumgard, L. H., Takle, E., and Wright-Morton, L. (2013). *Climate Change and Agriculture in the United States: Effects and Adaptation ii Climate Change and Agriculture in the United States: Effects and Adaptation. Geol. Atmos. Sci. Rep.* 1.

Yerushalmi, S., and Green, R. M. (2009). Evidence for the adaptive significance of circadian rhythms. *Ecol. Lett.* 12, 970–981. doi: 10.1111/j.1461-0248.2009.01343.x

Conflict of Interest Statement: BG was employed by Benson Hill Biosystems.

The remaining authors declare that the research was conducted in the absence of any commercial or financial relationships that could be construed as a potential conflict of interest.

frontiers in Plant Science

ORIGINAL RESEARCH
published: 14 November 2018
doi: 10.3389/fpls.2018.01650

Screening of Mutants Related to the C_4 Photosynthetic Kranz Structure in Foxtail Millet

Mingzhao Luo, Shuo Zhang, Chanjuan Tang, Guanqing Jia, Sha Tang, Hui Zhi and Xianmin Diao**

Institute of Crop Sciences, Chinese Academy of Agricultural Sciences, Beijing, China

C_4 plants exhibit significantly higher photosynthetic, water and nutrient use efficiency compared with C_3 plants. Kranz anatomy is associated with many C_4 plants in which bundle sheath cells surround the veins and are themselves surrounded by mesophyll cells. This specialized Kranz anatomy is elucidated as an important contributor to C_4 photosynthetic activities in C_4 plant. Characterizing the molecular basis of Kranz structure formation has become a key objective for studies of C_4 photosynthesis. However, severe mutants that specifically disrupt Kranz anatomy have not been identified. In this study, we detected 549 stable ethyl methane sulfonate-induced foxtail millet (cultivar Yugu1) mutants related to leaf development and photosynthesis among 2,709 mutants screened (M_3/M_4 generation). The identified mutants included 52 that had abnormal leaf veins (with abnormal starch accumulation based on iodine staining). Each of the 52 mutants was characterized through an analysis of leaf morphology, and through microscopic observations of leaf tissue sections embedded in resin and paraffin. In total, 14 mutants were identified with abnormal Kranz structures exemplified by small bundle sheath cell size. Additional phenotypes of the mutants included poorly differentiated mesophyll and bundle sheath cells, increased vein density and the absence of chloroplasts in the bundle sheath cells. Kranz structure mutations were accompanied by varying leaf thickness, implying these mutations induced complex effects. We identified mutations related to Kranz structure development in this trial, which may be useful for the mapping and cloning of genes responsible for mediating Kranz structure development.

Keywords: foxtail millet, C_4 photosynthesis, Kranz structure, EMS mutant, leaf mutant

OPEN ACCESS

Edited by:
Thomas P. Brutnell, Shandong Agricultural University, China

Reviewed by:
Thomas Edward Hughes, University of Oxford, United Kingdom
Thomas L. Slewinski, Bayer CropScience, Belgium

****Correspondence:***
Guanqing Jia
jiaguanqing@caas.cn
Xianmin Diao
diaoxianmin@caas.cn

Specialty section:
This article was submitted to Plant Breeding, a section of the journal Frontiers in Plant Science

Received: *29 November 2017*
Accepted: *24 October 2018*
Published: *14 November 2018*

Citation:
Luo M, Zhang S, Tang C, Jia G, Tang S, Zhi H and Diao X (2018) Screening of Mutants Related to the C_4 Photosynthetic Kranz Structure in Foxtail Millet. Front. Plant Sci. 9:1650. doi: 10.3389/fpls.2018.01650

INTRODUCTION

Photosynthesis, the driver for life on this planet, includes many carbon fixation pathways (e.g., C_3, C_4, and crassulacean acid metabolism). In all photosynthetic pathways, a bi-functional enzyme-ribulose-1,5-bisphosphate carboxylase/oxygenase (Rubisco) is needed to fix CO_2 into carbohydrates. The C_4 photosynthetic pathway completes the initial and secondary CO_2 fixations using two distinct photosynthetic cell types, which form a distinct CO_2-concentrating mechanism that significantly improves the carboxylation efficiency of Rubisco. Consequently, C_4 plants exhibit a higher photosynthetic efficiency, biomass production, and water and nutrient usage than C_3

plants under hot, dry conditions that favor stomatal closure (Diao et al., 2014; Saha and Blumwald, 2016). These characteristics enhance the ability of plants to grow in increasingly arid environments and decrease the need for fertilizer applications. However, many agriculturally important crops, such as rice, wheat, soybean, and potato, are C_3 plants. Thus, the suggestion that introducing the C_4 pathway into C_3 plants may improve productivity (Zhu et al., 2010; Li et al., 2011; Rizal et al., 2012; Wang et al., 2017) prompted the initiation of The C_4 Rice Project[1] by a group that included leading rice researchers. Promising results have included the successful transfer of genes encoding key C_4 pathway enzymes into C_3 plants to improve photosynthetic efficiency (Ku et al., 1999; Chi et al., 2004). However, researchers have been unable to generate C_3 plants with a highly efficient CO_2-concentrating mechanism even after transferring one or more genes encoding C_4 cycle metabolic enzymes (Westhoff and Gowik, 2010). This inability has been partly due to a lack of a leaf Kranz structure, which is important for the spatial separation of enzymatic activities related to carbon fixation (Kromdijk et al., 2014).

All grass family C_4 crops have a typical Kranz structure (Christin et al., 2013) consisting of an inner layer of relatively large bundle sheath cells around a vascular bundle. The bundle sheath cells are surrounded by a layer of mesophyll cells that are compactly arranged to form a concentric ring-shaped structure. These are generally only two mesophyll cells between vascular bundles in C_4 leaves as opposed to up to 18 cells in C_3 leaves (Sage et al., 2014). Elucidating the regulatory mechanisms underlying the development of Kranz structure has been the focus of research into C_4 photosynthesis (Langdale, 2011). Some researchers have examined genes differentially expressed between C_3 and C_4 plants (Wang et al., 2014) or tissues (Wang et al., 2013). Other studies of C_4 plants have applied genome and transcriptome sequencing techniques to analyze bundle sheath and mesophyll cells (Li J. et al., 2010; Covshoff et al., 2013) at different developmental stages (Li P. et al., 2010). These studies identified several differentially expressed genes between leaf development stages before and after the formation of the Kranz structure, and between mesophyll and bundle sheath cells. Although these studies have suggested several candidate genes, no functional tests of these candidates have revealed regulators of the process.

Geological studies (e.g., involving carbon isotopes) and phylogenetic analyses of various species have suggested that C_4 plants evolved from C_3 plants, with structural and gene expression changes having occurred over time. More than 66 independent events took place that caused some C_3 plants to evolve into C_4 plants, which is considered as the best example of convergent evolution (Hibberd, 2002; Sage et al., 2011; Rizal et al., 2012; Christin and Osborne, 2013). The first stage of this evolution involved structural changes, including the development of a higher leaf vein density, larger bundle sheath cell volume, as well as increased abundance and altered localization of organelles (e.g., chloroplasts and mitochondria) in bundle sheath cells. Additionally, genes encoding specific enzymes (e.g., PEPC and GDC) began to show cell-type specific enrichment. Moreover, CO_2 fixation occurred first in the outer leaf cells, after which the carbohydrates derived from CO_2 were fixed in the inner bundle sheath cells (Mckown and Dengler, 2007, 2009; Sage and Zhu, 2011). Studies revealed that some positive/negative regulators in the developing endoderm might have been important for the formation of C_4 structures (Slewinski et al., 2012). Researchers have mined for genes related to the development of C_4 structures by selecting and identifying mutants, including maize mutants with abnormal leaf veins (Slewinski et al., 2012), rice mutants with increased leaf vein density (Feldman et al., 2014), and sorghum mutants with decreased leaf vein density (Rizal et al., 2015). Several transcription factors that help regulate BSC differentiation in C_4 species have been identified, including SCR and SHR (Gardiner et al., 2011; Slewinski et al., 2012).

Maize and sorghum have been important model organisms in studies of C_4 plants, but they are large plant species with complex genomes. In contrast, green foxtail and foxtail millet are small in stature and have simpler genomes. Foxtail millet originated in the Yellow River basin of China, and represents a domesticated form of green foxtail. The self-pollinating diploid foxtail millet exhibits characteristics that make it useful for research, including a high seed set per spike, compact size, simple growth condition requirements, relatively small genome (490 Mb), and a high transformation efficiency. Therefore, this plant species is gradually being used as a new model organism for studies of the C_4 photosynthetic mechanism (Doust et al., 2009; Diao et al., 2014; Saha and Blumwald, 2016). Mutant lines exhibiting abnormal development of C_4 photosynthetic structures may be very important for identifying and cloning of responsible genes. In this study, genetically stable ethyl methanesulfonate (EMS) mutants generated using the Yugu1 cultivar were analyzed for screening of changes in leaf appearance and vein density, sugar accumulation, and Kranz structural features. Mutants with abnormal leaf veins and Kranz structures were identified, and may be useful for elucidating the molecular mechanism underlying Kranz structure and development.

MATERIALS AND METHODS

Tested Materials

We previously developed EMS-based methods for mutagenizing foxtail millet (Li W. et al., 2010) to establish a stable mutant library for foxtail millet cultivar Yugu1. A total of 2,709 M_3/M_4-generation mutants with stable phenotypes were preliminarily screened. Wild-type Yugu1 (maintained in our laboratory through many generations of self-pollinations) was used as the C_4 control plant, while the wild-type Nipponbare rice cultivar (provided by Xingguo Ye from the Institute of Crop Sciences, Chinese Academy of Agricultural Sciences) was used as the C_3 control plant.

Growth Conditions

Plants were grown in a 3 m × 0.5 m plot using standard agronomic practices (e.g., irrigation, weeding, and pesticide spraying) at the Institute of Crop Sciences, Chinese Academy of Agricultural Sciences in Shunyi district, Beijing, China.

[1] https://c4rice.com

Fixation of Materials

For each mutant line, we selected 6–8 similarly growing and normally developing plants that were free of diseases and insect pests. The middle parts of completely unfolded leaves were collected at the 8-leaf stage. The FAA-fixed samples (about 0.5 cm × 1 cm) were placed in a vacuum for more than 0.5 h. Samples were then re-fixed in new FAA solution for 24 h, washed three times with 70% ethanol, and then preserved. The glutaraldehyde-fixed samples (about 1 mm × 2 mm) were placed in a vacuum for 3–4 h, after which they were fixed again in new glutaraldehyde solution.

Microscopic Observation

The Anyty V500IR/UV portable digital microscope (3R Eddytek Corp., Beijing, China) was used to observe and photograph the leaf veins of striped mutants, three individuals for each mutant line were sampled for observation.

Iodine Staining

Fixed samples preserved in 70% ethanol were dehydrated with increasing ethanol concentrations (85%, 95%, and 100%). They were then treated with different ethanol:xylene mixtures (2:1, 1:1, 1:2, and pure xylene). Samples were gradually exposed to absolute ethanol (ethanol:xylene mixtures, 1:2, 1:1, 2:1, and pure ethanol; kept in each concentration for 1 h), and then stained with I_2-KI for 12 h. Changes in leaf vein density and starch content were then observed microscopically. Image J[2] was used to calculate vein density and carbohydrate accumulation in mutant individuals.

Preparation of Paraffin Sections

Leaf cross-sections were further observed using paraffin sections, which were prepared using a modified version of a traditional method. Samples preserved in 70% ethanol were dehydrated in 85%, 90%, and 100% (twice) ethanol, and then treated with different ethanol:xylene mixtures [2:1, 1:1, 1:2, and pure xylene (twice)]. Each treatment lasted 40–60 min, with the duration determined based on the growth condition of mutants. Samples were then embedded in paraffin, and 10-μm sections were generated using the Leica RM2250 microtome. The sections were placed on distilled water on microscope slides to ensure they were sufficiently spread out before being heated for more than 48 h. The prepared sections were stained with 0.2% toluidine blue and then sealed with neutral balsam. Samples were observed and photographed using a Leica microscope.

Preparation of Resin Sections

We collected leaves from mutants with an abnormal Kranz structure as observed using the paraffin section. We also selected 6–8 mutant individuals per mutant line, and leaf samples were fixed with 2.5% glutaraldehyde and then rinsed three times (10 min each) with phosphate buffer. Samples were fixed in 1% osmic acid for 1 h, and then rinsed three times with double-distilled H_2O (10 min each). Samples were gradually dehydrated in different concentrations of ethanol and then incubated in acetone for 10 min. They were incubated overnight in a 1:1 acetone:resin mixture, with mild shaking, after which they were incubated overnight in pure resin before being embedded in resin polymer. Samples were sliced into 500–800 Å sections using an ultramicrotome, and then picked up by copper mesh, placed on microscope slides, and stained with toluidine blue. The sections were observed and photographed using a Leica microscope.

Reagents

(1) I_2-KI staining reagent: 1 g I_2 and 8 g KI were dissolved in distilled water for a final volume of 100 ml. The solution was stored in an amber laboratory bottle.

(2) FAA: 5 ml acetic acid, 5 ml formaldehyde, and 90 ml 70% ethanol were thoroughly mixed.

(3) 2.5% glutaraldehyde fixative: 10 ml 25% glutaraldehyde, 40 ml distilled water, and 0.2 M PBS were thoroughly mixed. The solution was stored at 4°C.

RESULTS

Preliminary Screening and Classification of EMS Mutants

A total of 549 mutants from 2,709 stable EMS mutants library was screened based on their phenotypes which show decrease biomass, such as decreased fertility, lax panicle, or leave color variation. We observed that 40.62% of the 549 mutants produced abnormal leaves, among the leaf mutants are list in **Table 1**.

There were many types of leaf mutants. The wild-type Yugu1 leaves were dark green with a uniformly arrayed leaf vein (**Figure 1A**). Meanwhile, leaf mutants produced abnormal leaves in terms of striped, shape, and color (**Figures 1B–P**). Abnormal striped (mainly white and yellow) were the most commonly observed leaf mutations. In some cases (e.g., *t81* and *t104*), white striped were present on the whole leaf (**Figures 1B,C**). Some mutants (e.g., *t11*) produced leaves with several large white striped (**Figure 1D**), while other mutants (e.g., *t71*) had normal-sized leaves that were covered with slender white striped (**Figure 1E**). In some cases (e.g., *t6*), mutants grew thin flag leaves with yellow striped (**Figure 1F**). Other mutants (e.g., *t53*) had thin yellow striped at the leaf tip, but the rest of the leaf was normal (**Figure 1G**). Some mutants produced leaves with abnormal sizes and shapes, including *t17*, which had relatively small leaves (**Figure 1H**) and *t57*, which had narrow leaves (**Figure 1I**). In mutants with abnormally colored leaves, some produced completely yellow leaves (e.g., *t124*; **Figure 1J**), while others had leaves that were yellow only at the tip (e.g., *t72*; **Figure 1K**). Many phenotypes were observed for mutants with lesions. For example, severe brick-red rust was detected on all leaves of some mutants (e.g., *t121*; **Figure 1L**), while other mutants had small punctum spots (e.g., *t33*; **Figure 1M**) or black rust spots (e.g., *t35*;

[2]https://imagej.nih.gov/ij/

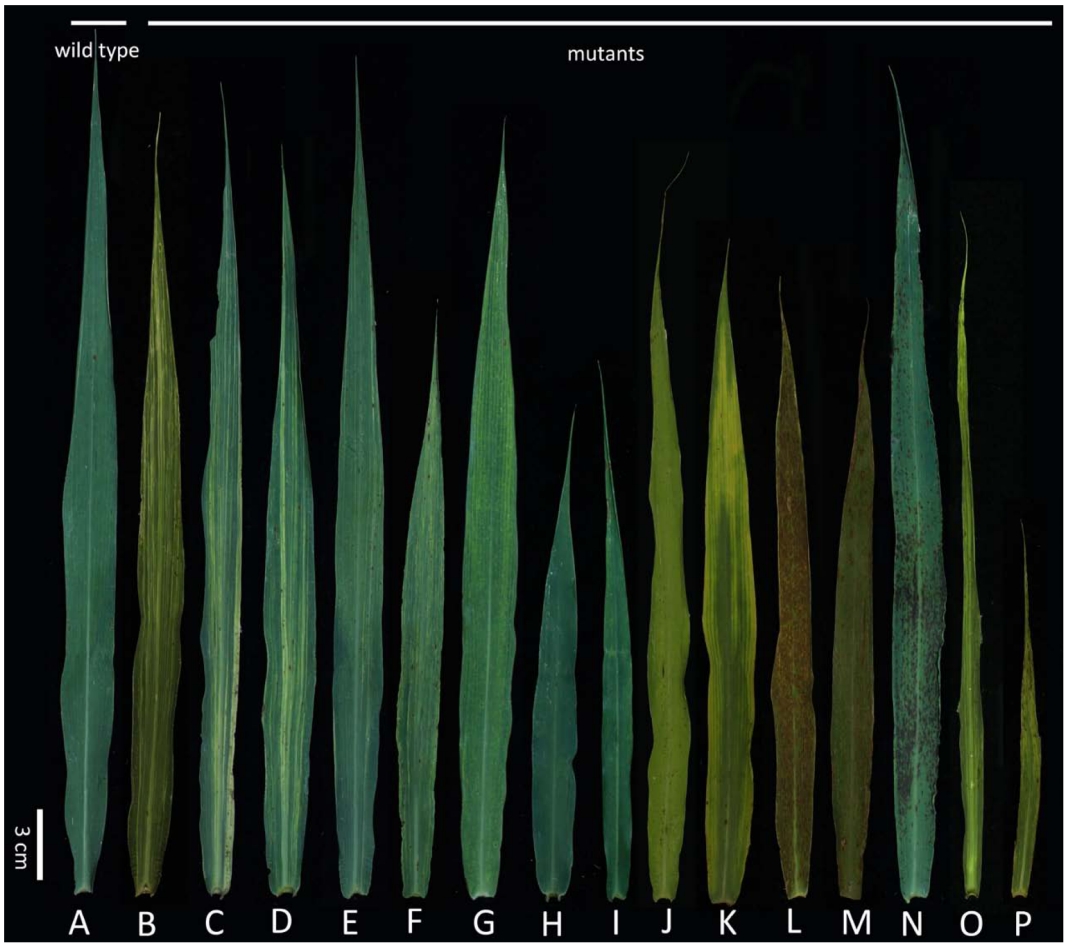

FIGURE 1 | Flag leaf of diverse mutants. **(A)** Wild-type Yugu1; **(B–P)** examples of leaf mutants; **(B)** light white striped; **(C–D)** white striped; **(E)** yellowish striped; **(F)** yellow striped; **(G)** yellowish striped; **(H,I)** abnormal leaf shape; **(J,K)** yellow leaf; **(L-N)** disease-spot leaf; **(O–P)** abnormal leaf striped and shape. Scale: 3 cm.

Figure 1N) on the leaves. Some mutants had abnormally shaped and striped leaves [e.g., *t14* (**Figure 1O**) and *t68* (**Figure 1P**)].

Microscopic Analysis of the Leaf Veins of Striped Mutants

To further characterize leaf vein tissue structures in striped mutants were observed and photographed using a microscope. The wild-type Yugu1 leaves were dark green with uniform leaf veination (**Figure 2A**). Varying leaf colors were observed among the striped mutants. Most yellow striped mutants produced abnormally colored leaves with a normal leaf veination, including some mutants with fully yellow leaves (e.g., *t15*; **Figure 2B**). We also detected yellow and green striped mutants with thick light green veins (e.g., *t216*; **Figure 2C**) as well as light green striped mutants with thick dark green veins (e.g., *t38*; **Figure 2D**). Yellow and green striped mutants produced yellow as well as green leaves

TABLE 1 | Phenotypes of 549 mutants after a preliminary screen.

Phenotypes	Numbers of mutants	Total	Ratio (%)	Phenotypes	Numbers of mutants	Total	Ratio (%)
White striped	48	549	8.74	Yellow leaf	22	549	4.01
Yellow striped	19	549	3.46	Lax panicle	54	549	9.84
Light white striped	39	549	7.10	Erect leaf	67	549	12.20
Yellowish striped	11	549	2.00	Decreased fertility	75	549	13.66
Disease-spot leaf	16	549	2.91	Tight spikelet	99	549	18.03
Abnormal leaf striped and shape	16	549	2.91	Early browning	20	549	3.64
Abnormal leaf shape	52	549	9.47	Late heading	11	549	2.00

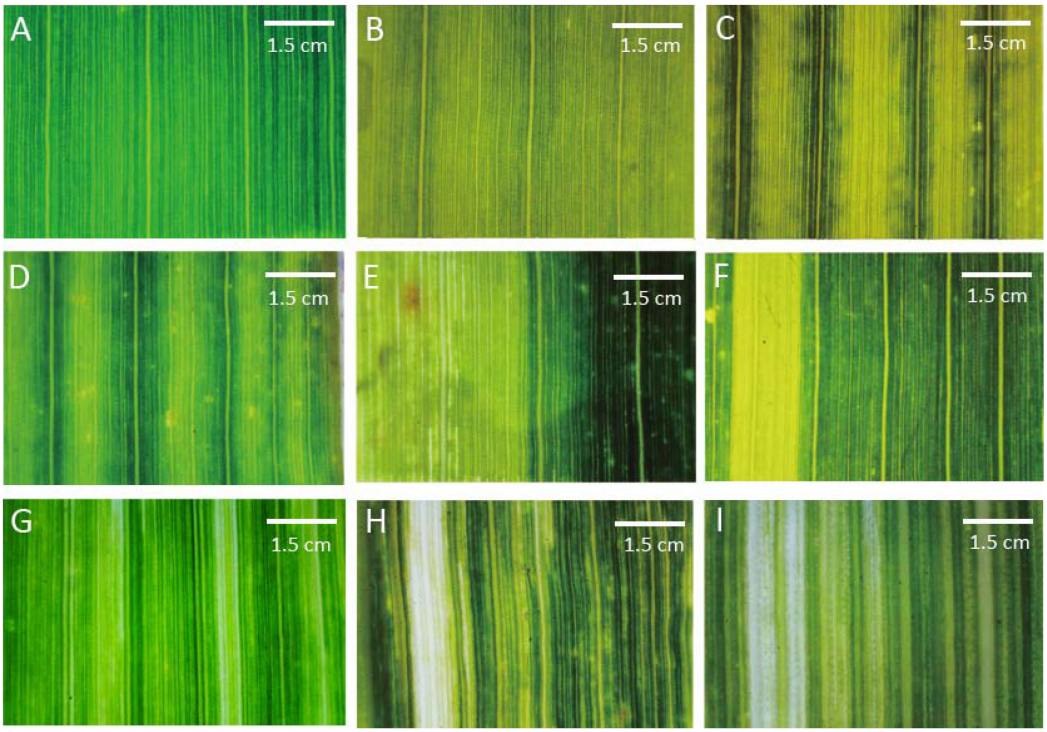

FIGURE 2 | Mutant classifications after a microscopic analysis of leaf vein arrangements. **(A)** Wild-type Yugu1; **(B)** light yellow leaves (*t15*); **(C)** yellow and green striped leaves (*t216*); **(D)** light green striped leaves (*t38*); **(E)** yellow and green leaves (*t261*); **(F)** thick yellow striped leaves (*t267*); **(G)** thin yellow striped leaves (*t198*); **(H)** thick white striped leaves (*t197*); and **(I)** thin white striped leaves (*t189*). Scale: 1.5 cm.

(e.g., *t261*; **Figure 2E**). Yellow wide striped mutants had leaves that were no longer green (e.g., *t267*; **Figure 2F**). The presence of striped on these mutants might affect chlorophyll synthesis or degradation or may be related to chloroplast structural damages.

A macro camera was used to observe a few striped mutants, including those with leaf veins that were no longer green and those with irregularly arranged leaf veins. The leaf veins of several yellow narrow striped mutants could not be clearly distinguished (e.g., *t198*; **Figure 2G**), while an increased number of irregularly arrayed and thick veins were observed in some wide white striped mutants (e.g., *t197*; **Figure 2H**). Additionally, leaf veins that could not be clearly distinguished were observed in narrow white striped mutants (e.g., *t189*; **Figure 2I**). The striped of these leaf mutants that were visible to the naked eye and the unclear veins observed by microscopy might be related to the abnormal development of cell structures. Moreover, this could also be the result of plastid mutations (similar to iojap and japonica of maize) or may be due to epigenetic effects of the mutagenesis. This possibility should be the main research focus of future studies involving the screening of leaf vein mutants.

Results of Iodine Staining

To more clearly observe the changes in leaf vein structure, the mature leaves from 549 plants were stained with iodine. The distance between leaf veins was greater for the Nipponbare C_3 control plant than for the Yugu1 C_4 plant. The average distances between leaf veins were 259.42 μm and 119.21 μm for Nipponbare (**Figure 3E**) and Yugu1 (**Figure 3F**) plants, respectively. After iodine staining, carbohydrates appeared bronze-colored and proteins were yellow. In C_3 plants, photosynthesis occurs in mesophyll cells that are rich in chloroplasts, resulting in the accumulation of carbohydrates. Bundle sheath cells have poorly developed chloroplasts (Langdale, 2011). After iodine staining, the area surrounding the leaf vein was yellow, while the mesophyll cells between leaf veins were brown. The yellow area between leaf veins consisted of bulliform cells with no chloroplasts. In C_4 plants, photosynthetic carbon fixation mainly takes place in bundle sheath cells, in which many carbohydrates accumulate. Thus, leaf veins were bronze-colored, while the mesophyll cells between the leaf veins were yellow (**Figures 3E,F**). Iodine staining reflected the accumulation of carbohydrates in leaves and enabled analyses of tissue structure changes due to mutations.

The iodine staining results revealed 52 mutants (**Supplementary Figures S1, S2**) with four types of abnormal leaf veins, based on the change of accumulation of carbohydrates revealed by color and veins variations detected in mutants (**Table 2**). We detected 34 Type-A mutants, which had relatively low sugar levels, resulting in an increase in the yellow-stained areas around leaf veins. Additionally, their leaf veins could be clearly distinguished (e.g., *t62*; **Figure 3A**). Type B included six mutants with relatively low sugar levels and an increase in the yellow-stained areas around leaf veins; however, some leaf

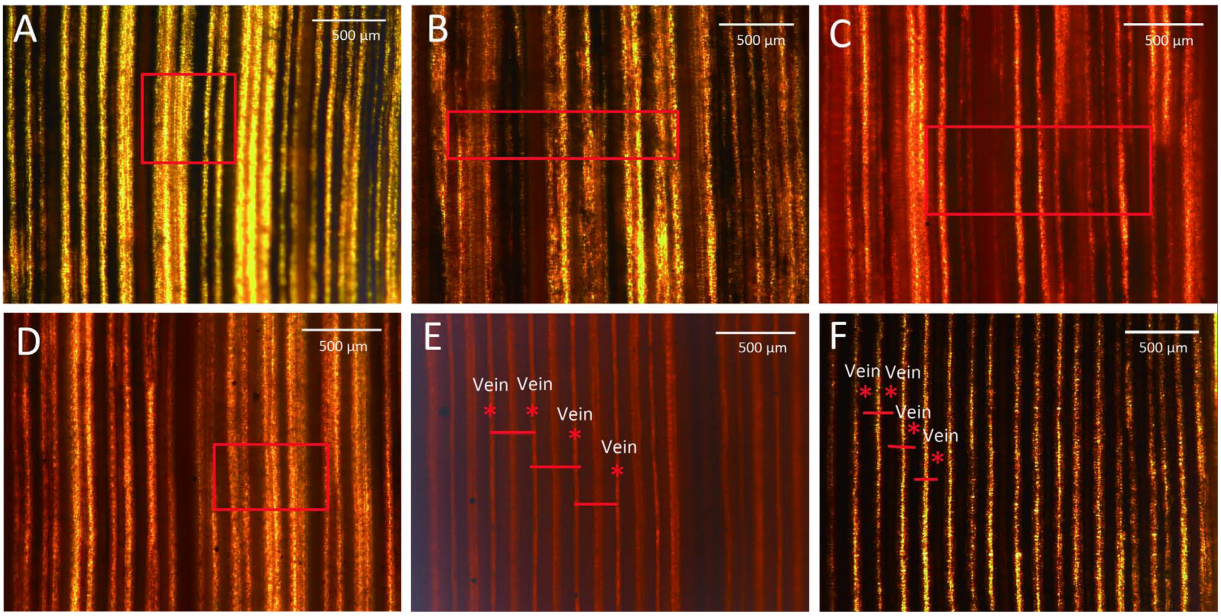

FIGURE 3 | Leaves stained with I_2-KI. **(A)** Decreased carbohydrate abundance and normal vein arrangement (*t62*); **(B)** decreased carbohydrate abundance and abnormal vein arrangement (*t95*); **(C)** increased carbohydrate abundance (*t66*); **(D)** unevenly stained (*t74*); **(E)** rice (C_3 control plant); and **(F)** wild-type Yugu1. Scale: 500 μm. Leaf veins are marked with an asterisk, and short red lines represent the distance between adjacent leaf veins. The red boxes in the picture means obvious differ between mutants and wild-type Yugu1.

veins could not be clearly distinguished (e.g., *t95*; **Figure 3B**). We identified nine Type-C mutants, with increased sugar levels that led to red-stained areas. These mutants also had irregularly arrayed leaf veins (e.g., *t66*; **Figure 3C**). Three mutants were categorized as Type D because of the observed uneven distribution of sugars, with increased and decreased sugar levels surrounding leaf veins (e.g., *t49*, *t50*, and *t74*; **Figure 3D**). Thus, although almost all striped mutants exhibited abnormal sugar accumulation and irregular leaf vein arrangements, we did not detect any mutants with severely defective leaf vein development. This result might be associated with chloroplast development in bundle sheath cells and the inhibition of part of the sugar synthesis and transportation mechanism of a photosynthetic pathway.

Analysis of Resin Sections

According to previously published results (Sage et al., 2014), C_4 Kranz anatomy possesses enlarged bundle sheath cells compared with C_3 species. To analyze the cross sections of leaf vein mutants, paraffin and resin sections were prepared for the 52 iodine-stained mutants. Aligned Kranz structures were observed in the Yugu1 leaf cross sections. Mature vascular bundles were surrounded by a layer of large circular or oval bundle sheath cells and an outer layer of spindly mesophyll cells. We detected two or three mesophyll cell layers between bundle sheath cells of two adjacent Kranz structures. Chloroplasts in bundle sheath cells were bluish violet after staining with toluidine blue (**Figure 4A**).

Abnormally developed Kranz structures were observed in 14 mutants (e.g., Kranz structure dysplasia and fewer mesophyll cell layers), and the red arrows indicated the altered part in the leaf tissue cross sections (**Supplementary Figure S3**). In the *t6* mutant, vascular tissue that did not develop into a Kranz structure existed between normally developed Kranz structures. This vascular tissue was surrounded by chloroplast-containing bundle sheath cells that were abnormally small and were not associated with tightly arrayed mesophyll cells (**Figure 4B**). Meanwhile in the *t11* mutant, the vascular bundles were not surrounded by enlarged bundle sheath cells full of chloroplasts. Additionally, mesophyll cells were circular and similarly sized, and some individual vascular tissues were underdeveloped (**Figure 4C**). The *t14* and *t18* mutants had

TABLE 2 | Classification of I_2-KI–stained mutants based on the change of accumulation of carbohydrates revealed by color and veins variations.

Types	Mutant numbers	Total number	Ratio
A	*t6, t10, t14, t17, t18, t20, t23, t26, t27, t28, t39, t40, t41, t43, t45, t48, t53, t54, t56, t62, t63, t64, t65, t68, t69, t71, t72, t75, t76, t78, t81, t92, t93, t115*	34	65.4%
B	*t11, t46, t47, t95, t104, t106*	6	11.5%
C	*t22, t42, t44, t66, t67, t87, t91, t105, t114*	9	17.3%
D	*t49, t50, t74*	3	5.8%

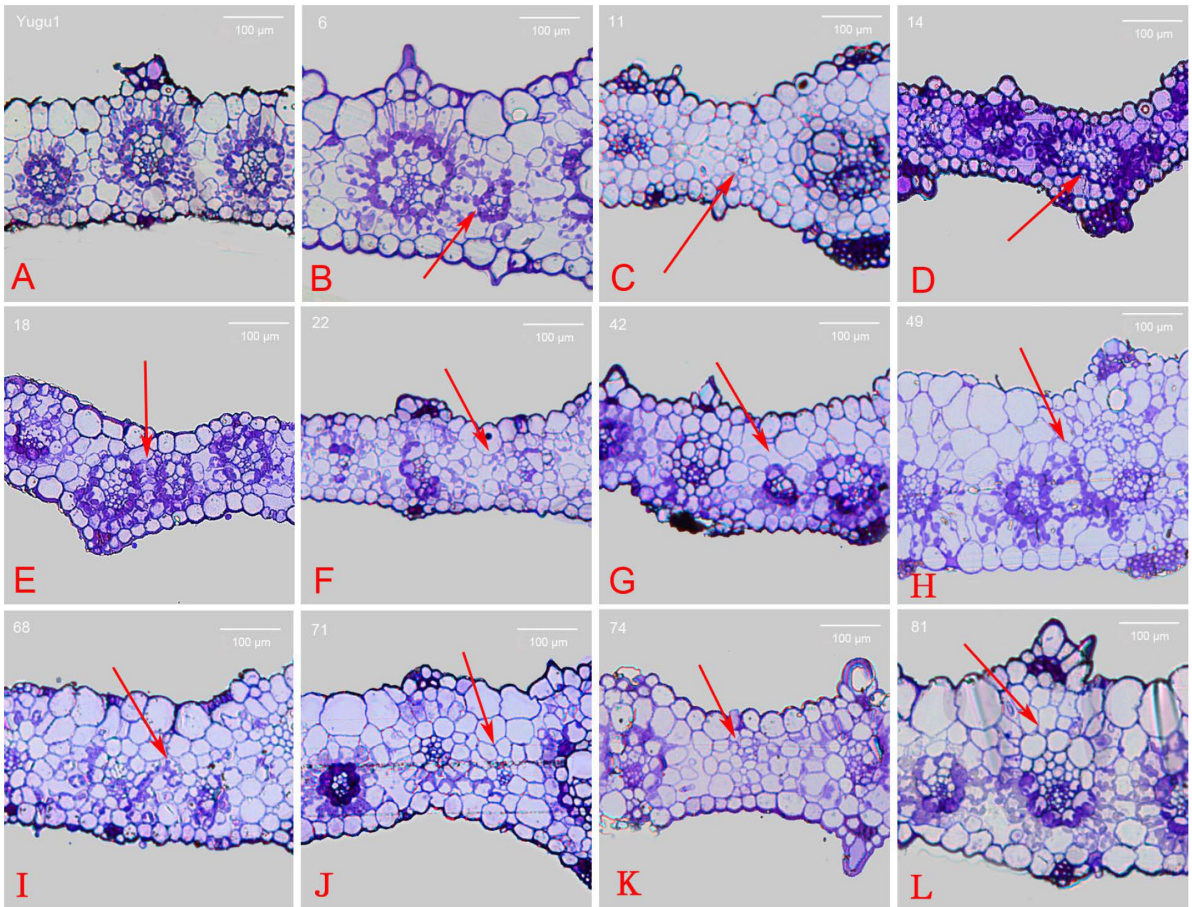

FIGURE 4 | Cross section of wild-type and mutant leaves embedded in resin. **(A)** wild-type Yugu1; **(B)** *t6*; **(C)** *t11*; **(D)** *t14*; **(E)** *t18*; **(F)** *t22*; **(G)** *t42*; **(H)** *t49*; **(I)** *t68*; **(J)** *t71*; **(K)** *t74*; and **(L)** *t81*. Scale: 100 μm. The red arrows indicated the altered part in the leaf tissue cross sections.

apparently differentiated bundle sheath and mesophyll cells with both distinct chloroplast distribution and cell size, but the cells were obviously smaller than those of the wild-type leaves. These mutants also had a relatively thin leaf cross section and closely linked adjacent Kranz structures (**Figures 4D,E**). The *t49* mutant produced mesophyll cells that were bigger than bundle sheath cells, and the cells lacking chloroplasts were also bigger than normal. Moreover, the leaf cross sections were thicker than the wild-type cross sections (**Figure 4H**). Furthermore, *t22*, *t42*, *t71*, and *t74* mutants produced abnormal Kranz structures that lacked bundle sheath cells surrounding vascular bundles. Additionally, no chloroplasts were detected (**Figures 4F,G,J,K**). The cross section of the *t68* mutant leaf revealed a disordered cell arrangement, with circular or oval mesophyll and bundle sheath cells (**Figure 4I**). The *t81* mutant mesophyll cells contained an increased abundance of chloroplasts, while some photosynthetic cells (bundle sheath and mesophyll cells) at the adaxial side of the Kranz structure lacked chloroplasts (**Figure 4L**).

The *t50* and *t62* mutants developed small, but otherwise normal, Kranz structures. All Kranz structure cells had differentiated normally except for the abnormally small bundle sheath cells surrounding the vascular bundle. The Kranz structure of the *t50* mutant was surrounded by relatively small bundle sheath cells, with an outer layer of large mesophyll cells. In contrast, all of the Kranz structure cells were smaller than normal in the *t62* mutant. The bundle sheath and mesophyll cells of the *t91* mutant differentiated and developed normally, with an orderly arrayed Kranz structure. However, the leaf cross section indicated the parenchymal cells at the adaxial side were larger than normal, resulting in thicker leaves.

DISCUSSION

Genetic Analysis of Kranz Anatomy in the Grasses

The identification of mutants in which key characteristics of C_4 photosynthesis have been disrupted represents a reliable and efficient method for elucidating the molecular basis for these traits. Rizal et al. (2015) identified two sorghum (C_4 plant) mutants with relatively low leaf vein densities. A further analysis confirmed that the brassinolide synthesis pathway was blocked, implying this pathway may induce an increase in leaf vein density (Rizal et al., 2015). Comparative genomics and bioinformatics

investigations led researchers to identify many transcription factors, *cis*-acting elements, and differentially expressed enzyme-coding genes possibly related to the C_4 pathway based on transcriptome sequencing data. Several transcription factors have been identified, including SCR, SCL23, and SHR, which may regulate both root endodermal cell fate and leaf bundle sheath determination (Slewinski et al., 2012; Slewinski, 2013). Therefore, the genetic network controlling root endodermal cell fate may be wired very similarly to the leaf bundle sheath developmental program. Although some insight has been gained from the genetic analysis of Kranz anatomy in the grasses, much remains to be discovered. Here we show through the characterization of EMS induced mutations of *S. italica*, that forward genetic screens offer an attractive path to understanding Kranz anatomy.

In this study, we identified several mutants with disorderly arrayed leaf veins and undeveloped or abnormally developed bundle sheath cells. For example, the *t22*, *t42*, *t71*, and *t74* mutants lacked large, chloroplast-filled, and sheath-shaped cells surrounding vascular bundles (**Figures 4F,G,J,K**), suggesting the mutated genes were associated with bundle sheath cell development, or related to the disruption of developmental regulators like SHR or SCR. Thus, these mutants may be useful materials for comprehensive analyses of bundle sheath cell development (e.g., gene localization and cloning studies). We observed that, in addition to not forming normal bundle sheath cells, the mutants produced thin and irregularly shaped leaves, as well as abnormally arranged epidermal and mesophyll cells (**Figures 4F,G,I**). These complex mutant phenotypes suggest the regulation of the relevant genes or their functional networks is also complex.

Combining with pictures of mutants' phenotype in field (data were not shown), mutant *t22* and *t71* identified in study exhibited similar plant height, panicle type and leaf size compared with wild-type Yugu1. Especially for *t22,* no significant change of carbohydrate accumulation and vein space (**Supplementary Figure S1**) has been observed between the mutant and wild type, which might illustrate that genetic dissection of *t22* would definitely provide us more detailed information of Kranz structure formation in Setaria. Further studies focused on genetic dissections of Kranz structure mutants through MutMap or transcriptome approaches would be helpful for clarifying how Kranz anatomy came into being in the grasses. Although we really have acquired one or two mutants that maybe special for Kranz structure, most of mutants identified in this trial may not directly relate to the Kranz structure, and exhibited pleiotropic effect (photosynthetic, chloroplast, leaf size) that may be of limited use for dissecting Kranz development. Furthermore, some Kranz structure mutants may be missed during screening processes, despite this is a fast way for mutant identification. Several severe mutants may not have been identified because Kranz anatomy maybe regulated by many genes and possibly redundant, thus making single or limited gene mutations a difficult way to screen mutations with completely terminated Kranz anatomy. Also, mutations that disrupt Kranz anatomy beyond what was found in this study may be seedling lethal, and thus not detected. Former investigations always only focused on vein density and very less leaf tissue cross sections were identified, this may be why these reports have failed to identify Kranz structure mutants. Large scale of cross section analysis may be the only efficient way to identify Kranz structure variations occurred in mutant library.

Forward Genetics Analyses of Mutations May Accelerate the Molecular Characterization of the Development of Key Structures in C_4 Plants

Leaf vein density, bundle sheath cell size, and organelle quantity and localization in bundle sheath cells are key structural features that differ between C_3 and C_4 plants. Many researchers are interested in elucidating the mechanisms responsible for the development of these structures. Slewinski have suggested that identifying the positive/negative regulatory factors influencing endoderm development might provide useful information regarding the production of the Kranz structure in C_3 plants (Slewinski, 2013). Because of a lack of C_4 mutants with key phenotypes, transcriptomics data have been used to compare whole-genome expression levels between C_3 and C_4 plants and to analyze the leaves or specific tissues of C_4 plants at different developmental stages. By applying genomics and bioinformatics methods, researchers have also identified several transcription factors, *cis*-elements, and differentially expressed genes encoding enzymes possibly related to the C_4 pathway based on transcriptome sequencing data (Huang and Brutnell, 2016; Huang et al., 2016).

The mechanism responsible for the development of the Kranz structure has not been characterized. In this study, relevant EMS mutants were screened, and the genes associated with these mutants will be cloned. Our data would be combined with the existing gene expression profiles for a subsequent analysis to identify genetic factors that mediate the development of the Kranz structure. Additionally, cloning the related target genes for functional verifications may provide new insights into the evolution and development of the Kranz structure in C_4 plants.

Impacts of Chloroplast and Mitochondrial Development Related Genes on Identification of Real C_4 Related Leaf Striped Mutants

Researchers have studied several leaf striped mutants of rice and maize, and gene localization observations and functional verifications have indicated that striped mutants are usually the result of abnormal chloroplast or mitochondrial development and are severely affected by environmental conditions (e.g., temperature and light) (Yoo et al., 2009; Li P. et al., 2010). We also revealed that many striped mutant phenotypes are affected by the growth period and tissues. Some striped mutants exhibit diverse gene expression patterns during different developmental periods. In some mutants, the striped phenotype might appear only during the seedling stage. For example, the leaves of the *t22* mutant contain white striped during the seedling stage, but then subsequently appear normal. Conversely, the leaves of some mutants, such as *t53*, exhibit obvious striped phenotypes during later growth stages. Other mutants, including *t41*, *t42*, and *t91*,

produce a white striped phenotype at all growth and development stages. Leaf abnormalities may also appear at specific sites. For example, the leaf tip of *t19* and *t72* mutants is yellow, while the rest of the leaf is normal, which is in contrast to *t56* leaves, in which white striped are produced toward the bottom.

Leaf veins and Kranz structures developed essentially normally in some striped mutants (e.g., *t56*, *t72*, and *t91*). The Kranz structure is a core structural feature of C_4 plants. Identifying mutants with significant Kranz structural changes, but that are otherwise normal, is critical for elucidating the development of this structure. Microscopy techniques are invaluable for this type of research. However, an initial analysis of untreated leaf sections may be advisable. Preparing paraffin or resin sections of specific mutants selected based on the initial universal screen of mutants may decrease the workload and improve efficiency.

CONCLUSION

In this study, the emerging model species of Setaria was used for dissecting C_4 Kranz anatomy through forward genetic approaches. Many stable EMS-induced mutants with abnormal Kranz structures in foxtail millet were identified for advancing research efforts on verifying the molecular mechanisms of this important anatomic structure in formation of C_4 photosynthetic activities. Results of this trial would lay out the foundation of the development of Setaria as an essential model for deciphering genetic basis of plant C_4 photosynthesis in future.

AUTHOR CONTRIBUTIONS

XD designed the experiments. ML, SZ, CT, GJ, and ST performed the experiments. HZ provided materials. ML, SZ, CT, and GJ analyzed the data. ML, GJ, and XD wrote the paper.

FUNDING

This work was supported by the National Natural Science Foundation of China (31522040), Fundamental Research Funds of CAAS (Y2016XT05, Y2017JC15, and CAAS-XTCX2016002), China Agricultural Research System (CARS06-13.5-A04), and the Agricultural Science and Technology Innovation Program of the Chinese Academy of Agricultural Sciences.

ACKNOWLEDGMENTS

We thank Liwen Bianji, Edanz Editing China (www.liwenbianji.cn/ac) for translating and editing the English text of a draft of this manuscript.

SUPPLEMENTARY MATERIAL

The Supplementary Material for this article can be found online at: https://www.frontiersin.org/articles/10.3389/fpls.2018.01650/full#supplementary-material

REFERENCES

Chi, W., Zhou, J. S., Zhang, F., and Wu, N. H. (2004). Photosynthetic features of transgenic rice expressing *Sorghum* C4 type NADP-ME. *Acta Bot. Sin.* 46, 873–882.

Christin, P. A., and Osborne, C. P. (2013). The recurrent assembly of C4 photosynthesis, an evolutionary tale. *Photosynth. Res.* 117, 163–175. doi: 10.1007/s11120-013-9852-z

Christin, P. A., Osborneb, C. P., Chateleta, D. S., Columbusc, J. T., Besnardd, G., and Hodkinsone, T. R. (2013). Anatomical enablers and the evolution of C4 photosynthesis in grasses. *Proc. Natl. Acad. Sci. U.S.A.* 110, 1381–1386. doi: 10.1073/pnas.1216777110

Covshoff, S., Furbank, R. T., Leegood, R. C., and Hibberd, J. M. (2013). Leaf rolling allows quantification of mRNA abundance in mesophyll cells of *Sorghum*. *J. Exp. Bot.* 64, 807–813. doi: 10.1093/jxb/errs321836

Diao, X. M., Schnable, J., Bennetzen, J. L., and Li, J. Y. (2014). Initiation of setaria as a model plant. *Front. Agric. Sci. Eng.* 1, 16–20. doi: 10.15302/j-fase-2014011

Doust, A. N., Kellogg, E. A., Devos, K. M., and Bennetzen, J. L. (2009). Foxtail millet: a sequence-driven grass model system. *Plant Physiol.* 149, 137–141. doi: 10.1104/pp.108.129627

Feldman, A. B., Murchie, E. H., Leung, H., Baraoidan, M., Coe, R., and Yu, S. M. (2014). Increasing leaf vein density by mutagenesis: laying the foundations for C4 rice. *PLoS One* 9:e94947. doi: 10.1371/journal.pone.0094947

Gardiner, J., Donner, T. J., and Scarpella, E. (2011). Simultaneous activation of SHR and ATHB8 expression defines switch to preprocambial cell state in Arabidopsis leaf development. *Dev. Dyn.* 240, 261–270. doi: 10.1002/dvdy.22516

Hibberd, J. M. (2002). Characteristics of C4 photosynthesis in the stems and petioles of C3 flowering plants. *Nature* 415, 451–454. doi: 10.1038/415451a

Huang, C. F., Chang, Y. M., Lin, J. J., Yu, C. P., Lin, H. H., and Liu, W. Y. (2016). Insights into the regulation of C4 leaf development from comparative transcriptomic analysis. *Curr. Opin. Plant Biol.* 30, 1–10. doi: 10.1016/j.pbi.2015.12.011

Huang, P., and Brutnell, T. P. (2016). A synthesis of transcriptomic surveys to dissect the genetic basis of C4 photosynthesis. *Curr. Opin. Plant Biol.* 31, 91–99. doi: 10.1016/j.pbi.2016.03.014

Kromdijk, J., Ubierna, N., Cousins, A. B., and Griffiths, H. (2014). Bundle-sheath leakiness in C4 photosynthesis: a careful balancing act between CO2 concentration and assimilation. *J. Exp. Bot.* 65, 3443–3457. doi: 10.1093/jxb/eru157

Ku, M. S., Agarie, S., Nomura, M., Fukayama, H., Tsuchida, H., and Ono, K. (1999). High-level expression of maize phosphoenolpyruvate carboxylase in transgenic rice plants. *Nat. Biotechnol.* 17, 76–80. doi: 10.1038/5256

Langdale, J. A. (2011). C4 cycles: past, present, and future research on C4 photosynthesis. *Plant Cell* 23, 3879–3892. doi: 10.1105/tpc.111.092098

Li, J., Pandeya, D., Nath, K., Zulfugarov, I. S., Yoo, S. C., and Zhang, H. (2010). Zebra-necrosis, a thylakoid-bound protein, is critical for the photoprotection of developing chloroplasts during early leaf development. *Plant J.* 62, 713–725. doi: 10.1111/j.1365-313X.2010.04183.x

Li, P., Ponnala, L., Gandotra, N., Wang, L., Si, Y., and Tausta, S. L. (2010). The developmental dynamics of the maize leaf transcriptome. *Nat. Genet.* 42, 1060–1067. doi: 10.1038/ng.703

Li, W., Zhi, H., and Wang, Y. F. (2010). Analysis on the conditions of EMS treatment on foxtail millet. *J. Hebei Agric. Sci.* 14, 77–79. doi: 10.16318/j.cnki.hbnykx.2010.11.029

Li, Y. Y., Zhang, H., and Zhu., X. G. (2011). C4 rice: are we ready for the challenge? a historical perspective. *Plant Physiol. J.* 47, 1127–1136.

Mckown, A. D., and Dengler, N. G. (2007). Key innovations in the evolution of kranz anatomy and C4 vein pattern in *Flaveria*. *Am. J. Bot.* 94, 382–399. doi: 10.3732/ajb.94.3.382

Mckown, A. D., and Dengler, N. G. (2009). Shifts in leaf vein density through accelerated vein formation in C4 *Flaveria*. *Ann. Bot.* 104, 1085–1098. doi: 10.1093/aob/mcp210

Rizal, G., Karki, S., Thakur, V., Chatterjee, J., Coe, R. A., and Wanchana, S. (2012). Towards a C4 rice. *Asian J. Cell Biol.* 7, 13–31. doi: 10.3923/ajcb.2012.13.31

Rizal, G., Thakur, V., Dionora, J., Karki, S., Wanchana, S., and Acebron, K. (2015). Two forward genetic screens for vein density mutants in *Sorghum* converge on a cytochrome P450 gene in the brassinosteroid pathway. *Plant J.* 84, 257–266. doi: 10.1111/tpj.13007

Sage, R. F., and Zhu, X. G. (2011). Exploiting the engine of C4 photosynthesis. *J. Exp. Bot.* 62, 2989–3000. doi: 10.1093/jxb/err179

Sage, R. F., Christin, P. A., and Edwards, E. J. (2011). The C4 plant lineages of planet earth. *J. Exp. Bot.* 62, 3155–3169. doi: 10.1093/jxb/err048

Sage, R. F., Khoshravesh, R., and Sage, T. L. (2014). From proto-Kranz to C4 Kranz: building the bridge to C4 photosynthesis. *J. Exp. Bot.* 65, 3341–3356. doi: 10.1093/jxb/eru180

Saha, P., and Blumwald, E. (2016). Spike-dip transformation of *Setaria viridis*. *Plant J.* 86, 89–101. doi: 10.1111/tpj.13148

Slewinski, T. L., Anderson, A. A., Zhang, C., and Turgeon, R. (2012). Scarecrow plays a role in establishing kranz anatomy in maize leaves. *Plant Cell Physiol.* 53, 2030–2037. doi: 10.1093/pcp/pcs147

Slewinski, T. L. (2013). Using evolution as a guide to engineer kranz-type C4 photosynthesis. *Front. Plant Sci.* 4:212. doi: 10.3389/fpls.2013.00212

Wang, L., Czedik-Eysenberg, A., Mertz, R. A., Si, Y., Tohge, T., and Nunes-Nesi, A. (2014). Comparative analyses of C4 and C3 photosynthesis in developing leaves of maize and rice. *Nat. Biotechnol.* 32, 1158–1165. doi: 10.1038/nbt.3019

Wang, P., Kelly, S., Fouracre, J. P., and Langdale, J. A. (2013). Genome-wide transcript analysis of early maize leaf development reveals gene cohorts associated with the differentiation of C4 kranz anatomy. *Plant J.* 75, 656–670. doi: 10.1111/tpj.12229

Wang, S., Tholen, D., and Zhu, X. G. (2017). C4 photosynthesis in C3 rice: a theoretical analysis of biochemical and anatomical factors. *Plant Cell Environ.* 40, 80–94. doi: 10.1111/pce.12834

Westhoff, P., and Gowik, U. (2010). Evolution of C4 photosynthesis-looking for the master switch. *Plant Physiol.* 154, 598–601. doi: 10.1104/pp.110.161729

Yoo, S. C., Cho, S. H., Sugimoto, H., Li, J., Kusumi, K., and Koh, H. J. (2009). Rice virescent3 and stripe1 encoding the large and small subunits of ribonucleotide reductase are required for chloroplast biogenesis during early leaf development. *Plant Physiol.* 150, 388–401. doi: 10.1104/pp.109.136648

Zhu, X. G., Shan, L., Wang, Y., and Quick, W. P. (2010). C4 rice-an ideal arena for systems biology research. *J. Integr. Plant Biol.* 52, 762–770. doi: 10.1111/j.1744-7909.2010.00983.x

Conflict of Interest Statement: The authors declare that the research was conducted in the absence of any commercial or financial relationships that could be construed as a potential conflict of interest.

Advantages of publishing in Frontiers

OPEN ACCESS
Articles are free to read for greatest visibility and readership

FAST PUBLICATION
Around 90 days from submission to decision

HIGH QUALITY PEER-REVIEW
Rigorous, collaborative, and constructive peer-review

TRANSPARENT PEER-REVIEW
Editors and reviewers acknowledged by name on published articles

Frontiers
Avenue du Tribunal-Fédéral 34
1005 Lausanne | Switzerland

Visit us: www.frontiersin.org
Contact us: info@frontiersin.org | +41 21 510 17 00

REPRODUCIBILITY OF RESEARCH
Support open data and methods to enhance research reproducibility

DIGITAL PUBLISHING
Articles designed for optimal readership across devices

FOLLOW US
@frontiersin

IMPACT METRICS
Advanced article metrics track visibility across digital media

EXTENSIVE PROMOTION
Marketing and promotion of impactful research

LOOP RESEARCH NETWORK
Our network increases your article's readership